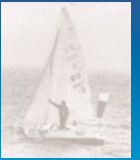




EU FP7 IRSES 2011 Project



COMPLEX RESEARCH OF EARTHQUAKE'S FORECASTING POSSIBILITIES, SEISMICITY AND CLIMATE CHANGE CORRELATIONS

Acronym: *BlackSeaHazNet*
Scientific Panel: ENVIRONMENT
Duration of the project: 36 months

Person in charge for the project: Strachimir Mavrodiev
Person in charge of administrative, legal and financial aspects of the project: Boyko Vachev



BlackSeaHazNet Workshop,
16-19 Dec 2013, INRNE, BAS, BG, Tzarigradsko shose, 72, Sofia

BlackSeaHazNet Series
Volume 3

BlackSeaHazNet Series
Volume 3

BlackSeaHazNet Conclusion Workshop

16-20 December, 2013, Sofia, Bulgaria

BlackSeaHazNet FP7 IRSES Project 246874
”Complex Research of Earthquake’s Forecasting Possibilities,
Seismicity and Climate Change Correlations”

BlackSeaHazNet Серия
Книга 3

BlackSeaHazNet Заключителен семинар

16-20 декември, 2013, София, България

BlackSeaHazNet FP7 IRSES проект 246874
”Комплексно изследване на възможностите за
прогнозиране на земетресения и корелациите между
измененията на климата и сеизмичността”

The information provided in this book is the sole responsibility of the authors and does not reflect the Community's opinion, and Community is not responsible for any use that might be made of data appearing in the proceedings.

BlackSeaHazNet, Project of 7-th Framework Programme of European Commission

© Institute for Nuclear Research and Nuclear Energy of Bulgarian Academy of Sciences

BlackSeaHazNet, FP7 IRSES MSCA Project, PIRSES-GA-2009-246874

Coordinator: INRNE, BAS, Sofia, Bulgaria

ISBN

Sofia, 2014

BlackSeaHazNet, Проект от Седма рамкова програма на Европейската комисия

© Институт за ядрени изследвания и ядрена енергетика Българска академия на науките

BlackSeaHazNet, Проект IRSES MSCA от Седма рамкова програма, PIRSES-GA-2009-246874

Координатор: ИЯИЯЕ, БАН, София, България

ISBN

София, 2014

CONTENTS

	<i>S. Cht. Mavrodiev</i>	5
Results of BlackSeaHazNet - FP7 IRSES project. Extended Executive Summary		
<i>G. Melikadze, M. Todadze, G. Kobzev, T. Jimsheladze, A.Sborshchikovi, N.Kapanadze</i>		22
Evaluation of water level observation and technology on the territory of Georgia		
<i>G.Melikadze, G.Kobzev, T.Jimsheladze, A.Sborshchikovi</i>		27
Water level's variation in boreholes of Georgia (2011-2013)		
<i>A.Sborshchikovi, G.Kobzev, S.Cht.Mavrodiev, G.Melikadze</i>		39
Boreholes water level and earthquake's prediction (2011-2013)		
<i>Hrachya Petrosyan</i>		48
Change in the intensity of manifestation precursors as it approaches the time of the earthquake		
<i>Y. Chapanov</i>		54
Solar, geomagnetic, climate and seismic impulse variations		
<i>Y. Chapanov</i>		60
Seismic and volcanic variations driven by solar and geomagnetic cycles		
<i>Y.Chapanov, C. Ron, J. Vondrák</i>		66
Millennial cycles of mean sea level and Earth rotation excited by total solar irradiance variations		
<i>I. Logvinov, B.Srebrov, L. Rakhlin, S. Kovachikova</i>		70
Geoelectrical studies at the geophysical observatories of Bulgaria		
<i>M.Adibekyan, A.Gevorgyan, A. Khangaldyan</i>		80
Method of standard deviation for analysis of hydrodynamic and geomagnetic variations for estimation of regional seismic situation		
<i>Y. Bogdanov, V. Pavlovych, S. Prokopenko, D. Gergova, B. Vachev</i>		92
Electromagnetic Sounding of Thracian Tumuli in the sboryanovo national reserve, near the town of Iserpoh , Razgrad District, North east Bulgaria		
<i>A.Gevorgyan, A. Khangaldyan, S.Mavrodiev, M. Adibekyan, G.Melikadze, A.Sborshchikovi, G.Kobzev, T.Jimsheladze</i>		100
Method of standard deviation for analysis of Caucasus borehole water level data		
<i>N. Zhukova, T. Matcharashvili, T. Chelidze</i>		107
Analysis of temporal variation of earthquake occurrences in Caucasus from 1960 to 2011		
<i>I. Kachalin, O. Liashchuk, S. Šebela, J. Vaupotic,</i>		116
Underground geophysical observations in caves		
<i>G. Kikuashvili, Lazo Pekevski, Schteriumir Mavrodiev</i>		122
Shumann Resonance monitoring device		
<i>S. Mihajlovic, M. Cukavac</i>		129
Measurement of geomagnetic field in Serbia at geomagnetic observatories Grocka and in seismically active areas in Serbia		
<i>E. Alparslan, C. Seyis</i>		137
Validation of satellite monitored earthquake precursor anomalies by geochemical monitoring		

	<i>L. Ries</i>	143
Data Acquisition – Dafit a new toolset for time effective and traceable data preparation and data validation of time series data		
	<i>L. Dobrodnyak, I. Logvinov, E.Nakalov, L. Rakhlin, S. Timoshin</i>	148
Application of magneto-telluric stations (Geomag -02) in geoelectric studies on the territory of Bulgaria		
	<i>G.Melikadze, M. Todadze, N. Kapanadze, Olga Körting, Birgit Müller, J. Vaupotic P. Andreeva, Hr. Kiselinov</i>	152
Study of interaction between seismicity and gas emission on the territory of Georgia		
	<i>N. Kapanadze, M. Bezek, J. Vaupotic, G. Melikadze</i>	158
Radon and thoron levels in air at selected places in Georgia		
	<i>G. Melikadze, N. Kapanadze, M. Todadze, Ch Tsabaris, E.Androulakaki, F. Pappa, G. Eleftheriou, D. Patiris, M. Schubert, K. Knoeller, R. Stollberg, U. Mallast</i>	162
Using environment tracers for investigation of Black sea pollution		
	<i>N. Dobrev, P. Ivanov, K. Kostov, O. Dimitrov, M. Krastanov, V. Nikolov, B. Berov</i>	169
Identification of types of exogenic geological hazards along Bulgarian Black Sea coast		
	<i>N.A. Kilifarska, V.G. Bakhmutov, G. V. Melnyk</i>	176
Global warming or climate variability – the role of geomagnetic field and lower stratospheric ozone		
	<i>N.A. Kilifarska, V.G. Bakhmutov, G. V. Melnyk, T. Mozgova</i>	187
Geomagnetic field–Ozone influence on the surface air temperature in epicentral regions of Balkan’s earthquakes		



Results of BlackSaHazNet - FP7 IRSES project

Extended Executive Summary

Strachimir Cht. Mavrodiev

With the help of
Lazo Pekevski, Macedonia
Georgi Kikuashvili, Georgia

The aims of the project are in the project's title: **Complex Research of Earthquake's Forecasting Possibilities, Seismicity and Climate Change Correlations**

The main results achieved are as follows:

1. Creating a group which is able to fulfill a Complex Research of Earthquake's Forecasting Possibilities. The result is imminent forecasting for seismic regional activity on the basis of the geomagnetic monitoring in the framework of special created data- acquisition system for archiving, visualization and analysis.

2. The data-acquisition system (<http://theo.inrne.bas.bg/~mavrodi>), applied for **BlackSeaHazNet** every day geomagnetic and earthquake monitoring use:

- the Balkan Intermagnet (<http://www.intermagnet.org/>) geomagnetic stations minute data,
- software for calculation of the daily and minute Earth tide behavior (Dennis Milbert, NASA, <http://home.comcast.net/~dmilbert/softs/solid.htm>),
- the Earth tide extremes (daily average maximum, minimum and inflexed point) as trigger of earthquakes,
- the data for World A- indices (<http://www.swpc.noaa.gov/alerts/a-index.html>),

The simple mathematics for calculation of the Precursor signal and software for illustration the reliability of forecasting and its statistic estimation:

- a. The variables X_m, Y_m, Z_m are the component of minute averaged values of Geomagnetic vector or its variations, $m=1440$.
- b. The variables dX_h, dY_h, dZ_h are standard deviation of X_m, Y_m, Z_m , calculated for 1 hour ($h=1, \dots, 24$):

$$X_h = 1/60 \sum_{m=1}^{60} X_m, \text{ where } h=1, \dots, 24,$$

$$dX_h = \sqrt{1/60 \sum_{m=1}^{60} \left(1 - \frac{X_m}{X_h}\right)^2}.$$

- c. And geomagnetic signal

$$GeomHourSig_h = \sqrt{\frac{dX_h^2 + dY_h^2 + dZ_h^2}{X_h^2 + Y_h^2 + Z_h^2}}$$

- d. The A indices are the Low, Medium, High a- indices calculated by NOAA, Space weather prediction center: <http://www.swpc.noaa.gov/alerts/a-index.html>.
- e. The variable $GmSig_{day}$ is diurnal mean value of $GmHourSig_h$:

$$GeomSig_{day} = 1/24 \sum_{m=1}^{24} GeomHourSig_h$$

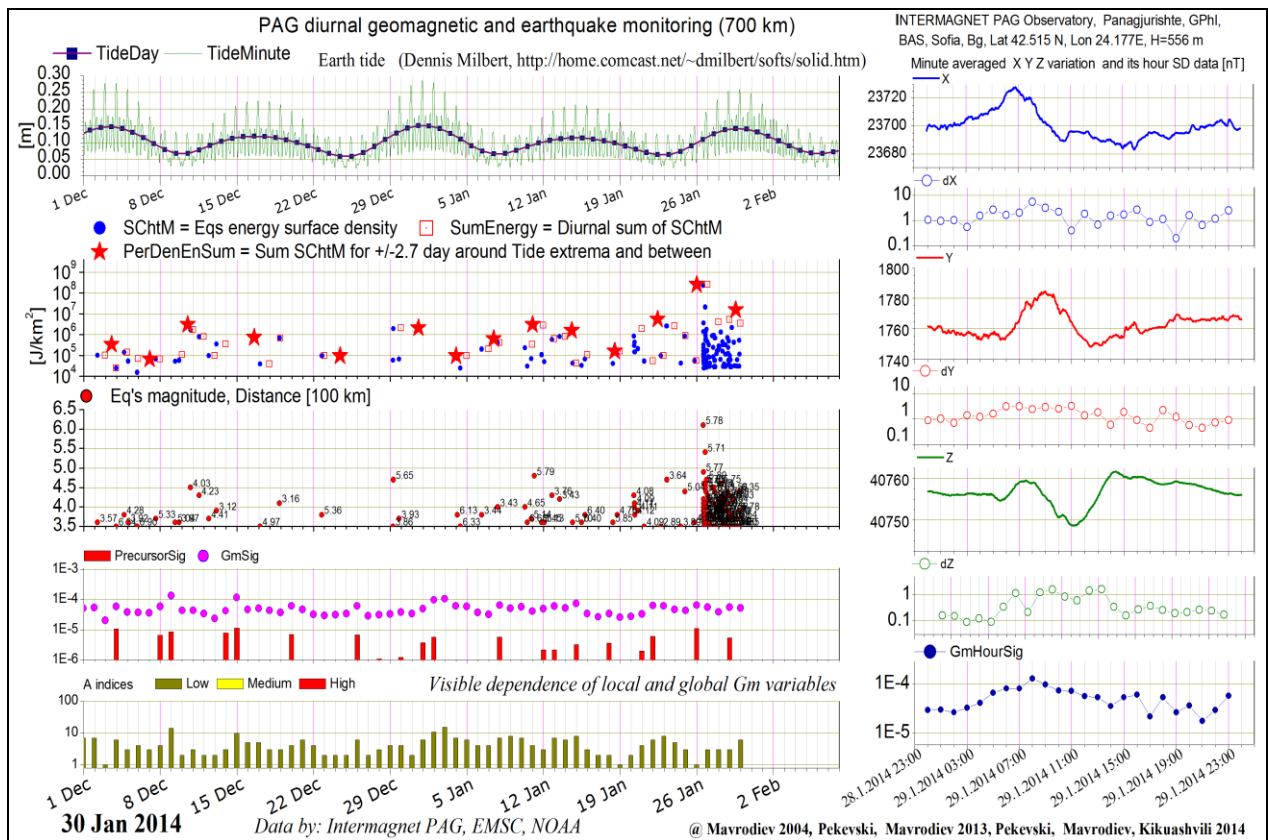
and

$$PrecursorSig_{day} = 2 \frac{GeomSig_{day} - GeomSig_{yesterday}}{Amg_{day} + Amg_{yesterday}}$$

- f. The indices of Eq's magnitude value are the distance in hundred km from the monitoring point.
- g. The variable SChTM is the eq's energy surface density in the monitoring point [J/km^2] :

$$SChTM = \frac{\exp(1.4M + 4.8)}{(40 + Depth^2 + Distance^2)}$$

- h. The variable PerDenEqSum is the sum of energy density of all eq's, occurred in the time period +/- 2.7 days before and next of the tide extreme.
- i. For seconds and more samples per second the generalization has to calculate geomagnetic components for every minute and correspondingly the $GmSig_{day}$ has to be the mean value for 1440 minutes.



For boreholes water level data one do not use the A indices data, the $GmSig$ has to be changed with Water level signal $WISig$ and Precursor signal is only a derivative:

$$PrecursorSig_{day} = WISig_{day} - WISig_{yesterday}$$

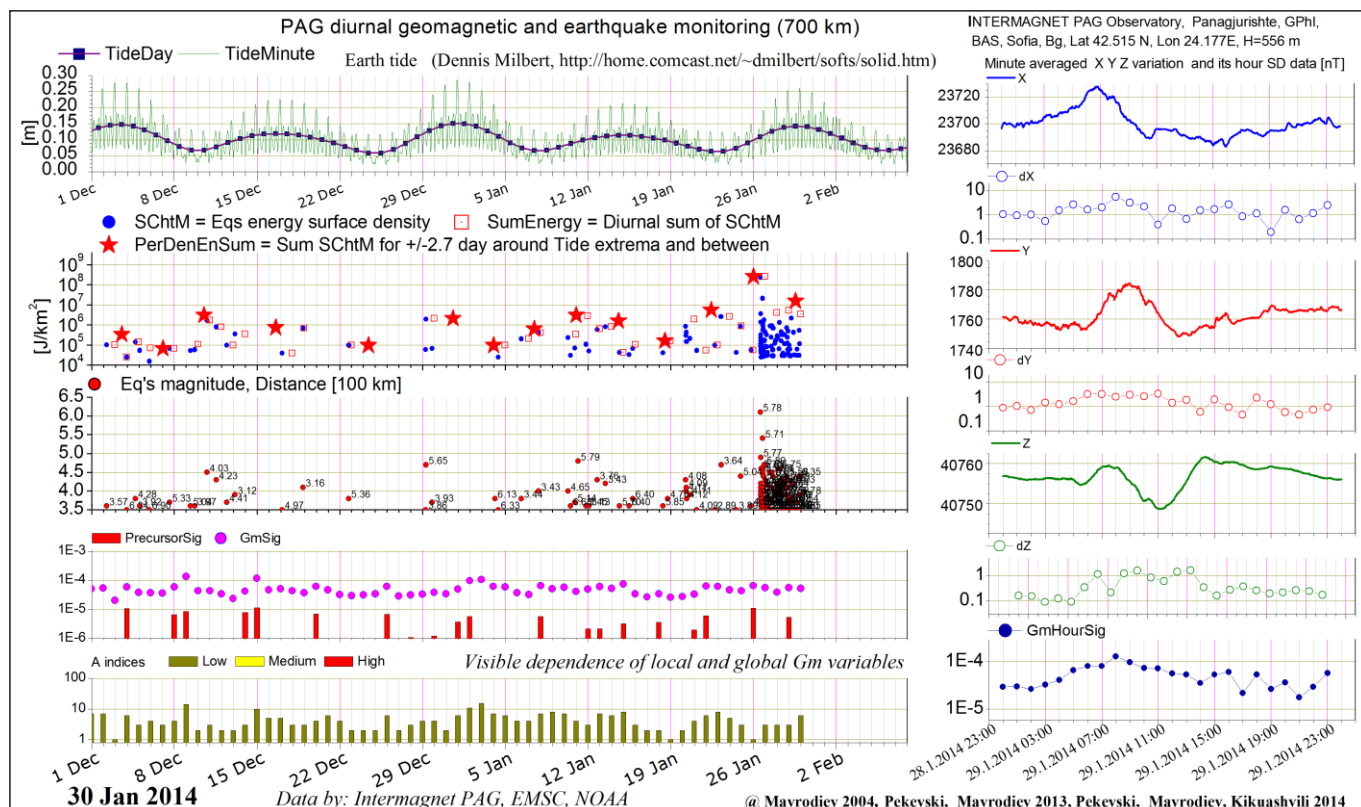
For statistic estimation of the reliability we calculate the variable day difference

$$\text{DayDiff} = \text{EqTime} - \text{TideExtremTime}$$

and calculate the distribution for those earthquakes with biggest values of SChtM.

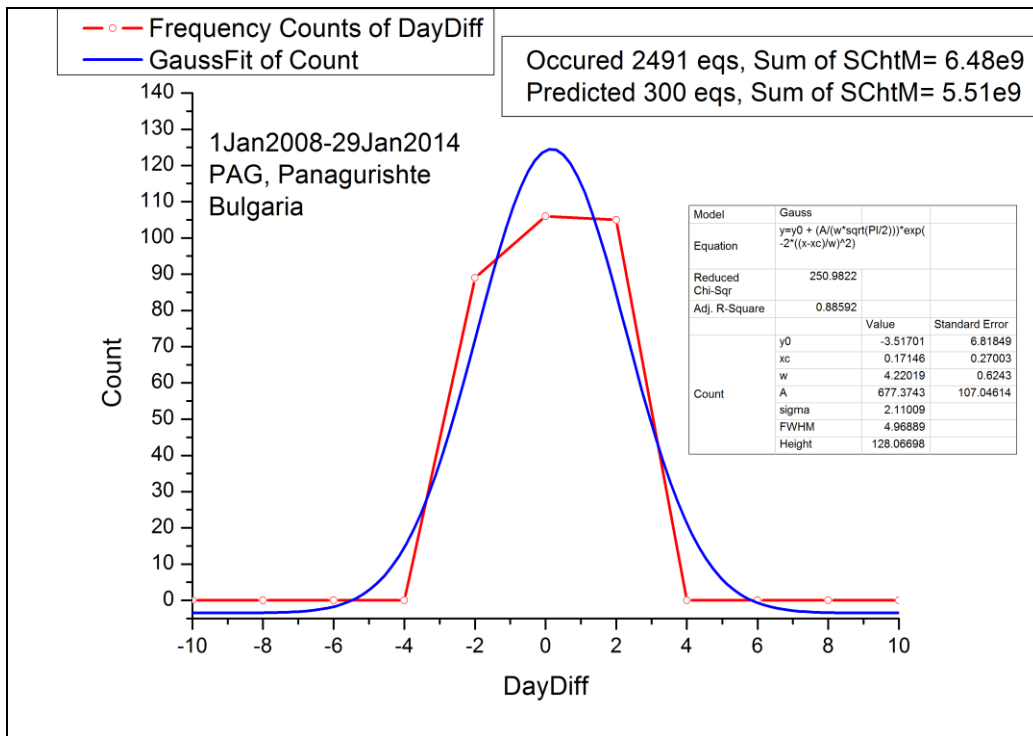
3. The reliability of regional imminent seismic condition on the basis of Geomagnetic quake approach were tested statistically using the geomagnetic data of monitoring stations:

- Intermagnet PAG (Panagurichte, Bulgaria),

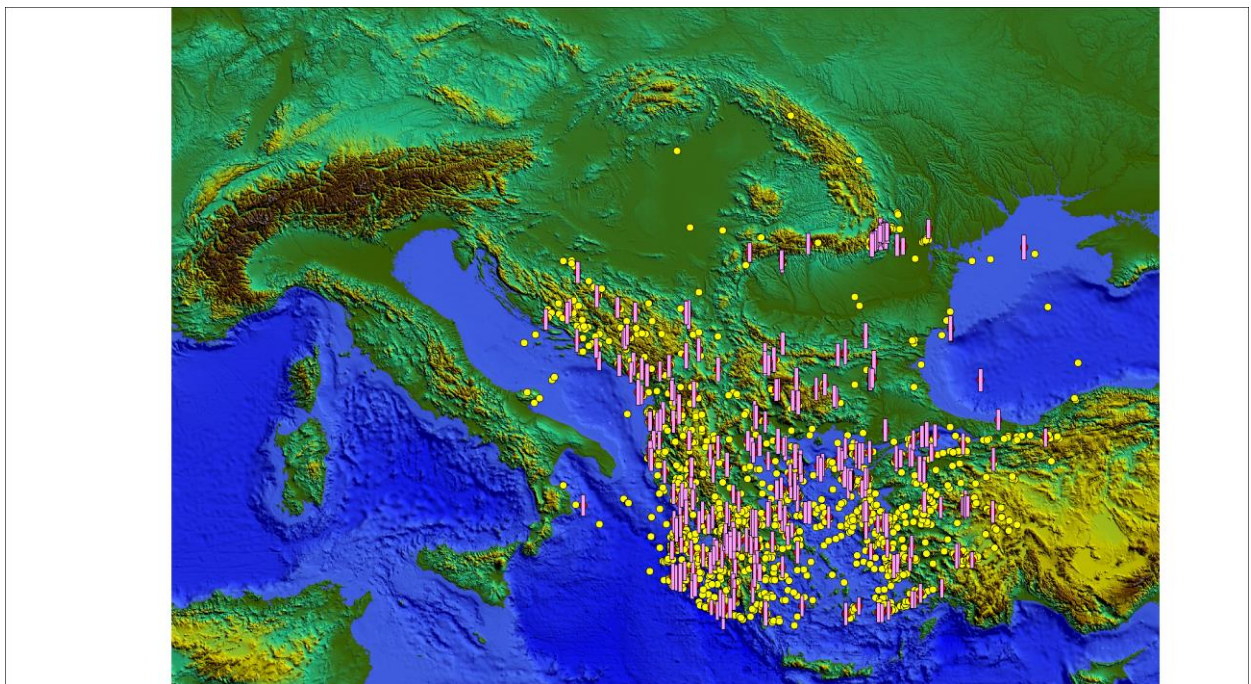


For the period from January 1, 2008 to 29 January 2014 were calculated the values of day difference between the times of predicted (by definition we suppose that predicted earthquakes are those which have maximal energy density in the monitoring point and occurred in +/- 2.7 days around tide's extreme) and occurred earthquakes.

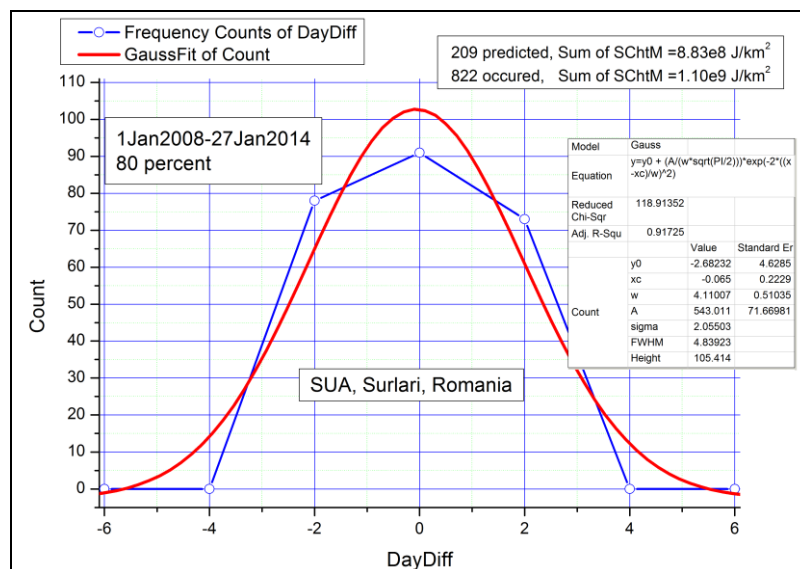
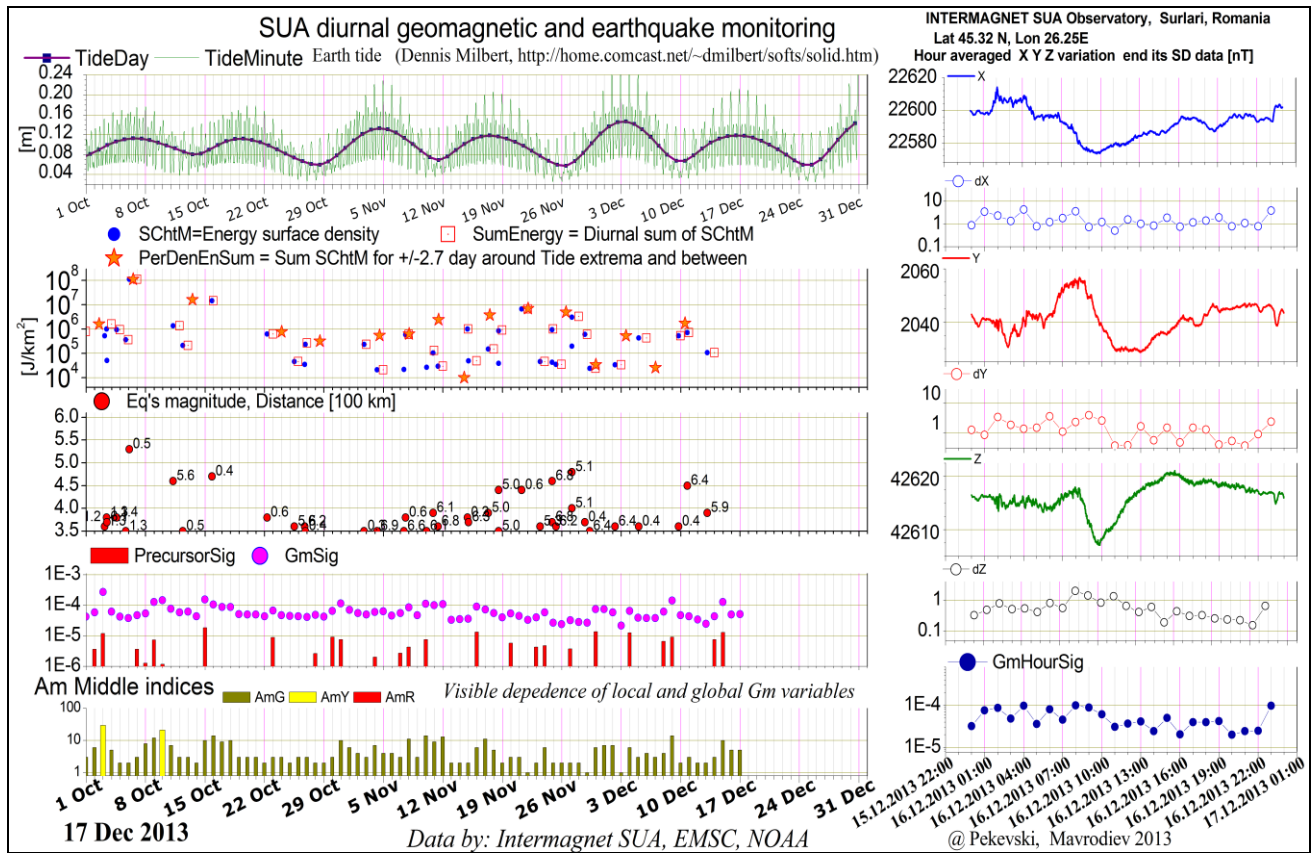
As one can see from the next figure the distribution is near to the Gauss one with $hi^2 = 0.89$. The relation between sum of energies of occurred and predicted earthquakes $r = 6.48/5.51$. **This facts can be interpreted as statistical prove that the geomagnetic quake approach is reliable for estimation of imminent regional seismic conditions.**



For illustration the map of predicted (column/bar with values logarithm of variable SChtM) and occurred (circles) earthquakes is presented:

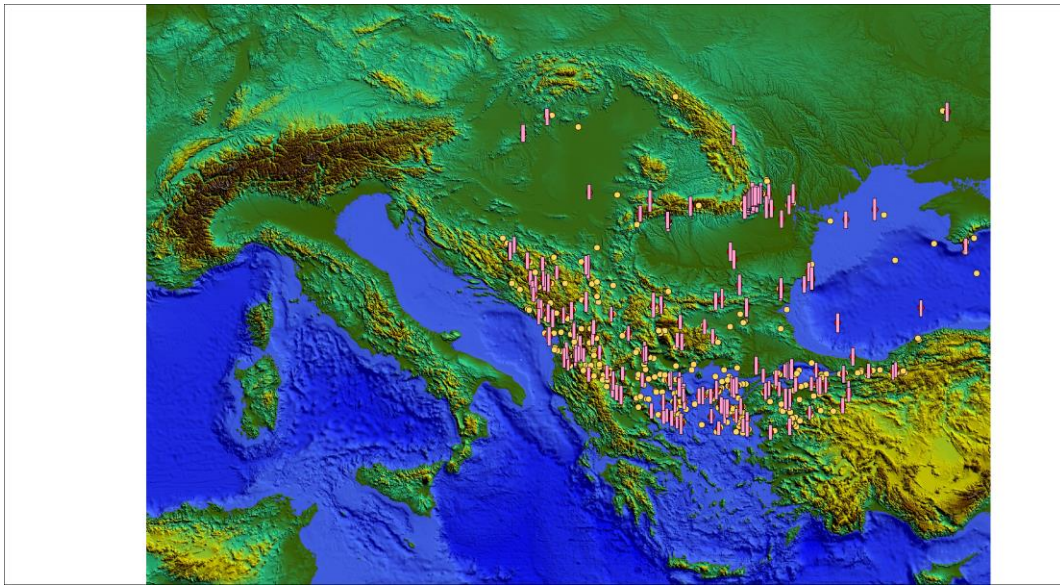


Intermagnet SUA (Surlari, Romania):

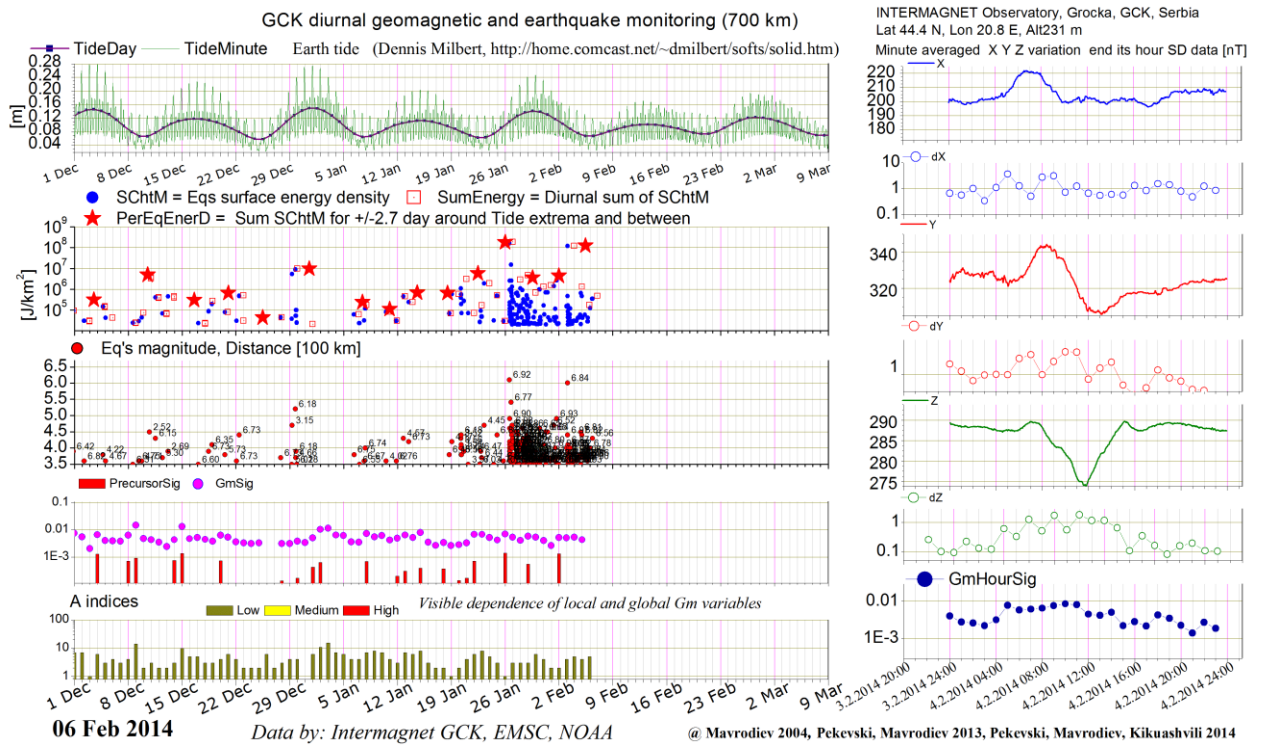


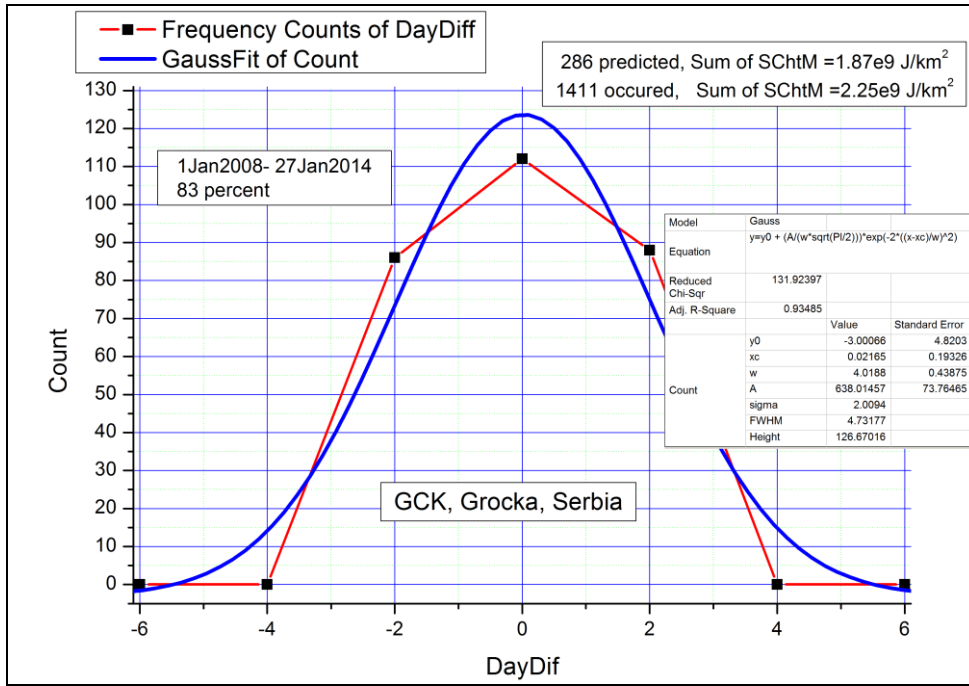
As one can see from the above figure the distribution is near to the Gauss one with $\chi^2 = 0.92$. The relation between sum of energies of occurred and predicted earthquakes

$$r = 11.0/8.83$$



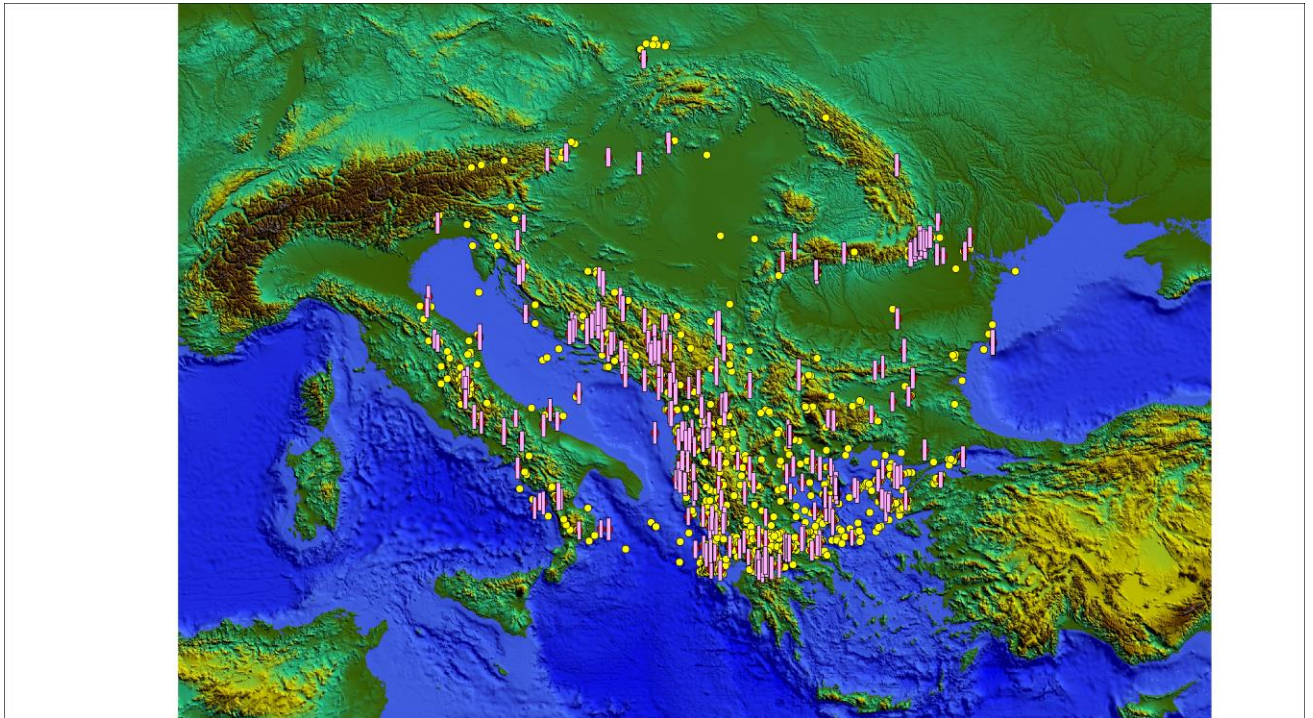
- Intermagnet GCK (Grocka, Serbia)



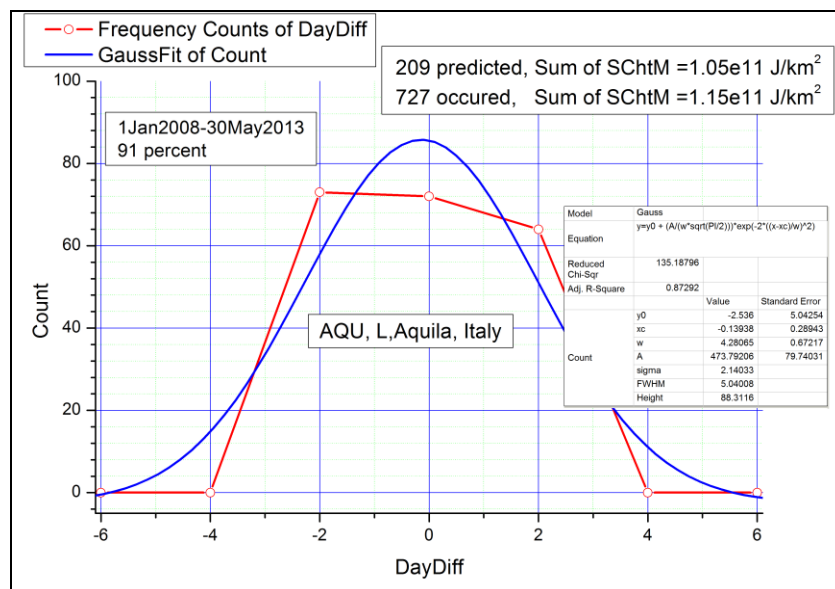
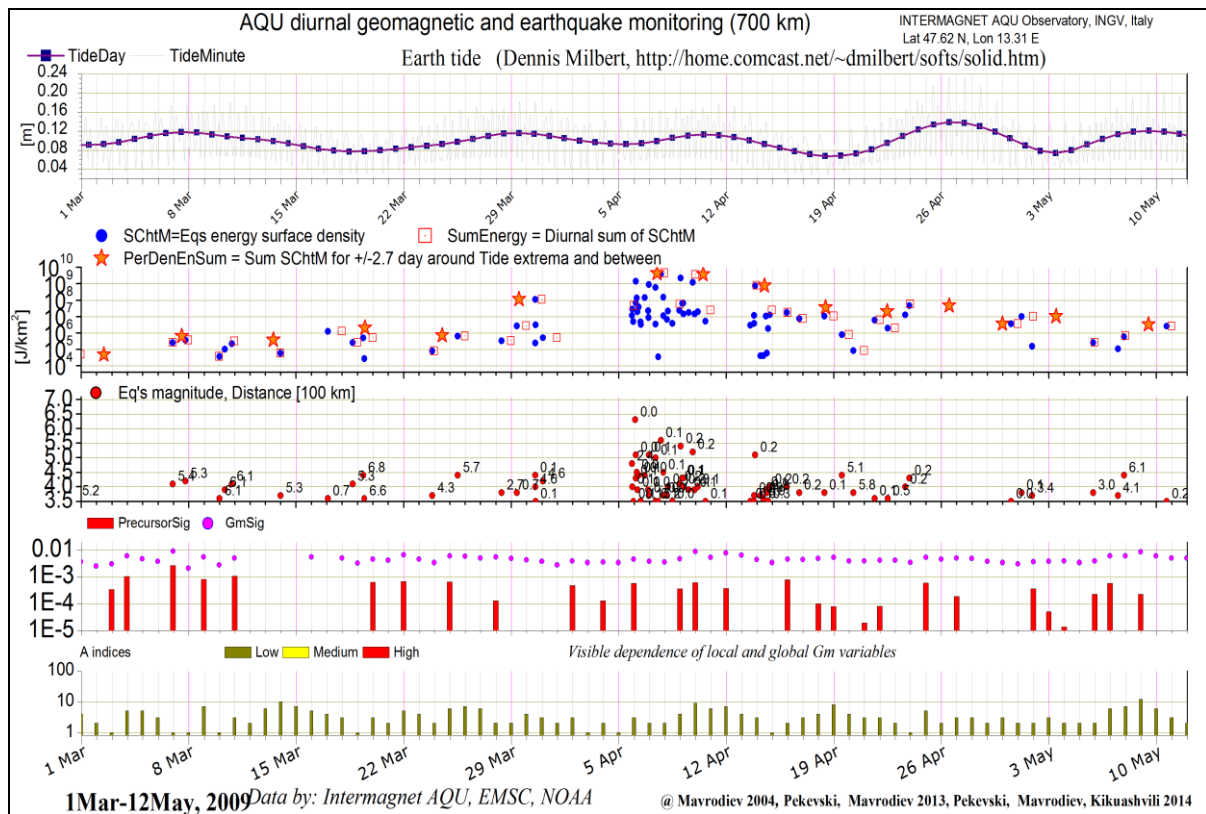


As one can see from the above figure the distribution is near to the Gauss one with $\chi^2 = 0.93$. The relation between sum of energies of occurred and predicted earthquakes

$$r = 2.25/1.87$$

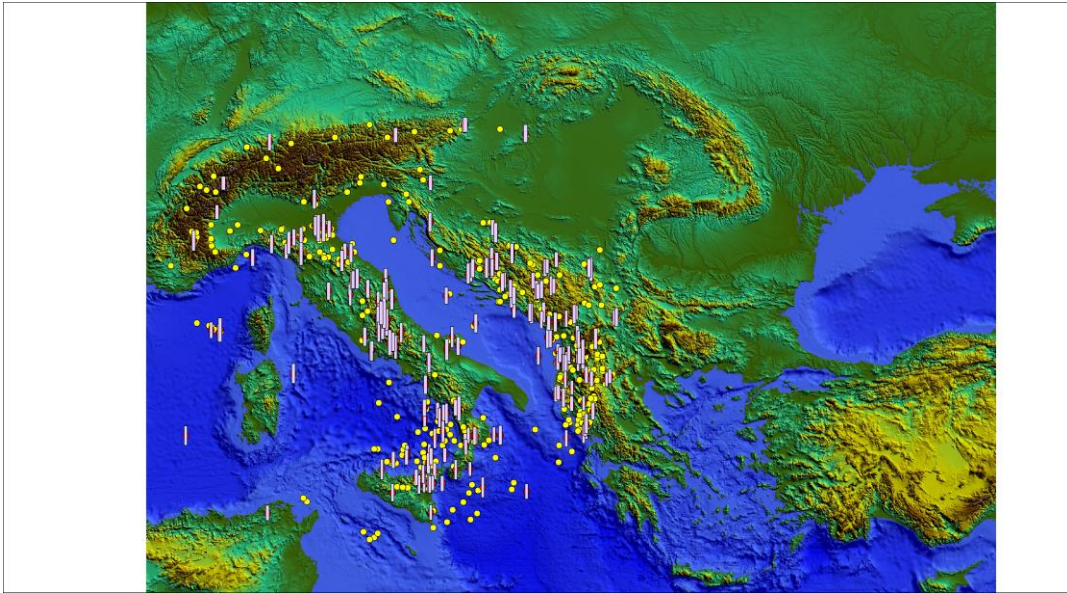


- Intermagnet L'Aquila (AQU, Italy)

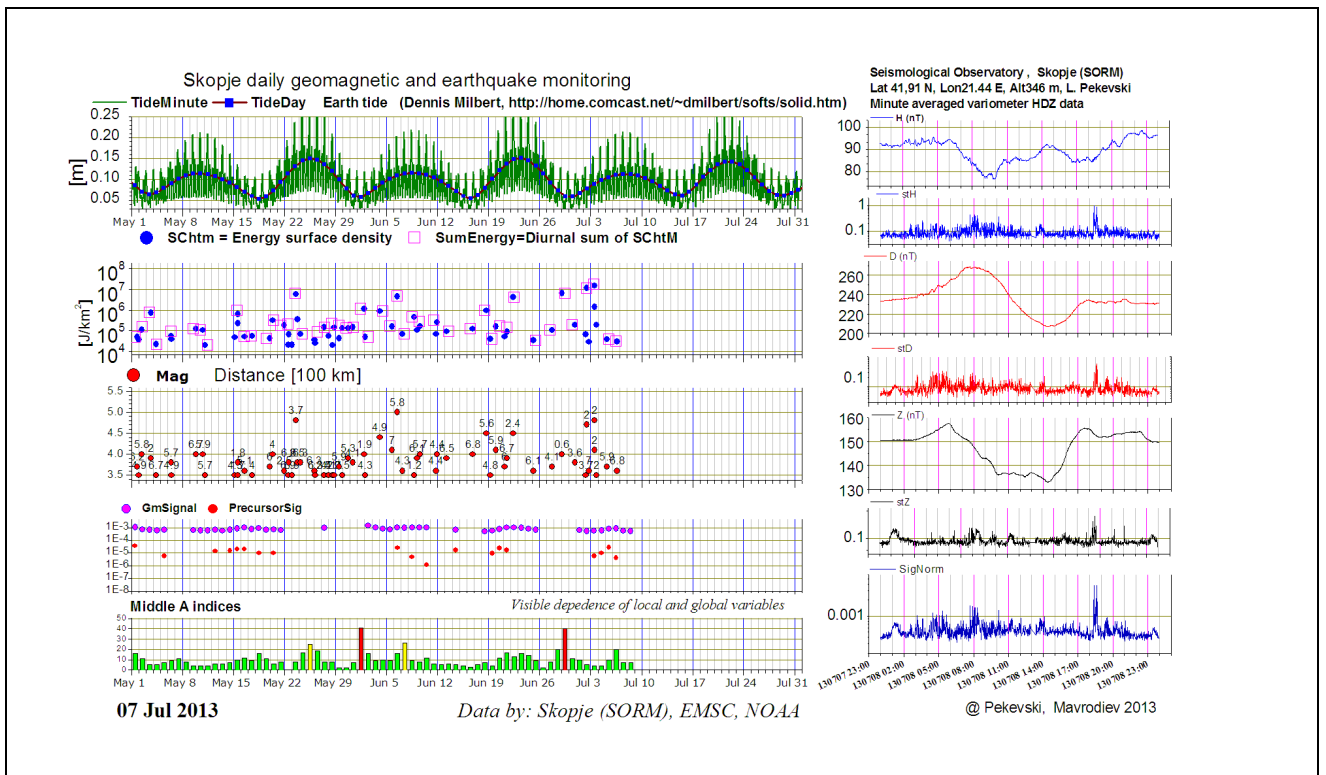


As one can see from the above figure the distribution is near to the Gauss one with $\chi^2 = 0.87$. The relation between sum of energies of occurred and predicted earthquakes

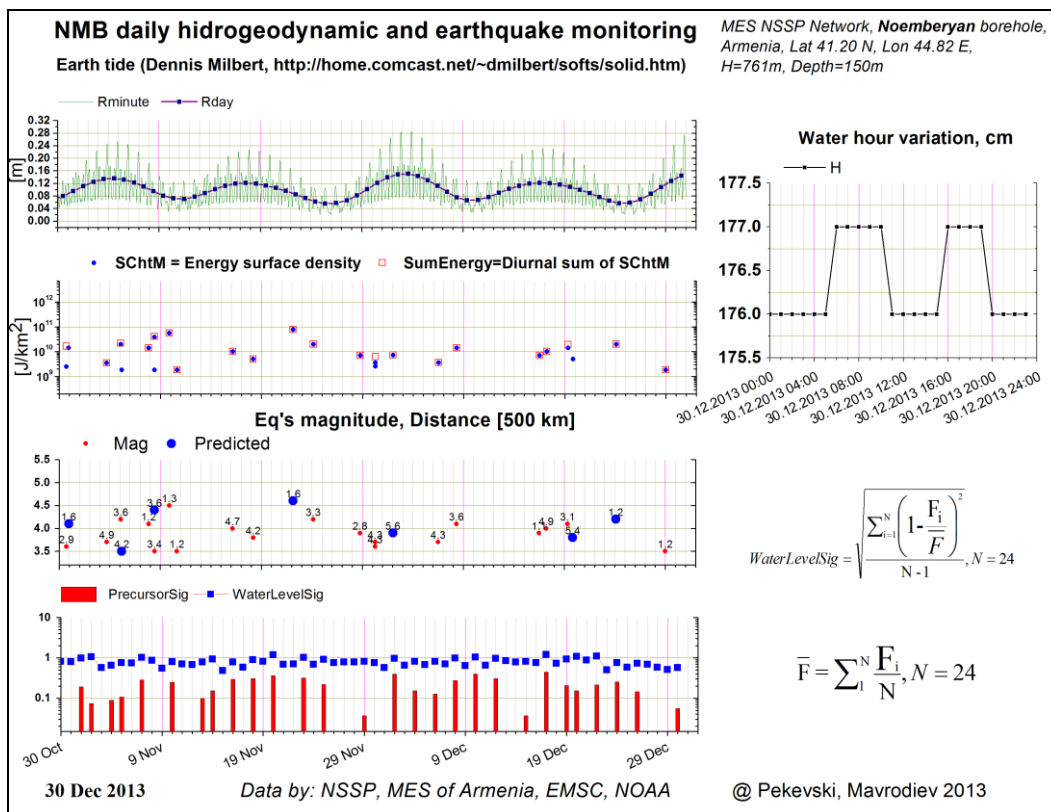
$$r = 1.15/1.05$$



- BlackSeaHazNet 1second station, Skopje, Macedonia,

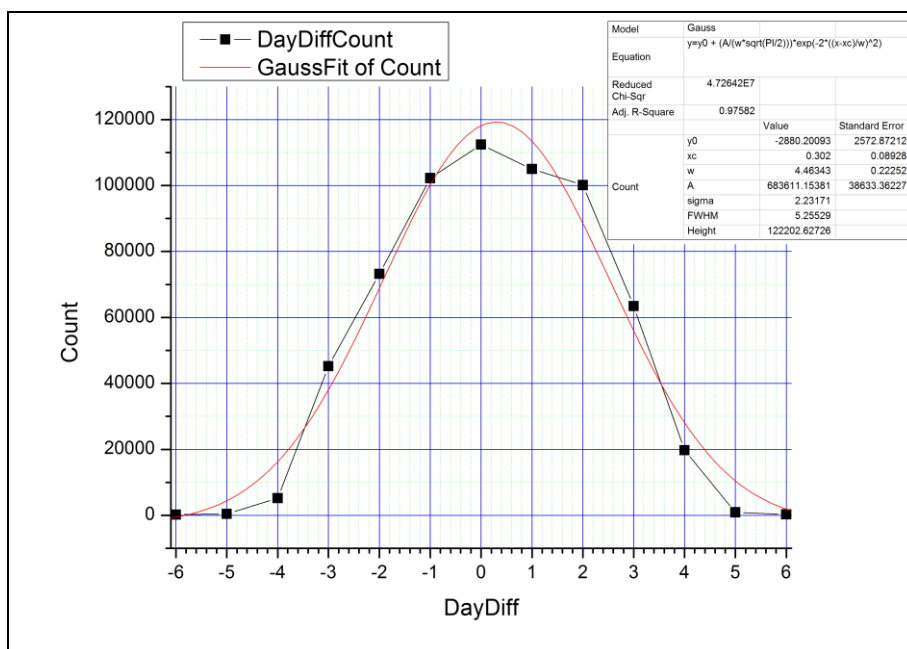


4. Imminent regional confirmation of forecasting based on the geomagnetic quake (positive jump of PrecursorSig_{day}) approach:
 - Dusheti, Georgia flux gate second magnetometer - Mw 7.1, depth 7.2 km, 2011, 23 Oct, 36.63N, 43.49E, Van, Turkey earthquake;
 - Skopje, Macedonia (second) and Panagurichte (minute) flux gate magnetometers – Mw 5.6, Depth 9.4 km, 42.66 N, 23.01 E, 00.00 hour, 22 May, 2012;
 - Grocka, Serbia and Panagurichte (minute) flux gate magnetometers – Mw 6.1, Depth 18km, 26 Jan 2014, 13:55, 38.19 N, 20.41 E; Mw 6.0, depth 2km, 3 Feb, 2014, 03:08, 38,25 N, 20.32 E, Mw5.6, Depth 9.4km.
5. Big world earthquakes and Intermagnet data. During our investigation of relation between regional geomagnetic and seismic activity in areas of interest, close to particular Intermagnet geomagnetic observatories (GMO), it was found that in case of strong earthquake occurred on epicenter distances less than 600 - 1000km from geomagnetic observatory, clear precursor signal was evident.
6. The acquisition system for archiving, visualization and analysis of the water level variations in boreholes as earthquake precursor was created for Georgia and Armenia data (<http://theo.inrne.bas.bg/~mavrodi> , <http://dSPACE.nplg.gov.ge/handle/1234/9101>):

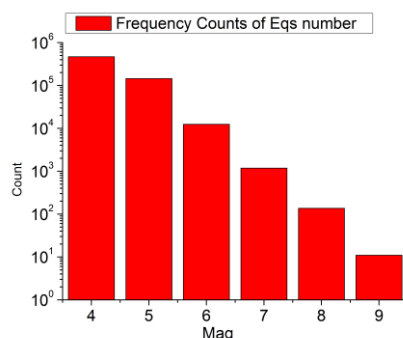


7. Why the forecasting's are reliable- the Moon- Sun tides waves of Earth surface as trigger of earthquakes.

The time differences **DayDiff** between the time of all 628873 occurred earthquakes with $M \geq 3.5$ from 1981 and the local tide extremes time, were calculated. The next figure illustrates that the time extremes are the earthquakes trigger with $\chi^2 = 0.95$



The value at DayDiff = 2 can be interpreted as a count of aftershocks. From the next figure one can see the number of earthquakes vs magnitude:



8. Another geophysical network was tested in Ukraine and Antarctica: seismic, meteorological, electromagnetic (VLF), geomagnetic, infrasound, radon monitoring. Estimated probability for earthquakes with $M > 5$ was 0.8, Vranča, Romania and earthquakes with $M > 6.5$ was 0.6 for the Scotia Sea region, Antarctica.

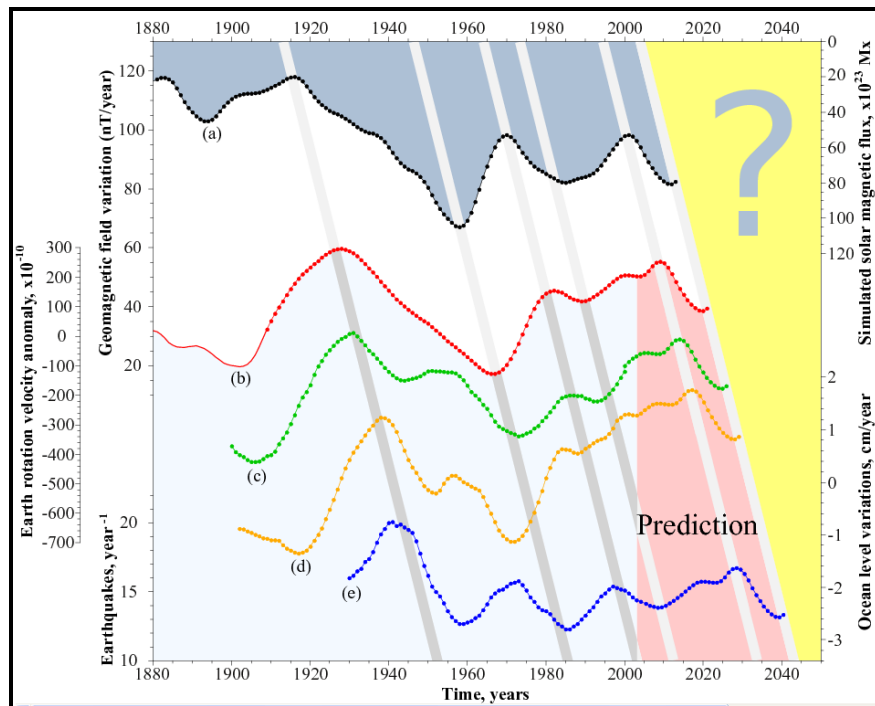
9. The reality of Climate Seismicity correlation and axion- geo -nuclear -reactors hypothesis for Climate changes reasons
 In the Rusov's talk in Ohrid, Macedonia 2011 workshop was presented the hypothesis and some experimentally argumentations that Solar processes are the host power pacemaker of Earth climate behavior and its seismicity.

The causality link processes are as follows:

- the burn of one Sun axion from two gamma quanta in the field of iron nuclei (the strait Primakoff effect);
- the burn of two gamma quanta (the inverse Primakoff effect) in the field of iron nuclei in the Earth's nuclei and the increasing of temperature, which leads to the activation of geo nuclear set

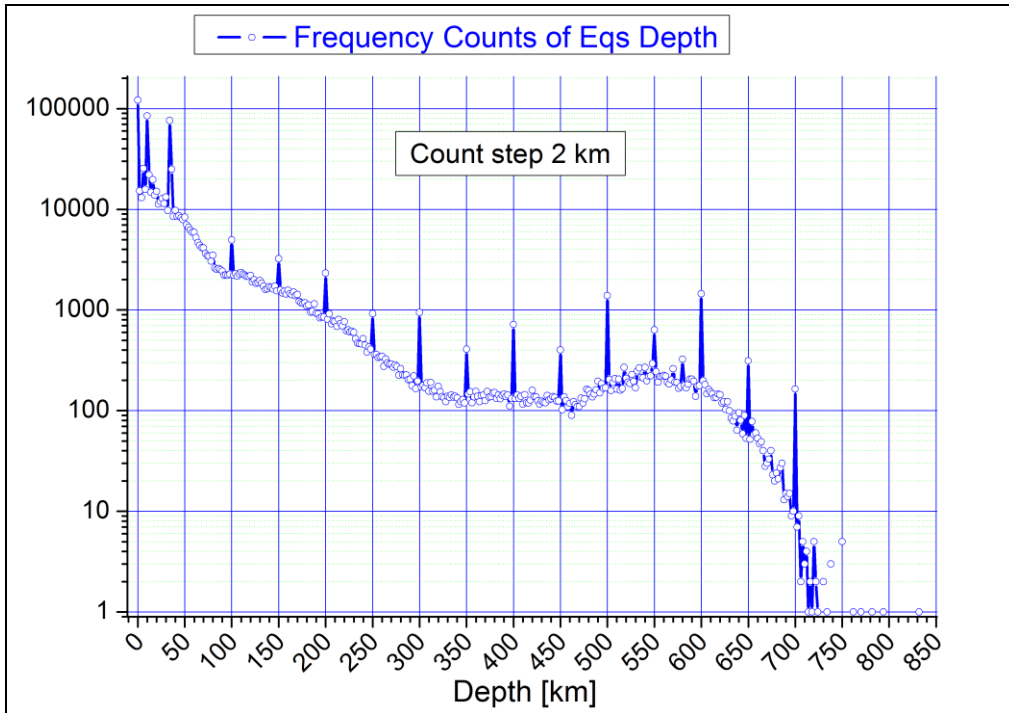
of reactors (Feoktistov type ^{238}U , ^{232}Th reactors with fast neutrons) in the canyons on the nuclei's surface;

- as a result there is more heat, more intensive lifting of magma, more activity in the oceans rift zones, more intensive Wegener's plates movement, and, consequently, more seismic and volcanic activity as well as change of climate behavior.
- as well as the discovery of neutrino was based on the conservation laws, we can hope that some estimations for the axions existence, its mass, the spatial distribution and characteristics of geo – reactors will be achieved after creation of the more accurate Earth's heat balance models and the experimental measuring of neutrino's type and energy distribution.

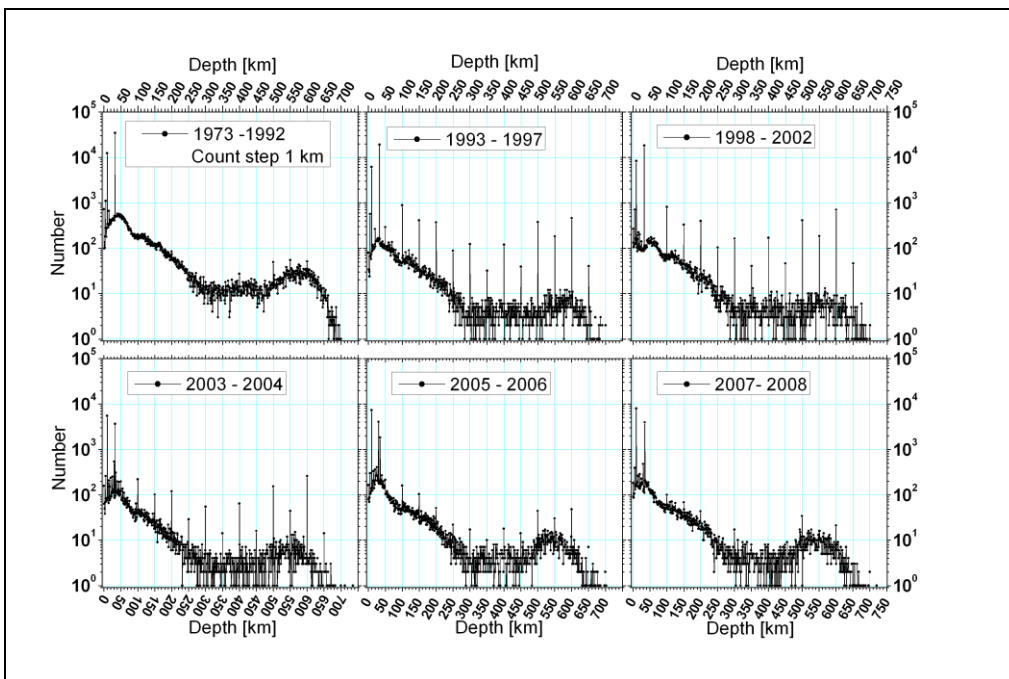


Time evolution: (a) of the variations of magnetic flux in the bottom of the Sun convective zone (tachocline zone); (b) of the geomagnetic field secular variations (Y -component, nT/year), the values of which are obtained at the Eskdalemuir Observatory (England), where the variations ($\delta Y/\delta t$) are directly proportional to the westward drift of magnetic features; (c) of the variation of the Earth rotation velocity; (d) of the variations of the average global ocean level (PDO+AMO, cm/year); (e) the number of large earthquakes (with magnitude $M > 7.0$). All curves are smoothed by sliding intervals in 5 and 11 years. The pink area is the prediction region. Note: formation of the second peaks on curves (c) – (e) is mainly predetermined by nuclear tests in 1945–1990.

Some possible evidence for existing of geo- reactors set can be illustrated from the next figure, which presents the distribution of earthquakes number with depth (citata na saita):

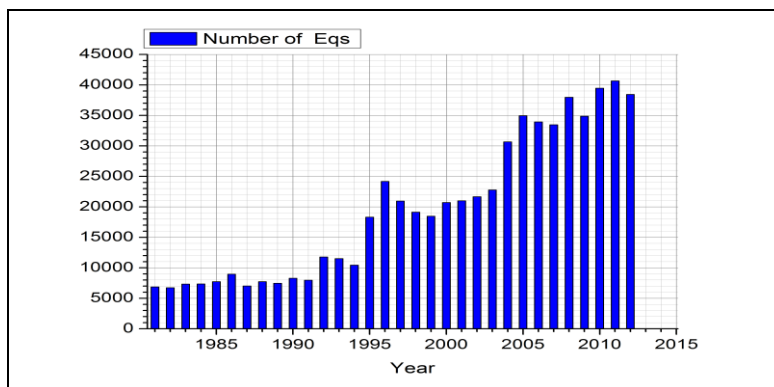
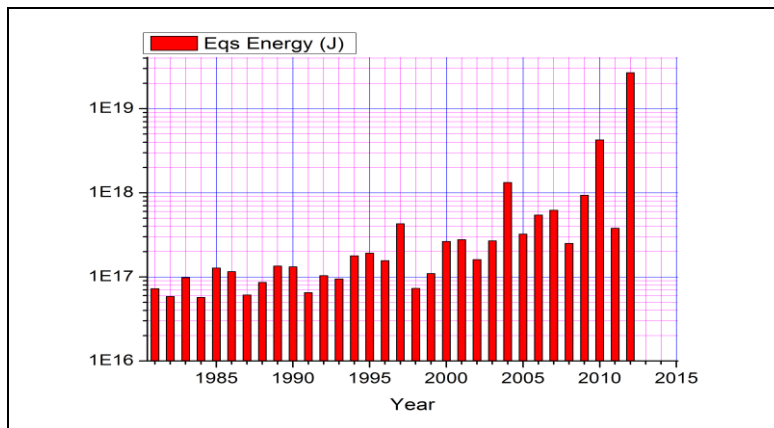


The year's dynamics is illustrated in the next figure:



Such dynamics can be explained in the framework of our Axion- Geo- reactors hypothesis.

Also in next valance model of climate behavior one have to include the influence of the earthquakes heat, the friction between atmosphere and Earth surface in a case of stronger earthquakes.. See for example the next two figures which gives the year's dynamics of World earthquakes with $M \geq 3.5$ and their energy:



10. Geo-electromagnetic measurements: for the first time in Bulgaria territory were measured in the same point the Earth electric currents and geomagnetic field component using the station GEOMAG-02 and magnetometers GEOMAG-02M: Main technical characteristics of MTS GEOMAG-02 are: measuring range of full MF \pm 65000nT; measuring range of MF variations \pm 3200nT; resolution of MF variation registration to FLASH-card 0.01nT; temperature drift <0.2nT/ $^{\circ}$ C; tolerance of component non-orthogonally of MF sensor <30ang. min; automatic compensation range of contact MF in each component \pm 65000nT; EF variation measuring range \pm 200mV; \pm 2000mV; resolution of EF variation registration to FLASH-card 1 μ V; measuring channel frequency band DC - 1 (3, 10)Hz; measuring channel information sampling numbers 10-15 in sec; data averaging during recording to FLASH-card 0.1...60s; capacity of FLASH-card «CompactFlash» (FAT-16, FAT-32) 64MB...64GB; operating temperature range 10 $^{\circ}$ -40 $^{\circ}$; connecting cable length between MF sensor and electronic unit up to 50m; power consumption 12V; 0.1A.

11. Radon mapping was caring out on the territory Georgia and Slovenia for fixed active fault system and gas concentration monitoring was starting, including in the cave system. Bat there was not enough long time series for receiving the estimation of Radon concentration variations as regional earthquake's precursor.

12. Meteorology and seismicity correlations: Investigation of the possible correlation between meteorology variables and regional seismic activity was started.

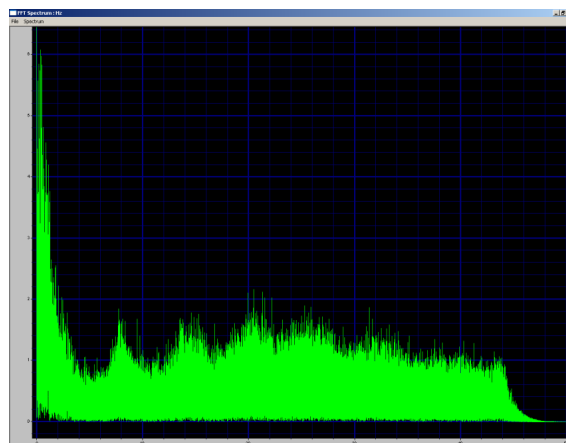
13. Ozone and temperature spatial distributions and its possible correlations with regional seismic activity: There is a good correspondence between geomagnetic field, near surface air temperature and pressure spatial distributions in Northern hemisphere during XX century. The alteration of the near

tropopause temperature (by O₃ variations at these levels) changes the amount of the water vapor in the driest part of the upper troposphere/lower stratosphere. Application of non-linear statistical methods for analysis of climatic and magnetic field data reveals the important role of energetic particles and lower stratospheric ozone in climate variations.

14. Electromagnetic scanning: The research of deep Earth's crust structure and upper mantle study using the inverse problem analysis of the Earth electromagnetic radiation in radio diapason, measured with Astrogon device was performed in Greece and Bulgaria in different profiles. The device is a passive sensor type sensitive to the three components of the magnetic field within a wide range of frequencies (5 – 100 kHz). The comparison with geological knowledge for the Crust in the profiles and the inverse problem results give a hope for perspectives of such kind of studies and that the method has to be included in the permanent regional monitoring. Really, during the project fulfilling, the method of the electromagnetic tomography of the Earth crust and upper mantle was developed, which gives the possibility to determine the location of the future earthquake hypocenters as the most stressed volume of the crust (or mantle). Moreover, the stationary EM measurements by the same device (or new one DS-4, designed and produced during the project fulfilling) show the existence of electromagnetic precursor in a wide frequency diapason, which coincide with that of low frequency signal in Intermagnet data. So the base of the project task solution – where and when – is grounded.

15. Other precursors research are as follows: The first is TM 71 extensometer monitoring, which is carried out to observe micro-displacements along fault movements (or landslide movements connected with active tectonics) in karst caves, fault scarps or in trenches where was found anomaly in velocities 3-4 months before regional strong earthquake. The second represents 2D displacements of static vertical pendulum in 25m deep karst shaft that are registered each 10 seconds. Changes in stress direction are detected. The studies were oriented towards the aim to connect the periods of micro-displacements with local and worldwide seismicity. The third represents the temperature monitoring of two sulphidic waters, which are situated near important regional faults. The fourth includes microbiological monitoring site on the fault planes in the Postojna Cave (Slovenia) to find the possible connection between microbial biomass and tectonic displacements.

16. Schuman resonance measurement device: it was developed and the construction design and software for measuring device were tested.



17. The website of the Project was created: <http://theo.inrne.bas.bg/~mavrodi/blackseahaznet/>

During the project many young scientists visited research centers of the Black Sea region, which facilitated their contacts with colleagues. They take part in project conferences, seminars, joint field

works and processing data in hosting countries. As a result, joint publications were published in journals and conference proceedings.

In the case of project prolongation until the end of 2014 in the frame of the remaining budget (around 34% or approximately 160.000 EUR) **the main expected results which are based on the project current achievements will be:**

A. Preparation of the project proposal for regional electromagnetic monitoring under, on and above Earth's surface and near space and as well meteorological data for creating of complex data acquisition system on the basis of which to start solving the inverse problem for regional imminent forecasting of time, coordinates, depth, magnitude and intensity of incoming earthquakes.

B. Creation of project proposal/s for Sun – Earth interaction balances models which describe its influences on climate change, seismicity, volcanism and continental plate's movement.

C. Development of long term collaboration for complex research in the framework of bilateral, regional and other European 2020 programs.

Acknowledgments:

We are very thankful to all participation of the project for active work and enthusiasm.

Without the everlasting efforts of coordinators Natalia Kilifarska, Christos Tsabaris, Jania Vaupotich, Stanka Sebel, Nikolai Dobrev, Katia Georgieva, Lazo Pekevski, Erham Alparslan, Hrachya Petrosyan, Tamaz Chelidze, George Melikadze, Vladymyr Bakhmutov, Vazira Martazinova, Oleksandr Lyashchuk, Vitalii Rusov and Volodymyr Pavlovych the results of Project could not be so good.

We have to note the special roll and big work of Person in charge of administrative, legal and financial aspects of the Project Boyko Vachev.

We would like to thank heartly the REA project officers heartly Dr. Oscar Perez-Punzano and Dr. Atantza Uriarte-Iraola, for their invaluable support in the process of negotiation and executing the project.

We would like also to express our sincere gratitude to the DG Institute for Nuclear Research and Nuclear Energy, BAS in the face of Directore Assoc. Prof. Dr. Dimitar Tonev and Vice Director Assoc. Prof. Dr. Lachezar Georgiev, for the encouragement and valusble assistance, as well as to Dr. Frank Marx, and in his face – to the European Commission, for the financial support for the BlackSeaHazNet project realisation.

EVALUATION OF WATER LEVEL OBSERVATION TECHNOLOGY ON THE TERRITORY OF GEORGIA

G. Melikadze, M. Todadze, G. Kobzev, T. Jimsheladze, A.Sborshchikovi, N.Kapanadze
M.Nodia Institute of Geophysics Iv. Javakhishvili Tbilisi State University

melikadze@gmail.com

Abstract

Approach to methodology of earthquake's forecasting developed and evaluated since 1980 up today. At first was developing a hydro-chemical network on the territory of all Caucasus. During observations a lot of anomalies were fixed, but because of the diversity of chemical water content it was impossible to conduct observations of the unified parameters for creating the complete picture of strains on the whole territory. This is the reason why we decided to conduct observations for those parameters which could fix tidal variations with deformation of 10^{-8} degree, what is compared with strains differences during earthquakes preparation period. Besides, it was possible to conduct unified observations. Water level in the deep boreholes was one of them. That way since 1985, the network of 10 boreholes of different depth (from 250 up to 3500 m) covers the whole territory of Georgia. Boreholes characterize all basic geo-plates and open waters of deep aquifer, actually they represent sensitive volumetric strainmeters, and react on the deformations about 10^{-7} - 10^{-8} , caused both by endogenous, and exogenous factors. A borehole was considered informative if it was fixing tidal variations and was included in the network. Special monitoring equipment is installed at boreholes which record several parameters, i.e. water level and micro-temperature, atmosphere pressure and surface temperature, tilt, magnetic field and others. Data is collected by datalogger XR5-SE-M. The data can be gathered in real time using the GSM net. Frequency of data collection is 1 minute. For the visualization and manipulation of data using special program which are developed at M. Nodia Institute of Geophysics.

1. Introduction

Georgia is a part of a big geodynamical active region. As a result of plate migration, strong compressive strains are being built in the crust. The energy released during sudden stress drop events may trigger earthquakes.

All over the world and in Georgia also, various anomalies (Hydro-dynamical, hydro-chemical, micro-temperature etc) are observed before earthquakes, besides in most cases, on enough distant places from epicentres. Therefore studying the geodynamical processes may help to forecast the natural catastrophes with reasonable probability.

1.1. HYDROCEMICAL MONITORING

Since 1979, the researches for the forecast of earthquakes promoted development of a hydro-chemical network of special regime regional observation. On the territory of Georgia hydro-chemical observations are carried out on the 23 boreholes (Fig. 1).

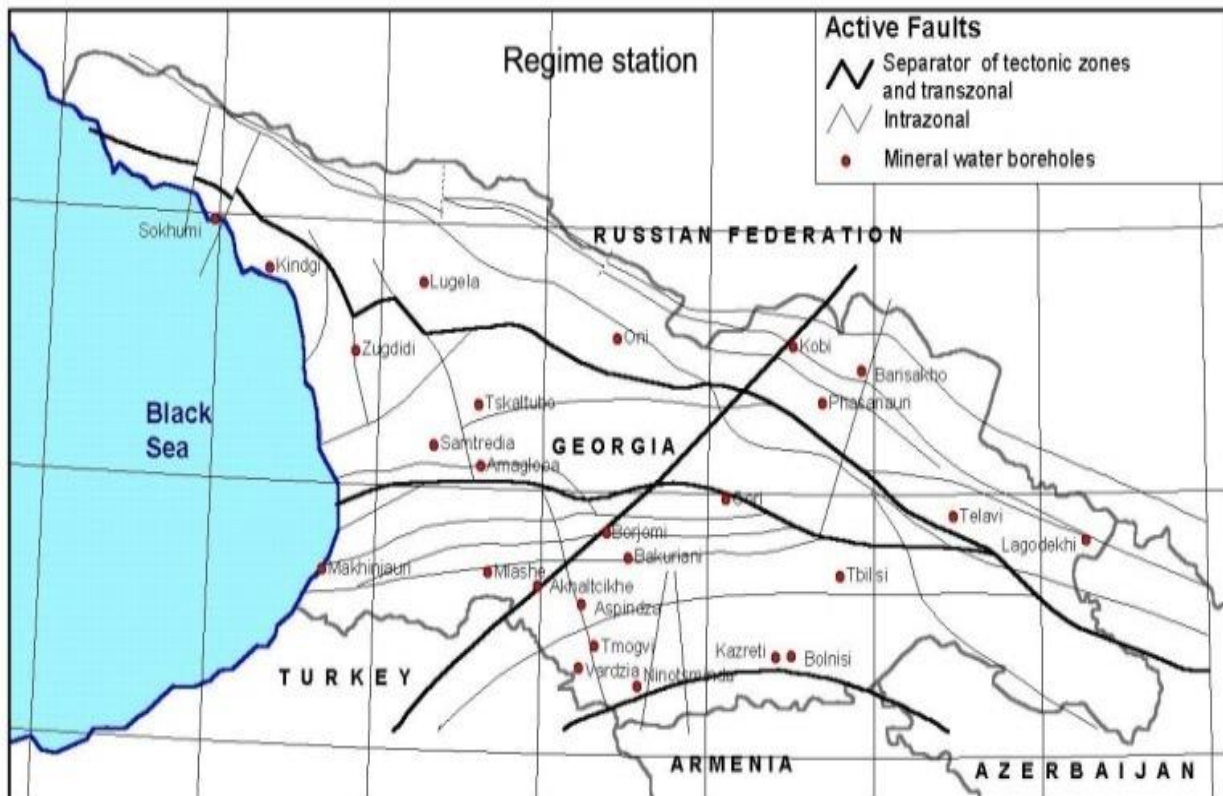


Fig.1. Scheme of hydro-chemical monitoring stations on the territory of Georgia

Measurements of water debit- by volumetric method, temperature of water and air - by mercury thermometer were daily carried out on the water points. Helium concentration was directly defined on the water points with the same frequency. Chemical composition of water was assessed on 20 components (HCO_3 , Cl, SO_4 , Na, K, Ca, Mg, J, Br-, Zn, Cu, Fe, Mn, He etc). Water chemical analysis was done by standard methodology.

1.2. WATER LEVEL VARIATION MONITORING IN THE BOREHOLES

The modern methods of earthquakes forecast allow watching temporal and spatial changes of strain in the terrestrial crust. One of them is the monitoring method of hydrogeodeformation ground field (HGF). A regime network, according to the development of VSEGINGEO, in Caucasus has been established since 1985. Till now the network of 10 boreholes of different depth (from 250 up to 3500 m) covers the whole territory of Georgia. Boreholes characterize all basic geo-plates and open waters of deep aquifer, actually they represent sensitive volumetric strainmeters, and react on the deformations about 10^{-7} - 10^{-8} , caused both by endogenous, and exogenous factors. A borehole was considered informative if it was fixing tidal variations and was included in the network (Melikadze G. et al., 1989).

They are situated in different tectonic areas. The deep boreholes with undisturbed regime were chosen for the observations which were not influenced by other boreholes.

Boreholes are equally spread all over the territory, basically on main geo-plates. These wells record all kinds of deformation caused by exogenous (atmospheric pressure, tidal variations and precipitation), as well as endogenous\ tectonic processes (Rojstaczer S. et al., 1998, Melikadze et al., 2002). On some boreholes, reaction of tidal-variation or atmosphere pressure dominated. For example, the atmospheric pressure is dominant at Adjameti and Oni boreholes and then tidal variations. But the tides are dominant on the Marneuli and Lagodekhi boreholes (Melikadze et al, 2004).

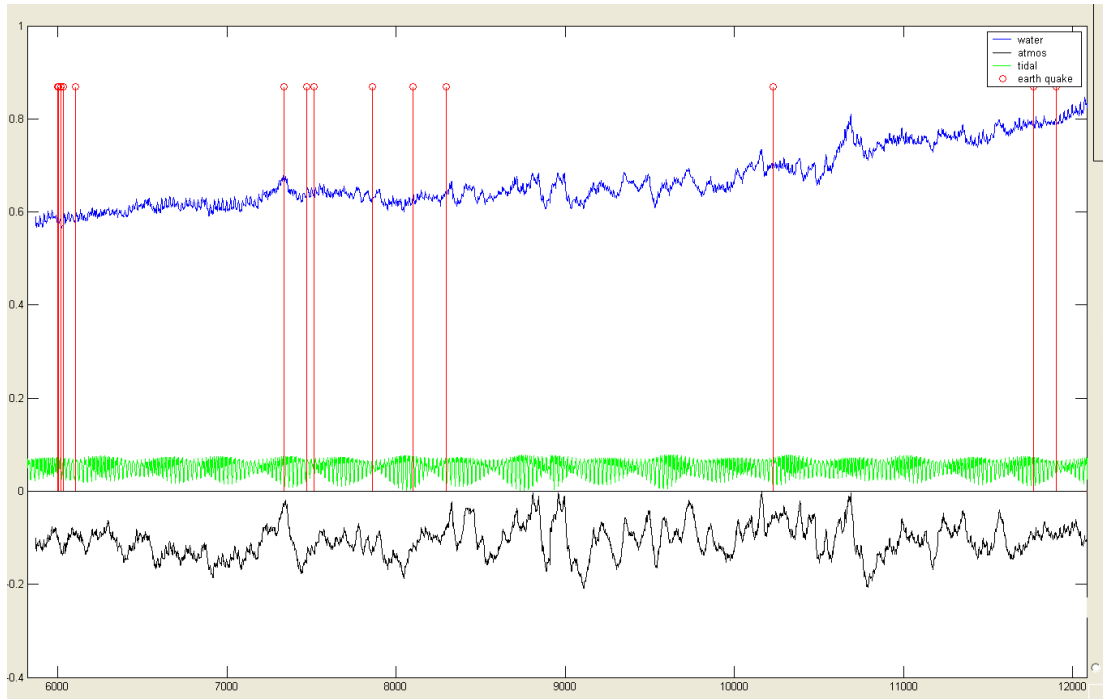


Fig. 2 Variations in time of water level (the bottom line), atmospheric pressure (the top line) and the tides (an average line) in the Adjameti borehole. Vertical lines correspond to the occurrence of earthquakes.

2.1 Data collection

Primary data is collected by datalogger **XR5-SE-M** and modem **SiemensMc35i**. Frequency of data collection is usually 1 minute.



Fig.3 Data Logger XR5-SE-M

Let discuss some properties of datalogger XR5-SE-M. It has 8 analog inputs, can log at any interval from 1 sec. to 24 hours; internal batteries life is about 2 year under typical usage.

Retrieved from XR5 data is a text-file. The data is entered first into Excel, then into the database, created on Delphy-language and MatLab programs. Delphy-base contains data for each well separately. Each well is characterized by: water level, atmosphere pressure and theoretical values of tidal. There is also a database for all earthquakes.

Delphy-base of the merged data for individual wells, combined with earthquakes can be used in the MatLab-programs. If we want to study one individual well, we use the programs **RestDance**, **WaterAndQuakes** (made in MatLab). If we want to look behavior of all wells together, than we use the programs **GeorgiaMap**, **StationsMany**.

Data can be transferred with help of GSM modem. We use two models:

- a) Wavecom model 1206B (recommended by manufactures);
- b) Siemens MS35i

Modems must be configured.

The program LogXR can automatically receive the data, from start time to last data. There is no possibility to receive only a portions of data. Here works the principle: all or nothing.

Sometimes it happens, there is no connections, so we manually connect, transfer (save) data and then clear memory for next portion of data (typically data should be collected everyday, otherwise the memory maximum is one month) . Setting of time is extracting from the computer during Setup, so the time on computer must be according Greenwich

2.2 Internal batteries and GSM connection.

The XR5 uses two AA size, 3.6v lithium batteries. If the XR5's battery voltage reads below 6.0v, the batteries should be replaced (**Tadiran TL-5903/S**). Battery life is greater than 2 years under typical usage. An external power input is provided. If external power is used, the batteries will power the unit during power outages; battery shelf life is up to 10 years.

The stability of GSM connection depends on the region , where the borehole is situated. We use Magti GSM connection , digital mode. The connection with east Georgia is more stable than in west Georgia.

Conclusion.

According to the new methodology, we have selected informatively deep boreholes for the special network, which covers the whole territory of Georgia and characterizes all basic geo-plates. They represent sensitive strainmeters and fix the deformations processes about 10^{-7} - 10^{-8} , caused both by endogenous and exogenous factors.

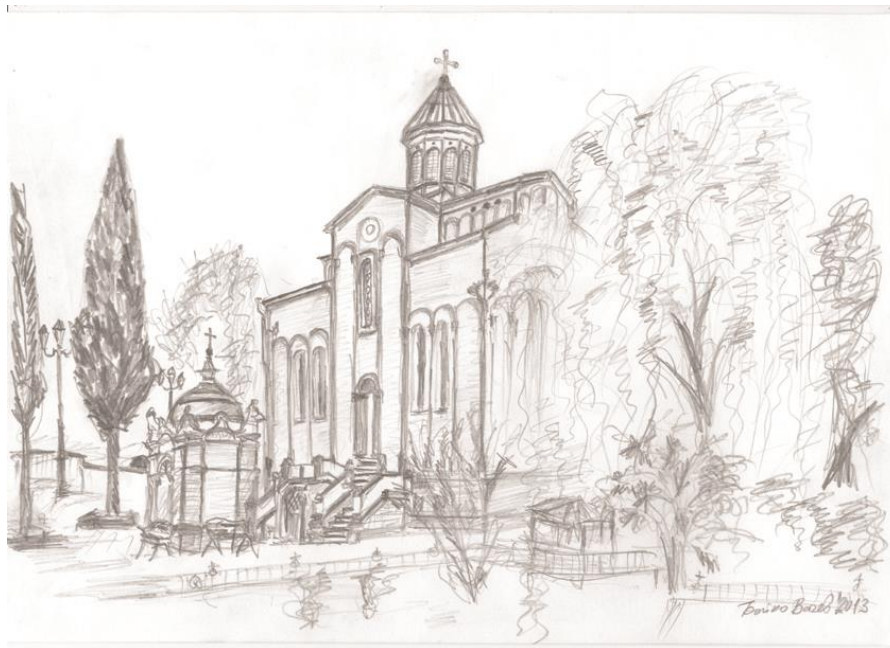
All over the world including Georgia, various anomalies (Hydro-dynamical, hydro-chemical, micro-temperature etc) are observed before earthquakes, besides in most cases, on enough distant places from epicentres. Therefore, studying the geodynamical processes may help to forecast the natural catastrophes with reasonable probability.

Analyzing data of different parameters show us the importance of improving the existing multiparametric observation network by adding new parameters as well as to expansion of contacts and collaboration with colleagues from our neighbouring countries in order to exchange data and to create the observation network on the territory of whole Caucasus and Black Sea region.

References

1. **Melikadze G., Adamchuk Y., Todadze M.** Search informational harbingers of earthquakes on the territory Georgia. A series Geology «Gruziinti» N10, P.,1989 **Research workshop on Exploration and Exploitation of Groundwater and Thermal Water Systems in Georgia** 59
2. **Hsieh, P. A., I. D. Bredehoeft, I. M. Farr.** Determination of Aquifer Transmissivity from Earth Tide Analysis. Water resources research. vol. 23. 10. 1987, p.p. 1824-1832.
3. **Hsieh, P. A., I. D. Bredehoeft, S. A. Rojstaczer.** Response of Well-Aquifer Systems to Earth Ties: Problems Revisited. Water resources Research vol. 24. No. 3. 1988, p.p. 468-472.

4. **Melikadze, G., Popov E. A.** Technique of Hydro-geological supervision with the purposes of the forecast earthquake on territory of Georgia. A series geology «Gruziinti» N7, 1989.
5. **Rojstaczer, S.** 1988. Intermediate period response of water wells to crustal strain: Sensitivity and noise level, J. Geophys. Res., 93, 13,387-12,402.
6. **Melikadze G., Matcharashvili T., Chelidze T., Ghlonti E.** Earthquake related disturbance in stationarity of water level variation. Bulletin of the Academy of sciences of the Georgian, 165 № 1, 2002
7. **Nino Kapanadze, George Melikadze, Zurab Machaidze ,Shota Kimotidze, Khatuna Bedianishvili** Evolution of methodology multi-parametrical observation on the territory of Georgia
8. **Melikadze G., Buntebarth G., Chelidze T.** Hydrodynamic and microtemperature monitoring in seismic areas. Georgian Engineering News, # 3, 2004 , p.p 12-132



Церковь Каишвети Св. Георгия 1, Тбилиси Бойко Вачев'2013
Kashveti Church „St. George” 1, Tbilisi Boyko Vachev'2013

WATER LEVEL'S VARIATION IN BOREHOLES OF GEORGIA (2011-2013)

George Melikadze¹, Genadi Kobzev¹, Tamar Jimsheladze¹,
Alexander Sborshchikovi¹

¹ M.Nodia Institute of Geophysics Iv. Javakhishvili Tbilisi State University, Georgia

Abstract:

Water level in boreholes, atmosphere pressure and temperature monitoring is performed for deep boreholes: Kobuleti, Borjomi, Akhalkalaki, Marneuli, Lagodekhi, Ajameti and Oni. We have one minute data for three years (2011-2013) and demonstrate as example measured parameters for Marneuli borehole. Water level (WL) in Marneuli borehole is related with tidal and atmosphere pressure variation. During far and strong earthquakes we observed seismic waves influence on background WL variation. Similar reaction we fixed for other deep boreholes. In MATLAB environment StationsMany, WaterAndQuakes applications have been developed at M.Nodia Institute of Geophysics. These programs allow to exclude influence of isogenic factors (tidal and atmosphere pressure variations) and create real geodynamical fields and investigate their evolution in time and space.

Introduction

Water level monitoring is made at the following deep boreholes of Georgia: Kobuleti, Borjomi, Akhalkalaki, Marneuli, Lagodekhi, Ajameti and Oni. Measuring on all stations is taken every one minute. For data recording we use datalogger XR5-SE-M and the program LogXR. Data transferring is made by GSM modules Siemens and Wavecom-type. Data processing and figures creation is realized by program StationsMany. This program is evolutionary development of programs WaterAndQuakes and RestDance. These programs are written on MatLab-language.

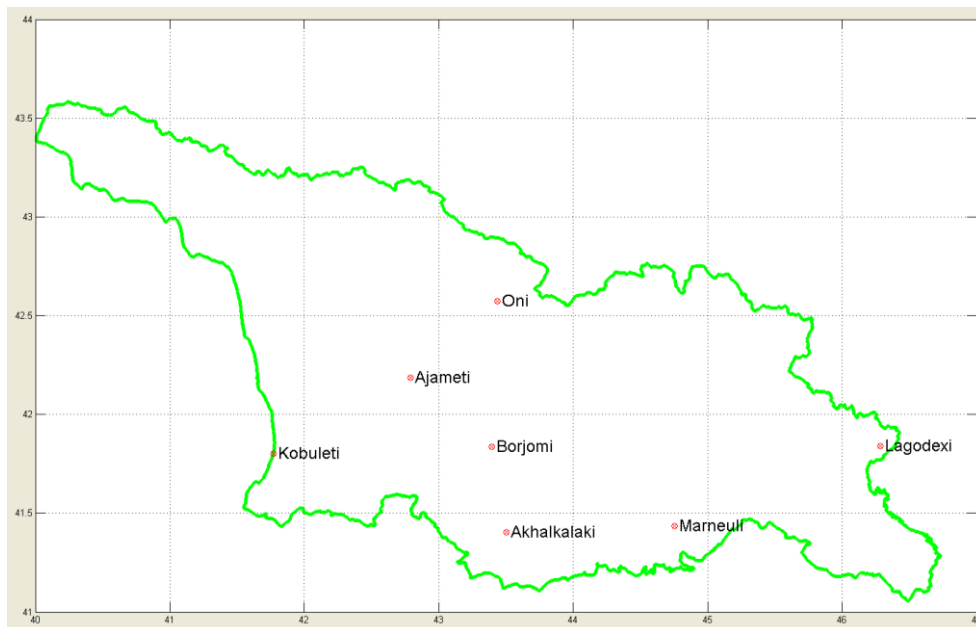


Figure 1. Location of deep boreholes in Georgia

Here is the detail description of the boreholes:

Borehole	Depth, meters	Filter interval, meters	Lithology	Geological intervals, meters	Waterlevel, meters
Ajameti	1330	520-740	Litostone	520-740	-6
Akhalkalaki	1400	1000	Tuff, andezit, basalt, dolomite	580-1000	-0.2
Borjomi-70	1330	1260-1300	Clay	0-12	-22
Kobuleti	2000	187-640	Tuff, andezit, bazalt	0-150 150-2000	-0.5
Lagodekhi	800	255-367	Sand+gravel	0-24	-15.8
Marneuli	3500	1235-1600	Tuff, diabases, bazalt	3100-3505	-5

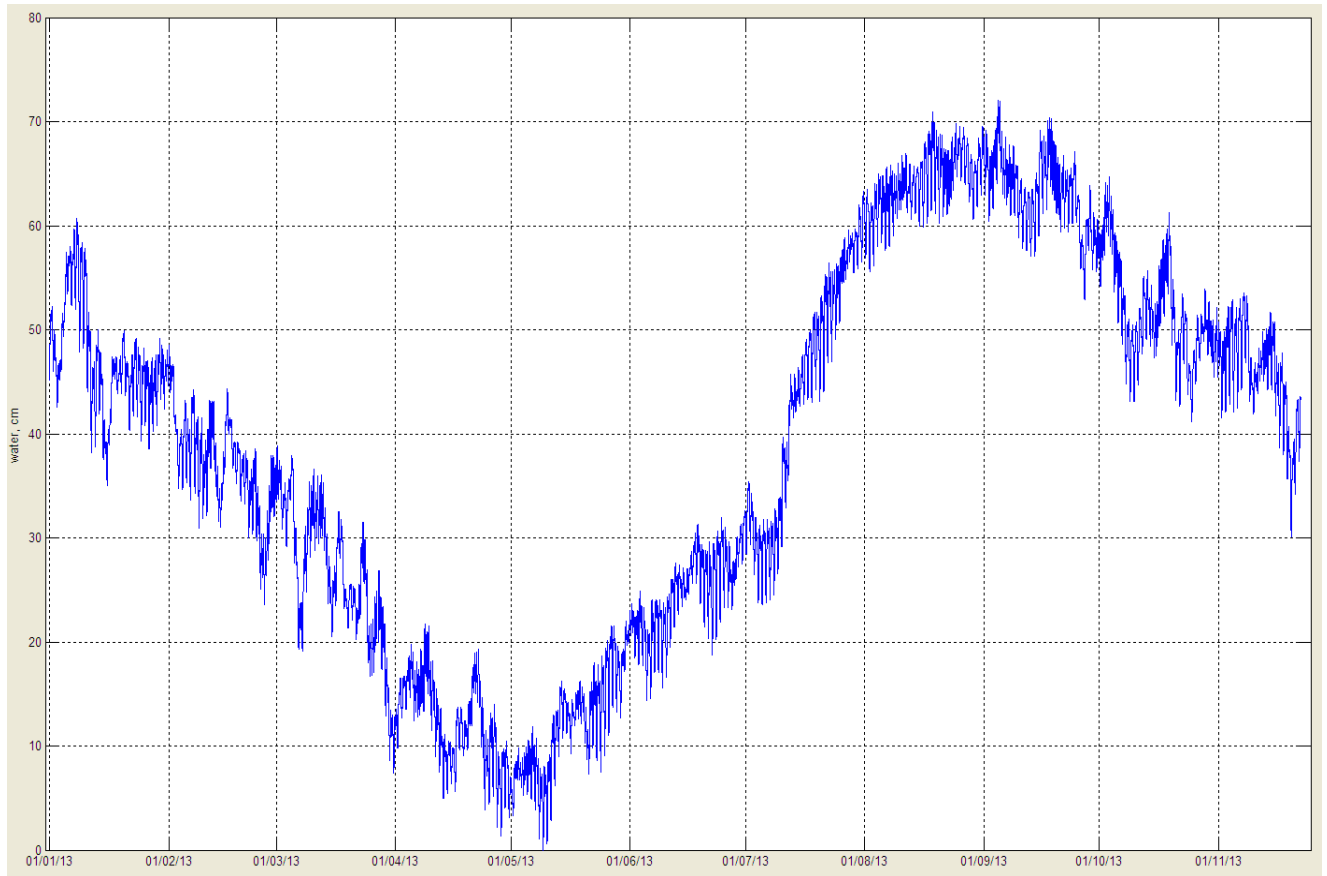


Figure 2. Marneuli water level, 2013

Here we have data of water level monitoring for Marneuli borehole during 2013 year (fig.2).

On examples (fig.2-4) we can see that water level at Marneuli borehole has season variation, have tidal (Sun & Moon) and atmosphere influence. Also it has reaction on the earthquakes.

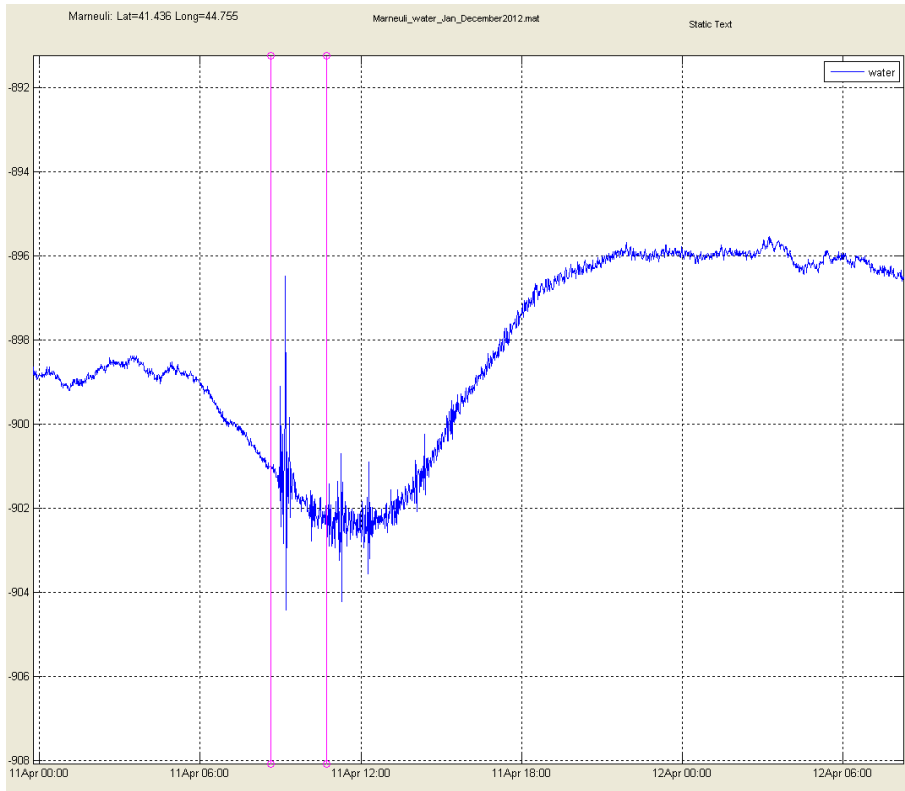


Figure 3. Marneuli, 11 April 2012, Sumatra, Mag=8.4, distance 6500 km, east direction

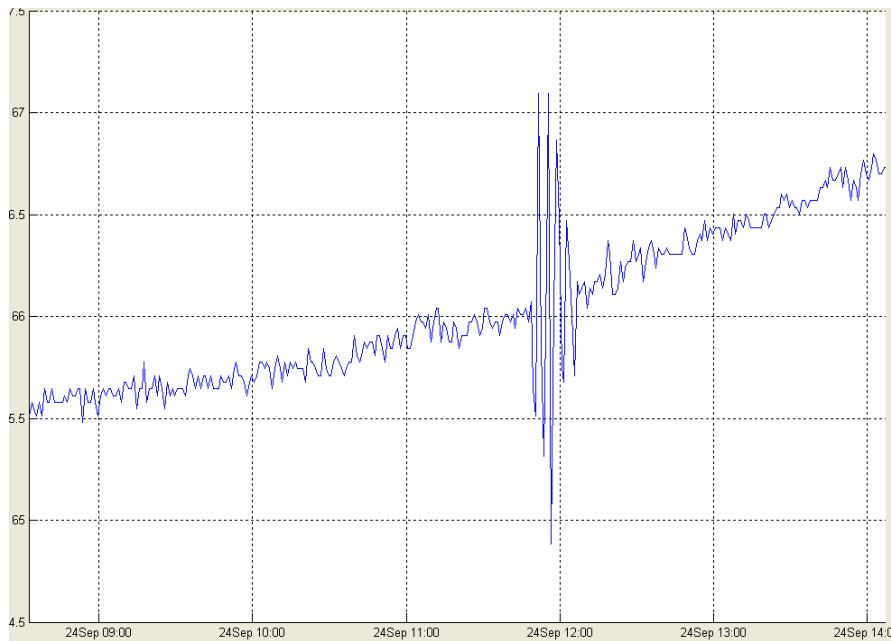


Figure 4. Marneuli, 24 September 2013, Pakistan, Mag=7.7, distance 2500 km, east direction

Our aim is studying water level behavior in the boreholes, visualization and finding methods of extraction earthquakes signals.

Visualization and simple conversions

Let us look at water level changing in various boreholes, which are made during four days before Turkey (Vani) earthquake 23 October 2011, Mag=7.2 (about 300 km on the south from Georgia). Here are water levels for Marneuli (top of picture, east), Kobuleti (west), Borjomi (center of Georgia), Ajameti and Akhalkalaki (to north and to south from Borjomi). So on the east it was small jump (Marneuli, top of picture); on the west (Kobuleti) the water was up; in the center there was jump (Borjomi); and small water down on north and south from center.

In time 19-21 October (from 4 up to 2 days before earthquake) there is water nonstandard behavior on four boreholes; than from 2 up to 0 day begin stabilization and ... earthquake.

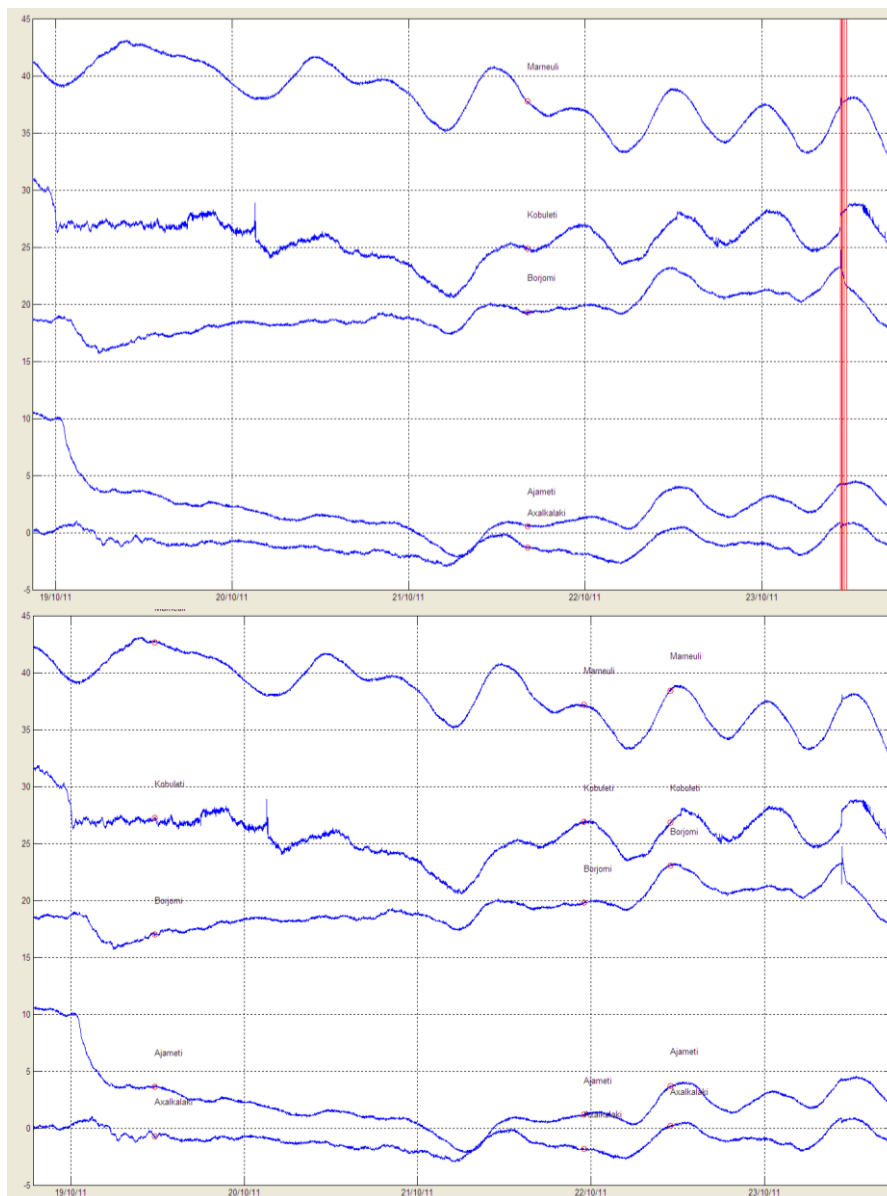


Figure 5. Water levels in 5 boreholes (Georgia) and earthquake in Turkey 23 October 2011, Mag= 7.2

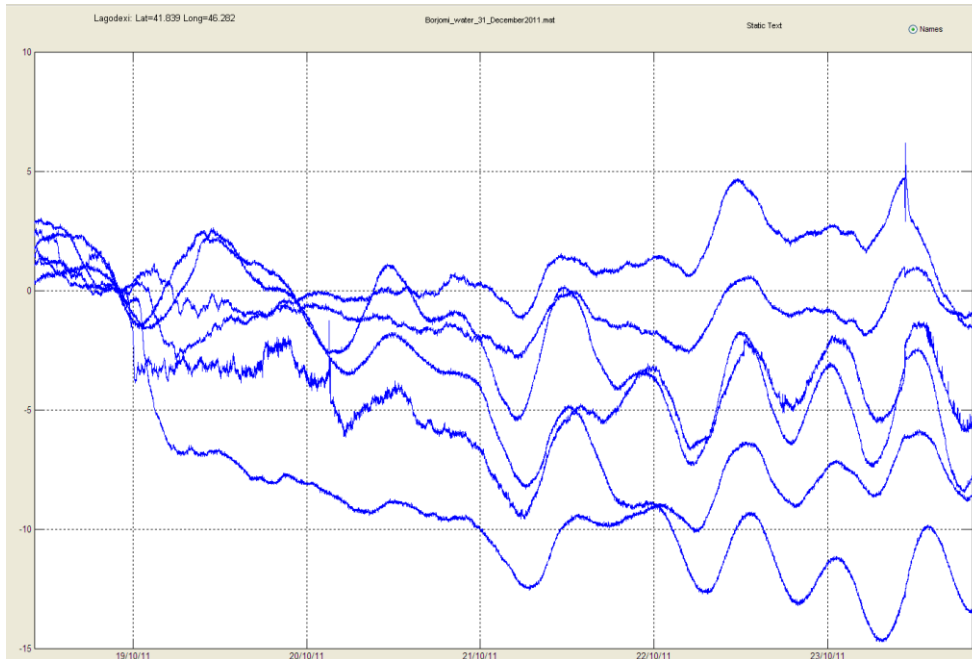
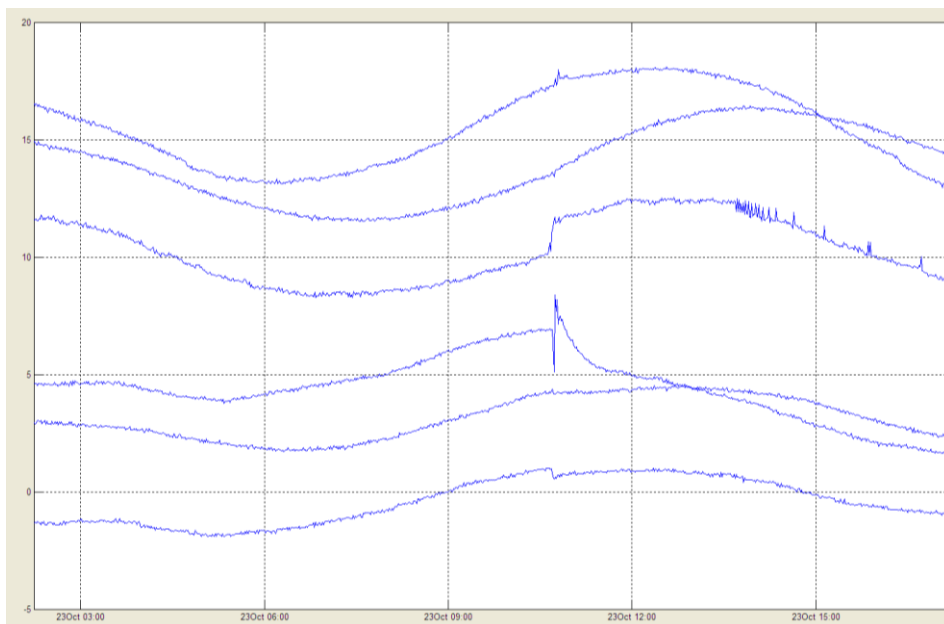


Figure 6. Conversions: Water levels are set to 0 for all stations on 19 October 2011; water moving from 19 October till 23 October and earthquakes on 23 October 2011



**Figure 7. Water levels in Georgian boreholes, 23 October (03:00 - 15:00) and earthquake in Turkey 23 October 2011, magnitude 7.2, south direction.
From top to bottom: Marneuli, Lagodekhi, Kobuleti, Borjomi, Ajameti, Akhalkalaki**

Relationship of water with atmosphere and tidal

Let us discuss more closely tidal and atmosphere influence on water level and make attempt to eliminate it from the water. Fig. 8-10 shows, these influences can be very strong.

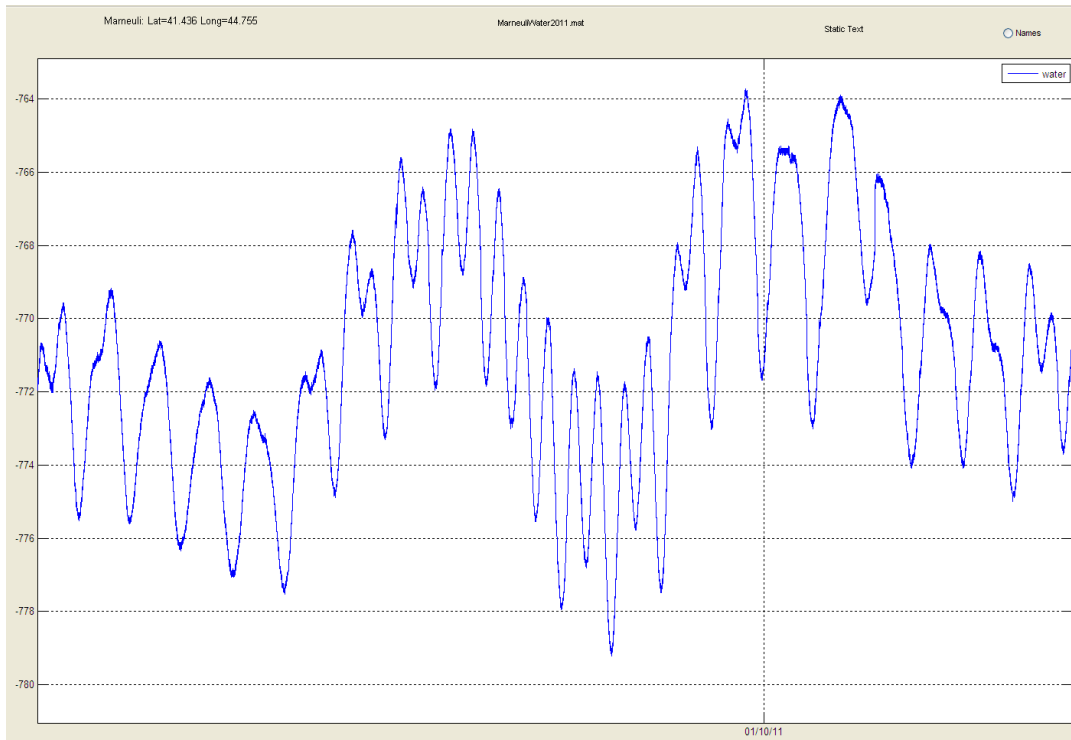


Figure 8. Water level, Marneuli

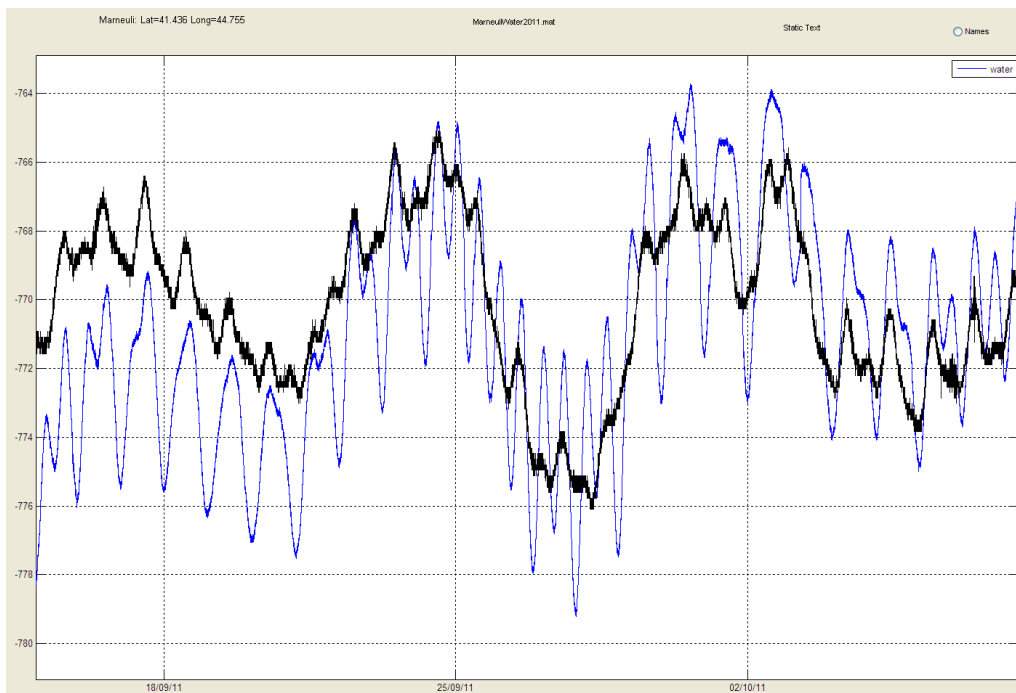


Figure 9. Influence of atmosphere on water level: water (blue) and atmos (black)

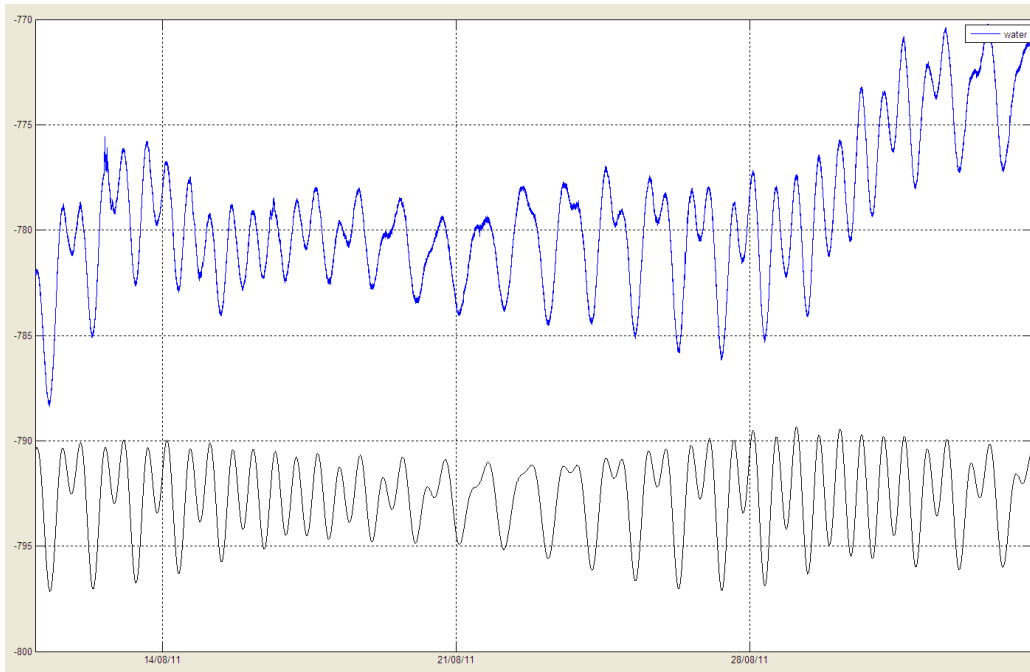


Figure 10. Water level (top, blue), tidalZ (bottom, black)

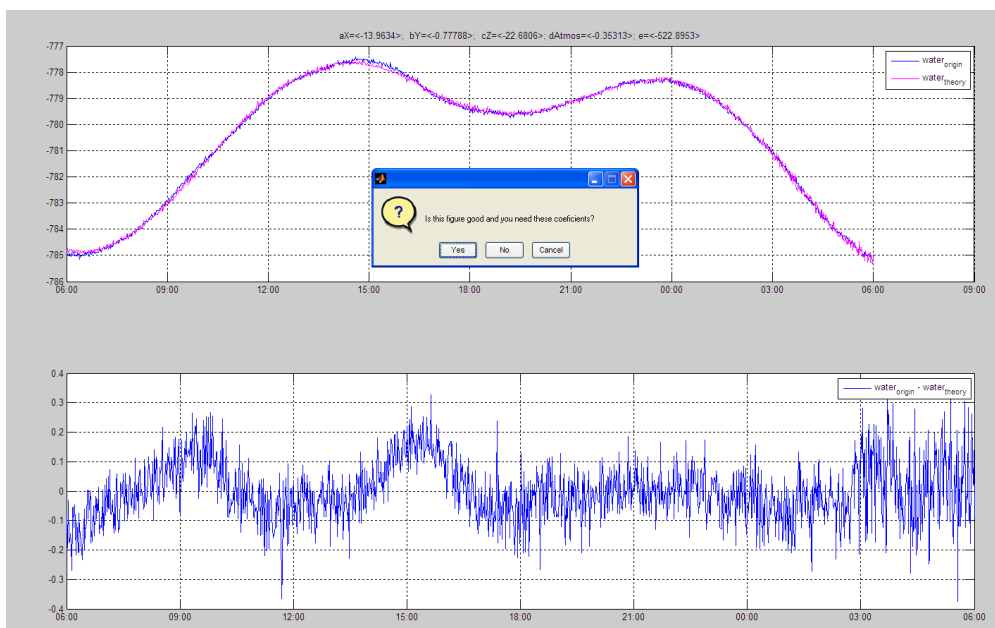


Figure 11. Water (top, blue), water_theory (top, magenta) and rest=water-water_theory (bottom)

$$\text{where } \text{water_theory} = a * \text{atmosphere} + b * \text{tidal} + c$$

Define $\text{water_theory} = a * \text{atmosphere} + b * \text{tidal} + c$ with appropriate coefficients **a, b, c** (in fact, **tidal** has 3 components: **tidalX**, **tidalY**, **tidalZ** and every this component has his coefficient too). On fig. 11 (top) graphs for **water** and **water_theory** almost coincide, but **rest** (fig.11, bottom) shows the difference between them.

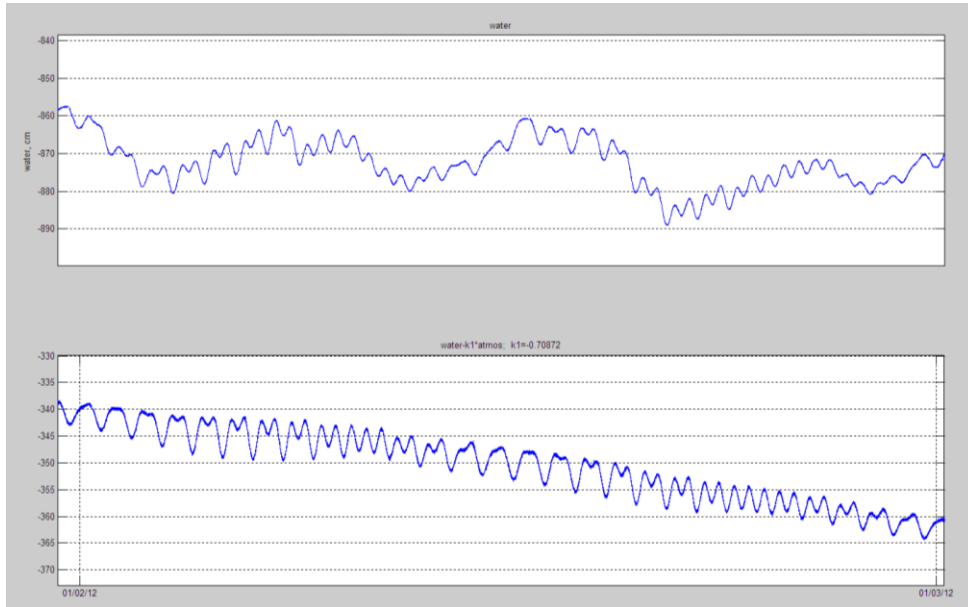


Figure 12. Marneuli 2012: water (top) and water-a*atmos (bottom)

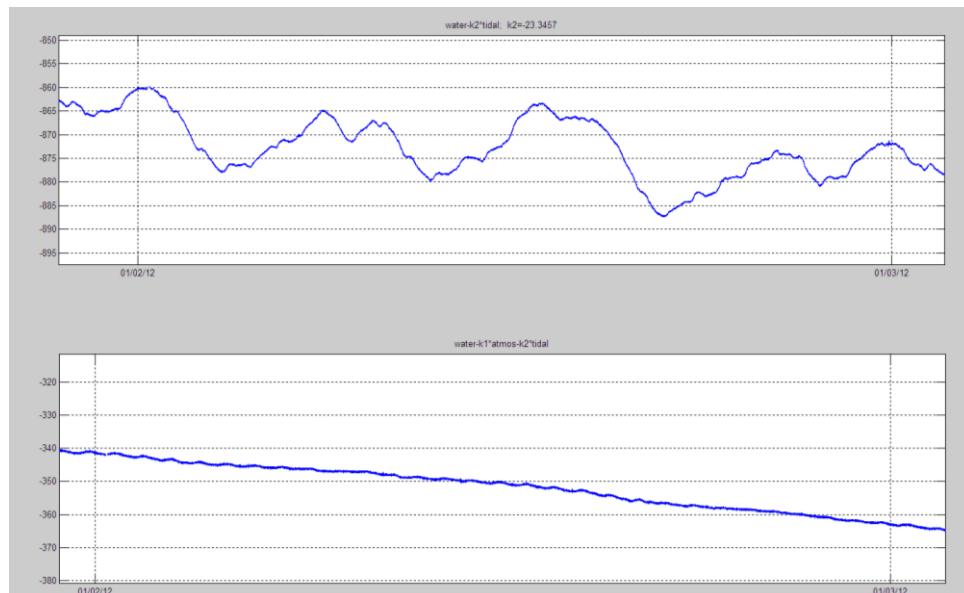


Figure 13. Marneuli 2012: water - b*tidal (top) and water - a*atmos - b*tidal (bottom)

On the fig.12 (top) there is original water level and result after extraction atmosphere influence (fig.12,bottom). On the fig.13(top) there is result of extraction of tidal from the water. Fig.13 (bottom) shows: after extraction atmosphere and tidal, **we can eliminate atmosphere and tidal influence on water.**

Speed for water level

Seasonal trend does not allow us to compare water levels of boreholes. Definition of speed for water level will help to manage with this problem and give to us additional information.

Definition: $Speed(m+i)=(water(m+i)-water(i))/m, \quad i=1,2,3,\dots$

where m is fixed number of minutes. For example $m=180$ minutes.

On fig.14-15 for visualization comparability speeds-data are multiplied on some coefficients. On this pictures we see, that seasonal water trend does not exist (has small value). Also on fig.14 and 15 it can be seen anomaly in days 18-21 October, than stabilization and jumps on 23 October (earthquakes).

Speed examples

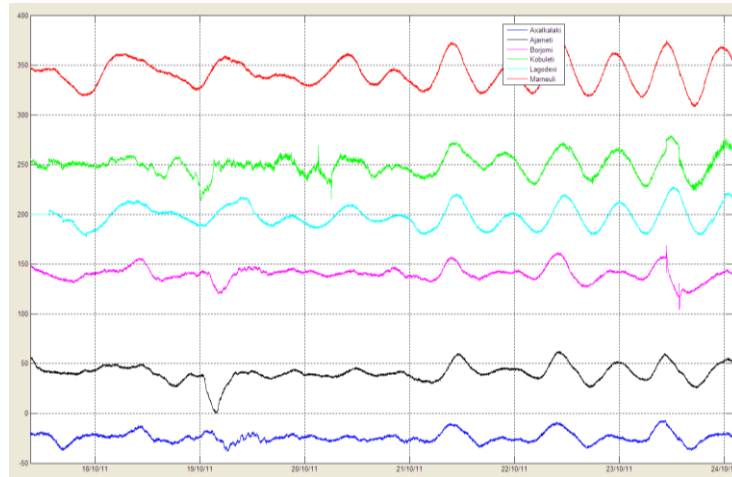


Figure 14. Speeds: $m=180$ minutes for boreholes of Georgia, 2011

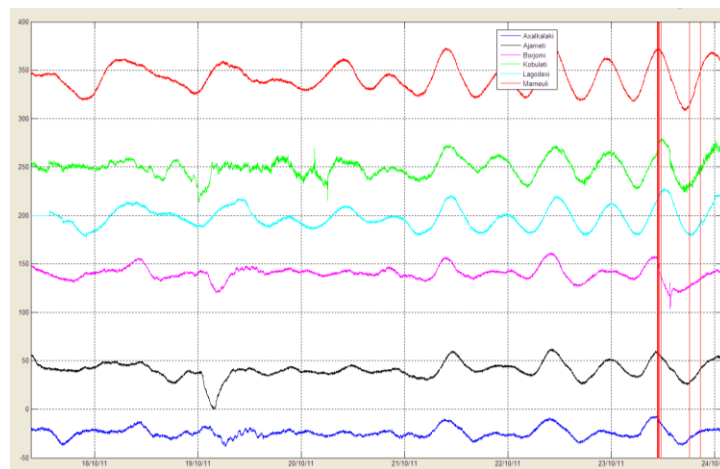


Figure 15. Speeds: $m=180$ minutes interval for boreholes of Georgia, 18-24 October and Turkey (Vani) earthquakes 23 October 2011, Mag=7.2

From top: Marneuli, Kobuleti, Lagodekhi, Borjomi, Ajameti, Akhalkalaki

Fields

By definition field is a map for the values of some parameter, measured on different points of area at the same time. For all boreholes we set the water level to zero for some days before earthquake, than construct fields and look at the water variations during 2 days up to earthquake.

Water fields, original water

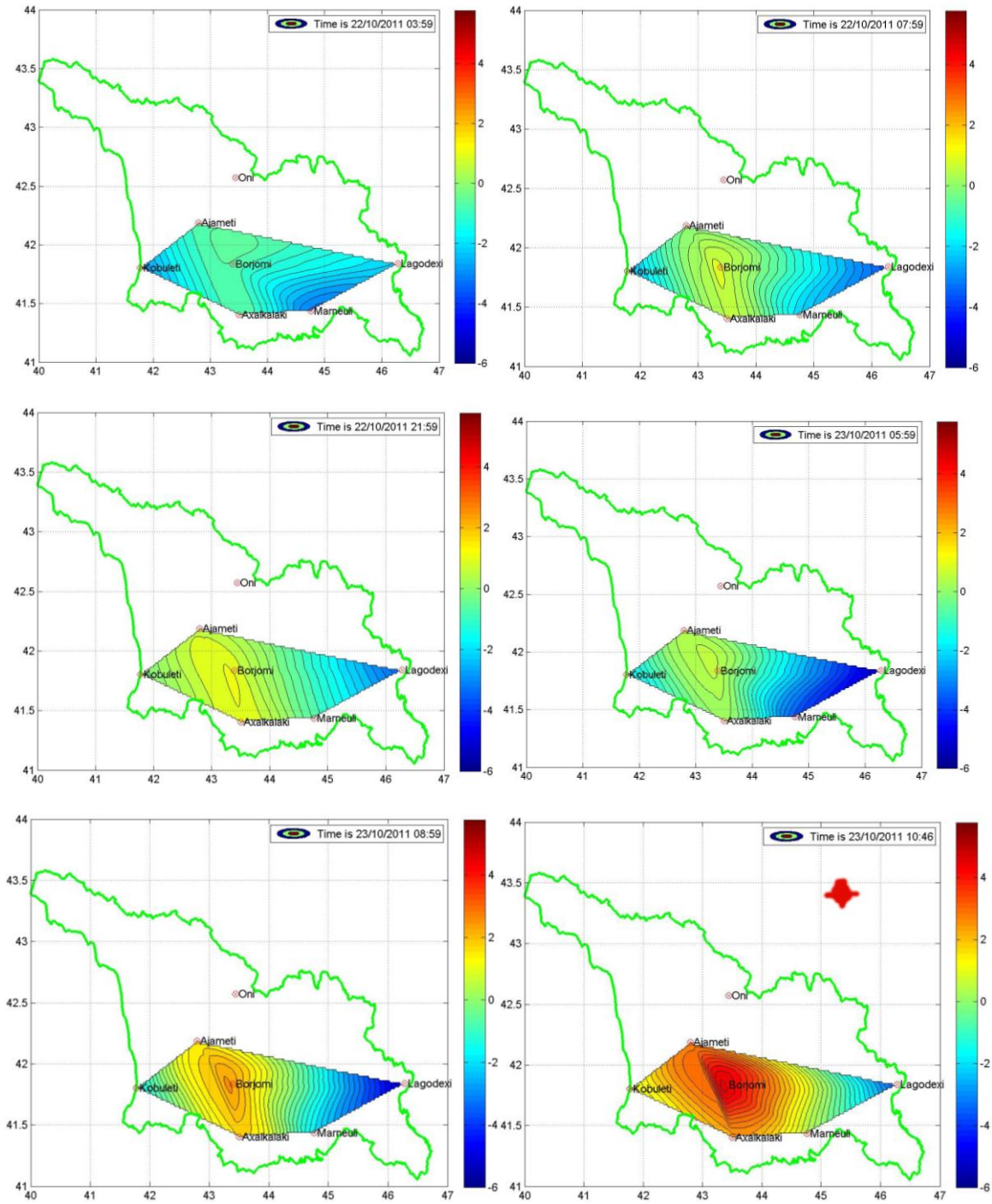


Figure 16. Field for water level in Georgia during 2 days before earthquake in Turkey 23 October 2011

Fields for water-level speed, Georgia

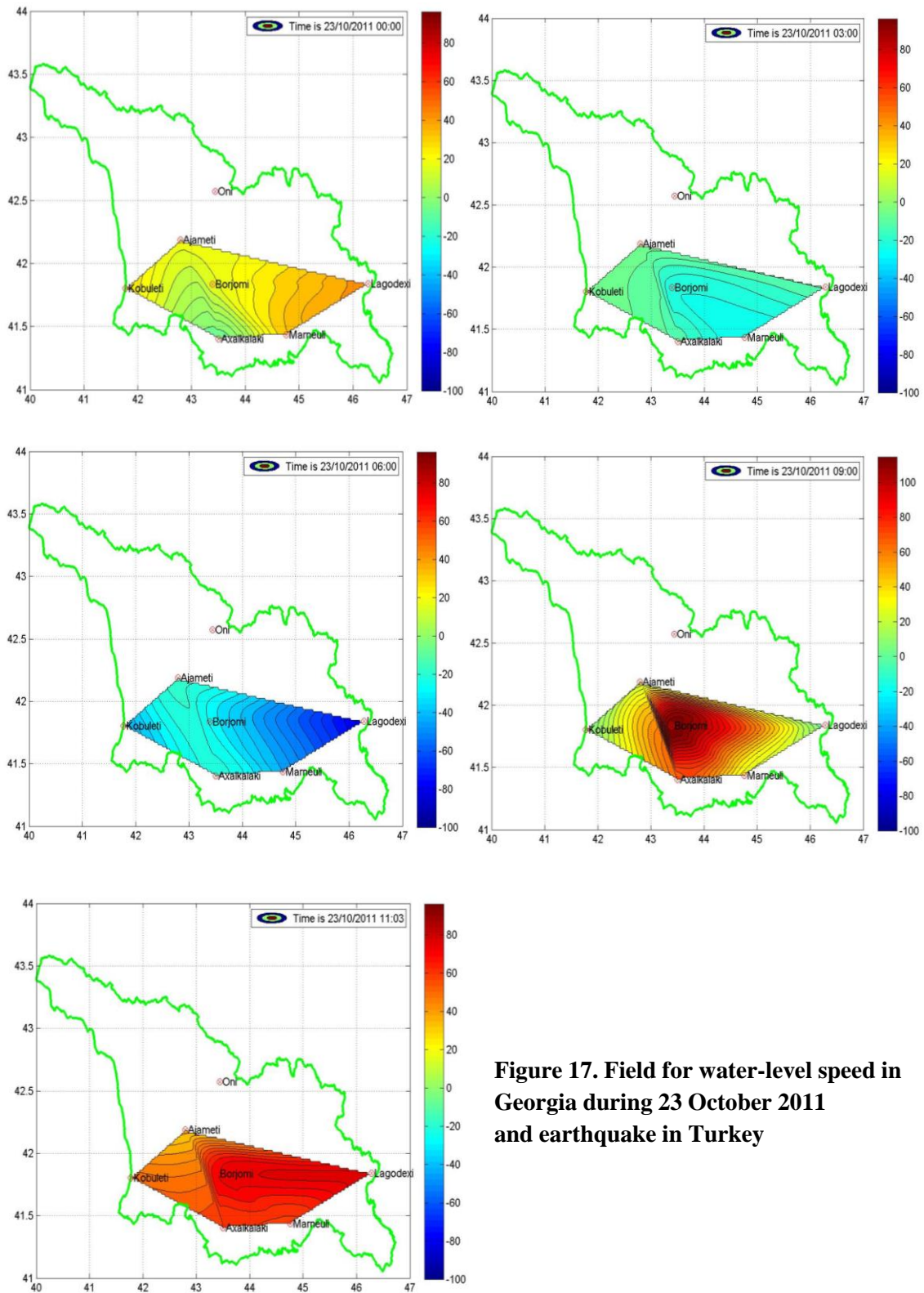


Figure 17. Field for water-level speed in Georgia during 23 October 2011 and earthquake in Turkey

Conclusion

There was shown a relation of water level variations with atmosphere and tidal behavior. The meaning of speed and field was demonstrated in this article. So in this work was shown three methods of visualization and anomaly during great earthquakes: speed, field and original behavior of water level using StationsMany-program.

References:

- [1] G. Melikadze, Y. Adamchuk, M. Todadze, (1989) A series Geology “Gruziinti”. Research workshop on Exploration and Exploitation of Groundwater and Thermal Water Systems in Georgia, **10**(59).
- [2] P.A. Hsieh, I.D. Bredehoeft, I.M. Farr, (1987) Water resources research, **23**(10), 1824-1832.
- [3] P.A. Hsieh, I.D. Bredehoeft, S.A. Rojstaczer, (1988) Water resources Research **24**(3), 468-472.
- [4] G. Melikadze, E.A. Popov, (1989) A series geology ‘Gruziinti’ **7**.
- [5] S. Rojstaczer, (1988) J. Geophys. Res., **93** (13), 387-12, 402.
- [6] G. Melikadze, T. Matcharashvili, T. Chelidze, E. Ghloni (2002), Bulletin of the Academy of sciences of the Georgian, **165** № 1
- [7] G. Melikadze, G. Buntebarth, T. Chelidze, (2004) Georgian Engineering News, **3**, 12-132



Церковь Кашвети Св. Георгия 2, Тбилиси Бойко Вачев'2013
Kashveti Church „St. George” 2, Tbilisi Boyko Vachev'2013

BOREHOLES WATER LEVEL AND EARTHQUAKE'S PREDICTION (2011-2013)

A.Sborshchikovi^{1,2}, G.Kobzev^{1,2}, S.Cht.Mavrodiev², G.Melikadze¹

¹ M.Nodia Institute of Geophysics, Georgia, ² Institute for Nuclear Research and Nuclear Energy, Bulgarian Academy of Sciences,

rossoneri08@yandex.ru

Abstract

Studies of precursors and events that occur before an earthquake is one of the most important problem that arose in today's seismology. Earthquake prediction has become the issue that needs to be solved, it will help us to forecast destructive earthquake. In this article we will discuss water level daily monitoring in several boreholes located in different parts of Georgia.

Keywords: water level, precursors, earthquake prediction, geoelectromagnetism

Introduction

The main reason of this research was to find the answer to the question is the change of water level in the boreholes the same effect on the incoming earthquake appearance as the variations of magnetic fields or not.

The hypothesis for possible correlations between the earthquakes and the variations of magnetic fields, Earth's horizontal and vertical currents in the atmosphere, was born when in the when the historical data on the Black Sea was systemized. The achievement in the Earth surface tidal potential modeling, with the ocean and atmosphere tidal influences being included, makes an essential part of the research. In this sense, the comparison of the Earth tides analysis codes [1] was very useful. The possible tidal triggering of earthquakes has been investigated for a long period of time [2].

The earthquake-related part of the models has to be infinitely repeated in the "theory-experiment-theory" process, using nonlinear inverse problem methods in looking for correlations between the different fields in dynamically changing space and time scales. Each approximate model supported by some experimental evidence should be included in the analysis. The adequate physical understanding of the correlations among electromagnetic precursors, tidal extremes and a impendant earthquake is related to the progress of an adequate Earth magnetism theory and electrical currents distribution, as well as to the quantum mechanical understanding of the processes in the earthquake source volume before and during the earthquake.

Simultaneous analysis of more accurate space and time measuring sets for the Earth crust condition parameters, including the monitoring data of the electromagnetic field under and over the Earth surface, as well as the temperature distribution and other possible geophysical precursors, would be the basis of nonlinear inverse problem methods. It could be promising for studying and solving the "when, where and how" earthquake prediction problem.

The discovery of geomagnetic quake as reliable precursor for increasing of regional seismicity

In December 1989, a continuous measurement of a projection of the Earth's magnetic field (F) with a magnetometer (know-how of JINR, Dubna, Boris Vasiliev) with absolute precision less than one nano-Tesla at a sampling rate of 2.5 samples per second was started. The minute's mean value of F , its error mean value, the minute's standard deviation SDF , and its error were calculated, i.e., every 24 hours, 1440 quartets of data were recorded.

Minute standard deviation of F is defined as:

$$SDF_m = \left(\left(\frac{1}{N} \right) \sum_{i=1}^{N_m} (1 - F_{mean} / F_i)^2 \right)^{\frac{1}{2}} \quad (1)$$

where m is the chosen time interval and n is the number of samples during the period,

$$F_{mean} = \left(\frac{1}{N} \right) \sum_{i=1}^{N_m} F_i \quad (2)$$

and N_m is the number of samples per minute.

The connection between variations of local geomagnetic field and the Earth currents was established in INRNE, BAS, Sofia, 2001 seminar [3]. The statistic of earthquakes that occurred in the region (1989-2001), confirmed the Tamrazyan notes [4,5], that the extremes of tides are the earthquake's trigger. The Venedikov's code [6,7] for calculating the regional tide force was used [8].

The signal for imminent increasing regional seismic activity (incoming earthquakes) is the "geomagnetic quake" (Gq), which is defined as a jump (positive derivative) of daily averaged SDF_{mean} , devoted to half sum of middle geomagnetic field indices. Such approach permits to compare by numbers the daily behavior of the geomagnetic field with those in other days.

Among the earthquakes occurred on the territory under consideration in certain time period, the "predicted" one is the earthquake with magnitude M and distance between epicenter and monitoring point $Dist$, which is identified by the maximum value of the function:

$$S_{ChM} = 10^{1.5M+4.8} / (D + Depth + Dist)^2 \left[J / km^2 \right] \quad (3)$$

where $D = 40$ km is a fit parameter. Probably, its sense is connected with the mean of Earth crust thickness.

The physical meaning of the function S_{ChM} is a surface density of earthquake's energy in the point of measurement. It is important to stress out that the first consideration of the earthquake magnitude M and epicenter distance dependence was obtained using nonlinear inverse problem methods. Obviously, the close distance strong earthquake (with relatively high value of S_{ChM}) will bear more local Earth currents variations, which will generate more power geomagnetic quake.

It is very important to note that in the time scale of one minute, the correlation between the time period of increasing regional seismic activity (incoming earthquake), and tide extrema, recognized of predicted earthquake was established using the Alexandrov's code REGN for solving the over - determined nonlinear systems [8,9]. The very big worthiness of Alexandrov's theory and its code is possibility to choose between two functions, which describe the experimental data with the same *hi*-squared, the better one.

Day-Difference analysis

The role of the electromagnetic variations as earthquake's precursor can be explained in general by the hypothesis: the strain accumulation in the Earth Crust during the earthquake preparation causes medium's density change, within which a chemical phase ("dehydration") shift and a corresponding electrical charges shift appears. The Earth tides extreme as earthquake's trigger could be based on the hypothesis of "convergence of tidal surface waves" in the region (territory with prominent tectonic activity as consequences of chemical phase shift) of impending seismic activity.

For every occurred earthquake was calculated “day-difference”; the smaller absolute time difference between the hypocenter time and the daily times of pre and post tide’s extreme time at that site on the Earth surface (the earthquake epicenter). This procedure was provided on all reported earthquakes in ISC catalogue (<http://www.isc.ac.uk/>) for the time period 1981-2011 and $M \geq 3.5$. The program for calculating of daily averaged module of vector movement T_{mean} is based on Dennis Milbert TIDE program (solid.for), by which Tide data could be calculated only for the time period after 1981. The DailyTide time of the Tide extremes T_{mean} were calculated by analogy of center mass calculation.

The statistic of day-differences for the earthquakes that occurred worldwide (1981-2011) and the Gaussian fitted curve (Fig.4), confirmed the Tamrazyan notes [5,6] from 1960-th, that the extremes of tides play a role of earthquake’s trigger.

Data and stations

The main reason of this research was to find the answer to the question was is the change of water level in the boreholes has the same effect for earthquake appearance as the variations of magnetic fields or not.

The hypothesis for possible correlations between the earthquakes, the variations of magnetic fields, Earth’s horizontal and vertical currents in the atmosphere, was born when in early 1988, the historical data on the Black Sea was systemized. The achievement in the Earth surface tidal potential modeling, with the ocean and atmosphere tidal influences being included, makes an essential part of the research. In this sense, the comparison of the Earth tides analysis codes [6] is very useful. The possible tidal triggering of earthquakes has been investigated for a long period of time [7].

After studying this fact a hypothesis was born may be we can forecast earthquake using the same methodology.

Before discussing our methodology let stop our attention on the boreholes, which are located in different parts of Georgia. We have Ajameti borehole (depth 1300 m); Axalkalaki (1400 m); Borjomi-70 (1300 m); Kobuleti (2000 m); Lagodehi (800m) and Marneuli (3500m).

The location of these boreholes is shown in Fig.1a.

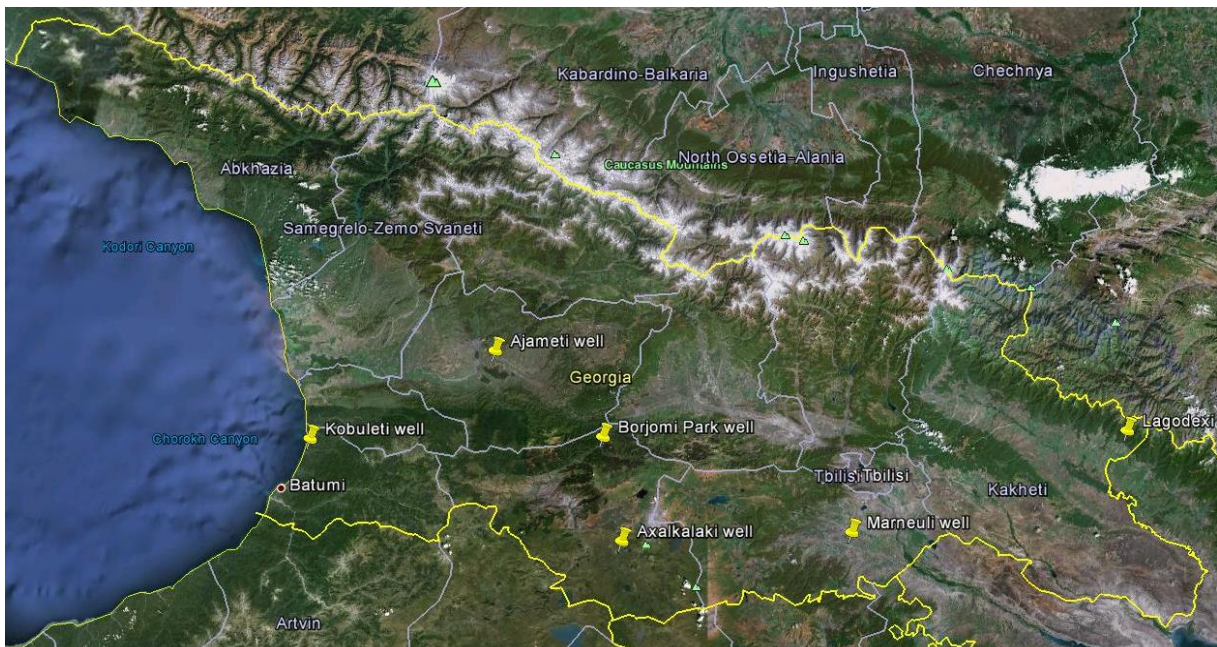


Fig.1a Map of boreholes in Georgia

Here is the detail description of the boreholes:

Borehole	Depth, meters	Filter interval, meters	Lithology	Geological intervals, meters	Water level, meters
Ajameti	1330	520-740	Litostone	520-740	-6
Ahalkalaki	1400	1000	Tuff, andezit, basalt, dolomite	580-1000	-0.2
Borjomi-70	1330	1260-1300	Clay	0-12	-22
Kobuleti	2000	187-640	Tuff, andezit, bazalt	0-150 150-2000	-0.5
Lagodehi	800	255-367	Sand+gravel	0-24	-15.8
Marneuli	3500	1235-1600	Gravel	0-50	-5

Methodology of analysis

We have selected earthquakes with magnitude $M \geq 3.5$ at distance $D \leq 500\text{km}$ from boreholes for 2011, 2012 and 2013 years. After format conversion of water level data we calculate the daily standard deviation (daily level signal). When we have the jump of today and yesterday signals we say that we have a precursor for incoming regional seismicity. After this we analyze the day difference between occurred earthquakes and next extreme of the tide, calculated using Dennis Milbert FORTRAN code for local tidal behavior, <http://home.comcast.net/~dmilbert/softs/solid.htm>.

For precursors calculation we used one hour water level data. The statistic evidence that water level precursors can be used for estimation of incoming regional seismic situation is illustrated in the figures 2,3 and 4,5.

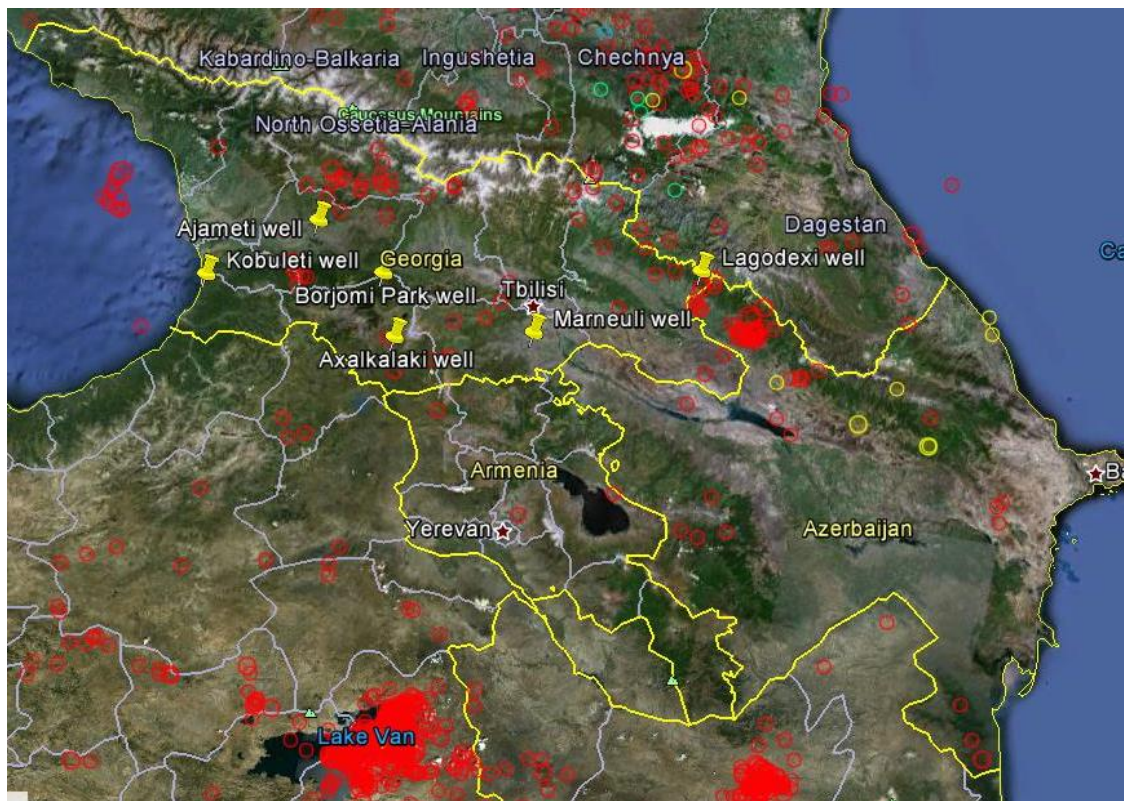


Fig.1b The map of earthquakes during 2011-2012

Georgia Boreholes Water Level and Earthquake's daily monitoring

Earth tide (Dennis Milbert, <http://home.comcast.net/~dmilbert/softs/solid.htm>)

Water Observatory, **Marneuli** borehole, Georgia (DSH)
 Lat 41.43 N, Lon 44.86 E, Alt 397 m

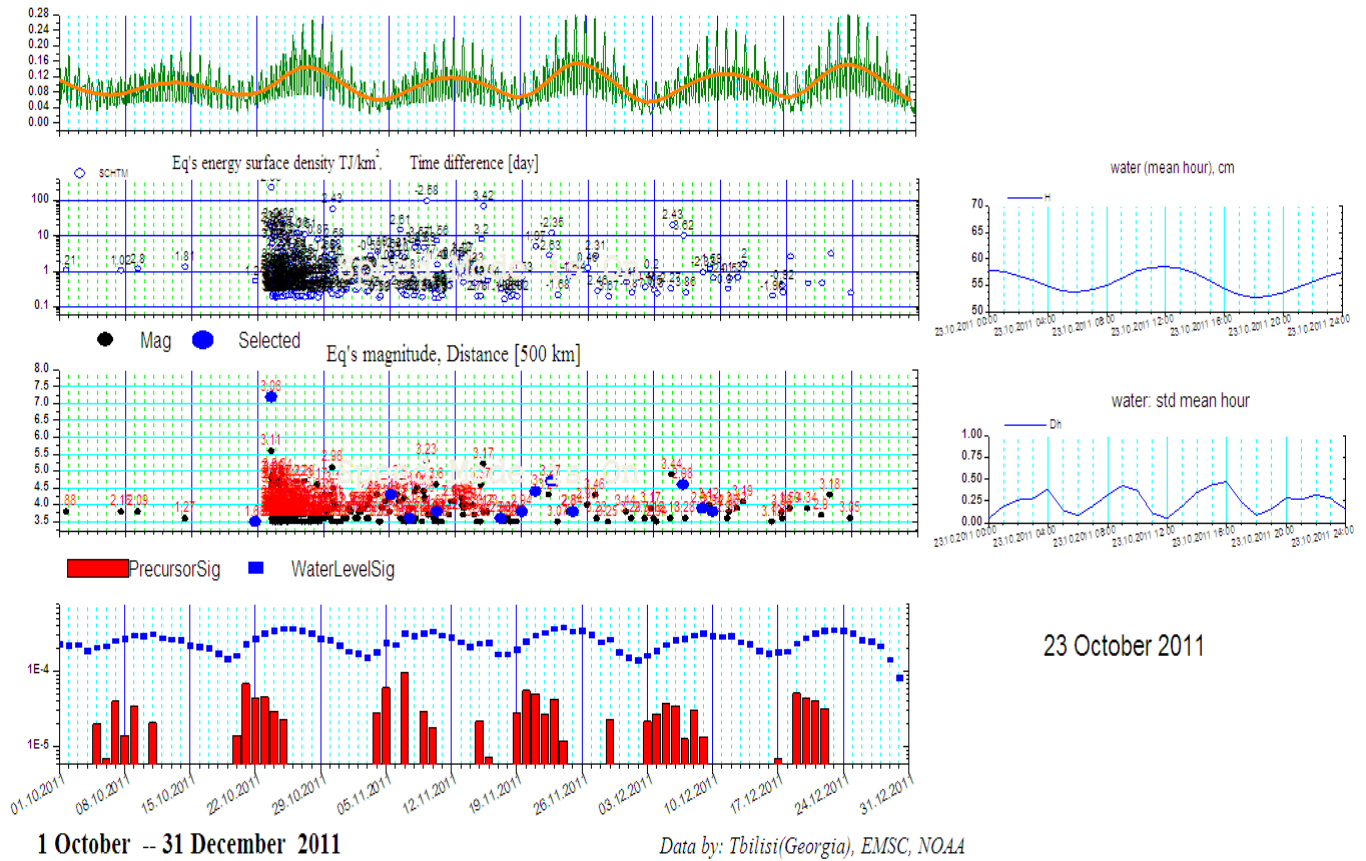


Fig.2 Marneuli borehole daily monitoring including period of great earthquake in Turkey (2011)

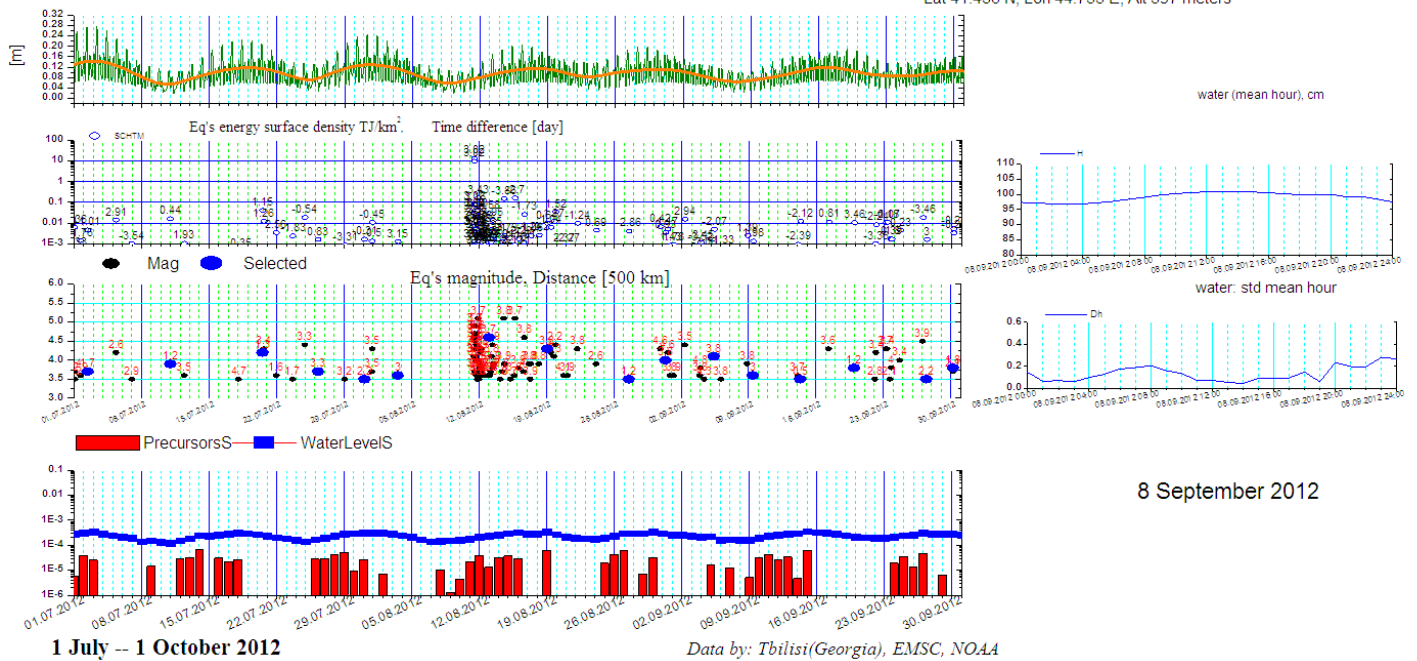
As we see in figure 2 the first graph in the left corner is the picture of tidal behavior [m], the next shows the energy (J/km^2), the next – magnitude, and the last describes precursors (red columns) and water level signals (blue points). The blue points has been count using normal standard deviation and the red columns so called precursors were obtain by subtraction of the daily standard deviation of today and the previous day [10,11]. The first graph in the right corner is water mean during 23 October the period of great Turkey earthquake and the next describes standard deviation of water level [12].

The same emplacement is shown for another period in the figure 3.

1 2 3 4 5 6

Georgia Boreholes Water Level and Earthquake's daily monitoring

Water Observatory, **Marneuli (Tamarisi)** borehole, Georgia (DSH)
Lat 41.436 N, Lon 44.755 E, Alt 397 meters



8 September 2012

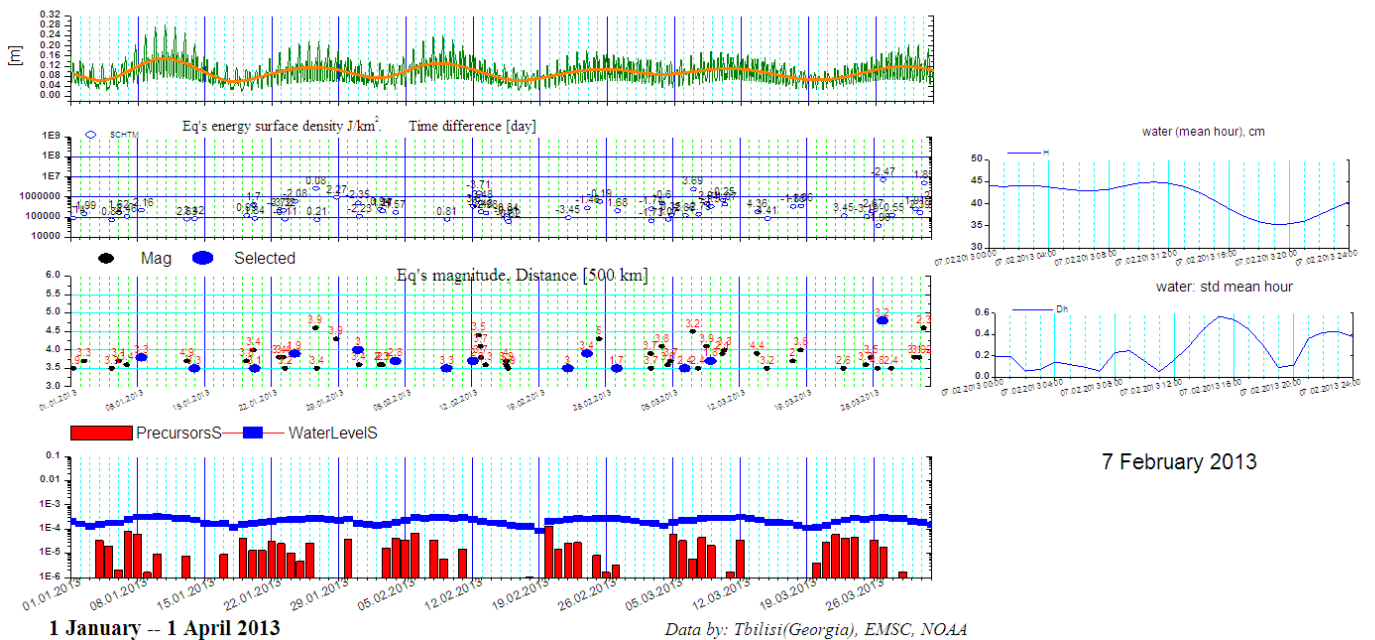
Data by: Tbilisi(Georgia), EMSC, NOAA

1 2 3 4 5 6

Georgia Boreholes Water Level and Earthquake's daily monitoring

Earth tide (Dennis Milbert, <http://home.comcast.net/~dmilbert/softs/solid.htm>)

Water Observatory, **Marneuli (Tamarisi)** borehole, Georgia (DSH)
Lat 41.436 N, Lon 44.755 E, Alt 397 meters



7 February 2013

Data by: Tbilisi(Georgia), EMSC, NOAA

Fig.3 Marneuli borehole daily monitoring (2012,2013)

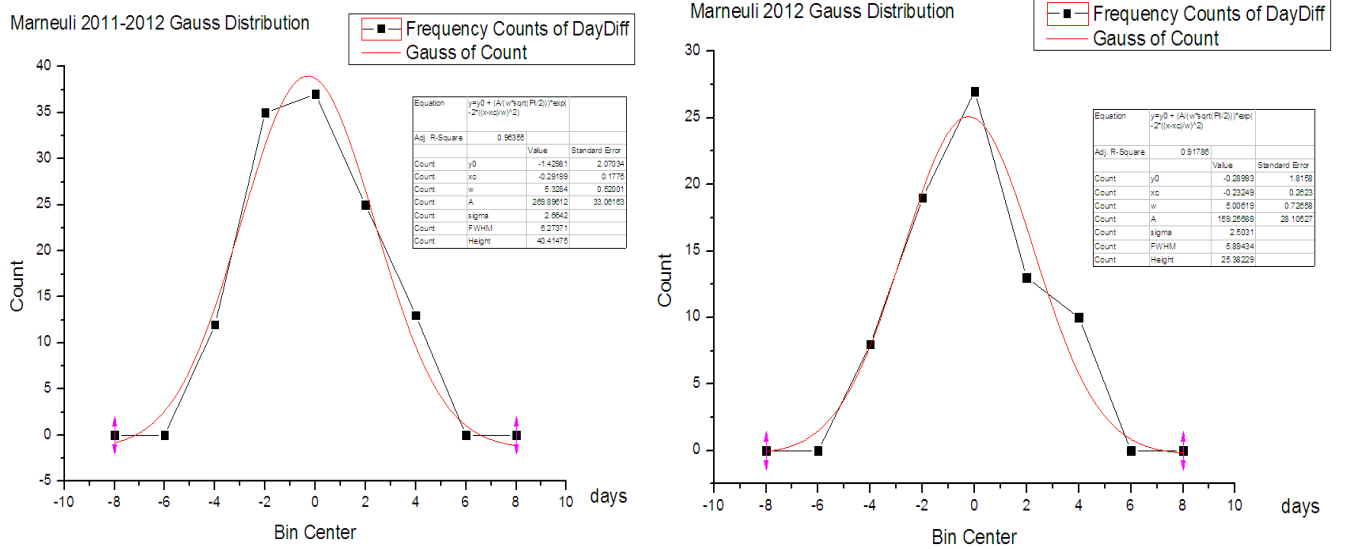


Fig.4 Marneuli borehole Gauss Distribution for day difference (2011-2012,2012)

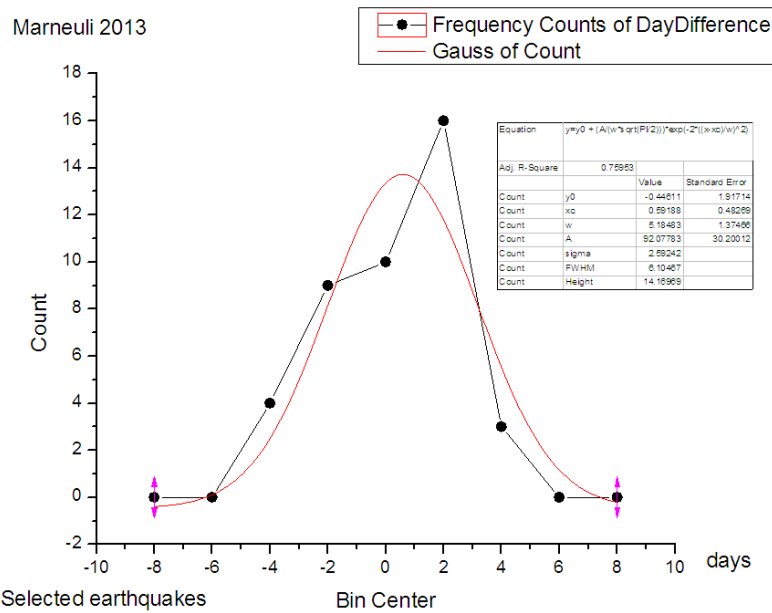


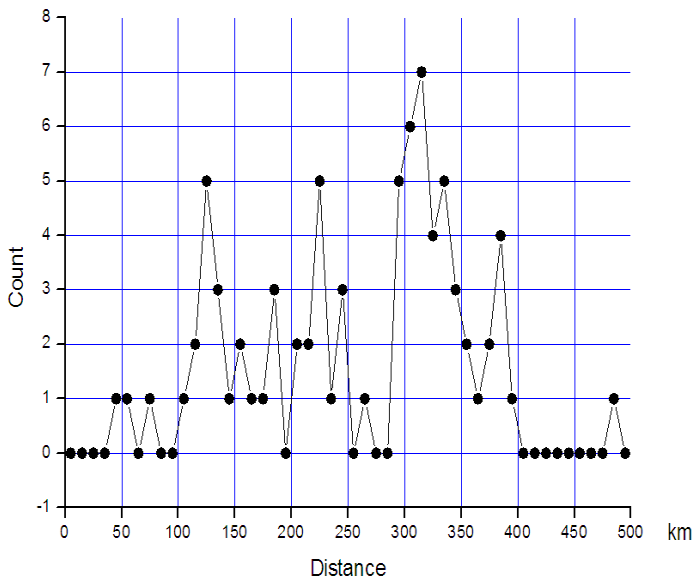
Fig.5 Marneuli borehole Gauss Distribution for day difference (2013)

From the figures 4 and 5 we see that the day difference distribution from 2011 until 2013 are described well by Gaussian curve with the R-square not less than 0.90.

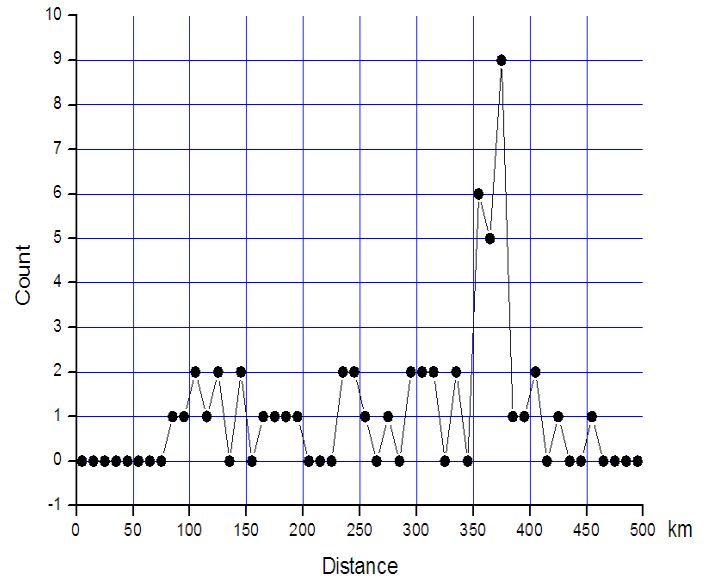
The figure 6 presents frequency count for the distance of the selected by precursors earthquakes with maximal energy density in monitoring point with increment 10 km.

The highest number of the earthquakes is at the distance 300-350 km (Turkey earthquakes), the earthquake at distance 350-450 km are Iran earthquakes and the other one that are at distance less than 300 km are regional local earthquakes.

Marneuli 2012 Selected quakes Distance -●- Distribution number of earthquake



Kobuleti 2012 Selected quakes Distance -●- Distribution number of earthquakes



Marneuli 2013

-●- Frequency Counts of Distance

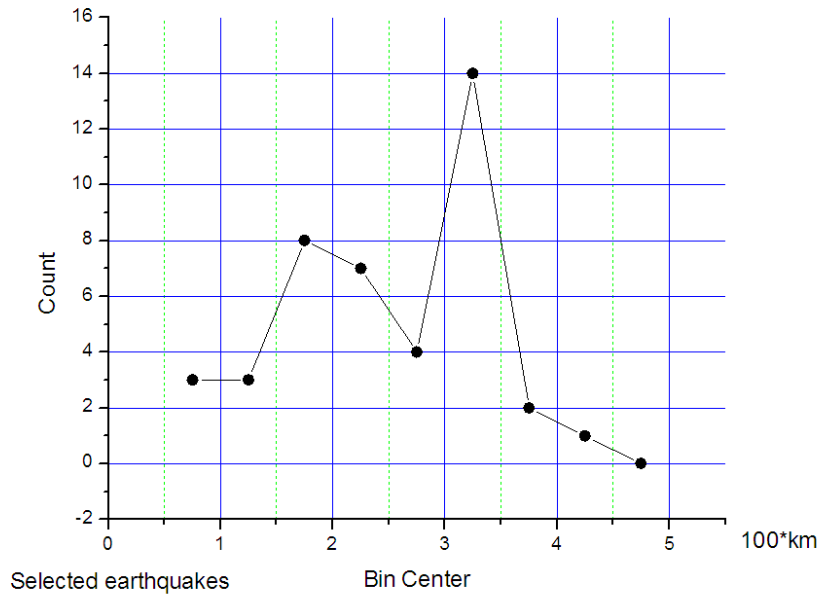


Fig.6 Two boreholes frequency counts for distance of selected by precursors quakes And frequency count of distance on Marneuli borehole 2013

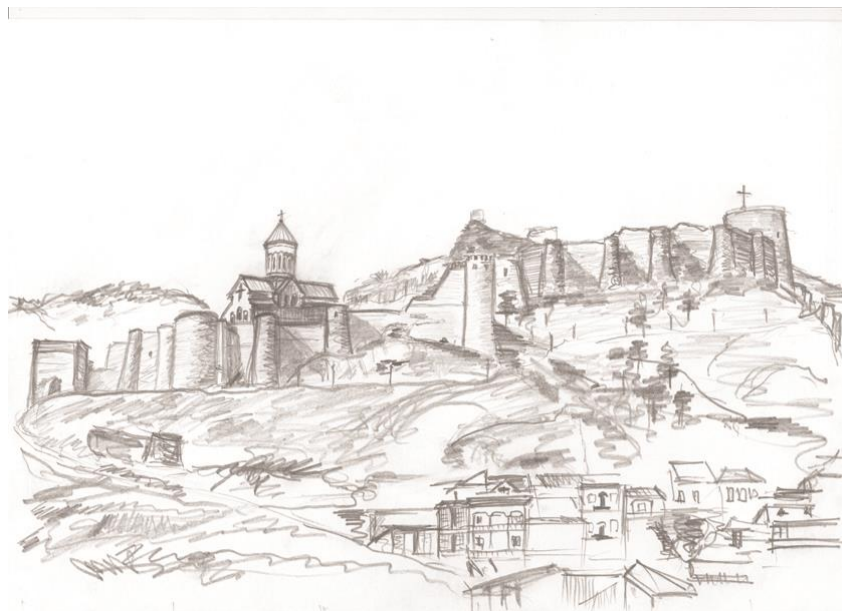
Conclusion

As conclusion we can say that the using in analogy of geomagnetic quake approach of daily boreholes water data level analyzes can serve as precursor of increasing regional seismic activity.

References

1. Venedikov A. P., Arnoso R., and Vieira R.: A program for tidaldata processing, Computer & Geosciences, 29, 4, 487–502,2003.
2. Tamrazyan G.P., Tide-forming forces and earthquakes, ICARUS, Vol.7, pp.59-65, 1967.

3. Mavrodiev S.Cht., Thanassoulas C., "Possible correlation between electromagnetic earth fields and future earthquakes", ISBN 954-9820-05-X, Seminar proceedings, 23-27 July, 2001, INRNE-BAS, Sofia, Bulgaria, 2001.
4. Knopoff L., Earth tides as a triggering mechanism for earthquakes, Bull. Seism. Soc. Am. 54:1865–1870, 1964.
5. Tamrazyan G.P., Tide-forming forces and earthquakes, ICARUS, Vol.7, pp.59-65, 1967.
6. Tamrazyan G.P., Principal ragularities in the distribution of major earthquakes relative to Solar and Lubar tades and other Cosmic forces, ICARUS, Vol.9, pp.574-592, 1968,15.
7. Venedikov A. and Arnoso R.: Program VAV/2000 for Tidal Analysis of Unevenly Spaced Data with Irregular Drift and Colored Noise, J. Geodetic Society of Japan, 47, 1, 281–286, 2001.
8. Alexandrov L., Program code REGN, PSR 165 RSIK ORNL, Oak Ridge, Tennessee,
9. Mavrodiev S.Cht., and Pekevski L., Complex Regional Network for Earthquake Researching and Imminent Prediction, Electromagnetic phenomena related to earthquakes and volcanoes, Editor: Birbal Singh, Publ., Narosa Pub. House, New Delhi, pp.135–146, 2008.
10. T. Chelidze, T. Matcharashvili, and G. Melikadze, Earthquakes' Signatures in Dynamics of Water Level Variations in Boreholes, In: Synchronization and Triggering: from Fracture to Earthquake Processes, Eds.V.de Rubeis, Z. Czechowski, R. Teisseyre, Geoplanet: Earth and Planetary Sciences, 2010, Vol. 1, Part 3, 287-304, DOI: 10.1007/978-3-642-12300-9_20, Springer.
11. G. Kobzev, G. Melikadze, T. Jimsheladze., New method of hydrodynamical data analyse, Workshop-ceminarmaterials "BlackSeaHazNet Series, Vol. 25-72, 2011, Tbilisi, Georgia
12. .A.Sborshchikovi, G.Kobzev, S.Cht.Mavrodiev, G. Melikadze BOREHOLES WATER LEVEL AND EARTHQUAKE'S DAILY MONITORING, Nano Studies 2013 8 203-212



Крепость Нарикала, Тбилиси Бойко Вачев'2013
Cidatel Narikala, Tbilisi Boyko Vachev'2013

CHANGE IN THE INTENSITY OF MANIFESTATION PRECURSORS AS IT APPROACHES THE TIME OF THE EARTHQUAKE

Hrachya Petrosyan

Survey for Seismic Protection, MES of RA, hrachikp@gmail.com

Summary: *First time in Armenia studied the change in intensity of manifestation precursors as we approach the time of the earthquake, in order to assess the most complex parameter predictive of future earthquake - his time. The emergence of short-term operational and precursors, likely indicates the occurrence of the last stage of the increasing destruction of rocks, the high intensity of the processes of destruction. These processes are often recognized: 1) the presence of anomalies in different orders, 2) the appearance of signals at a higher frequency, 3) a change in the intensity of manifestation of a precursor for several years before the event, 4) the rapid growth shortly before the earthquake characteristics (anomalies) on that accelerating oscillations are superimposed (availability regime with peaking).*

1. Introduction

Research on the prediction of earthquakes, according K.Kasahara is still at a stage where a significant role is played by empiricism. Hence the importance of documentation already occurred seismic events. The statistical approach to forecasting earthquakes play a major role periodicity of the sequence of earthquakes, as well as the correlation between earthquakes and other phenomena [1].

We have studied more than 650 anomalies and the various parameters which are reflected in more than 150 test anomalies-precursors 18 earthquakes with M from 3.7 to 7.7. Summary table of the parameters of earthquakes and tests are presented in [4, 5]. Each of the statistical properties of the studied anomalies reflects an average of more than 4 anomalies, therefore, are the subject of predictive test statistically significant anomalies. Forerunners differentiated by types (methods and parameters) and type (medium - ΔT over 1 year, early short ΔT for more than 3 months and less than 1 year later short - ΔT for more than 3 days and less than 3 months, operational - ΔT 3 days or less).

2. The results of the works

The time sequence of the appearance of precursors reflects the physical nature of the phenomena that cause abnormal variations of geophysical and other fields.

The sequence of steps of the earthquake preparation and development of the process of destruction of rocks reflected in the presence of anomalies of different orders, which are superimposed on each other as they approach the moment of formation of the main rupture during an earthquake. Example overlay anomalies of different orders is shown in fig.1.

C, ml/l

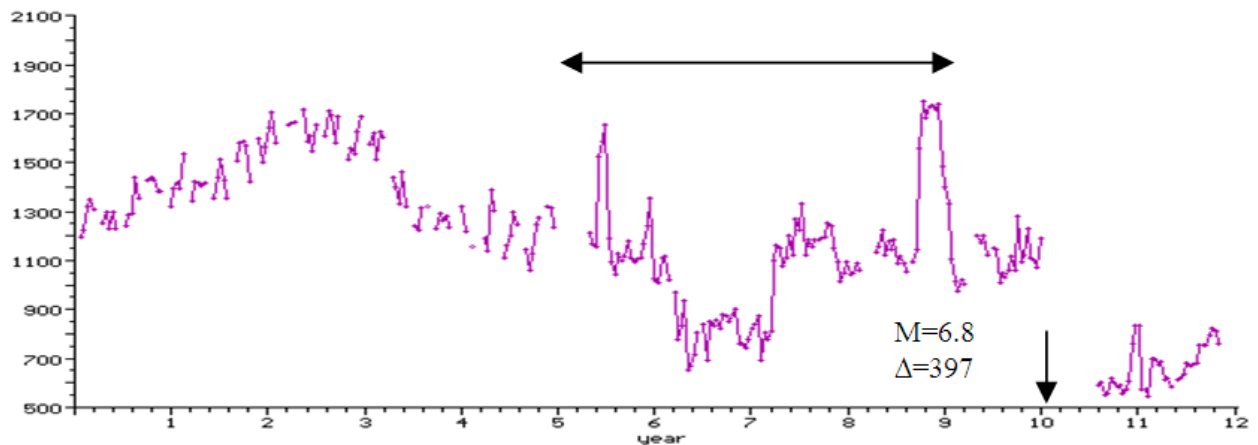


Fig.1. Changes in the concentration ($\text{mg/L} \times 10^{-6}$) dissolved in saline water helium on st. Kajaran Narman (Turkey 30.10.1983, $M=6.8$) earthquake.

As we approach the moment of formation of the main break on time series signals appear at a higher frequency, which distort the shape of the time series, without changing its course. An example is shown in fig.2.

H, m

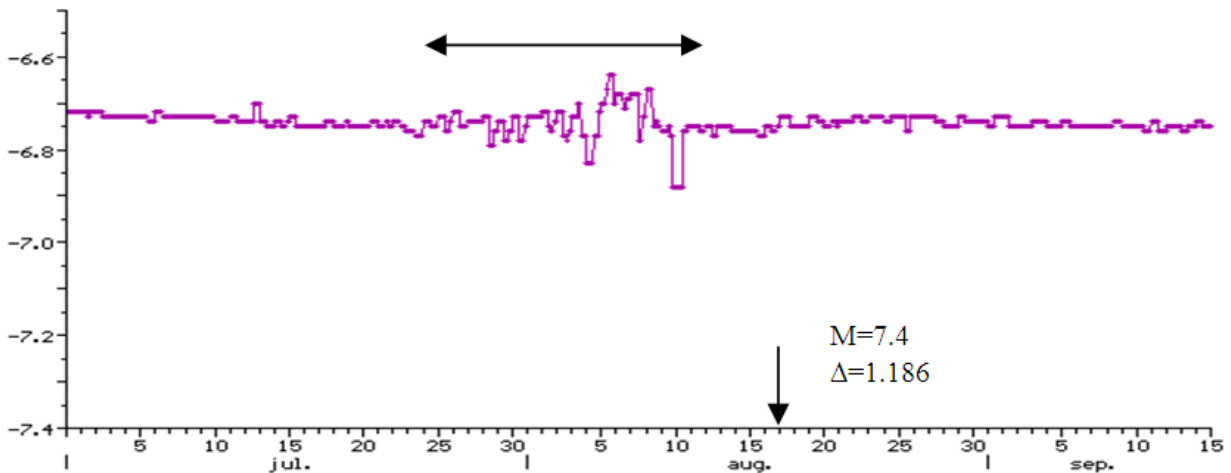


Fig.2. Variations of groundwater levels at the st. Ashotsk.

Izmit (Turkey 17.08.1999, $M=7.4$) earthquake

Change in the intensity of manifestation precursor as we approach the seismic event often begins several years before the event. This pattern is most often manifested in variations in groundwater levels, as changes HGD-field are a direct deformometer that reflects changes in the stress-strain state of the earth's crust. Below is an example of anomalous decrease of groundwater level, reflecting the expansion processes in the earth crust in the areas of installation HGD-monitoring station (fig.3).

H, m

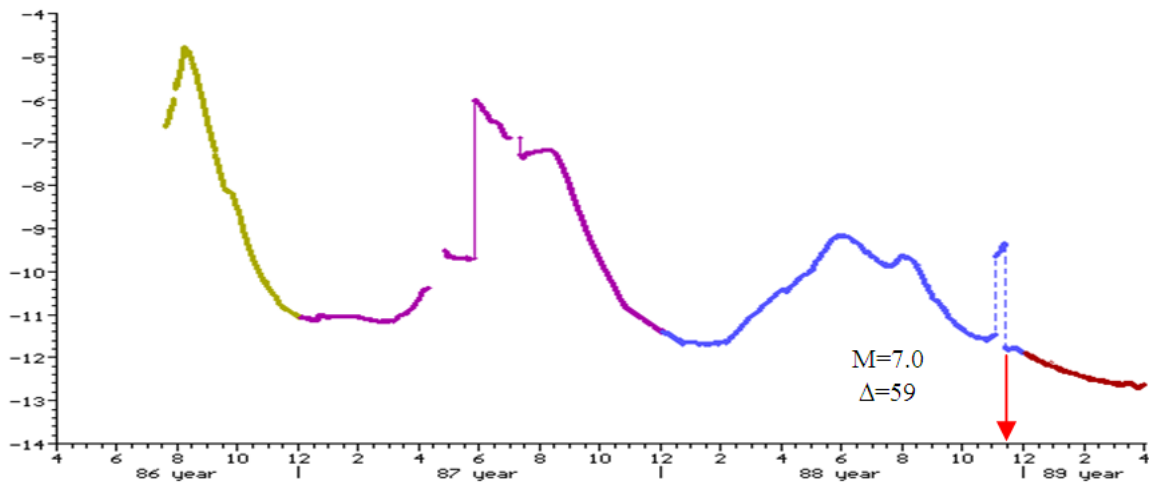


Fig.3. Changes in groundwater levels at the st. Noyemberyan.

Spitak (07.12.1988, M=7.0) earthquake.

G.G.Malinetsky and S.P.Kurdyumov [2] believe that "graphics behavior characteristics describing complexly organized hierarchical system-tectonic fault-just before a catastrophe demonstrate fastest growth, which accelerating oscillations are superimposed. It should be noted that the asymptotic behavior of such processes before the disaster is the so-called blow-up regime (where one or more variables characterizing the system in a finite time grow to infinity)". As a typical type of dependence arising before disasters in complex systems, the authors present the development of geochemical precursors of earthquakes 17.01.1995, M=6.9 in Kobe (fig.4).

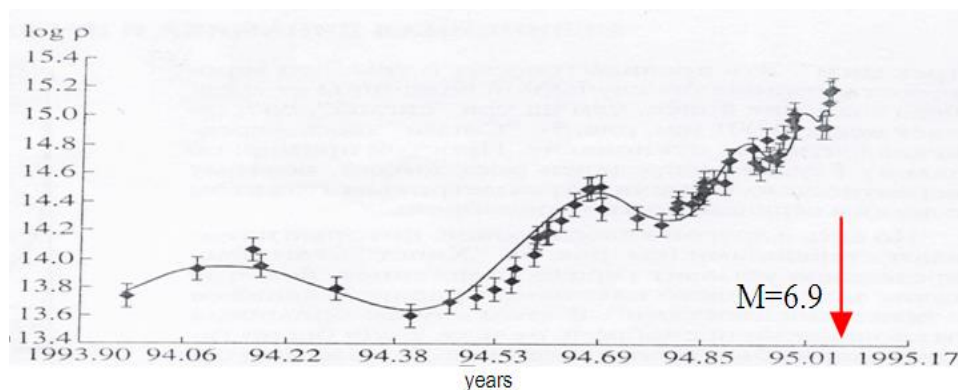


Fig.4. Time dependence of the logarithm of the concentration of chloride ions in the springs before the catastrophic earthquake in Kobe (Japan) in 1995. Point - it's accurate, solid curve - smoothed dependence of constructed on them [2].

As rightly consider the authors of [2], in order to improve the quality of the forecast, we need long series of reliable and sufficiently accurate data describing the different aspects of the studied object.

That such data are available in the database NSSP. On the current understanding of self-organized criticality (SOC), which in the annex to describe the interaction of Seismology

discontinuities of different ranks, the collective effects and acceleration of their formation before a strong earthquake, based in their research and known seismologists G.A.Sobolev and A.V. Ponomarev [3].

We estimate in the light of these ideas, the behavior of all test anomalies-precursors ("characteristics") included in the catalog of earthquake precursors tested [4, 5]. Field displays all 11 precursors and strong regional ($M \geq 6.0$) and 7 local and tangible ($3.7 \leq M \leq 5.0$) seismic events is shown in fig.5.

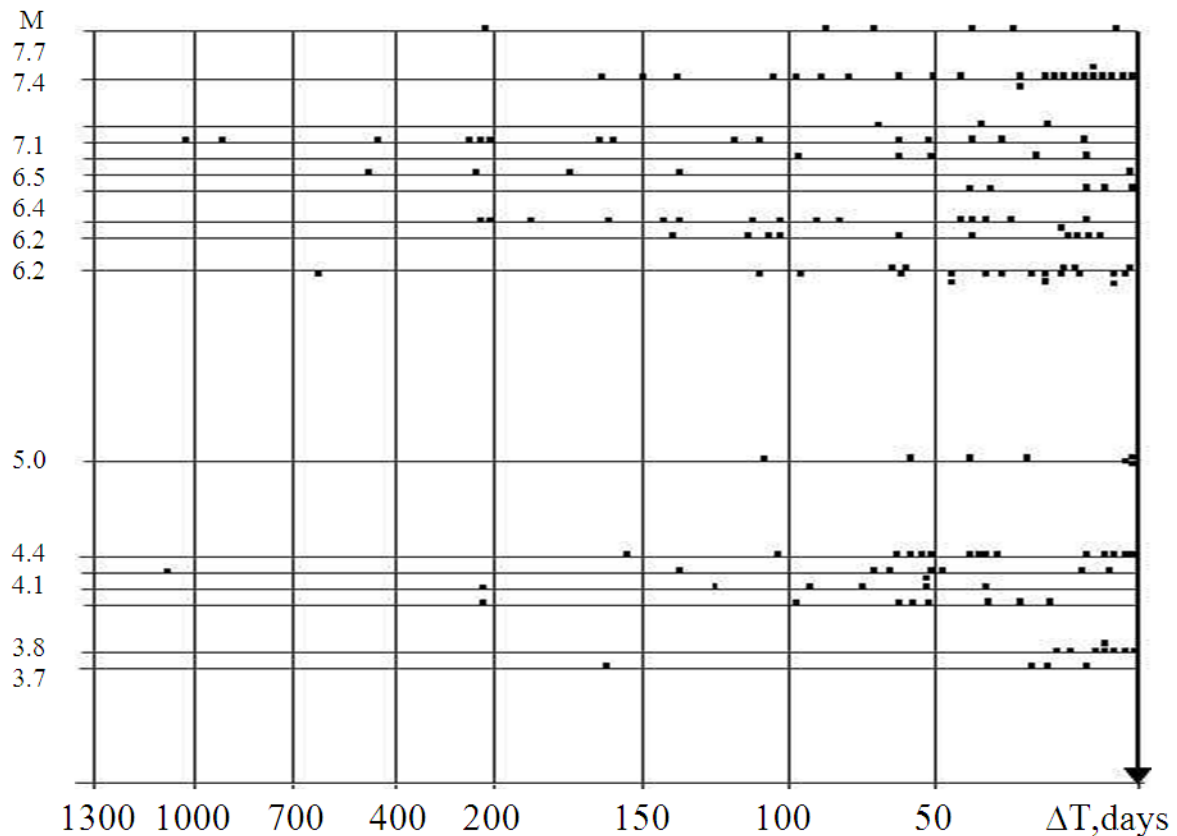


Fig.5. Field displays all the precursors 18 and earthquakes. Arrow denotes the combined time of all earthquakes, the dots represent precursors, M-magnitude earthquake tested, ΔT -times manifestations precursors.

As can be seen from fig.5, the number of precursors increases as the time of the earthquake as strong at both regional and local seismic events tangible. The greatest number of precursors and their diversity as parameters and according to the forms of manifestation is observed in the last 4 months before the event.

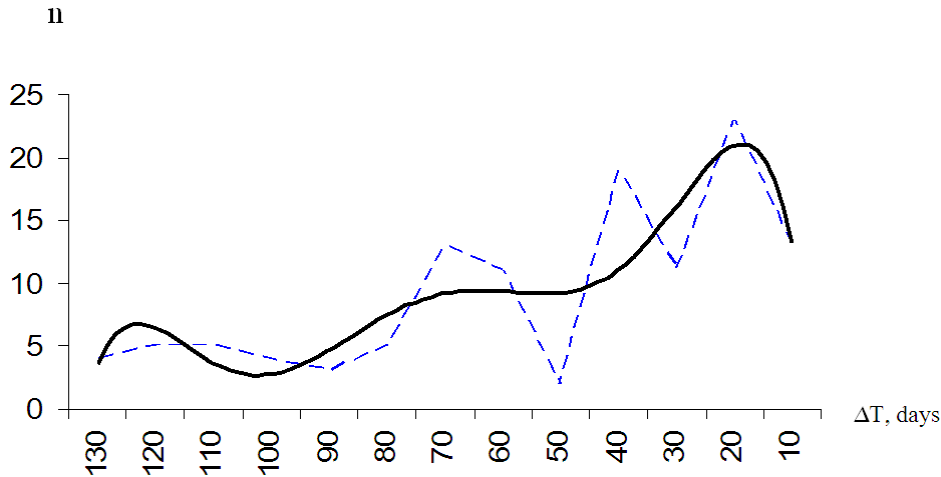


Fig.6. Changing the number of precursors of n in the last 4 months before the earthquake. The dashed curves are constructed from raw data, and solid curves-it smoothed dependence constructed from them.

More detailed picture of the increase in the number of precursors for all the events in the last 4 months before the seismic events (fig.5) is represented graphically in fig.6. Smoothed curve corresponds to a polynomial of order 6:

$$\hat{O} = -0.002x^6 + 0.068x^5 - 1.066x^4 + 8.089x^3 - 30.31x^2 + 51.11x - 24.26 \quad (1)$$

The resulting coefficients of the polynomial (1) reflect the increase in the number of precursors undulating n as approaching seismic events. At baseline and smoothed curves (fig.6) for all earthquakes for 100 days before the event there is an increase of the amplitude (the amount of precursors) and the change in frequency and curves themselves have a wave form. As mentioned above, the authors [2] argue that the graphics performance behavior shortly before the earthquake exhibit fast catastrophic growth, which accelerating oscillations are superimposed, where one or more variables describing a system in finite time grow to infinity (fig.4). In general, agreeing with them, we consider it necessary to note that in this case, there is one significant difference, namely shortly before earthquakes marked decrease in the number of precursors on average 20 days before the earthquake. In other words, reducing the number of precursors shortly before the earthquake an opportunity to assess the most difficult parameter predictive of future earthquake - his time.

3. Conclusions

Thus, we can draw the following conclusions:

1. Change in the intensity of manifestation of precursors on the territory of Armenia as it approaches the moment of the earthquake recorded:

- In the presence of anomalies of different orders,
- In the appearance of signals with a higher frequency,
- A change in the intensity of manifestation of a precursor for several years before the seismic event,
- Available modes with peaking (matching model criticality).

2. Have with peaking mode, in turn, reflected in the fact that:

- Maximum number of precursors and their diversity as parameters and according to the forms of manifestation is observed in the last 100 days before the event.
- Marked decrease in the number of precursors on average 20 days before the earthquake. An opportunity to assess the most complex parameter predictive of future earthquake - his time.

Literature:

- [1] K. Kasahara Mechanic earthquakes. M, Mir. 1985, p. 262 (on Russian).
- [2] G.G. Malinetskii, S.P. Kurdyumov Nonlinear dynamics and prediction problems. Herald of the Russian Academy of Sciences, 2001, v.71, N.3, p. 210-232 (on Russian).
- [3] G.A. Sobolev, A.V. Ponomarev Physics of earthquakes and precursors. M., Nauka, 2003, p. 270 (on Russian).
- [4] Hrachya Petrosyan. Testing and earthquake prediction. Yerevan, publishing house "Surb-Ser", 2004, p.160 (on Russian).
- [5] Hrachya Petrosyan. Forerunners and prediction of earthquakes on the territory of the Republic of Armenia. Yerevan, publishing house "Phenomenon", 2009, p. 134 (on Russian).



Площадь Республики, Ереван Бойко Вачев'2013
Republic Square, Yerevan Boyko Vachev'2013

SOLAR, GEOMAGNETIC, CLIMATE AND SEISMIC IMPULSE VARIATIONS

Yavor Chapanov

National Institute of Geophysics, Geodesy and Geography,
Bulgarian Academy of Sciences, Sofia, Bulgaria

astro@bas.bg

Abstract:

The global environmental changes consist mainly of quasi harmonic oscillations with variable phases and amplitudes and irregular variations, containing abrupt changes due to several natural sources of impulse excitations. The direct determination of small data jumps is difficult, because the jump values are very small relative to the amplitudes of the seasonal, interannual, short and long terms of the observed periodical variations. A new useful method of data jumps determination in long time series is proposed. The method consists of time series integration and determination of parts with significant linear or parabolic trends. The parts with linear trends of integrated data correspond to the constant behavior of the original data, where the ends of the linear trends are the epochs of the impulse variations. The parts of integrated data with significant parabolic trends correspond to linear variations of the original data. This method is applied for determination of the impulse variations of various solar, geomagnetic and climate indices. The interconnection between these jumps and variations of ice sulfate deposits and annual earthquakes numbers is investigated.

1. Introduction

The modern knowledge uses time series of many years' permanent observations. The data contain some small residual systematic deviations due to instrument and station changes. Determination of the systematic deviations from the mean values was applied in (Chapanov et al., 2007, 2008; Gambis et al., 2011) by means of linear trends in integrated time series. This approach is used here in a method of data and velocity jumps detection by means of parabolic and linear trends in integrated time series.

2. Method description

The method of data jumps determination consists of several steps. The first step is a removal of linear trend from the original data, followed by the integration of the resulting time series. The new integrated time series consists of oscillations with the amplitudes smaller than in the original data and of the parts with visible piecewise significant linear or parabolic trends. The parts with linear trends of integrated data correspond to the constant mean behavior of the original data, the sudden changes of the linear trends occur at the epochs of the jumps in the original data. The parts of integrated data with significant parabolic trends point out to the linear variations of the original data. The second step of the method is the creation of the table containing all the epochs of data jumps. The next step consists in calculating the mean values or trends in the original data parts, corresponding to the table of jump epochs, and the last step is the calculation of jump values between neighboring data parts.

2. Time series integration

The time series are integrating numerically by the well known trapezoid rule. Let consider function f of argument x , discretized into $N+1$ equidistant points $f(x_i)$, $i=1, 2, \dots, N+1$. Let the first argument

$x_1=a$, and last argument $x_{N+1}=b$. Then the grid spacing is $h=(b-a)/N$ and the trapezoid approximation to the integral is

$$\int_a^b f(x) dx \approx \frac{h}{2} \sum_{k=1}^N (f(x_{k+1}) + f(x_k))$$

(1)

$$= \frac{b-a}{2N} (f(x_1) + 2f(x_2) + 2f(x_3) + \dots + 2f(x_N) + f(x_{N+1})).$$

When the grid spacing is non-uniform, we can use the formula

$$(2) \int_a^b f(x) dx \approx \frac{1}{2} \sum_{k=1}^N (x_{k+1} - x_k) (f(x_{k+1}) + f(x_k)).$$

To obtain integral of a given time series $f(t_i)$, $i=1, 2, \dots, N+1$ it is necessary to integrate N times the function f with boundaries $a=t_1$ and $b = t_i$, $i=2, \dots, N+1$.

3. Data and velocity jumps

The solar, geomagnetic, climate, volcanic and seismic data consist of time series of Total Solar Irradiance TSI, Wolf's numbers W_n , Equatorial Solar Asymmetry ESA, global Palmer Drought Severity Index PDSI, Mean Sea Level MSL at Stockholm, total ice core sulfate from Greenland GISP2 borehole and earthquakes numbers with magnitude $M>6.0$. The original time series of these data are presented in parts (a) of Figures 1-7, where the parts (b) present the integrated time series. Both integrated and original data in each Figure contain identical sets of trends in order to determine data or velocity jumps, whose epochs are shown in Table 1.

Table 1. Epochs of data and velocity jumps of: 1 – TSI; 2 - W_n ; 3 – ESA; 4 – PDSI; 5 – MSL, 6 – total sulfate; 7 earthquakes numbers $M>6.0$.

1	1644, 1703, 1725, 1750, 1782, 1811, 1835, 1885, 1915, 1935, 1962
2	1742, 1793, 1826, 1837, 1870, 1917, 1963
3	1878, 1890, 1901, 1914, 1936 , 1959, 1963, 1974, 1982, 1995, 2000
4	1886 , 1897, 1913, 1917, 1936, 1942 , 1952, 1974, 1982, 1995, 2000
5	1869 , 1882, 1890, 1900 , 1924, 1937, 1942, 1957 , 1980, 1992
6	1608, 1641, 1690, 1785, 1888, 1902, 1955, 1972
7	1963 , 1970, 1990, 1997, 2011

At least half of the epochs of data and velocity jumps in Table 1 may be explained by systematic data errors, especially for the epochs before 1900, because these epochs are not repeatable in different time series. These epochs are written in Normal font in Table 1. Repeated epochs in different time series are written in bold font, while close epochs are denoted by Italic font, so these epochs are supposed to belong to common physical effects of solar-terrestrial-climate influences.

The largest set of common data and velocity jumps belong to equatorial solar asymmetry and climate index of dry/wet cycles PDSI. A few mean sea level jumps are connected with the solar or climate jumps. The abrupt increase of sulfate deposit in 1902 is probably connected with solar activity jump in 1901. We may suppose that sulfate jumps in 1955 and 1972 affect MSL jump in 1957 and climate change in 1974.

(a)

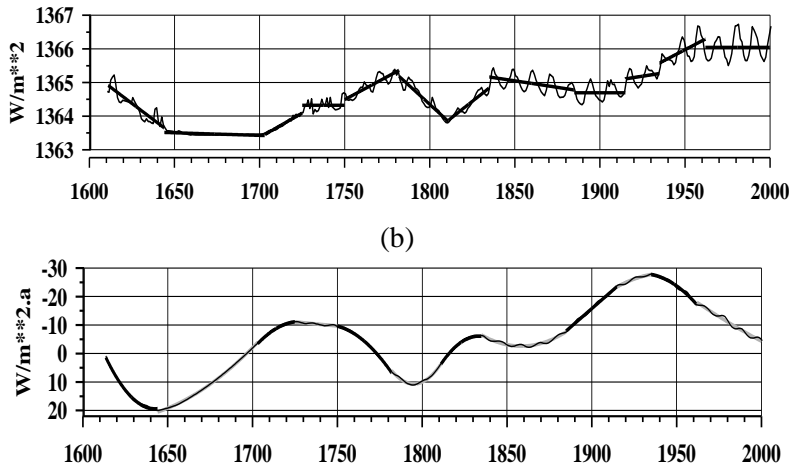


Figure 1. TSI jumps for the period 1600 - 2000: (a) – original data, (b) – integrated time series

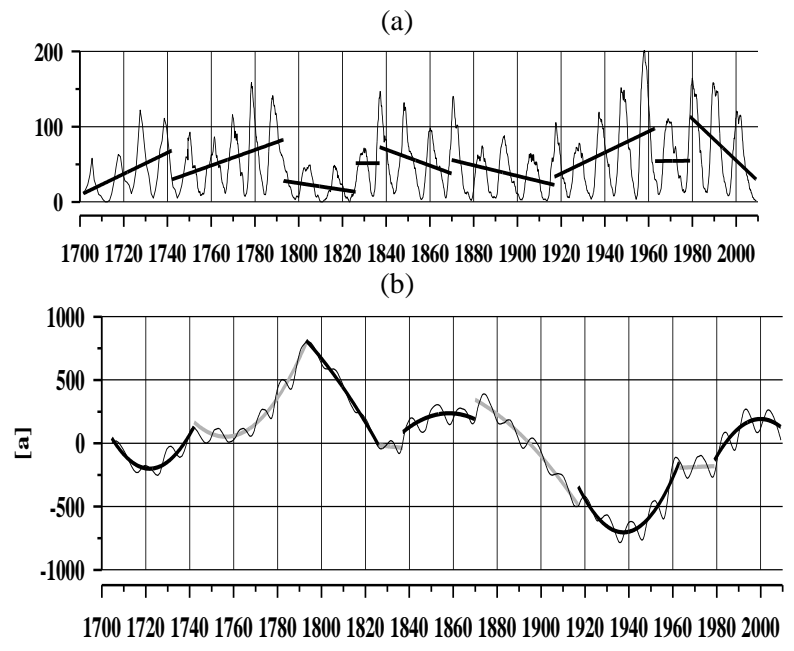


Figure 2. Wolf's numbers: (a) – original data, (b) – integrated time series

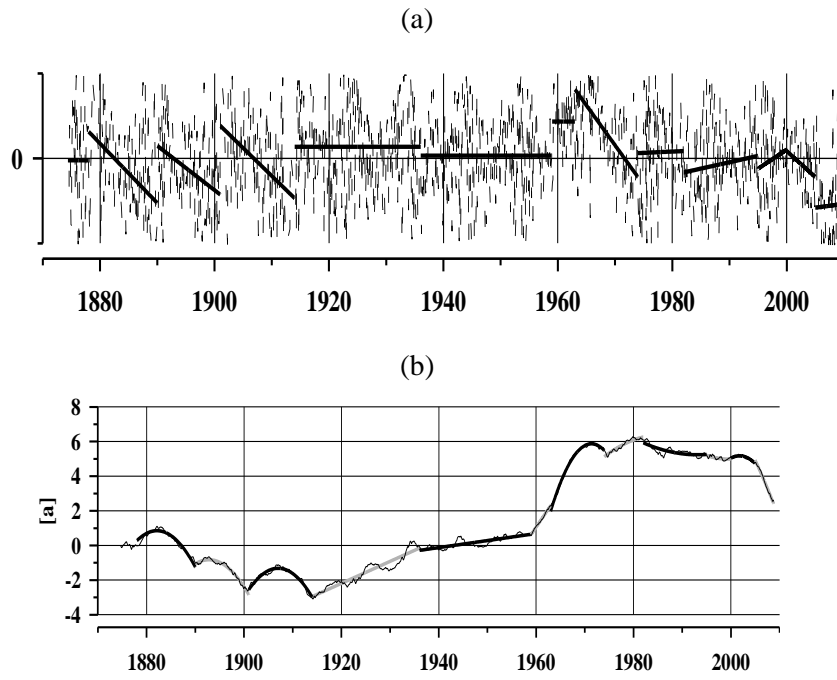


Figure 3. Equatorial solar asymmetry: (a) – original data, (b) – integrated time series

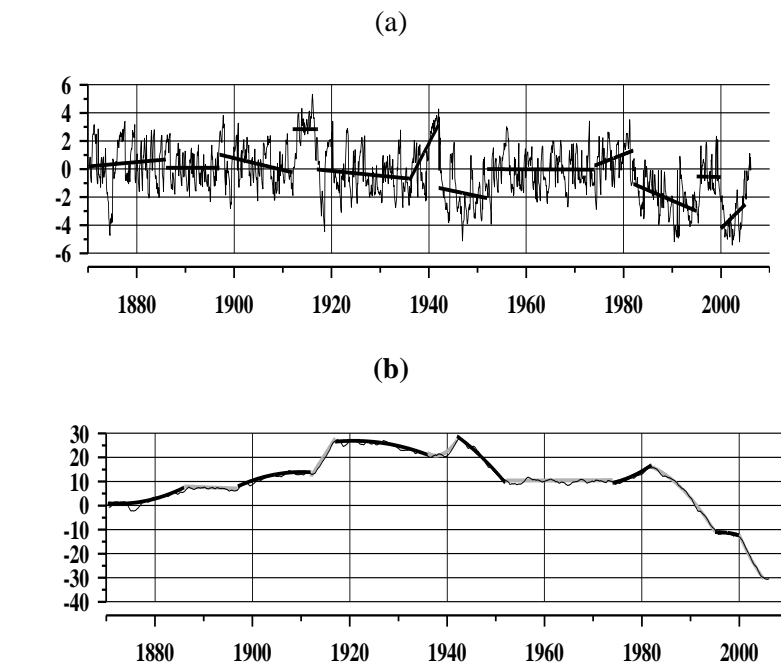


Figure 4. Global Palmer Drought Severity Index PDSI: (a) – original data, (b) – integrated time series

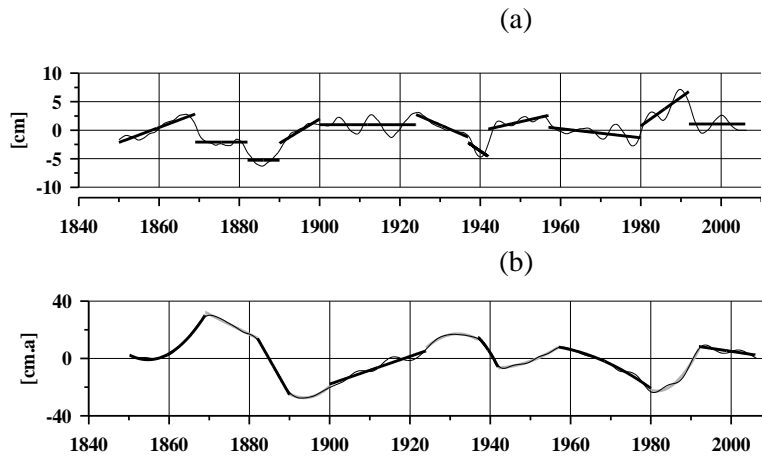


Figure 5. Mean sea level jumps: (a) – original data, (b) – integrated time series

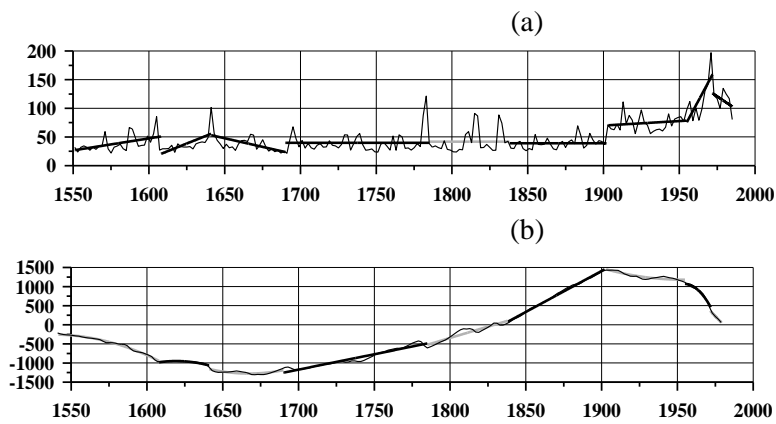


Figure 6. Total ice core sulfate jumps: (a) – original data, (b) – integrated time series

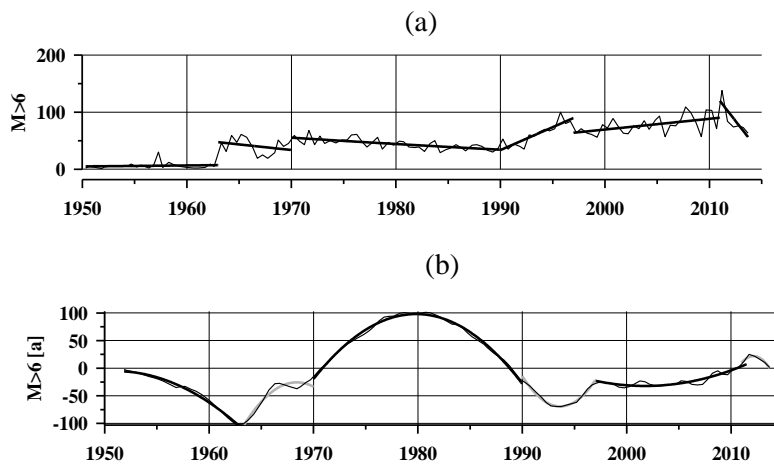


Figure 7. Earthquakes number $M > 6$ jumps: (a) – original data, (b) – integrated time series

4. Conclusions

The method of data and velocity jumps determination based on the linear and parabolic trends in the integrated time series is highly sensitive to any impulse behavior of the observed variations due to various geophysical processes like earthquakes, tornadoes, hurricanes, geomagnetic jerks or to some systematic data deviations.

The method is extremely sensitive to small data jumps hidden inside the level of random noise and high frequency oscillations of the data, because the integrated time series obtain almost zeroed amplitude of high frequency elements, while the original data with mean linear or constant behavior obtain magnitude in the integrated time series as large as the time intervals of these parts.

Most jumps of solar, geomagnetic, climate, volcanic and seismic data are not connected with other natural jumps, so it is possible to suppose their artificial origin as systematic errors.

Some jumps have common epochs, so their natural origin is supposed. The largest set of common data and velocity jumps belong to equatorial solar asymmetry and climate index of dry/wet cycles PDSI. A few mean sea level jumps are connected with the solar or climate jumps. The abrupt increase of sulfate deposit in 1902 is probably connected with solar activity jump in 1901. We may suppose that sulfate jumps in 1955 and 1972 affect MSL jump in 1957 and climate change in 1974.

References:

Chapanov, Ya., C. Ron, J. Vondrák, 2007, Proc. "Journées Systemes de Reference Spatio-Temporels", N. Capitaine (ed.), ISBN 978-2-901057-59-8, Observatoire de Paris, 2008, 208-209.

Chapanov, Ya., D. Gambis, 2008, AIP. Conf. Proc. Vol. 1043 "Exploring the Solar system and the Universe", ISSN 0094-243X, ISBN 978-0-7354-0571-4, Melville, New York, 218-219.

Gambis, D., D. Salstein, Ya. Chapanov, 2011, Proc. "Journées Systemes de Reference Spatio-Temporels", N. Capitaine (ed.), ISBN 978-2-901057-59-8, Observatoire de Paris, 2011, 208-209.



БАН и Софийският университет, от цикъла „БАН – ракурси“

Бойко Вачев'2005

BAS and Sofia University, from cycle "BAS - Racources"

Boyko Vachev'2005

SEISMIC AND VOLCANIC VARIATIONS DRIVEN BY SOLAR AND GEOMAGNETIC CYCLES

Yavor Chapanov¹

¹ National Institute of Geophysics, Geodesy and Geography,
Bulgarian Academy of Sciences, Sofia, Bulgaria

astro@bas.bg

Abstract:

The interannual and long term variations of the seismic and volcanic activity are compared with corresponding solar and geomagnetic cycles. The volcanic activity are presented by the data of the volcanic sulfate record in the GISP2 ice core from Greenland during the rapidly changing climate of the Pleistocene-Holocene transition. The seismic activity is determined by the annual earthquakes numbers from the Centennial Earthquake Catalog (Engdahl and Villaseñor, 2002), placed at the USGS server. The earthquakes numbers are separated into files according earthquakes with magnitude greater than 4.0; 5.0; 6.0 and 7.0. The solar variations are determined by the sunspot and Wolf,s numbers and reconstructed total solar irradiance variations. Partial correlation between the Schwabe and Hale solar cycles and the decadal variations of seismic and volcanic activity exists. The interannual seismic and volcanic variations show good agreement with corresponding variations of the geomagnetic index AA and equatorial solar asymmetry.

1. Introduction

The earthquakes and volcanic eruptions are the results of material circulation in the Earth that appear near the Earth's surface. Volcanoes and earthquakes have a lot in common. They both occur mostly near to the boundaries of tectonic plates. They have potential to cause significant damage. Volcanic eruptions are caused by the tectonic plates shifting and that can cause earthquakes. The seismic and volcanic activities cause frequent natural disasters in many Earth regions. It is necessary to study not only earthquakes and volcanoes themselves but also all processes affecting their activities to predict earthquakes and volcanic eruptions. The solar and geomagnetic activity affect significantly seismic and volcanic variations. The correlation between some solar and geomagnetic indices is presented in this work.

2. Time series data

The data consist of several time series of solar and geomagnetic indeces, earthquakes and sulfate content in Greenland ice core. The solar indeces are represented by sunspot numbers over the South S_s and North S_n solar hemisphere since 1875 (Fig.1), the Wolf's numbers (Fig.3) and their derivatives – index of equatorial solar asymmetry S_a (Fig.2) and extended time series of 22-year variations of Wolf's numbers, determined by sign alternation of even 11-year Schwabe cycles (Fig.3). The index of equatorial solar asymmetry S_a is a function of sunspot numbers S_s and S_n :

$$(1) \quad S_a = (S_n - S_s) / (S_n + S_s).$$

The index of equatorial solar asymmetry S_a vary frequently between -1 and +1 (Fig.2), so the long-period signals of S_a (Fig.2, bold line) are determined by Vondrák-Whitaker filtration (Vondrák, 1969, 1977).

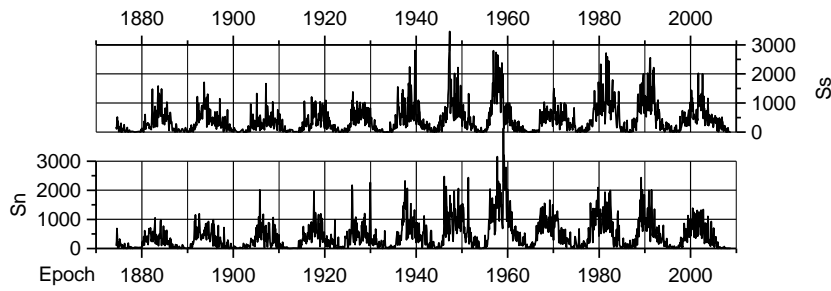


Figure 1. Numbers of solar spots over South solar hemisphere S_s (top graph) and over North hemisphere S_n (bottom graph).

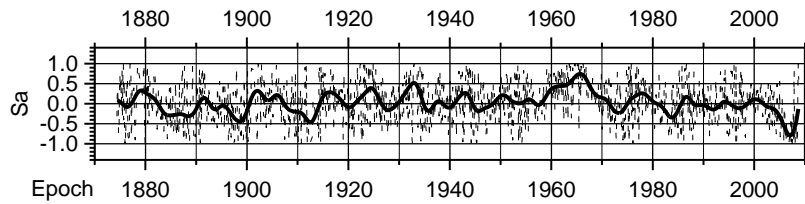


Figure 2. Equatorial solar asymmetry index S_a (dashed line) and smoothed curve of its long-term variations (bold line).

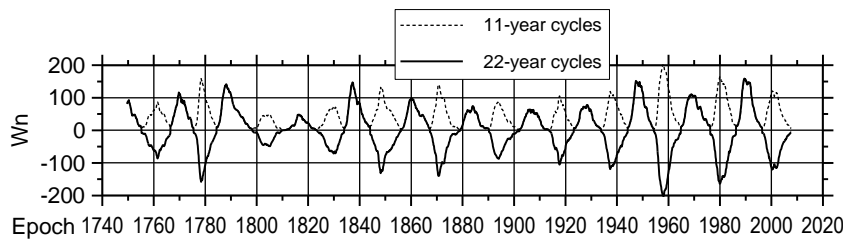


Figure 3. Wolf's numbers W_n (dashed line) and extended time series of 22-year variations (bold line).

The sulfate data contain the volcanic sulfate record from Greenland borehole GISP2 (Hempel and Thyssen, 1992; Palais et al., 1991). Each sample is approximately bi-annual for the last 12000 years with a consistent increase in the time covered by each sample to around 50 years/sample at 110,000 years ago (Mayewski et al., 1997). The volcanic sulfate record is derived by applying an empirical orthogonal function (EOF) analysis on the entire glaciochemical time series (Mayewski et al., 1997). EOF 5 was found to explain 12% of the variance in the sulfate record, but it did not significantly explain the variance in any other chemical species. The excellent correlation in the EOF time series and the volcanic sulfate record for the last 9000 years, based on sulfate residuals over a robust spline (Zielinski et al., 1994a) indicates that EOF5 is an indicator of volcanic sulfate deposition over the last 110,000 years.

The calculated volcanic sulfate data (Fig.4, b) contain a lot gaps or zero data parts and their harmonically analyses is difficult. The time series of the total and volcanic sulfate content correlate significantly, so it is preferable to use the time series of total sulfate content than the extracted time series of volcanic sulfate.

The seismic data (Fig.5) contain the number of earthquakes since 1900 with magnitudes $M > 7.0$; $M > 6.0$; $M > 5.0$ and $M > 4.0$, presented at the server of the US National Earthquake Information Center (NEIC).

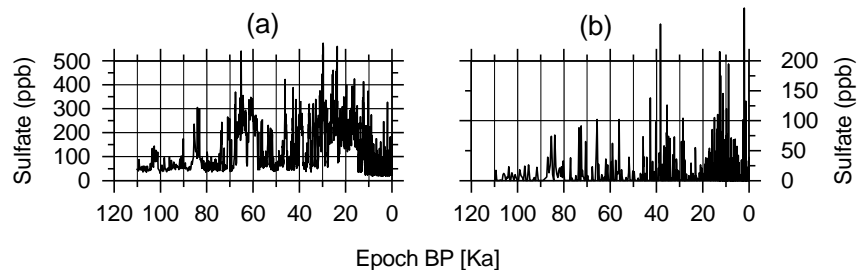


Figure 4. Sulfate record in the Greenland GISP2 ice core: total sulfate content (a) and volcanic sulfate record, derived by empirical orthogonal function (b). The time is thousand years before present (BP).

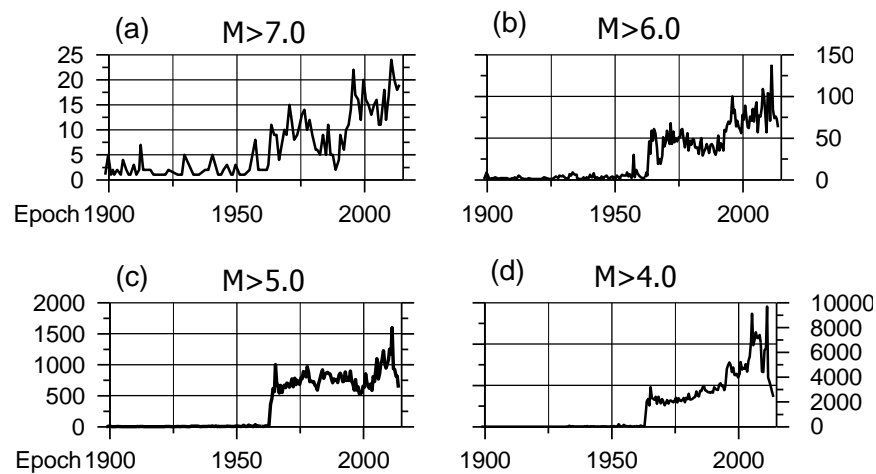


Figure 5. Numbers of earthquakes for the period 1900 – now with magnitudes $M>7.0$ (a); $M>6.0$ (b); $M>5.0$ (c) and $M>4.0$ (d).

3. Common 11- and 22-year cycles of solar, volcanic and seismic activity

The 11-year cycles of volcanic activity are determined by 5 harmonics with periods between 11a and 11.5a of the partial Fourier approximation of total sulfate for the period 1850-1985. The 11-year and 22-year of seismic activity are derived as a single wave from the numbers of earthquakes with magnitudes $M>4.0$ for the period 1968 – now.

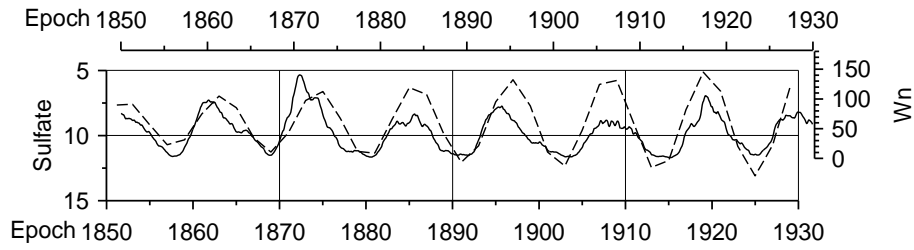


Figure 6. Comparison between the Wolf's numbers and 11-year sulfate cycles for the period 1850-1930.

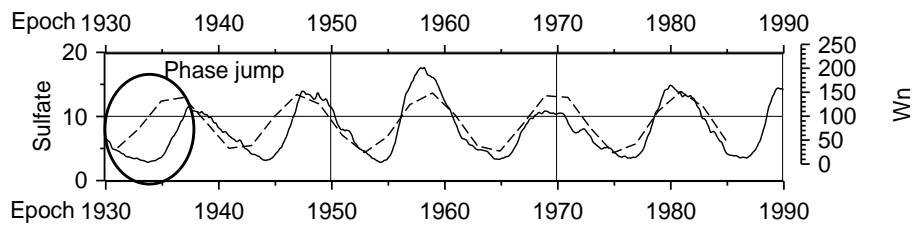


Figure 7. Comparison between the Wolf's numbers and 11-year sulfate cycles for the period 1930-1990.

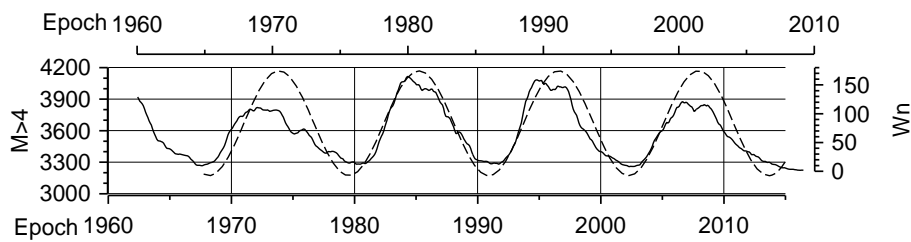


Figure 8. Comparison between the Wolf's numbers and 11-year cycles of numbers of earthquakes with magnitude $M > 4.0$.

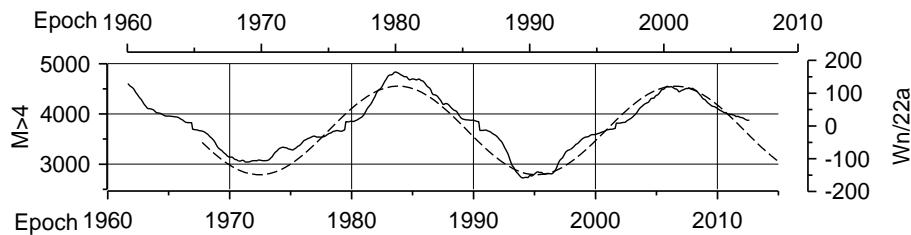


Figure 9. Comparison between 22-year cycles of solar activity and numbers of earthquakes with magnitude $M > 4.0$.

The comparison between the Wolf's numbers and 11- and 22-year cycles of volcanic and seismic activity yields excellent agreement (Figs. 6-9). The dependence of volcanic activity from the solar activity is broken in 1930, when significant phase jump occurred.

4. Equatorial solar asymmetry and geomagnetic influence on volcanic and seismic activity

The long-term variations of equatorial solar asymmetry, geomagnetic index AA, volcanic and seismic activity are compared in Figs. 10 and 11.

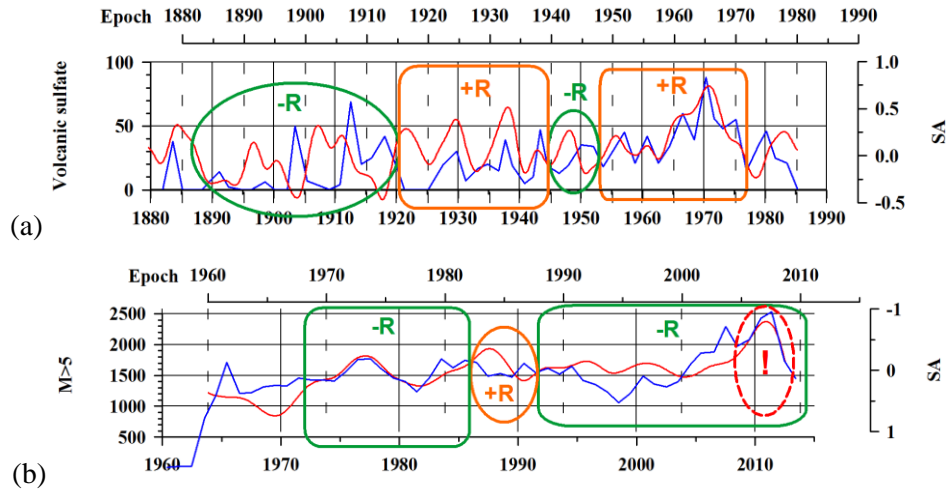


Figure 10. Comparison between long term cycles of equatorial solar asymmetry and volcanic sulfate (a); and numbers of earthquakes with magnitude $M>5.0$ (b). The positive/negative correlation is denoted by +R/-R.

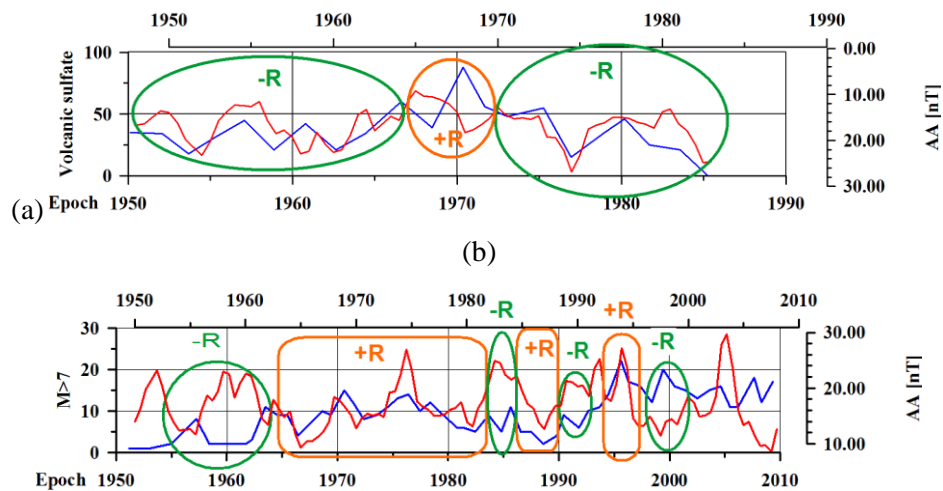


Figure 11. Comparison between long term cycles of geomagnetic index AA and volcanic sulfate (a); and numbers of earthquakes with magnitude $M>7.0$ (b). The positive/negative correlation is denoted by +R/-R.

The long-term variations of volcanic and seismic activity agree relatively well with the solar S_a and geomagnetic AA indices, taking into account several abrupt phase reverses, followed by sign change of the correlation coefficient. It is remarkable that the maximum of sulfate variations in 1970 and earthquakes numbers in 2011 agree with local extrema of equatorial solar asymmetry with a delay of about 3-5 years.

5. Conclusions

The total sulfate variations in the ice core contain 11-year signals partially correlated with the Wolf's numbers due to phase inverse in 1930. The 11-year and 22-year cycles of earthquakes numbers are highly correlated with Wolf's numbers since 1968 with 2 years delay.

Significant correlation between equatorial solar asymmetry and sulfate/earthquakes variations exists with 3 - 5 years delay and alternation between the positive and negative correlation coefficient. Excellent agreement between the local extrema of equatorial solar asymmetry variations and sulfate maximum in 1970 and earthquakes maximum in 2011 exists.

Minor geomagnetic effect on volcanic and seismic activity – partial correlation with phase reverse exists

References:

- Engdahl, E.R., and A. Villaseñor, Int. Handbook of Earthquake and Eng. Seismology, Part A, Chapter 41, pp. 665–690, Ac. Press, 2002.
- Engdahl, E.R., R. van der Hilst, and R. Buland, Bull. Seism. Soc. Am. 88, 722–743, 1998.
- Hempel, L., and F. Thyssen. 1992. Polarforschung 62, 11-16.
- Mayewski et al., 1997. Journal of Geophysical Research 102, 26345–2636
- Palais, J.M., M.S. Germani, and G.A. Zielinski. 1992. Geophysical Research Letters 19, 801-804
- Palais, J.M., K.C. Taylor, P.A. Mayewski, and P.M. Grootes. 1991. Geophysical Research Letters 18, 1241-1244.
- Vondrák, J.: 1969, Bull. Astron. Inst. Czechosl., 20, 349–355.
- Vondrák, J.: 1977, Bull. Astron. Inst. Czechosl., 28, 84–89.
- Zielinski, G.A., and G.R. Mershon. 1997. Geological Society of America Bulletin 109, 547-559.
- Zielinski, G.A., R.J. Fiacco, P.A. Mayewski, L.D. Meeker, S.I. Whitlow, M.S. Twickler, M.S. Germani, K. Endo, and M. Yasui. 1994. Geophysical Research Letters 21, 2365-2368.



„А нам нужна одна победа ...”, Одесская опера, 9 мая
„And we need one victory ...”, Odessa Opera, 9 of May

Бойко Вачев'2012
Boyko Vachev'2005

MILLENNIAL CYCLES OF MEAN SEA LEVEL AND EARTH ROTATION EXCITED BY TOTAL SOLAR IRRADIANCE VARIATIONS

Yavor Chapanov¹, Cyril Ron², Jan Vondrák²

¹National Institute of Geophysics, Geodesy and Geography, Bulgarian Academy of Sciences, Sofia,
Bulgaria, astro@bas.bg

²Astronomical Institute, Academy of Sciences of Czech Republic

Abstract:

The millennial cycles of the solar activity affect all geosystems, accompanied by global environmental changes. These cycles strongly affect Earth climatic variations, providing significant cooling effect especially over the polar ice, leading to decreasing the Mean Sea Level (MSL) and the principal moment of inertia C during the solar grand minima which is revealed by acceleration of the Earth rotation. The cooling effect is amplified significantly by the 2300-year Hallstatt cycles. The millennial solar-terrestrial influences simultaneously affect isotope content in the tree rings and ice boreholes, continental polar ice thickness, mean sea level, principal moments of inertia and Earth rotation. The common cycles of the solar activity, climate and Earth rotation are studied by means of reconstructed time series of the Total Solar Irradiance (TSI) for the last 9300 years, reconstructed MSL variations for the last 83Ka and Antarctica temperature variations for the last 800Ka. The millennial oscillations of the Earth rotation for the last 83Ka are reconstructed from the MSL variations on the assumption of angular momentum conservation. The models of the millennial cycles of the MSL, temperature and solar activity are proposed as Fourier approximations with different main periods, equal to 2300a, 4600a and 9200a. The proper values of the millennial Hallstatt cycles of the TSI and temperature are determined by varying the main period from 2200a to 2400a with 5-year steps, where the amplitudes have maxima when the periods are close to their real values.

2. Introduction

The Sun is the main energy source for all surface geosystems, including climate, weather, Mean Sea Level MSL, winds, rainfalls and etc. The essential energy transfer from the Sun to the Earth is the Total Solar Irradiance (TSI), which variations during the solar activity cycles cause various changes on the Earth surface. The climate and mean sea level response to the solar activity consists of cycles whose periods are close to the well known solar decadal, centennial and millennial periods and their harmonics. The 2300-year Hallstatt cycle, 6000-year cycle (Xapsos and Burke, 2009) and 11500-year cycle (Shopov et al., 2004) are the known millennial solar cycles. The millennial Earth rotation variations are reconstructed by a model based on dependence of inertial moment variations due to mean sea level and polar ice oscillations. The common millennial MSL, mean temperature and Length of Day (LOD) variations are compared with the corresponding variations of TSI. The periods of millennial oscillations of TSI and mean temperature are evaluated.

3. Data

The data consist of Mean Sea Level (MSL) for the period 13000-83000 before present (BP, epoch 1950, Arz et al., 2007, Fig.1, a), Antarctica Dome C ice core temperature variations for the past 800Ka (Jouzel et al., 2007, Fig.2, a), time series of Total Solar Irradiance (TSI) with duration 9300a (Steinhilber et al., 2009, Fig.3, a). The long term trends and periodicities below 10Ka (Fig. 1, 2, b) are determined by Fourier approximations and proper choice of harmonics. The superposition of 2300a TSI cycles and its harmonics yields significant cooling effect (Fig.3, b).

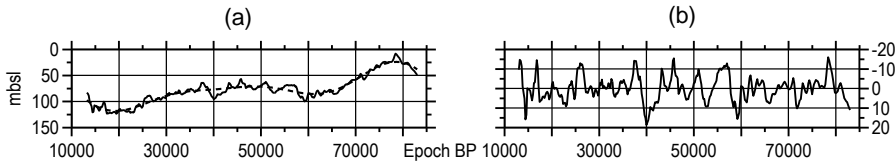


Figure 1. MSL variations (a, bold line), meters before sea level (mbsl), long term trend (a, dashed line) and periodicity below 10Ka (b).

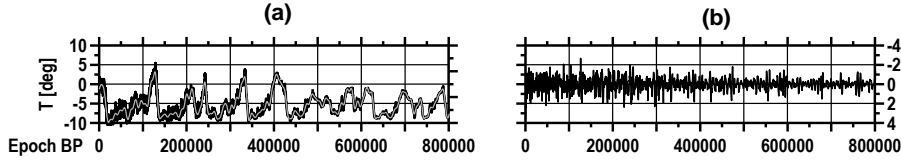


Figure 2. Antarctica Dome C ice core temperature variations (a, black), long terms (a, gray) and periodicity below 10Ka (b).

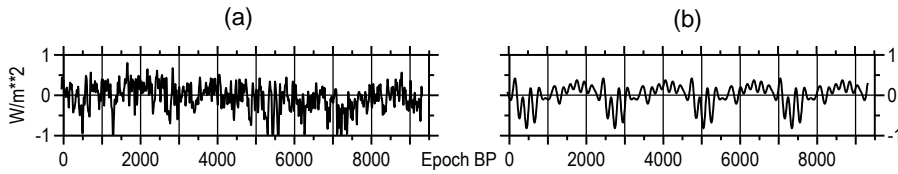


Figure 3. Total Solar Irradiance (TSI) variations (a), and cooling effects of 2300-year cycles (b).

4. Orbital influences

The climate variations of MSL and mean temperature with periods about 23Ka, 40Ka and 100Ka are mainly due to Earth orbital forcing. The 23Ka cycles are connected with the precession variations with opposite revealing on the South and North hemisphere. The 23Ka MSL variations depend on North latitude insolation, so the 23Ka mean temperature variations from Antarctic measurements are with opposite phases with the MSL variations, as it is seen in Fig.4, where the 3-d, 5-th and 10-th precession harmonics with periods 7.7Ka, 4.6Ka and 2.3Ka cause negative correlation between MSL and mean temperature variations.

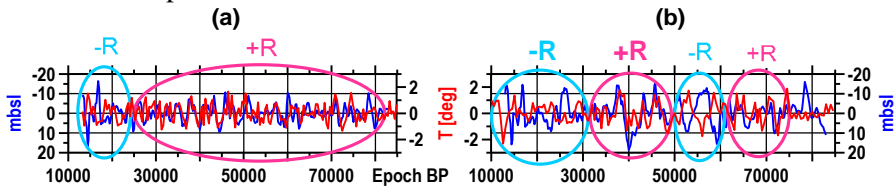


Figure 4. Comparison of MSL (blue line) and mean Earth temperature (red line) variations of 4600a (a) and 9200a (b) models. The negative correlation coefficients (-R) are denoted by blue circles and positive (+R) – by red circles.

The spectra of millennial MSL and temperature variations contain clear peaks corresponding to 9200a, 4600a and 2300a oscillations. The possible common TSI origin of these cycles and their harmonics is checked by comparison of corresponding phases (Table 1). Most of the phases are significantly different. Only a few harmonics have equal or opposite phases, so the common cycles of TSI and MSL are with periods 1533a and 1022a; TSI and temperature – with 920a period; and MSL and temperature – with 9300a period, which appears as 11-th harmonics of 100Ka orbital cycle. The orbital forcing of millennial MSL and temperature oscillations with periods below 10Ka is dominating, so the investigation of solar influence on millennial variations of Earth rotation and climate is possible after removing the orbital components and its harmonics. The reconstruction of the variations of the Earth rotation (LOD) from the MSL data is possible by means of the model (Chapanov and Gambis, 2010)

$$LOD = 2.583(1 - q)\Delta MSL, \quad q = S_o I_c / (S_{Ice} I_o), \quad (1)$$

where q is function of the total ocean and ice surface S_o , S_{ice} , and I_c , I_o - the total moment of inertia of thin ellipsoidal shell over the continental ice sheets and the ocean.

Table 1. TSI, MSL and temperature T phase comparison of the first 10 harmonics of 9200a oscillation. The equal phases are denoted in bold, the opposite phases (difference about 180 degrees) – in italic.

No	Period	TSI	MSL	T
1	9200	49.0	<i>130.5</i>	<i>-49.3</i>
2	4600	-140.1	-176.0	-45.0
3	3066	154.8	-98.8	-65.9
4	2300	130.5	82.6	-167.5
5	1840	-14.9	80.1	-79.0
6	1533	-62.3	<i>112.9</i>	<i>125.2</i>
7	1314	29.3	-177.3	115.2
8	1150	51.8	137.9	27.0
9	1022	<i>-40.1</i>	<i>136.0</i>	5.1
10	920	154.4	56.1	152.1

5. Parameters of millennial TSI variations

The millennial TSI variations, determined from 9.3Ka series, are represented by significant 2265a Hallstatt cycle and its harmonics, and a 5730a cycle (Fig.5, a, b, Fig. 6, b). The value of the Hallstatt cycle, determined by amplitude maximum of the varying period is 2265a and its second harmonic – 1146a (Fig.5). The same value (2265a) is determined for the 2300a mean temperature oscillations for the same time interval, but with second maximum corresponding to 2325a, probably due to the 10-th harmonic of precession cycles. The 5730a TSI oscillation should be the second harmonic of recently discovered 11500a solar cycle (Shopov et al., 2004). The time variations of the amplitudes and phases of the millennial 2265a and 1146a TSI cycles are determined in running 2300a window (Fig.7). The amplitudes increase to the maxima in 4000a BP and decrease after that. The phases change significantly all the time and this points out that the Hallstatt cycle and its harmonics are with variable periods.

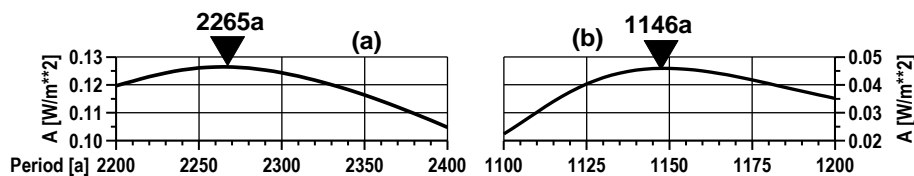


Figure 5. Amplitude maxima of the 2300a (a) and 1150a (b) TSI oscillations, determined by varying the period with 5-year steps.

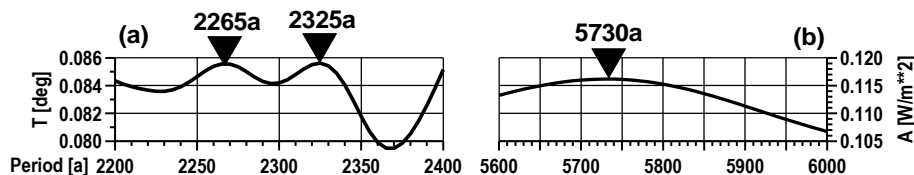


Figure 6. Amplitude maxima of the 2300a mean temperature variations (a) and 5700a TSI variations (b), determined by varying the period with 5-year steps.

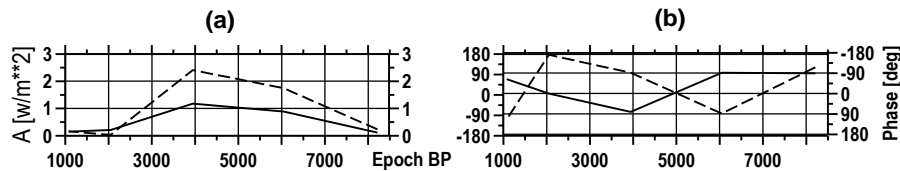


Figure 7. Variations of the amplitudes of the oscillations with periods 2265a (dashed line) and 1146a (bold line) (a) and corresponding phases (b), determined in running 2300a window.

6. Conclusions

The millennial oscillations of the total solar irradiance variations for the last 9.3Ka are represented by two main cycles with periods 2265a (Hallstatt solar cycle) and 5730a (second harmonic of 11500a solar cycle). The amplitude and phase of Hallstatt cycles are significantly variable in time with maximal amplitude around 4000a before present (BP), so the value of the Hallstatt period is also variable. Direct correlation between the millennial TSI variations and Mean Sea Level (MSL) and Mean Earth Temperature does not exist due to strong influences of the harmonics of precession forcing on the climate variations with periodicities below 10Ka, so the reconstructed Earth rotation variations from the MSL data are mainly based on orbital cycles.

It is necessary to create adequate models of the orbital influence on climate variations and to exclude all orbital terms from the long time series of MSL, temperature and other indices in order to study millennial cycles of solar-terrestrial influences.

Acknowledgements: The paper was supported by grant No. 13-15943S awarded by the Grant Agency of the Czech Republic.

References

- Arz, H.W., F. Lamy, A. Ganopolski, N. Nowaczyk, and J. Pätzold. 2007. *Quaternary Science Reviews*, Vol. 26, pp. 312-321.
- Chapanov Ya., J. Vondrák, and C. Ron, 2011. *Proc. Journées "Systèmes de référence spatio-temporels"*, Paris, 2011, ISBN978-2-901057-64-2, 149-152.
- Chapanov Ya., J. Vondrák, and C. Ron, 2012. *Proc. Journées "Systèmes de référence spatio-temporels"*, Vienna.
- Chapanov, Ya., D. Gambis, 2010. *Proc. BALWOIS 2010*, Ohrid.
- Jouzel, J., and 31 co-authors. 2007. *Sci.*, Vol. 317, No. 5839, pp.793-797.
- Ron, C., Ya. Chapanov, J. Vondrák, 2012. *Acta geodyn. et geomaterialia*, vol.9, No3(167).
- Shopov Y., D. Stoykova, L. Tsankov, M. Sanabria, D. Georgieva, D. Ford, L. Georgiev, 2004, *International Journal of Speleology*, v. 33 (1/4) pp. 19- 24.
- Steinhilber, F., J. Beer, and C. Frohlich. 2009, *Geophys. Res. Lett.*, 36, L19704, doi:10.1029/2009GL040142.
- Xapsos, M. A.; Burke, E. A., 2009. *Solar Phys.* V257, 363–369.

GEOELECTRIC STUDIES AT THE GEOPHYSICAL OBSERVATORIES IN BULGARIA

Logvinov I.¹, Srebrov B.², Rakhlin L.^{3,1}, Kovachikova S.⁴

¹Institute of Geophysical, NAS, Ukraine, Kiev, ²NIGGG, BAS, Bulgaria, Sofia, ³Research Centre GEOMAGNET, Ukraine, Lvov, ⁴Institute of Geophysics, Acad. Sci. Czech Rep., Czech Republic, Prague

Introduction

The availability of up-to date digital magnetotelluric instrumentation requires to perform geoelectric researches to the next level in Bulgaria. Long-term observations of variations in magnetotelluric (MT) field at the PAG Observatory discovered temporal variability of magnetic transfer functions [Srebrov et al., 2013]. An analysis of this variability suggests that it can be related to seismicity of the Balkans.

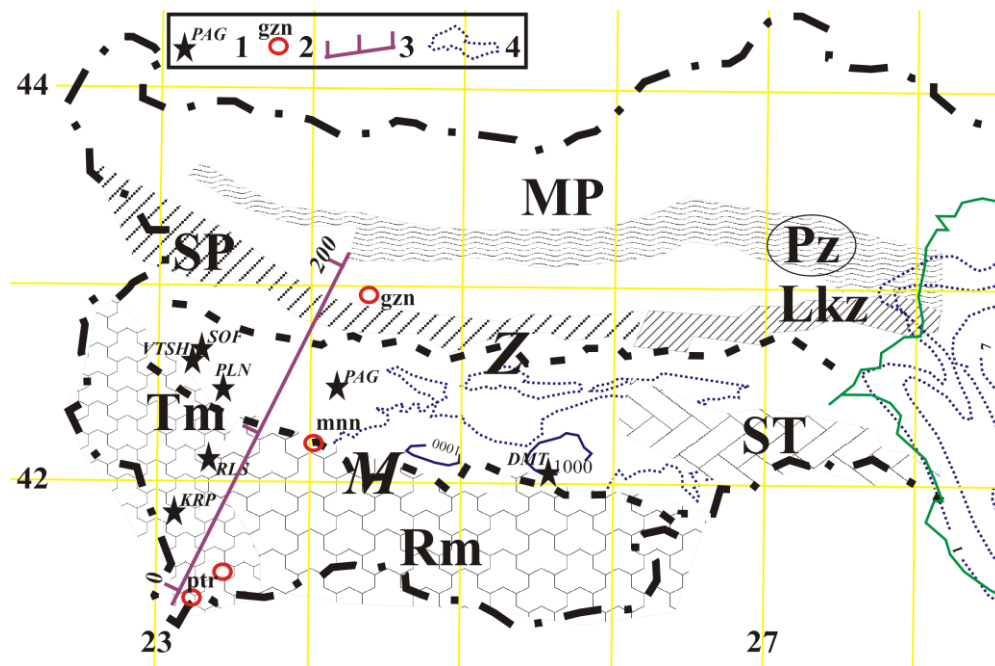


Fig.1. The location of the observation site. Tectonic setting [Structure..., 1979].

Data: 1 – the present authors; 2 – [Abramova et al, 1994]; 3 – the profile of 2D inversion; 4 – the roof of the pre-Paleogene sediments of the Srednogoria [Dachev, 1988] and the Black Sea [Tectonics ..., 1985]; Tectonic units: MP - Moesian Plate, TZ – transfer zone between Balkanids and the MP, SP – Stara Planina; Lkz - Ludokamchiyskaya zone, ST – Strandja; Tm and Rm – the Thracian and Rhodope Massifs; Regional fault zones: Z – Zabalkanskaya, M – Maritskaya.

The paper presents the first results of geoelectric studies in Bulgaria applying a set of the GEOMAG-02 digital equipment widely used for MT researches in countries worldwide [Rakhlin et al, 2005]. The observations were made at the geophysical observatories of the IGGG BAS (Fig. 1): PAG – geomagnetic; PLN – geodesic; KRP, VTSH, DMT – seismic. In addition, short-term observations were made on the southern outskirts of Sofia and Rila Monastery area. Five components of the MT were observed at the PAG, PLN and only magnetic components were registered at the rest of them. After processing measurements magnetic transfer functions were determined for all sites. Impedances were additionally obtained at the PAG and PLN. The problem is considered of detecting observations duration to obtain high-quality values of interpretation parameters. 1d, 2d and quasi3D

inversions were performed for experimental data. A comparison is made between the quasi3D inversion in the south–western Bulgaria and seismicity of the Balkans.

Technique of geoelectric studies

Methods of the magnetotelluric sounding (MTS) and magnetovariational profiling (deep geomagnetic sounding - DGS) are based on the presentation of the external source of the MT field as a plane wave falling on the horizontally layered Earth. There are different approaches to the interpretation of MTS curves. We applied a technique to interpret MTS curves along principal directions. On polar diagrams of principal and additional impedance the directions are found along which value of the principal impedance exceeds by many times that of additional one. Besides this, in selecting the principal directions invariants of a phase tensor are taken into account. Due to this approach, the data are most adequate to theoretical notions of magnetotelluric sounding.

The vertical component is zero at the surface of the Earth for a source field as a plane wave. In this case, the presence of the vertical component and differences in horizontal components of the the surrounding stations can be caused by inducing current in geoelectric inhomogeneities. The DGS method is based on finding anomalous behavior of the magnetic component of the MT field. In the method processing results are used from a single point, or the comparison of magnetic components from the area (profile). The results of processing from one station are usually based on the relationship (called the Wise-Parkinson relationship) between vertical component of the magnetic field and its horizontal components

$$H_z = W_{zx} H_x + W_{zy} H_y \quad (1),$$

where all the components are complex numbers. Magnetic transfer functions (W_{zx} and W_{zy}) can be presented in the form of C_u ($C_u = \text{Re } W_{zx} + \text{Re } W_{zy}$) and C_v ($C_v = \text{Im } W_{zx} + \text{Im } W_{zy}$) [Schmucker, 1970]. On a map the C_u and C_v can be presented as induction arrows (their positive values of azimuth are drawn clockwise relative north). Several important conclusions can be drawn from a ratio of the C_u and C_v about the geoelectric structure in the vicinity of an observation station.

A relationship is governed by the Biot-Savart law between conducting objects and geometry parameters of magnetovariational anomalies. Over the middle portion of a conductor oriented along the x-axis an induction arrow module is close to zero and has extremes of the left and right edges of the projections of the conducting object on the Earth's surface. The distance between the extremes increases with the depth of the conductor. The C_u changes sign and has a minimum and maximum on the right and left relative to the conductor center. Therefore, a close lateral or vertical position of the conductors results in the field superposition which strongly changes ratio mentioned above for the induction arrow. From the two-dimensional modelling it is known that the maximum frequency response of the tipper shifts to longer periods depending on increasing integrated conductivity of all conducting objects, causing magnetic variation anomaly.

Results of geoelectric studies

Experimental data. A digitization step of the GEOMAG-02 equipment of this study is 0.1 s. Processing the MT field observations was done by using computer programs of [Egbert, Booker, 1986; Egbert, 1997; Ladanivskyy, 2003]. Values of induction arrows were determined with an error of 0.05-0.1 and 5-8° (with periods less than 40s) and 0.03 and 3-5° (with periods greater than 40-10000s), respectively for the modules and their azimuths.

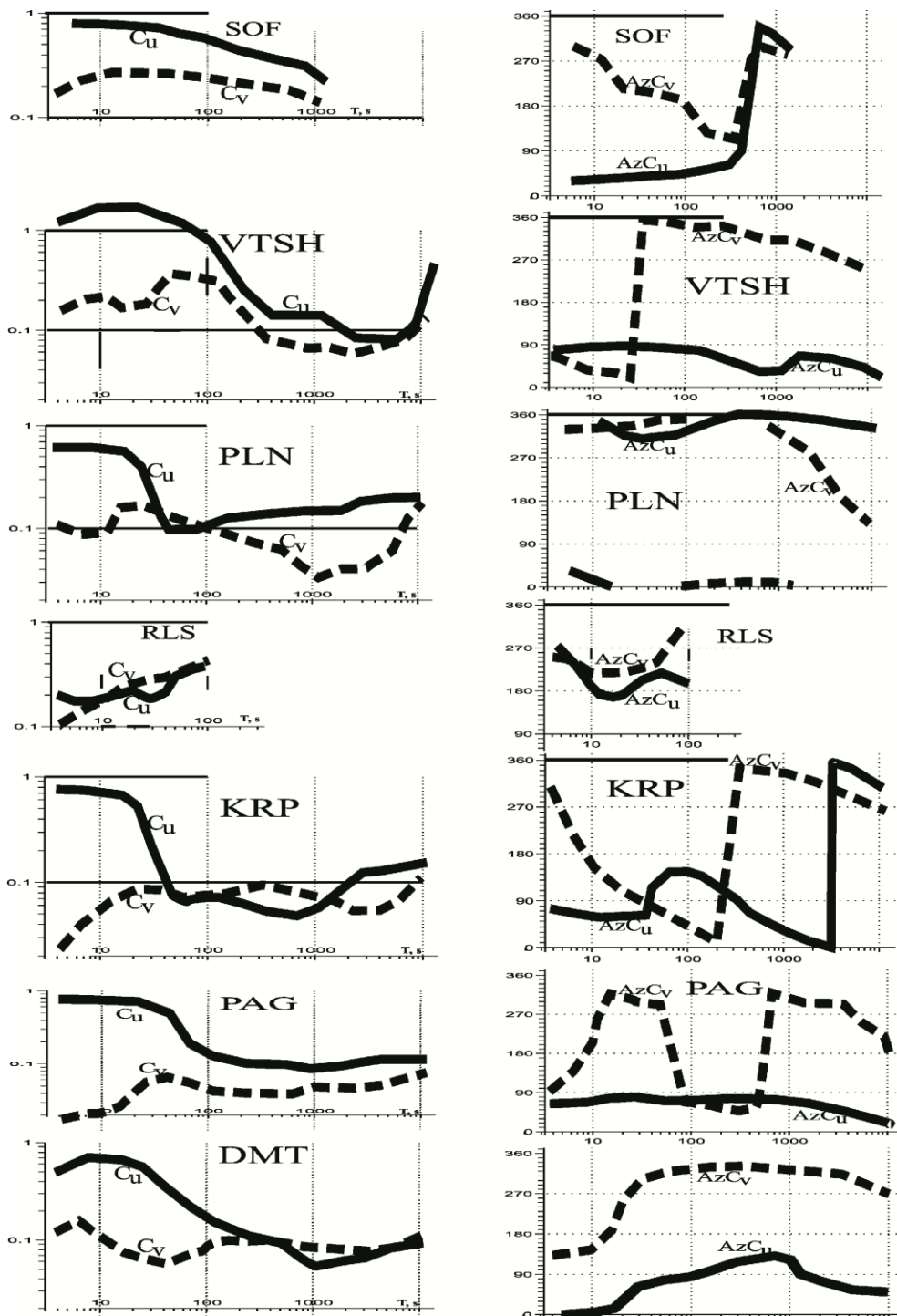


Fig. 2 Spectral characteristics of the C_u и C_v .

As preliminary processing records at the PLN and KRP resulted in abrupt changes the C_u azimuths it was interesting to delineate the spatial distribution of this behavior. For this purpose observations were made at 3 stations (RLS, VTSH, SOF) along the Krupnik–Sofia line. The least reliable results were obtained at RLS due to little time of record and large background noise. Nevertheless increasing observation stations along the profile allow us to identify more reliable zone of conductivity heterogeneity between PLN and KRP and localize it.

As it follows from Fig.2 two features of the C_u and C_v are clearly recognized on the frequency characteristics. Firstly, there occur very large the C_u values in the range of less than 30; secondly, there is a change in the C_u and AzC_u especially in the periods of 200-1000s.

A special study was performed to reveal a possible relationship between GEOMAG-02 characteristics and values of the C_u and C_v obtained for periods less than 100 s. Fig.3 shows the

frequency characteristics of all measurement channels. Peculiarity of GEOMAG-02 is complete equality of frequency characteristics of all channels (Fig. 3A,B).

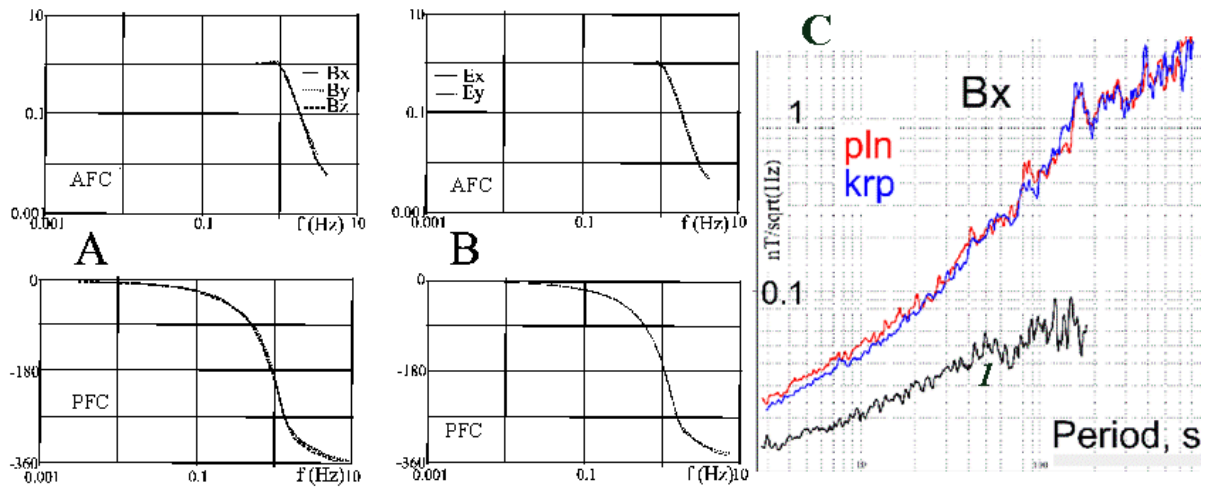


Fig. 3 Amplitude (AFC), phase (PFC) frequency magnetic characteristics (A) and electrical (B) channels. C – a comparison of the spectral densities of the channel obtained at the station KRP (krp) and PLN (pln) and intrinsic noise of the GEOMAG-02 magnetometer (1).

The magnitude of intrinsic noise of the GEOMAG-02 measurement channels was different for different instruments. A comparison of the spectral densities with the intrinsic noise of the apparatus shows that the latter is almost one order of magnitude smaller than the amplitude of variations in the magnetic field component of the MT in the range of 10-100 s (Fig.3C). Fig.3C demonstrates the worst-case frequency characteristic of the intrinsic noise of the instrument (amplitude noise is almost 2 times smaller for other instruments). Thus, it clearly follows that the technical characteristics of equipment for periods greater than 10 s cannot be responsible for the observed behavior of induction vectors.

Another argument in favour of a natural source of the observed effect is the difference between the frequency characteristics of the amplitudes and azimuths of the Cu and Cv from a station to a station. Note that the considered range corresponds to the geomagnetic pulsations Pc3-4, which are the most common types of oscillations recorded at the Earth's surface [Model Space, 2007], In the present days these oscillations are often termed as ULF-wave (ultra-low-frequency). In processing records of MT field variations in this frequency range very high values (> 0.85) are observed for multiple coherence of output channels for the largest number of fragments of records selected.

The arguments above suggest that a special effect was discovered in the behavior of magnetic variation parameters in the range of 4-40 s on the territory of Bulgaria. For a more thorough study of spatial-temporal features of the effect, long-term areal observations are required.

An interesting feature of the Cu and Cv behavior is observed in the range of 100-1000 s (Fig. 3C). The values and relationships of the Cu and Cv modules drastically change but the difference is most clearly seen in the azimuths of the Cu. At the KRP and DMT the Cu azimuth is $150-160^\circ$ (ie. the Cu is directed almost toward the south), whereas the Cu at the PLN is directed nearly toward the north (the Cu azimuth is close to 15°). This behavior is observed at the intersection of observation stations and conducting objects.

Magnetotelluric parameters. As a result of record processing MT-field, estimates of impedances were obtained at both stations in the range from 4-10 to 6400-10000 s. At the PLN great background noise is registered on the records of all channels because of working geodetic equipment, especially strong in electrical channels (Fig.4). To eliminate interferences, which occur on records of almost all stations, a special TARIG program of [Logvinov, Tarasov, 2010] was successfully applied.

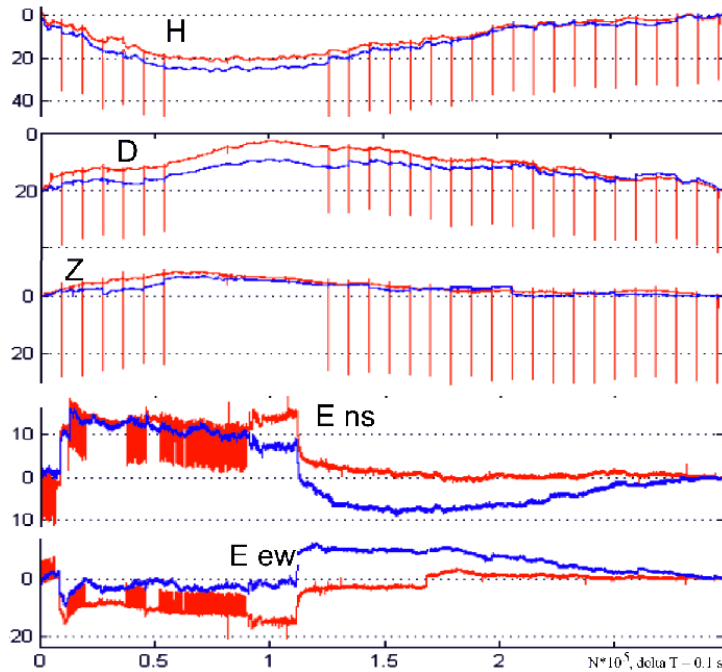


Fig. 4. Example of eliminating distortion of MT field variations using the TARIG program.
Data: red - observed, blue - corrected.

After eliminating interferences there were calculated different matrix decomposition of impedance and principal directions were obtained. Maximum values of the polar diagrams of impedance are observed at the PLN for the 90° azimuth. At the PAG maximum directions of polar diagrams of impedance has the 150° azimuth. If one assume that the induction vectors reflect a strike of conducting objects, the maximum MTS curves correspond to the longitudinal curve at both stations.

Variability of magnetic transfer functions.

In many European countries field missions take place in the summer time. It is interesting to examine how duration of observations of the MT field and the degree of disturbance of the MT field to influence on an estimate of a transfer function. Such a procedure was performed at two widely separated stations with sharply different geoelectric characteristics of sediments and level of seismicity. The estimates were made for 24 hours during a magnetic storm and a calm day from 3, 6 and 20 round the clock records. Fig. 5 presents the parameters of induction vectors during this experiment.

At the DMT in the maximum of the frequency characteristic of the Cu its estimates for the 24 hour record on a calm day differ from 3 and 6 ones by 25% while during a magnetic storm — by 2 times. Using the 24 hour record provided that it meets the requirements of the study for multiple coherence and the number of intervals, one can get assessments for at least up to 1000-1200s. The records of three or more nights and days estimates can be obtained for up to 1 hour or more. A scatter of Cv data is less, but it can be due to the small values. Azimuth discrepancies in the Cu and Cv reach 20° for any number of days and nights.

At the KRP differences in the induction vectors parameters depending on the duration of the registration is less noticeable, although appear during perturbations. One of the reasons for this difference at the two stations can be noise level. At the DMT records are distorted by large background noise of different origin. It is also interesting to compare the data obtained with the level of seismicity in the study areas during experiments.

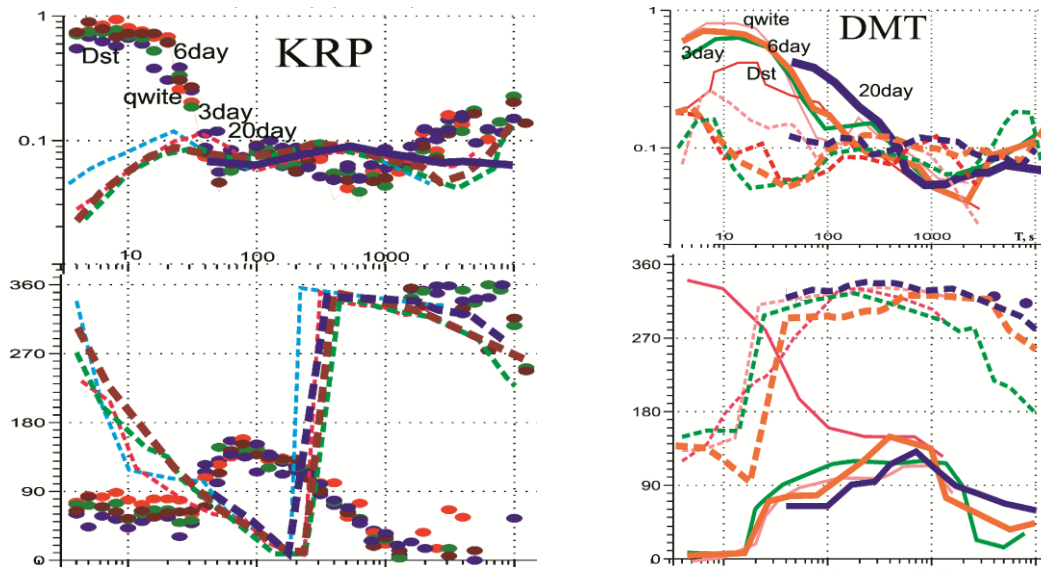


Fig. 5. Estimates of the parameters of induction vectors at Dimitrograd and Krupnik seismic observatories.

An analysis shows that the minimum duration of registration must be not less than 4 days and nights to determine magnetic variation parameters with acceptable errors in the range from 6000-8000 s.

One-dimensional (1D) inversion.

The technique and data. Fitting parameters of a deep geoelectric cross-section is based on one-dimensional inversion of sounding generalized curves. For this purpose two inversions were used [Parker, 1981] (D + algorithm) and [OCCAM, Constable et al., 1987]. The first method exploits a presentation of a cross-section in a form of a zero-thick layer of ultimate conductivity. It can estimate a total value of the longitudinal conductivity (S) of conductors occurring in the cross-section, with an apparent resistances curve (ρ_k) is being used simultaneously throughout a range observed. The second method is fitting a model which approximates experimental data by finite number of layers with smoothly varying conductivity. The OCCAM inversion gives priority to values of impedance phases.

The 1D inversion was performed for generalized sounding curves, constructed by combining the MTS curves at the PLN and PAG with a reference MTS curve. For the territory of Bulgaria it is reasonable to adopt a reference curve resulted from magnetovariational sounding at the PAG [Schultz, Larsen, 1987; Semenov, 1998; Olsen, 1998; Srebrov et al., 2013] .

The results of one-dimensional inversion. A layer of low resistance is defined as a layer which is determined from S by an inversion of D+ and has resistance (from the OCCAM inversion) of at least five times smaller (typically less than 100-200 Ohm) than host rocks.

The inversion results demonstrate that the MTS curves from both stations are subjected to galvanic distortions (shift effect). Fig. 6 shows the inversions of the generalized sounding curves where the MTS amplitude curves were corrected for the shift- effect.

As is shown from the results of two-dimensional modelling, more accurate depth to the conductors in the upper horizons of the crust is determined from the transverse curve. At the same time on this curve conductors situated below are weakly recognized.

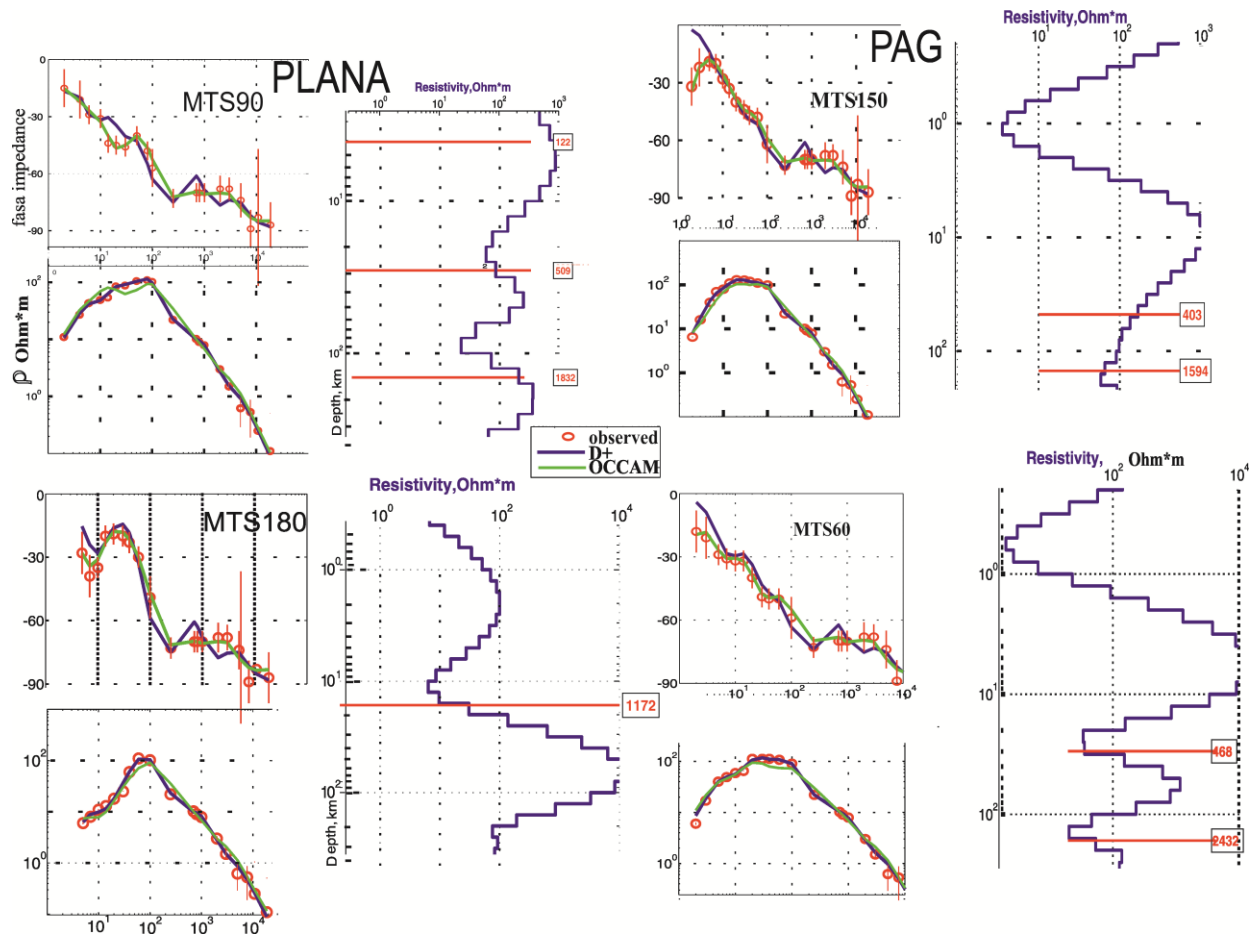


Fig. 6. Results of 1D inversion methods D + and OCCAM.

Based on the geoelectric sections of curves in two directions, following conclusions can be drawn. Resistance of the upper rocks of hundred meters thick reflects the lithological composition of the rocks in the vicinity of each station. At the PLN it is no less than 100 Ohm while at the PAG there is a thick conducting sedimentary layer whose resistance reaches values of less than 10 Ohm.

Geoelectric parameters of the consolidated crust are strongly different. At the PLN on the transverse curve a conducting object is observed in the range centre of the depth of 10-20 km. Its total longitudinal conductivity is about 1000 S/m. At the PAG similar object is recognized in the range of 20-30 km, with a total longitudinal conductivity is being of the order of 500 S/m.

At depths of ca. 100 km conducting layer is delineated, with its total longitudinal conductivity is being more than 1000 S.

Two-dimensional (2D) inversion.

An inversion is performed applying a two-dimensional modelling program (REBOCC algorithm) [Siripunvaraporn, Egbert, 2000]. Magnetic transfer functions were used which were obtained by the authors in the range from 10 to 7000 s. The results of previous investigations were added for the range of 600-7000 s [Abramova et al, 1994]. The data of past years were used to

increase density of the observation network. As a result, the profile extends from the Rhodopes on the south (ptr) to Balkans on the north (glzh) crossing the Rhodopes and Srednogorie (fig.1).

Fig.7 shows a geoelectric model with the smallest discrepancy (rms) between the experimental and model results. The model should be regarded as preliminary. At stations where experimental data are available throughout the whole range, rms is twice less than that for stations where the data were used for large periods longer 600 s. The main feature of this model is a low resistance objects in the Earth's crust near the Maritskiy fault.

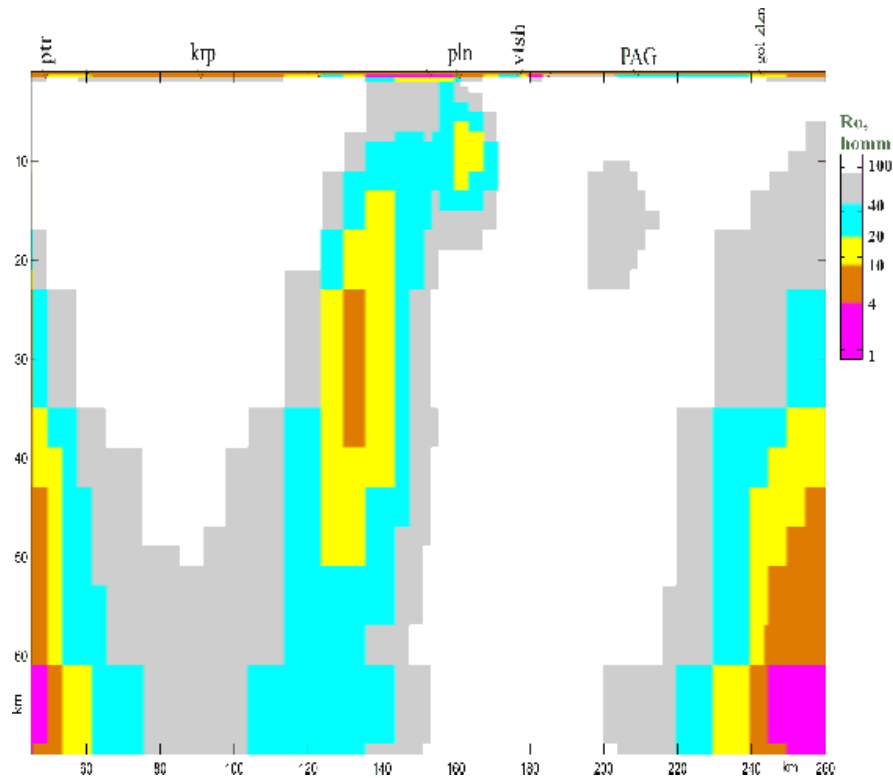


Figure 7. Geoelectric cross-section along the profile Rhodope-Balkans.

Quasi three-dimensional inversion

The inversion is based on a study of the distribution of anomalous currents (from which conductivity of a thin layer - D is determined) in a thin layer, placed in a horizontally layered medium [Kovacicova, 2001]. At this stage of the study the following model parameters were adopted: a thickness of a thin layer is 1 km whose upper edge is situated at 10 km. Magnetic transfer functions for the period of 2200s were applied for calculations [Abramova et al, 1994]

The most reliable results are obtained for the territory of Srednogorie and the Rhodopes, as here are located a majority of observation points. The distribution of conductors has a mosaic character that can be due to the irregularity of the observation network.

Conclusions and Descation.

It is interesting to compare the resulting distribution of conducting objects in the Earth's crust with that of earthquakes on the territory of Bulgaria. Fig.8 shows a histogram of the distribution of earthquakes during 1973-2010 (NEIC: Earthquake Search Results). It is seen that the most earthquake hypocenters (12,200) of a total number of 14,400 occur at the range depth of 10-12 km while much smaller (about 2000) are located at a depths of 4-6 km. Therefore, the resulting distribution of conductivity at a depth of 10 km can be compared with the seismicity of Bulgaria. As follows from Fig.8B there is tendency of a correlation of high conducting objects with seismicity.

There are practically no earthquakes in the areas where high conducting sources occur. The the depth of conductivity anomalies also confirms this inference.

The advantage of our results over previous ones is the use of more sophisticated digital instruments, applying up to date processing variations of the MT field and inversions for constructing geomagnetic models.

The application of modern equipment and processing technique allowed us to first obtain in Bulgaria interpretation parameters for periods from a few seconds to three hours. Based on the 1D inversion of magnetotelluric data, for the first time in Bulgaria a geoelectric model was constructed for Earth's the crust and upper mantle.

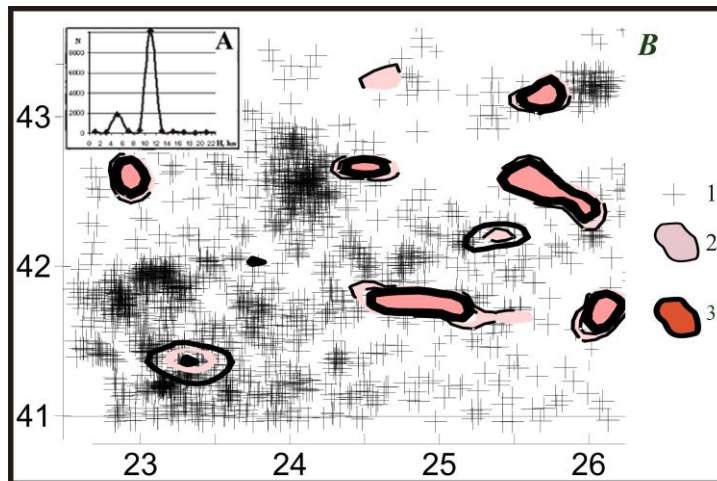


Fig.8. A. Dependence of the number of earthquakes on a depth of their hypocenter. B - State of earthquakes (1) and conductive objects (2- 2000 S, 3- 4000 S) with the upper edge at a depth of 10 km.

The 1D, 2D and quasi 3D inversions resulted in delineating abnormally conducting objects in the crust of the south- western Bulgaria. An integrated analysis of MT data and induction vectors suggests spatial coincidence of one of these objects from PLN zone and the Maritskiy fault zone where increased seismicity occurs along its whole length. A comparison of the distribution of high-conducting object, determined from the quasi 3D inversion, and seismicity indicates the absence of earthquakes within the conducting objects.

Acknowledgments. We are grateful to B. Ladanivskyy for their help in constructing frequency characteristics of the GEOMAG-02. Thanks are also due to L. Abramova, kindly provided data on a joint research of the Bulgarian and Moscow geoelectric teams.

This work was supported by the FP7 IRSES BlackSeaHazNet project.

Reference.

Abramov AM, Varentsov Iv.M., Velev A. Gavrilov, R., NG Golubev, MS Zhdanov, Martanus ER, Sokolova E.Yu., Schneier V.S. 1994. Investigation of deep geoelectric structure of Bulgaria // Physics of the Earth. 11. P.59- 69. (in Russian).

Geophysical parameters of the lithosphere of the southern sector of the Alpine Orogen / Eds. B.S.Volvovsky, V.I.Starostenko. 1996. Kiev: Naukova Dumka. 215 p. (in Russian).

Дачев X. Строеж на земна та кора в България. 1988. София: Техника. 334 p. (in Bulgarian).

Ladanivskiy B.T. MT data processing algorithm // V.V.Fedynskiy Fifth geophysical reading February 27 - March 1, 2003. Abstracts. p.134-135. (in Russian).

Logvinov I.M., Tarasov V.N. 2010. Geoelectric parameters of the crustal of the Dnieper-Elbe area, the East-European platform from the one-dimensional inversion of magnetotelluric sounding Geofiz. zhur, 32, 5. -P. 61-68. (in Russian).

Rahlin L., Guleyuk L., Nakalov E., Kuznetsov O. 2005. Magnitoteluric station "GEOMAG-02"// Novi geofizichni tehnologii prognozuvannya that monitoringu geologichnogo seredovischa. Lviv: Lviv branch IGF NAS of Ukraine. P.22-23. (in Ukrainian).

Crustal structure of Central and Eastern Europe from geophysical data. 1979. / Sologub V.B., Guterh A., Requests D. et al. Kiev: Naukova Dumka. 208 p. (in Russian).

Meso-Cenozoic tectonics of the Black Sea basin sediments. 1985. / Tugolesov D.A., Gorshkov A.C., Meisner L.B. etc. Moskow, Nedra. 215 p. (in Russian).

Constable S.C., Parker R.L., Constable C.G. 1987. Occam's inversion: a practical algorithm for the inversion of electromagnetic data// Geophysics. 52. P.289-300.

Egbert G.D., J.R.Booker 1986. Robust estimation of geomagnetic transfer function // Geophys. J. Royal Astron. Soc. 87. P. 173-194.

Egbert G.D. 1997. Robust multiple-station magnetotelluric data processing// Geophys. J. Int. 130. P.475-496.

Olsen N. 1998. The electrical conductivity of the mantle beneath Europe derived from C-responses from 3 to 720 hr. //Geophys. J.Int. 133. P. 298– 308.

Parker R.L., Whaler K.A. 1981. Numerical method for establishing solution to the inverse problem of electromagnetic induction// J. Geophys. Res. 86. P.9574- 9584.

Schmucker U. 1970. Anomalies of geomagnetic variations in the southwestern United States //Bull Scripps Inst. Oceanogr. 13.— 165 P.

Schultz, A., Larsen, J.C. 1987. On the electrical conductivity of the mid-mantle: I. Calculation of equivalent scalar magnetotelluric response functions//Geophys. J.R. Astron. Soc. 88. P.733– 761.

Semenov, V.Yu. 1998. Regional conductivity of the structures of the Earth's mantle//Publ. Inst. Geophys. Pol. Acad. Sci.- -C65 (302)- 122 P.

Srebrov B., Ladanyvskyy B., Logvinov I. 2013. Application of space generated geomagnetic variations for obtaining geoelectric characteristics in the Panagyurishte geomagnetic observatory region//Comptes rendus de l'Academie bulgare des Sciences. 66, 6. P.857-864.

Model Space: Scientific information publication: v.1. 2007.// Ed. M.I. Panasyuk, L.S. Novikov. - Moscow: MDU. 872 p. (in Russian).



БАН и бюстът на Борис Христов, от цикъла „БАН – ракурси“

Бойко Вачев'2006

BAS and monument of Boris Christov, from cycle "BAS - Racources"

Boyko Vachev'2006

METHOD OF STANDARD DEVIATION FOR ANALYSIS OF HYDRODYNAMIC AND GEOMAGNETIC VARIATIONS FOR ESTIMATION OF REGIONAL SEISMIC SITUATION

Margar Adibekyan¹, Ani Gevorgyan¹, Armine Khangaldyan²

¹Western Survey for Seismic Protection SNTO; adibekyan@yahoo.com; ani_gevorkjan@mail.ru

²“Survey for Seismic Protection” Agency at the MES of RA; arminenem@mail.ru

Abstract

In this work it is explored the Method of Standard Deviation for Analysis of Hydrodynamic and Geomagnetic Variations for Estimation of Regional Seismic Situation. Short introduction of method Standard deviation: The signal for imminent increasing regional seismic activity is the geomagnetic, hydrogeodynamic quake which is defined as a jump of daily averaged SDF (standard deviation function). Such approach permits to compare by numbers the daily behavior of the geomagnetic, hydrogeodynamic field with those in other days. Among the earthquakes occurred on the territory under consideration in certain time period, the “predicted” one is the earthquake with magnitude M and epicentral distance which is identified by the maximum value of the function: The physical meaning of the function is the surface density of earthquakes energy in the point of measurement. It is important to stress out that the first consideration of the earthquake magnitude and epicentral distance dependence was obtained using nonlinear inverse problem methods. The close distance strong earthquake will bear more electropotential variations, which will generate more power geomagnetic, hydrogeodynamic wave. The correlation between the time period of increasing regional seismic activity, and tide extreme, recognized of predicted earthquake was established using the Alexandrov’s code REGN.

For that it was researched several Hydrodynamic and Geomagnetic parameters of earthquakes in Armenia by following earthquakes in South Caucasus and for the comparative analysis it was used Hydrogeodynamic and Geomagnetic parameters of the Networks of Armenia.

The result of the work shows that Method Standard Deviation gives us the opportunity to get a signal for upcoming event. It can be used for operational forecasting purposes.

Introduction

Seismological investigations in the Caucasus, and particularly in Armenia, have been conducted since late XIX century. They were related mainly to investigations of strong earthquakes. The regional seismic network of Armenia was a part of the USSR United System of Seismic Observation (USSO). The Spitak earthquake showed the necessity of developing the existing seismic network and its technical re-equipment with contemporary high technology equipment and software. After the establishment of National Survey for Seismic Protection (NSSP) of the Republic of Armenia (RA) in 1991, new tasks were posed for Armenian seismology, directed to the population protection against strong earthquakes. Since then, the seismic network was being developed through its upgrading and increase of the number of seismic stations.

Ministry of Emergency Situations of RA

Ministry of Emergency Situations (MES) of RA is a republican body of executive authority, which in line with such competences as is vested in it by laws and other legal acts, develops, implements and coordinates RA government’s policy in the area of civil defense and protection of the population in emergency situations (figure 1).

MES of RA (www.mes.am)					
Rescue Service (including Crisis Management Center- the main body for planning, co-coordinating and implementing measures related to natural and other forms of disasters)	National Survey for Seismic Protection (NSSP)	Hydro-meteorology and State Service	National Technical Safety Center	Atmospheric Phenomena In Active Service Impact	State of Emergency Crisis Management Academy



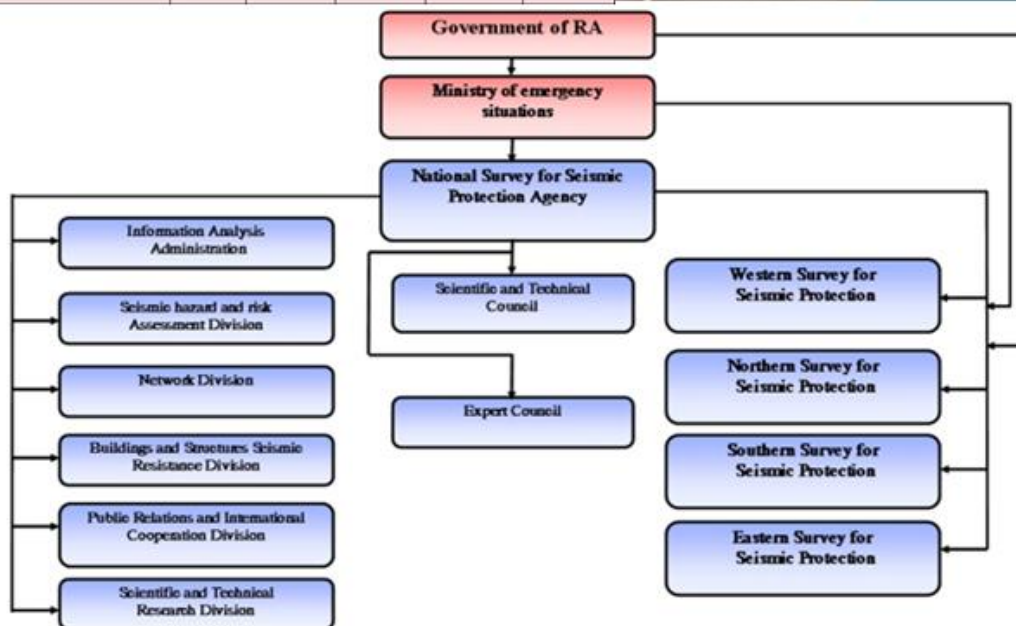


Figure 1. Structure Ministry of Emergency Situations (MES) of RA

Seismic Hazard Assessment

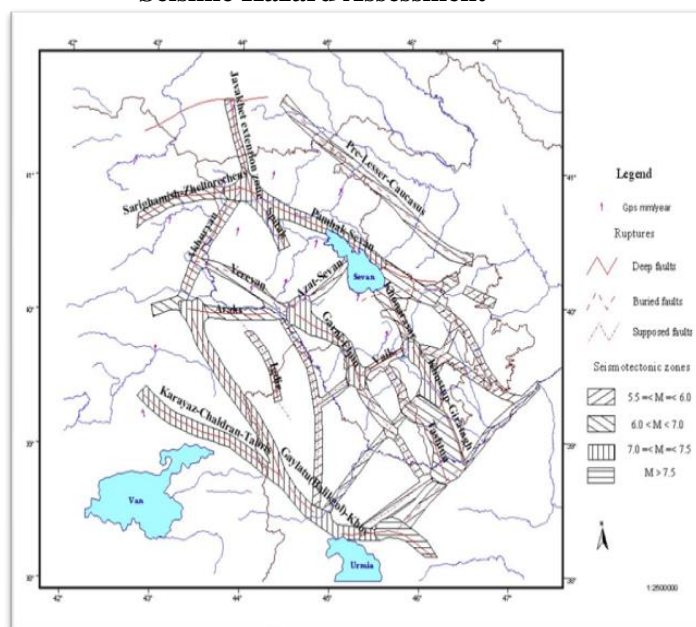


Figure 2. Active faults of RA and surrounding areas

Armenia is located in a region where seismic activities are active (figure 2). Earthquakes rupture faults, and large quakes rupture large faults. Seismic hazard assessments should therefore incorporate an inventory of active faults. Seismic hazard assessment elements are the primary seismic hazard

assessment and the secondary seismic hazard assessment. The primary seismic hazard assessment includes long-term and current assessment of seismic hazard. Current seismic hazard assessment is essential for population seismic safety and elaborating counter-measures by the central and local governments. Earthquake prediction has two approaches: scientific and societal. Probability approach (not the deterministic which includes site, time and magnitude of earthquake) allows from the scientific point of view to use intermediate research results for population and state safety. NSSP of RA experience reveals that intermediate results involve the current seismic hazard assessment with the precision sufficient for advocating the counter-measures for population earthquake protection.

Today, the contemporary digital seismic network is integrated into the unique multiparametric (Geomagnetic, Hydrodynamic, Ionosphere, Radon emission, Electromagnetic, etc.) multilevel Observation Network of NSSP of RA (figure 3), connected by modern communication means to NSSP. Observation Network of NSSP operates also for assessment of current seismic hazard in the territory of RA.

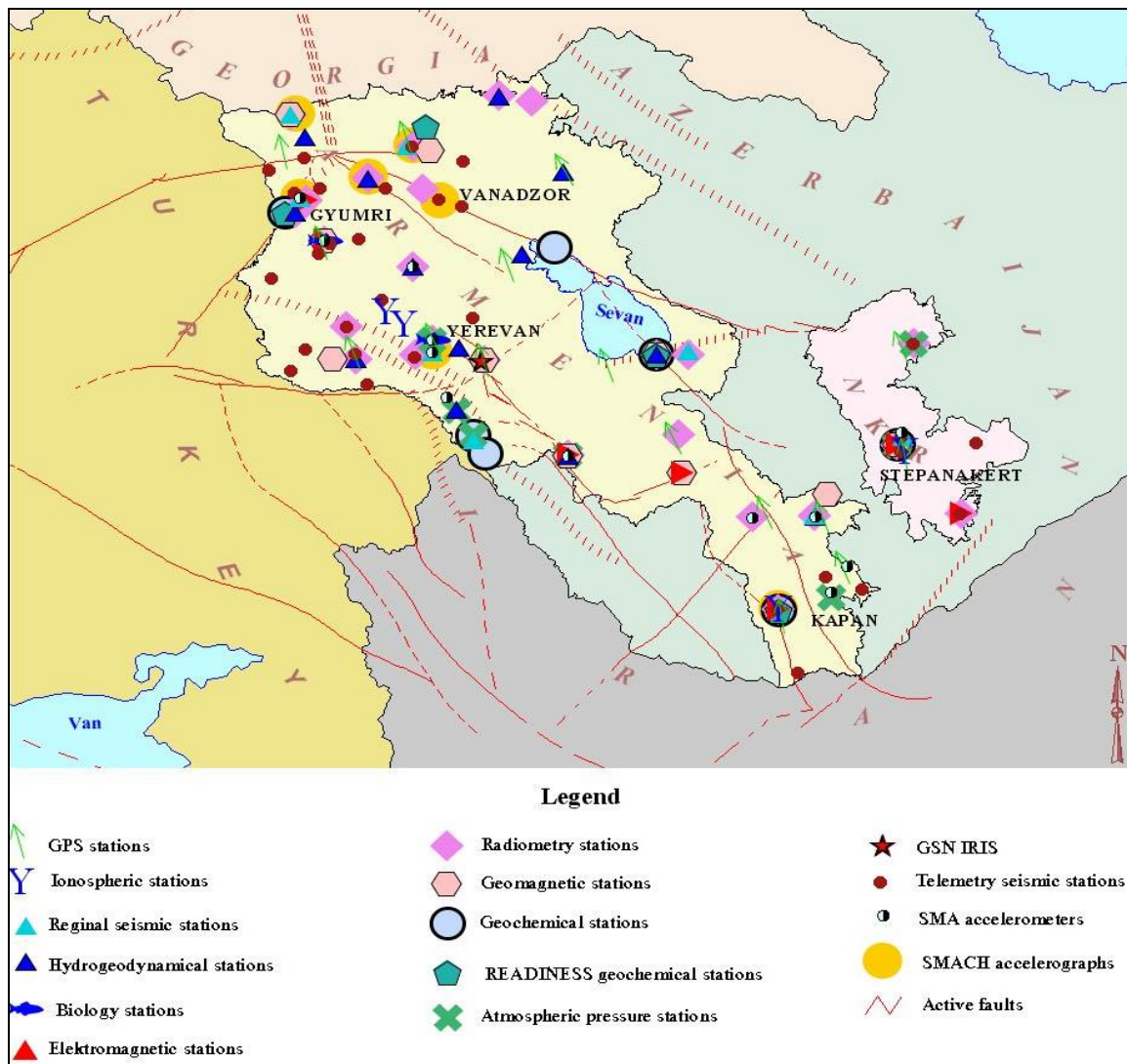


Figure 3. Observation Network of NSSP, RA

Geomagnetic monitoring: Geomagnetic earthquake precursors improvement formulation on the basis of Stepanavan (STE) geomagnetic data (figure 4).

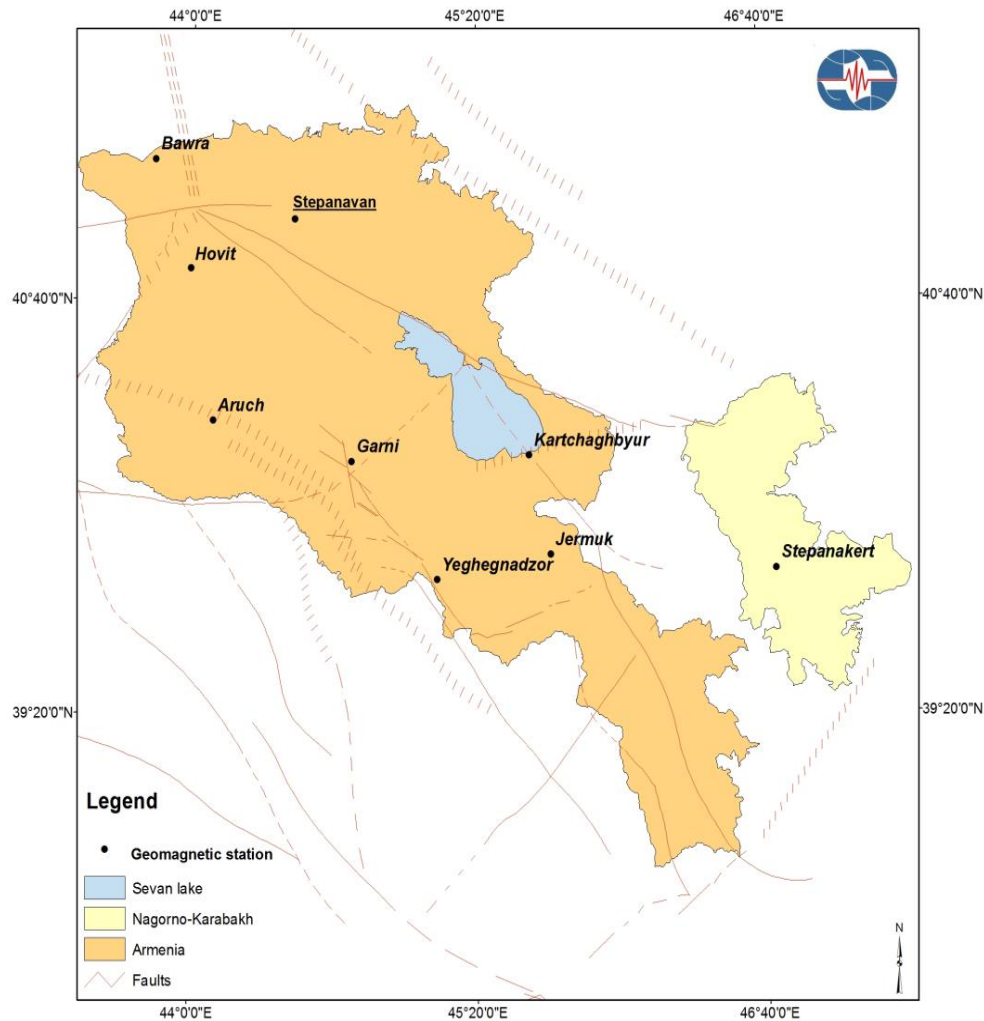


Figure 4. Geomagnetic stations of Observation Network NSSP, RA

Present the simple analysis of the local geomagnetic field behavior can be reliable imminent precursors for regional increasing seismicity. In the first step the problem was investigated using the Stepanavan ПИМ- high precise proton magnetometer. The monitoring result of this short period confirmed many articles of connection between one minute Earth tide and daily jump average of standard deviation of the geomagnetic field. The distribution of time difference such earthquakes origin times between local daily average tide's vector impending tides extremum movement confirms our thought that the increasing seismicity is realized in time period about ± 2.7 days.

Hydrogeodynamic monitoring: Observation of ground-water variations is an important part of research on earthquake prediction in RA (figure 5). Currently, there are 13 stations (borehole) in use. Factually, water level variations composition change in Earth interior is directly linked with mantle tension and deformation. Giving special attention to observations of these changes the specialists would try through them predict the earthquakes. Ground-water data played an important role in the successful prediction of several earthquakes, such as Spitak 1988 $M=7.0$, Martuni 1992 $M=5.0$, Noyemberyan 1997 $M=4.4$ in Armenia; Racha 1991 $M=7.1$, Barisakho 1992 $M=6.4$, Oni 2009 $M=5.9$ in Georgia, and Van 2011 $M=7.2$ and even Izmit 1999 $M=7.4$ (epicenter located 1300km far away). Ground-water can directly and sensitively reflect stress and strain changes in crustal rocks.

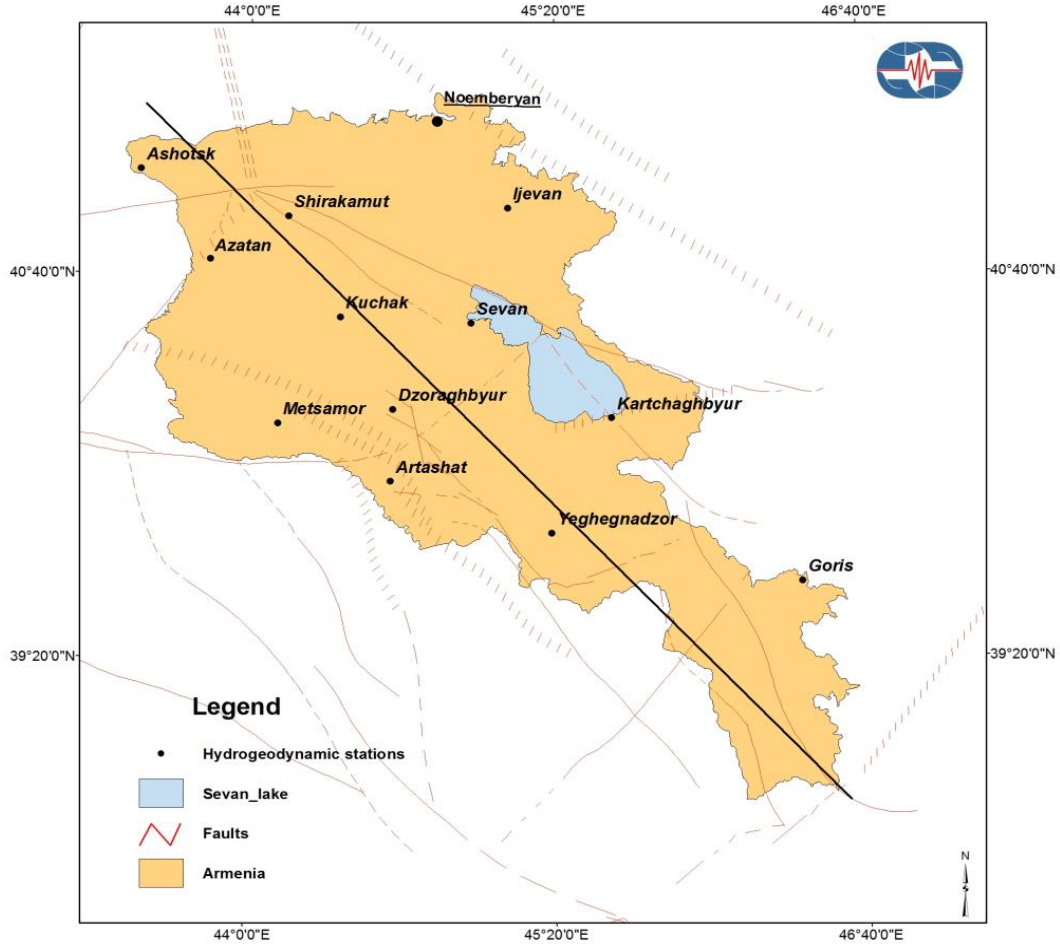


Figure 5. Hydrogeodynamic stations of Observation Network Nssp, RA

Main results

We have chance to study the possible correlations theory between the earthquakes and the variations of geomagnetic field, also ground-water level.

Analysis was done for Van (Turkey, 23.10.2011, $M=7.2$) [I], Garni (Armenia, 14.10.2011, $M=3.7$) [II], Khoy (Iran, 18.04.2013, $M=4.8$) [III], earthquakes in time-series have been studied using the geomagnetic parameter and earth tidal. Short introduction of method:

1. Standard deviate

$$SDF_m = \left(\left(\frac{1}{N} \right) \sum_{i=1}^{N_m} (1 - F_{mean} / F_i)^2 \right)^{\frac{1}{2}} \quad (1)$$

$$F_{mean} = \left(\frac{1}{N} \right) \sum_{i=1}^{N_m} F_i \quad (2)$$

where F_i , $i = 1, \dots, N$, $N = 24$ value of geomagnetic field and ground-water level, \bar{F} - average value of geomagnetic field and ground-water level

The signal for imminent increasing regional seismic activity is the geomagnetic quake which is defined as a jump o daily averaged SDF. Such approach permits to compare by numbers the daily behavior of the geomagnetic field with those in other days.

Among the earthquakes occurred on the territory under consideration in certain time period, the “predicted” one is the earthquake with magnitude M_p and epicentral distance which is identified by the maximum value of the function:

$$S_{Chm} = \frac{10^{1.5M+4.8}}{(D+Depth+Dist)^2}; \left[\frac{\text{energy}}{\text{km}^2} \right] \quad (3)$$

The physical meaning of the function is the surface density of earthquakes energy in the point of measurement. It is important to stress out that the first consideration of the earthquake magnitude and epicentral distance dependence was obtained using nonlinear inverse problem methods. The close distance strong earthquake will bear more electropotential variations, which will generate more power geomagnetic quake.

The correlation between the time period of increasing regional seismic activity, and tide extreme, recognized of predicted earthquake was established using the Alexandrov’s code REGN.

$$\text{StdDev} = \sqrt{\frac{\sum_{i=1}^N \left(1 - \frac{F_i}{F}\right)^2}{N-1}}, N = 24 \quad (4)$$

2. Daily signal.

$$DiornalSig_{today} = StdDev \quad (5)$$

3. The precursor signal.

$$PrecursorSig_{Today} = \frac{DiornalSig_{Today} - DiornalSig_{Yesterday}}{0.5(Am_{Today} + Am_{Yesterday})} \quad (5)$$

where the Am_{Today} , $Am_{yesterday}$ stand day by day geomagnetic activity Am middle indices. For example:

Now the geomagnetic quake is a signal for increasing of the imminent regional seismic activity and has more precise definition than previously. When this criterion is fulfilled one can say that the geomagnetic quake has a place.

Such quake is unique precursor for incoming earthquakes and in the next minimum or maximum of the local Tidal gravitational extreme, daily averaged module R of vector movement, somewhere in the region under consideration such predicted earthquake will occur.

The Standard Deviation Method we also used for date of ground-water level in the Noemberyan (NMB) station.

Description of the graphs

- The values of Am middle indices, averaged daily middle latitude geomagnetic activity indices.

- The next upper graph is presented the occurred earthquakes with index, which is the distance (≤ 500 km) from the station (monitoring point).

- The next graph presents the daily sum of function

- The upper graphs presents the behaviour of minutes and daily averaged values of earth’s surface tidal movment, calculated with Dennis Milbert’s code:

When the specific behaviour of field and its standard deviation are occurred more then one time at different houres of the day, it means the signals from future earthquakes with different epicenters are recorded.

Analysis comparison: Research results for Van (Turkey, 23.10.2011, $M=7.2$) [I], Garni (Armenia, 14.10.2011, $M=3.7$) [II], Khoy (Iran, 18.04.2013, $M=4.8$) [III] earthquakes.

I. Van (Turkey, 23.10.2011, M=7.2 (figure 6a, b, c))



Figure 6a. Map of the epicenters with magnitude $M \geq 3.5$ for time period 01 Sep - 01 Nov 2011

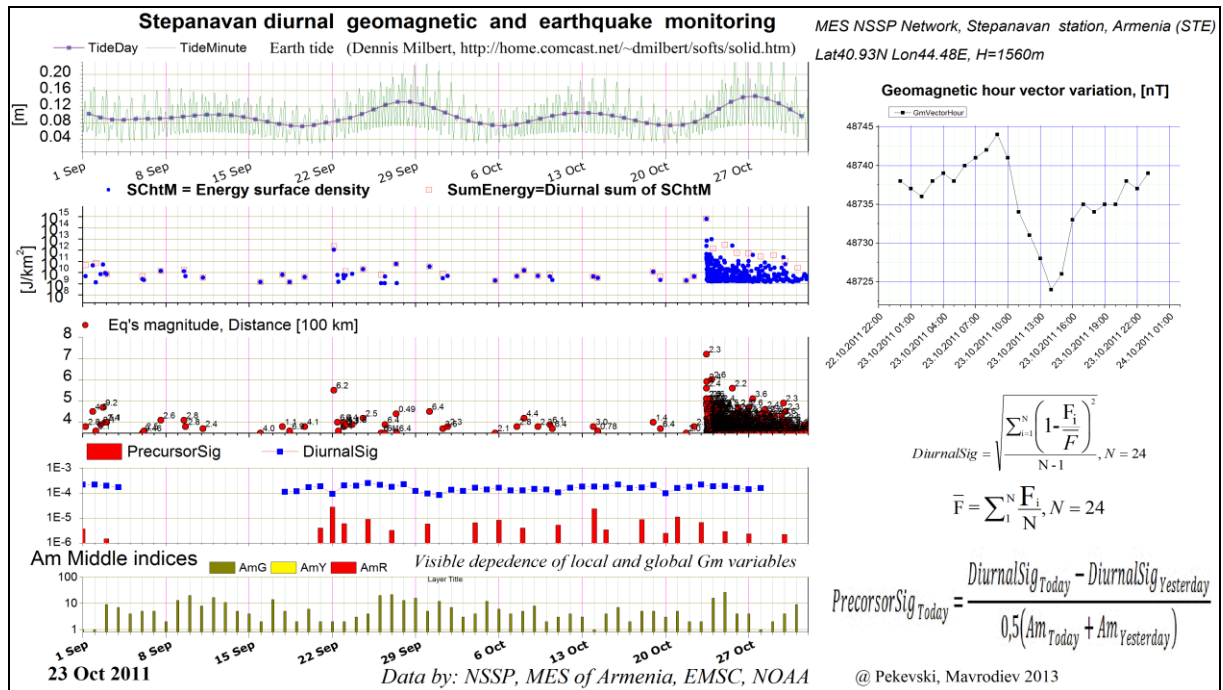


Figure 6b. "Stepanavan" geomagnetic daily monitoring including period of earthquake in Van (2011)

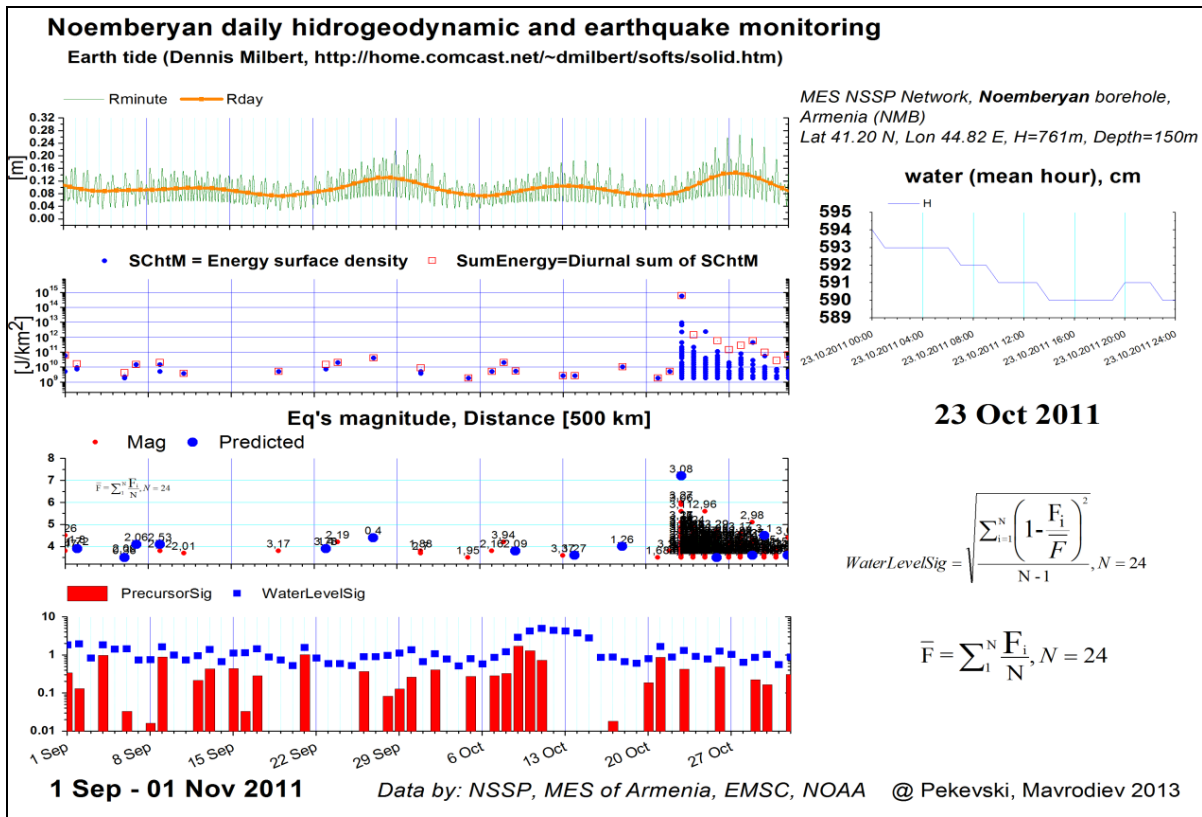


Figure 6c. “Noyemberyan” borehole daily monitoring including period of earthquake in Van (2011)

II. Garni (Armenia, 14.10.2011, M=3.7 (figure 7a, b, c))



Figure 7a. Map of the epicenters with magnitude $M \geq 3.5$ for time period 01 Sep - 22 Oct 2011

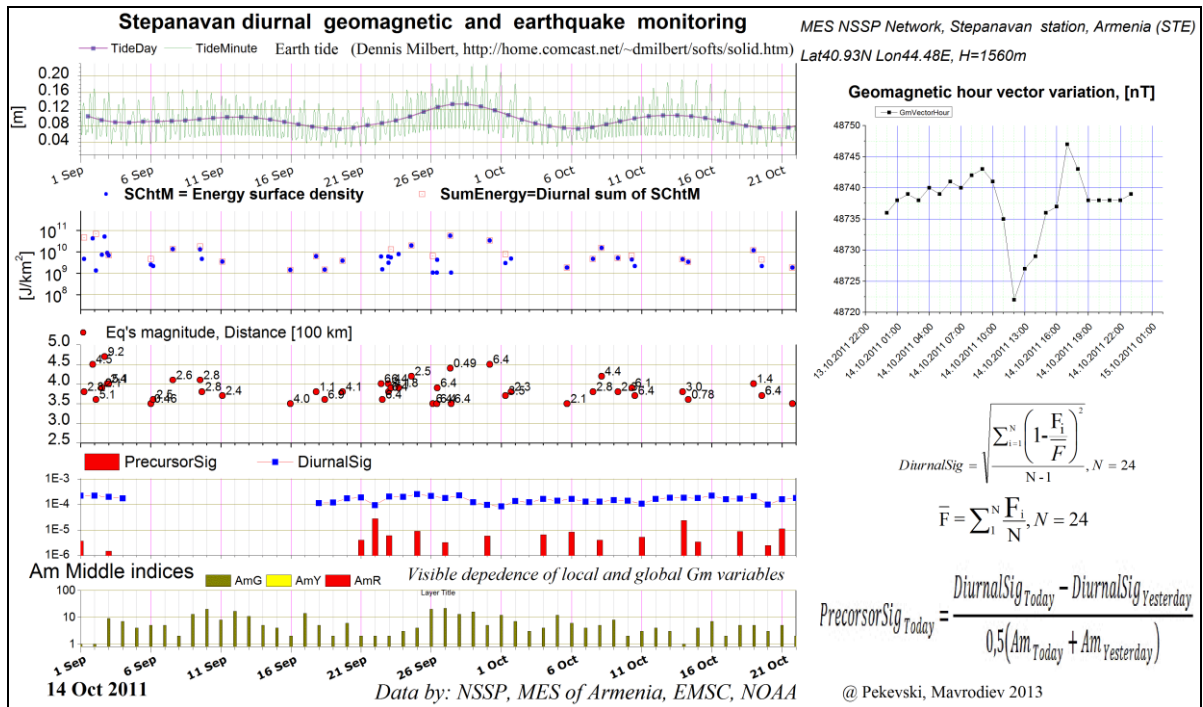


Figure 7b. “Stepanavan” geomagnetic daily monitoring including period of earthquake in Garni (2011)

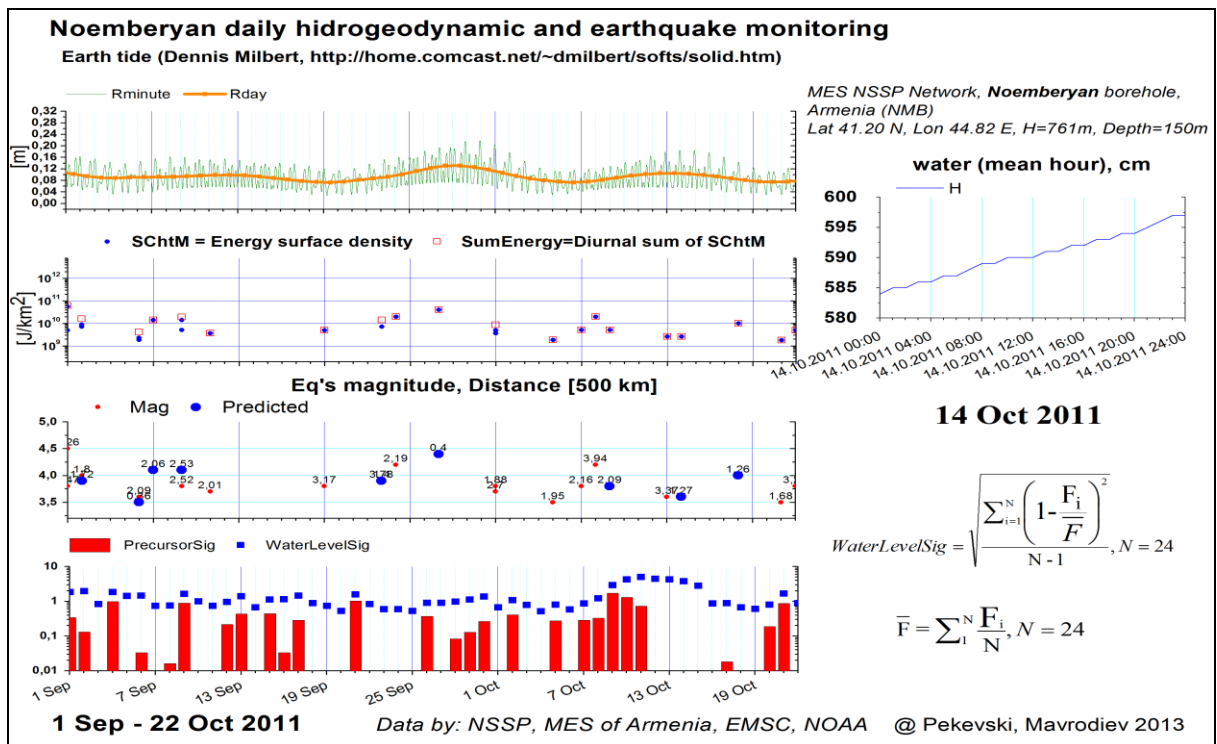


Figure 7c. “Noemberyan” borehole daily monitoring including period of earthquake in Garni (2011)

III. Khoy (Iran, 18.04.2013, M=4.8 (figure 8a, b, c))



Figure 8a. Map of the epicenters with magnitude $M \geq 3.5$ for time period 01 Mar - 22 May 2013

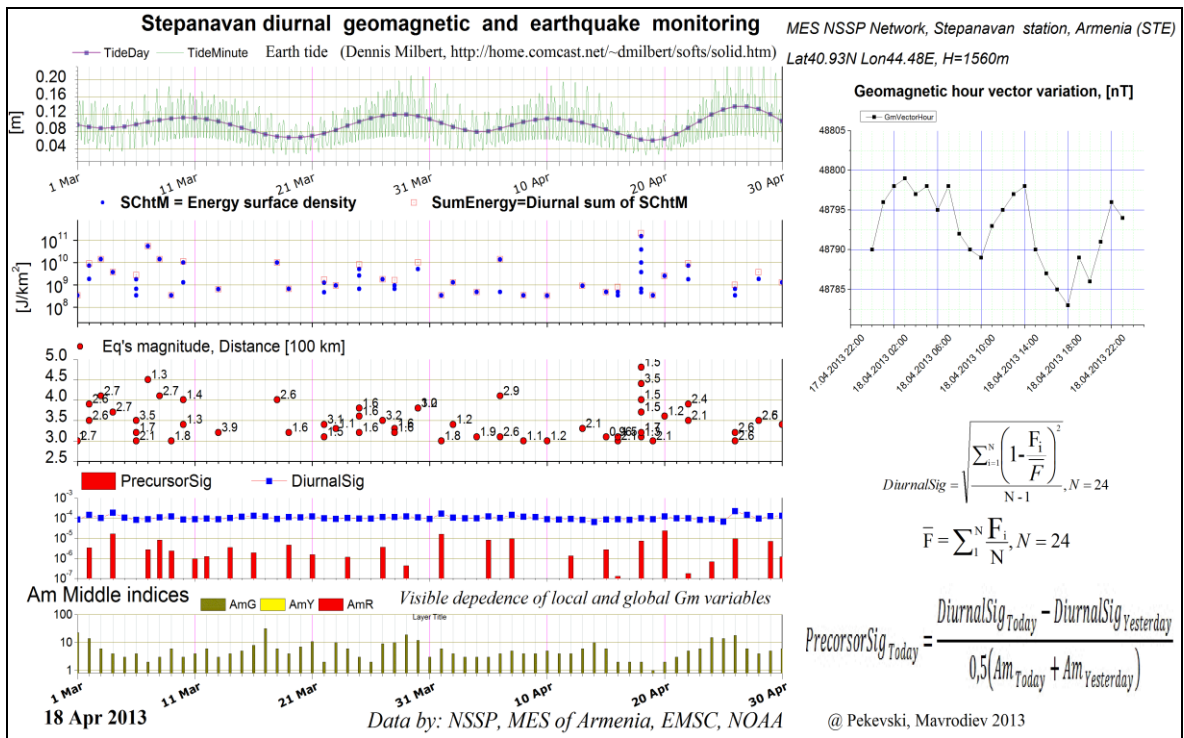


Figure 8b. “Stepanavan” geomagnetic daily monitoring including period of earthquake in Khoy (2013)

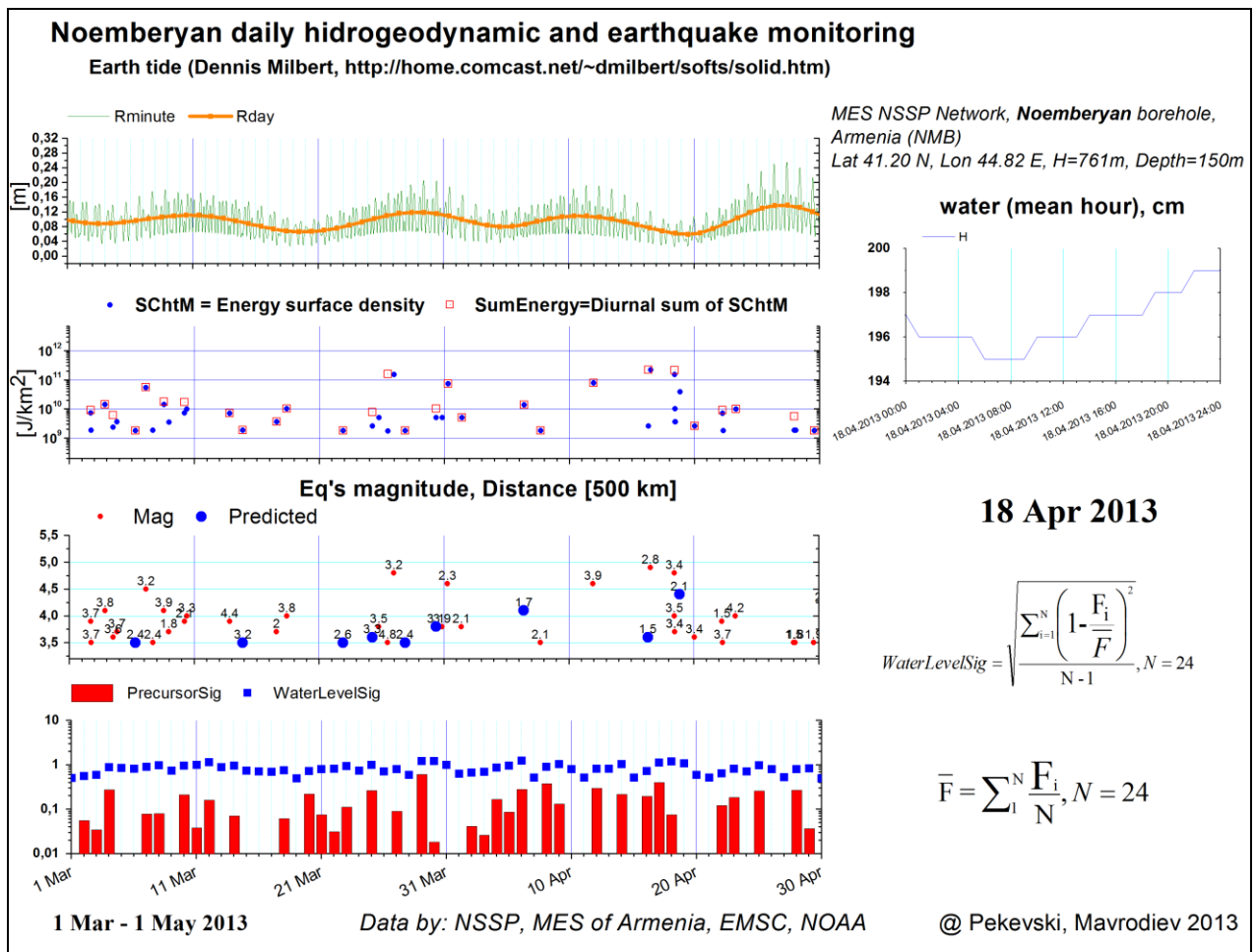


Figure 8c. “Noemberyan” borehole daily monitoring including period of earthquake in Khoy (2013)

Conclusion

Method Standard Deviation gives are the opportunity to get a signal for upcoming event. It can be used for operational forecasting purposes.

Reference

1. S. Cht. Mavrodiev, L.Pekevski. On reliability of the geomagnetic quake as regional imminent-earthquake precursor, complex research of earthquake’s forecasting possibilities, seismicity and climate change correlations, BlackSeaHazNet Methodological-Coordination Workshop 2-5 May 2011, Ohrid, Republic of Macedonia. BlackSeaHazNet Series, Volume 1, pp 49-63.
2. S. Cht. Mavrodiev, L.Pekevski. On the FP7 BlackSeaHazNet Project and its Possible Application for Harmonic Existence of the Regions. Black Sea Energy Resource Development and Hydrogen Energy Problems. Springer, Published in Cooperation with Nato Emerging Security Challenges Division 7-10 October 2012. pp 253-271.
3. T. Jimsheladze, G. Melikadze, G. Kikuashvili, S. Cht. Mavrodiev, L. Pekevski, M. Chkhitunidze. Study of Geomagnetic Variations in Georgia and establishment the Anomaly Nature of Earthquake Precursors, Complex research of earthquake’s forecasting possibilities, seismicity and climate change correlations, BlackSeaHazNet Training-Seminar Workshop 13-16 September, 2011, Tbilisi, Georgia BlackSeaHazNet Series, Volume 2, pp 205-214.
4. G.S. Vartanyan. Regional Geodynamic Monitoring System for Ensuring Safety in Geological and Exploratory Production of Oil and Gas // *Izvestia. Atmospheric and Oceanic Physics*. 2010. vol. 46 #8. pp. 952-964.

5. С.Ю Баласанян “Сейсмическая Защита и ее организация”, Гюмри Эльдорадо, 2004г, стр 164-169.
6. http://theo.inrne.bas.bg/~mavrodi/everyday_monitoring.html
7. <http://www.emsc-csem.org/#2>
8. <http://home.comcast.net/~dmilbert/softs/solid.htm>
9. http://www.swpc.noaa.gov/ftpdir/indices/old_indices/



*Трите сили или повеят на вятъра..., от цикъла „БАН – ракурси”
Three Powers or blowing of the wind ... , from cycle”BAS - Racources”*

*Бойко Вачев’2006
Boyko Vachev’2006*

ELECTROMAGNETIC SOUNDING OF THRACIAN TUMULI IN THE SBORYANOVO NATIONAL RESERVE, NEAR THE TOWN OF ISPERIH , RAZGRAD DISTRICT, NORTH EAST BULGARIA

**Yuriy Bogdanov^{1,2}, Volodymyr Pavlovych¹, Sergiy Prokopenko²,
Diana Gergova³, Boyko Vachev⁴**

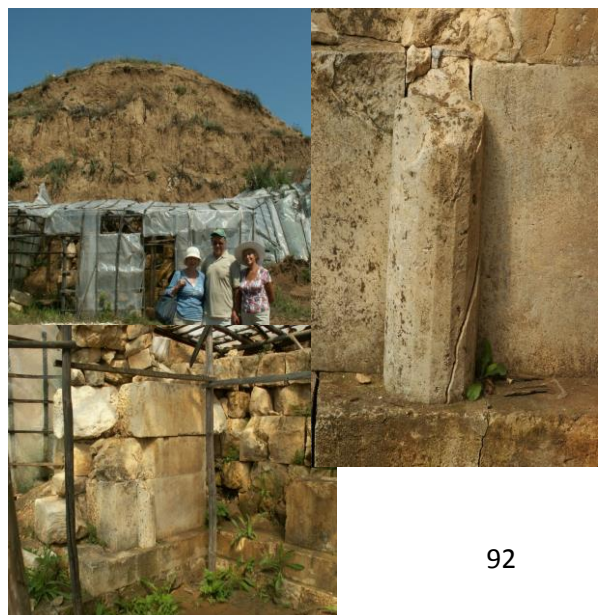
¹Institute of Nuclear Research, National Academy of Science of Ukraine,

²Spetsaviaindustry LTD, Kharkiv, ³Nationa Instiyute of Archaeology with Museum, Bulgarian Academy of Sciences ⁴Institute for Nuclear Research and Nuclear Energy, BAS

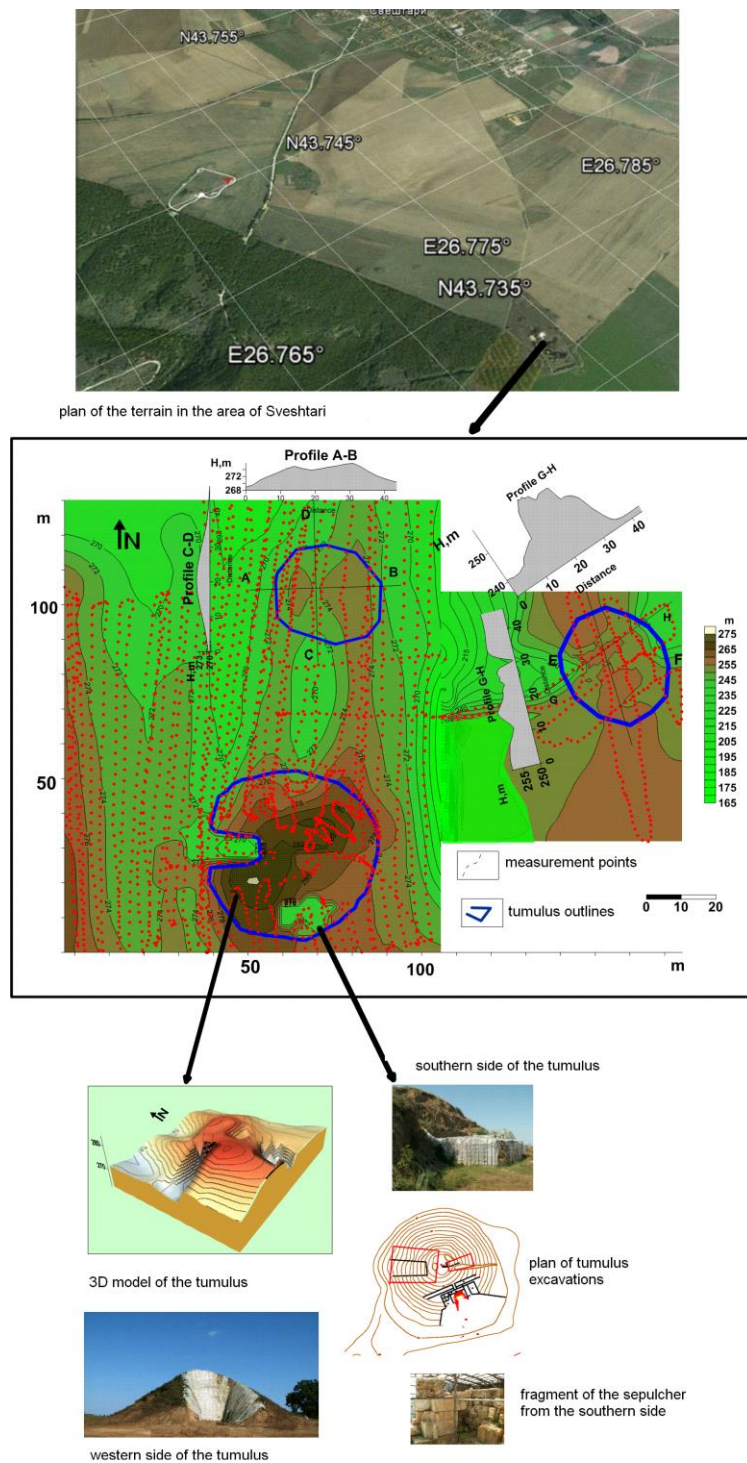
Complementing the existing data from various geophysical methods of investigating near-surface structures (the electrical resistivity and the georadar method) of the Thracian tumuli near the village of Sveshtari, in the Sboryanovo National Reserve (Gergova, Katevski 2008 374–379), detailed measurements of the natural electromagnetic radiation of the Earth were conducted in July 2013 in the area (Fig. 1). The neighboring region was studied with respect to seismicity using the same device and methodology (see presentation/report of Bogdanov, Pavlovych, Prokopenko on the conclusion BlackSeaHazNet workshop). The paleoseismic investigations had been carried out since the discovery of several tombs in the Eastern necropolis of Sboryanovo, including the Great Sveshtari tumulus, where evidence of ancient earthquakes was also found on the stone tomb in the southern part of the tumulus (see the photo below)

The essence of the method applied consists in the following. The Earth constantly emits electromagnetic waves over a sufficiently broad frequency range. According to present ideas, this radiation is generated throughout the thickness of the Earth's crust and mantle, and the intensity of radiation depends to a substantial extent on the stressed state of rock varieties – the greater the stress, the higher the radiation intensity. When passing through the near-surface layers, this radiation is scattered by internal inhomogeneities (and is reemitted in the most stressed areas) in such a manner that measuring the electromagnetic field in different points at the day surface provides actually a fixed diffraction pattern of electromagnetic wave scattering by internal inhomogeneities. The next main task is to decrypt the measurement results and to restore the internal structure of the near-surface layers (for the purposes of engineering geology, including the task of tumuli structure investigation). This method can be also implemented in the studies of the deeper strata of the Earth's crust and mantle, the depth being essentially determined by the measurement profile length at the surface in accordance with the laws of electromagnetic wave scattering (Bogdanov et al., 2002, 2008).

In this way the intensity of electromagnetic radiation (EMR) on the day surface represents the initial information for further analysis. To measure this value, a device has been developed that measures and records the amount of EMR pulses with amplitude exceeding a preset threshold per unit time. EMR is measured by means of a highly sensitive broadband antenna, which measures the magnetic component of the electromagnetic field (for higher accuracy the three components of the magnetic field vector – x,y,z, component x changes along NS direction, component y – along EW direction and component z – along the vertical). The time interval of pulse number measurement is set in advance. The time interval, accepted for the data of walking speed measurements, is equal to 0.2 s, which means that for an average pedestrian velocity of about 5 km/h the EMR pulse amount is recorded approximately at every 30 cm. The



GPS coordinates have been recorded for each measurement point.



Further on the EMR data were transferred together with the coordinates of each point from the device to the computer and processed using a special set of software programs.

The first stage of this processing is shown in Fig. 1: binding to the terrain according to the GPS coordinates (top), binding to the relief by plotting the route of measurements (middle) and constructing a 3D model of the site on the base of GPS coordinates and photos (bottom). The next stage of data processing consists in mapping the signal intensity and its gradients.

It must not be forgotten that the intensity data are recorded in the device for each component of the magnetic field vector separately and that all three components – x, y, z, have to be analyzed in order to build the complete picture of the structural features of the near-surface layer. As an example the map of the magnetic field x-component distribution in the area of Tumulus I is shown in Fig. 2.

The vortex pattern of the electromagnetic energy distribution around the tumulus is worth noticing, which, as shown by experience, is typical for EMR distribution around pyramidal structures.

Fig. 1. The first stage of EMR data processing – binding to the terrain.

Such a pattern is probably also typical for cone-shaped structures but this assertion needs additional verification since the present study is a first attempt of exploring sepulchral tumulus and large cone-like structures in general.

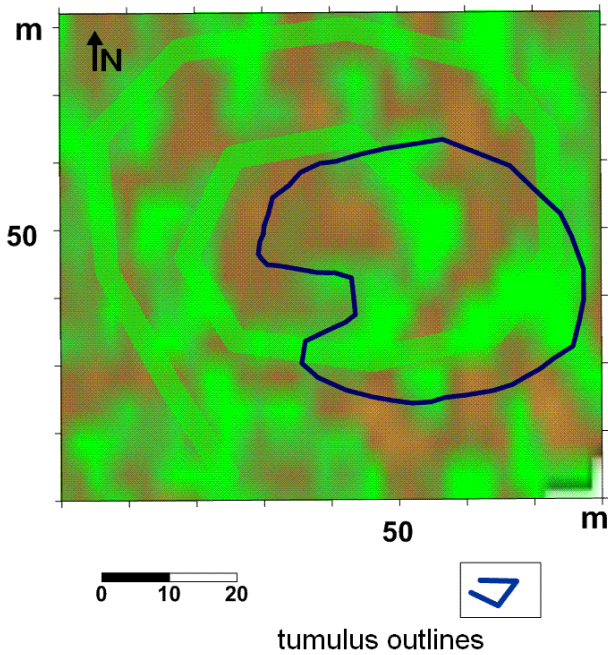


Fig. 2. Intensity distribution of the magnetic field x-component in the vicinity of Tumulus I (Great Sveshtari tumulus). Distribution of EMR energy around the tumulus in a vortex-like pattern. The tumulus outline is shown with a blue line taking into account the lower excavation.

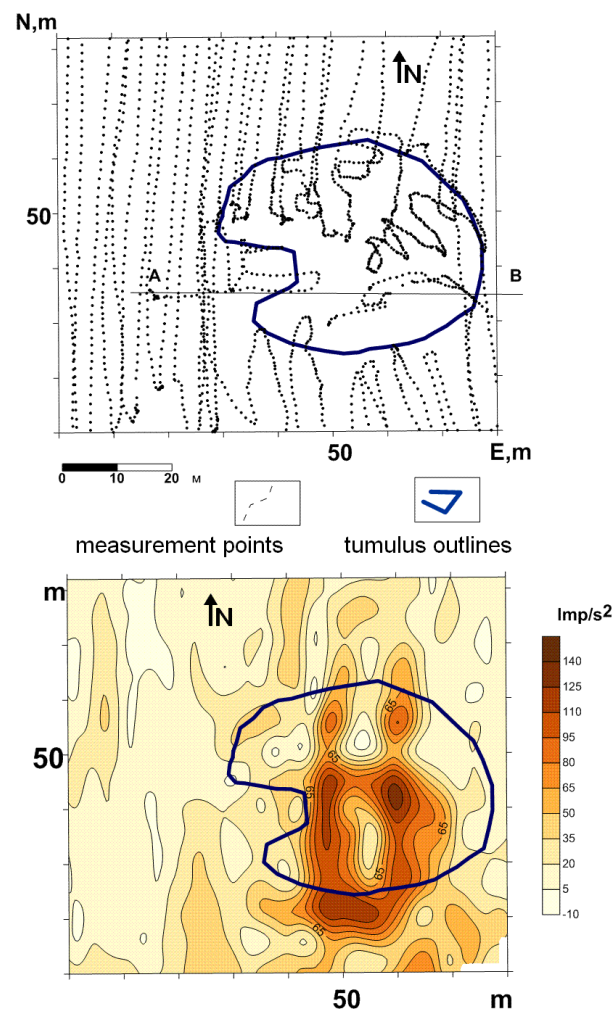
The maps with the distribution of intensity gradients of the field x-component are shown in Figs. 3 and 4. They are useful in detecting underground structures and sometimes it is expedient to present them in a different contrast. So, the distribution of the intensity gradient in the area of Tumulus I is shown in Fig. 3 with indication of the survey routes.

The distribution of the field intensity gradients across the survey area is presented in Fig. 4. Moreover, the distribution above Tumulus I (Great Sveshtari tumulus) is the same as in Fig. 3, but it is shown in black-and-white contrast.

The careful analysis of the figures proves that:

1. In the central, southern and southwestern part of Tumulus I (Great Sveshtari tumulus) anomalies in the EMR field are observed, which may be associated with underground structures, and the anomaly in the southern part is obviously related to the excavated destroyed sepulcher.
2. The field anomalies in Tumulus II (Tumulus 27) clearly exhibit geometric structures that can be associated with underground facilities.
3. The field above Tumulus III (Tumulus 31) is sufficiently homogeneous with the exception of its central part, which requires a more detailed study.
4. Typical strips are traced from Tumulus III (Tumulus 31) to Tumulus I (Great Sveshtari tumulus), which, as proved by experience in seismic structure investigation, may be associated with crustal faults due to paleoearthquakes.

Fig. 3. Anomalous field distribution in the vicinity of Tumulus I (Great Sveshtari tumulus). Measurement routes are shown in the top.



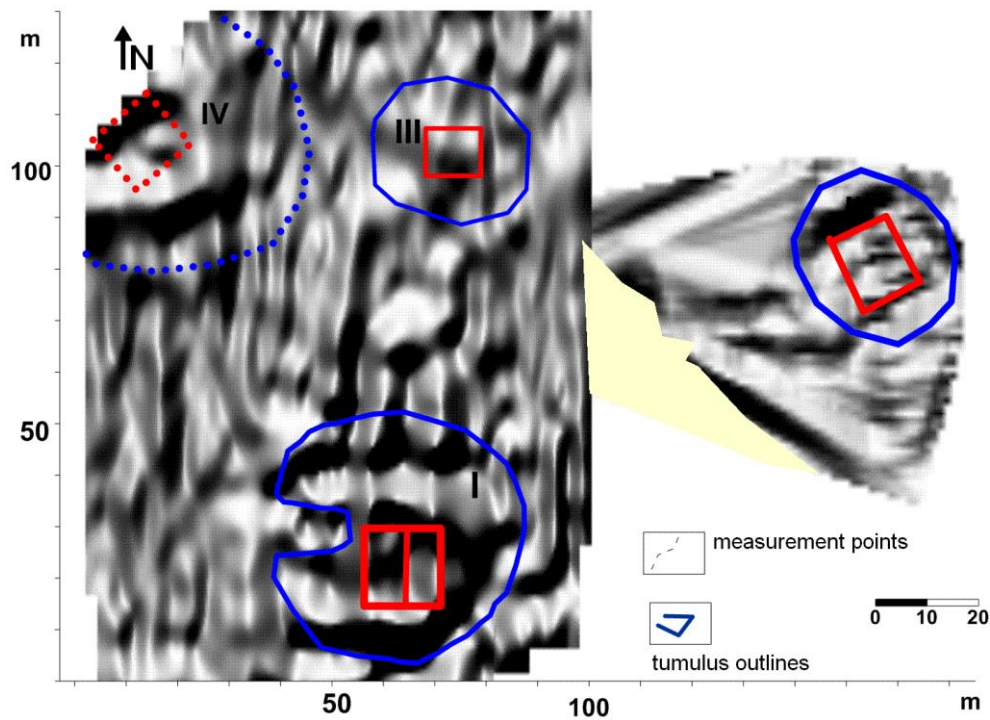


Fig. 4. Field distribution of intensity gradients on the surveyed site. The tumulus are indicated by blue outlines and numbers.

The next step in data processing is the composition of in-depth sections along the measurement profiles. The procedure of constructing the sections is sufficiently complicated mathematically and it will not be considered in detail here. It has to be noted only that it is based on the laws of electromagnetic wave scattering and on investigating the correlation functions.

Several sections of the surveyed Tumuli I(Great Sveshtari tumulus), II(Tumulus 27) and III(Tumulus 31) are presented below. It has to be reminded that the sections are constructed on the base of analysis only of the magnetic field x-component. The analysis of the other two components may contribute to introducing additional detail in the obtained patterns.

Figure 5 shows two sections of Tumulus I (Great Sveshtari tumulus) and their comparison with the geophysical section obtained by the electrical resistivity method. The location of the sections is clearly seen in the figure (profiles A-A' and B-B'). The places with suggested heterogeneous inclusions are shaded. An interesting feature of this tumulus is distinctly seen in section B-B': it seems as if this tumulus consists of three tumuli, formed on top of one another, with the destroyed sepulcher (left, bottom of profile B-B') being under the external tumulus.

The data from the exploration of Tumulus II (Tumulus 27) are shown in Fig. 6 – this is the most intriguing information from the viewpoint of underground structures that have not been discovered earlier. The scheme of survey routes and the distribution of field intensity at the surface are shown in the center of the top part of the figure. Field distribution anomalies are clearly visible here. Unfortunately, the data for this tumulus are not in sufficient detail because the manifestation of “surprises” has not been expected here at all. Further on, based on the analysis of six in-depth profiles (bottom of the figure) the supposed situation of underground structures has been localized (right, top part of the figure).

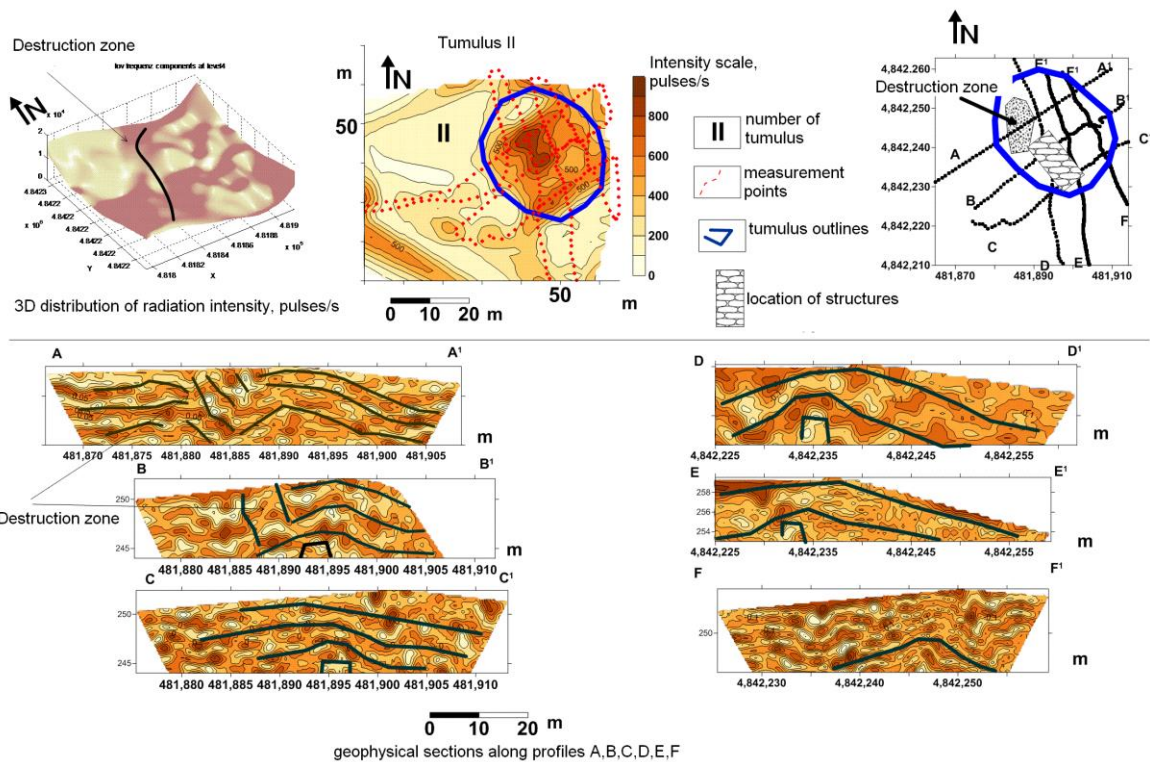
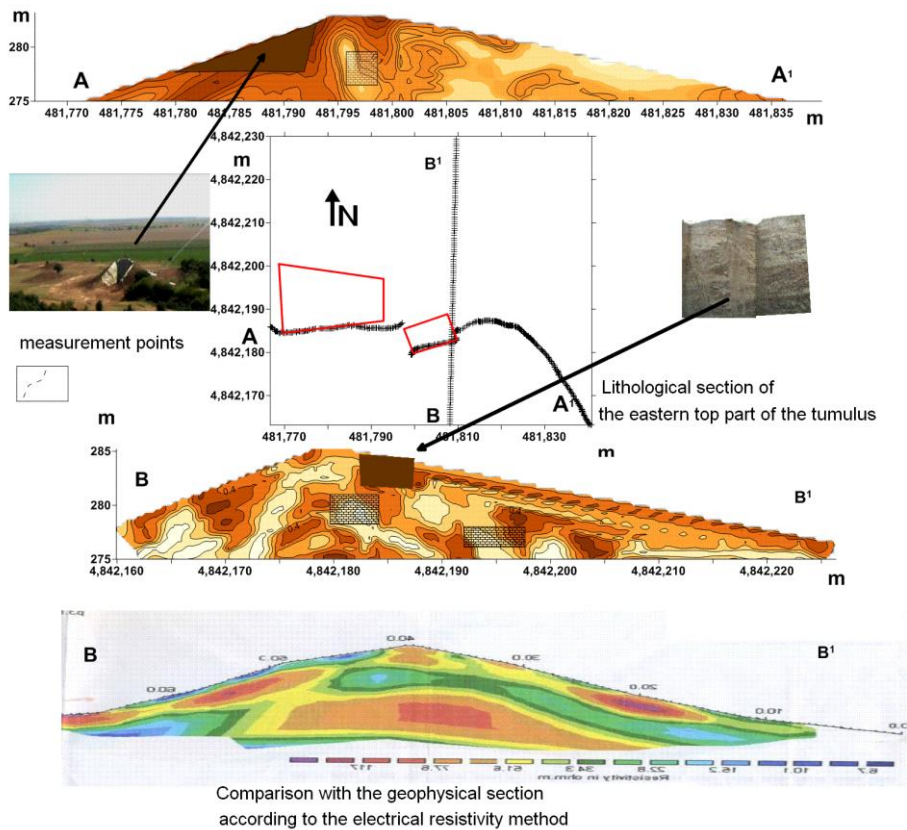


Fig. 6. Scheme of Tumulus II (Tumulus 27), location of survey routes, scheme of sections with supposed location of underground structures and 3D distribution of field intensity (top part of the figure); geophysical sections according to EMR data (bottom part of the figure)

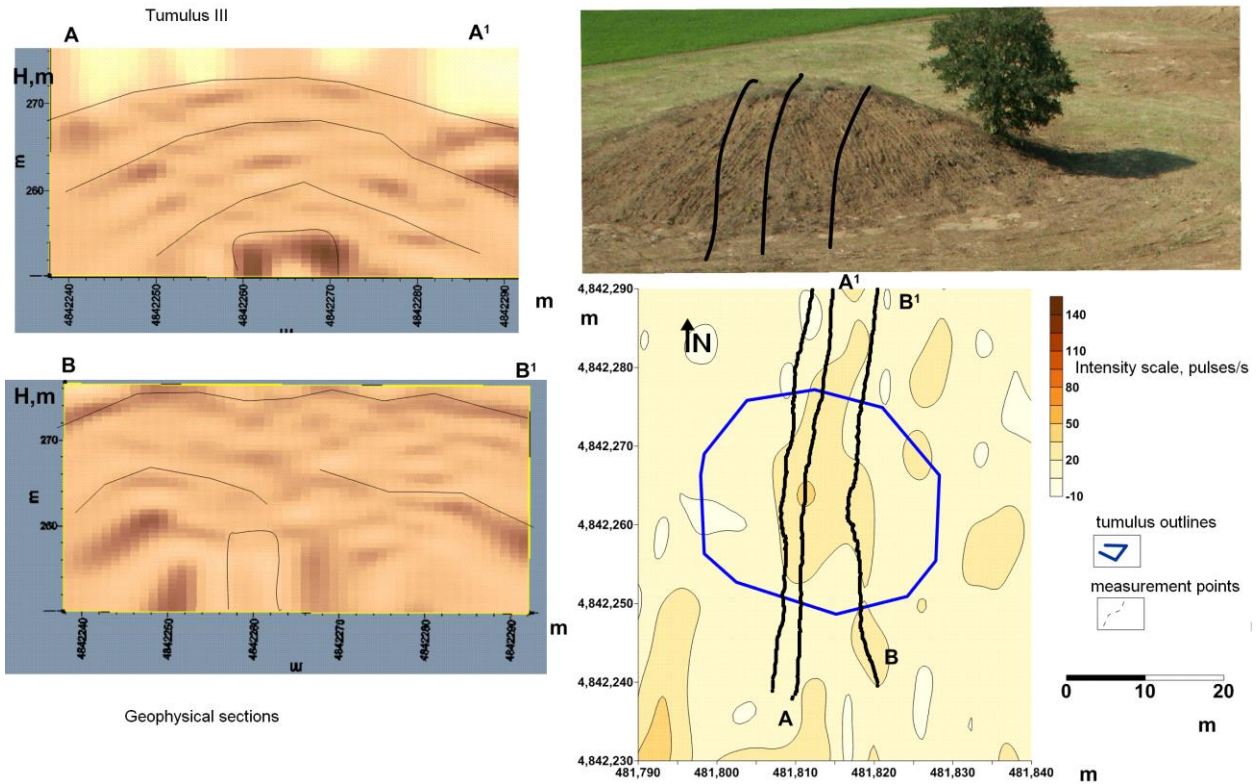


Fig.7. Distribution of survey routes, field intensity and geophysical sections of Tumulus III(Tumulus 31).

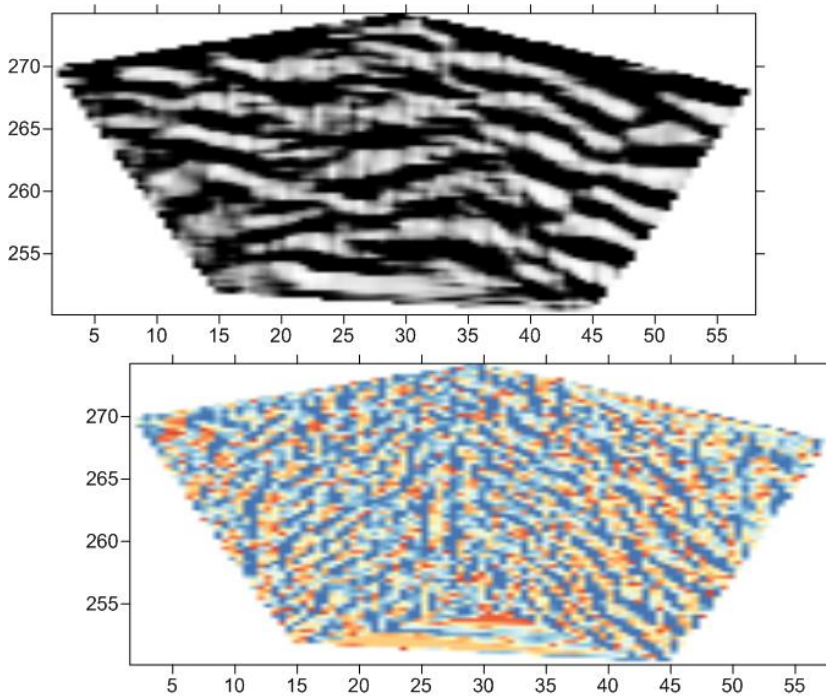


Fig. 8. Geophysical sections of Tumulus III Tumulus 31). The existence of geometric structures may be supposed in the center of the bottom part of the tumulus.

Tumulus III (Tumulus 31) (Figs. 7, 8) seems empty at first sight, but the detailed analysis of the sections suggests the existence of certain structures in its center.

To compose the conceptual models of information processing for the tumulus, an EMR survey was conducted along two profiles

of the well-studied sepulcher under Tumulus 13. These data provide information concerning the specific features of the geophysical sections that have to be taken into account when processing the results for unexplored tumulus.

Finally, the field intensity distribution was obtained from airborne survey.

In conclusion, it has to be pointed out that the above results have been obtained by processing only the EMR magnetic field x-component for a limited number of profiles, passing above the most interesting places of the tumulus. The processing of all profiles in all three coordinates, taking under consideration the additional information recorded (dispersion and automatic changes in the detection threshold in the course of measurement), may provide the possibility of obtaining three-dimensional distribution patterns of underground cavities and structures.

The excavations in Tumulus I (Great Sveshtari tumulus) in 2013 did not confirm the initial assumptions based on the existing anomalies.

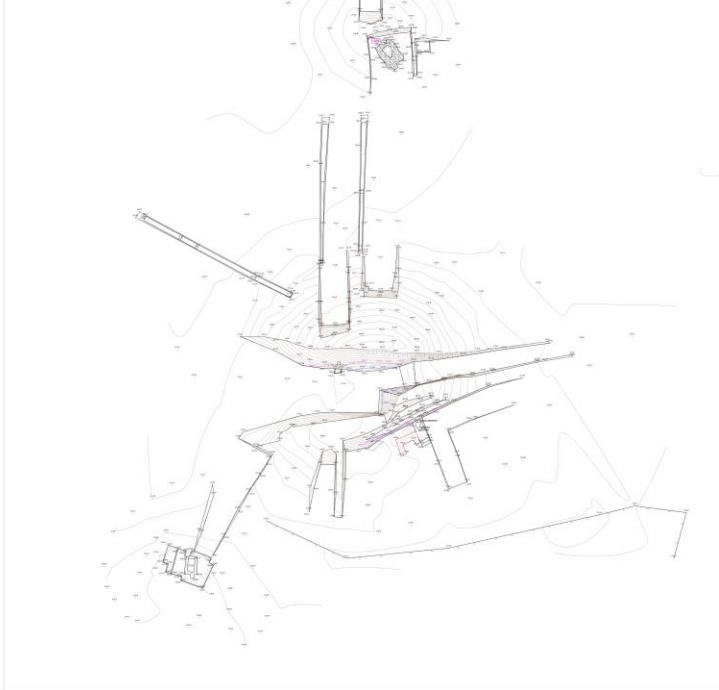
Subsequently, at the end of the year burials and remains of structures were found in Tumuli II(Tumulus 27) and III(Tumulus 31)(Gergova 2013; 2014 in print). The burial of horses with a 2-wheel chariot, encountered in Tumulus II(Tumulus 27) is the first of this type in Bulgaria and is of special interest(see photos below and Figs. 6 and 7).

References

- Bogdanov, Yu.A., Zakharov, I.G., Tyrnov, O.F. and M. Hayakawa, 2003. Electromagnetic effects Associated with Regional Seismic Activity in Crimea during the Interval July–August 2002, J. Atmospheric Electricity, Vol. 23, No. 2, pp 57-67
- Bogdanov, Yu. A., Bondarenko, N.V., Zakharov, I.G., Loiko, N.P., Lukin, V.V., Cherniakov, A.M. and O.R. Chertov, 2008. Instrument and methodical providing of the method of the Earth spontaneous electromagnetic emission analysis. Geophysical journal (Ukraine), V30, 2, pp 32 – 41.
- Gergova, D., 1995 Christoskov, L., Rizzo, V. *Traces of Seismic Effect on Archaeological Sites in Bulgaria*. In: Annali di geofisica, vol. XXXVIII, № 5-6, November-December 1995, 907-918
- Gergova D., 1995 I. Iliev, Rizzo, V. Evidence of a seismic event on Thracian Tombs., dated to the Hellenistic period. In: Annali di geofisica, vol. XXXVIII, № 5-6, November-December 1995.
- Gergova, D., 2005 D. Evstatiev, B. Vachev.. *Archaeological and Geological Analogues for the Safety of the Radioactive Waste Repositories*. – Annual Report 2005. Institute for Nuclear Research and Nuclear Energy. Sofia, 84–88.
- Gergova D.,D. 2005 Evstatiev, V. Rizzo. *Geoarchaeological characteristics of the Thracian tumuli in Bulgaria*. – Helis, 4, 156–168.
- Gergova, D., 2008 I. Katevski. *Archaeology and Geophysics in the Sboryanovo National Reserve*. – In: Geoarchaeology and Archaeomineralogy. Proceedings of the International Conference 29-30 October, Sofia, 374–379.
- Gergova D. *Under the Sign of Orion. Latest Discoveries from the Royal Necropolis of the Getae*. Credo Bonum . 2013
- Гергова Д. 2014 .*Проучвания на Голямата Свещарска могила през 2013 година*.- АОР за 2013г., София 2014(под печат)
- Гергова Д. 2014 а. *Проучвания на три могили от Южната група на Източния могилен некропол в Сборяново през 2013година*.- АОР за 2013 г. ,София 2014(под печат)



The tomb in Tumulus III(Tumulus 27)



Plan of the Great Sveshtari tumulus,
Tumuli II(Tumulus 27)
and III(Tumulus 31)



The Charriot with two horses in Tumulus 27



METHOD OF STANDARD DEVIATION FOR ANALYSIS OF CAUCASUS BOREHOLE WATER LEVEL DATA

Ani Gevorgyan², Armine Khangaldyan³, Strachimir Cth. Mavrodiev¹, Margar Adibekyan², George Melikadze⁴, Aleksandre Sborshchikovi⁴, Genadi Kobzev⁴ and Tamar Jimsheladze⁴

¹ *Institute Nuclear Research and Nuclear Energy - Bulgarian Academy of Sciences;*
schtmavr@yahoo.com

² *Western Survey for Seismic Protection SNTO; adibekyan@yahoo.com; ani_gevorkjan@mail.ru*

³ *“Survey for Seismic Protection” Agency at the MES of RA; arminenem@mail.ru*

⁴ *M. Nodia Institute of Geophysics, Iv. Javakhishvili Tbilisi State Universit; melikadze@gmail.com*

Abstract

In this work it is explored by Method of Standard Deviation for Analysis of Hydrodynamic parameter. For that it was researched Hydrogeodynamic parameters of several earthquakes in Armenia and Georgia by following the earthquakes in South Caucasus and for comparative analysis it was used Hydrogeodynamic parameter of the Networks of Armenia and Georgia. The result of the monitoring of water level variation parameter indicated a direct connection between deformation processes to strong earthquakes.

Introduction

Seismological investigations in the Caucasus, and particularly in Armenia, have been conducted since late XIX century. They were related mainly to investigations of strong earthquakes. The regional seismic network of Armenia was a part of the USSR United System of Seismic Observation (USSO). The “Spitak” earthquake showed the necessity of developing the existing seismic network and its technical re-equipment with contemporary high technology equipment and software. After the establishment of National Survey for Seismic Protection (NSSP) of the Republic of Armenia (RA) in 1991, new tasks were posed for Armenian seismology, directed to the population protection against strong earthquakes. Since then, the seismic network was being developed through its upgrading and increase of the number of seismic stations.

Experiment was done for earthquakes in time-series have been studied using the variation of water level in boreholes and earth tidal. Short introduction of method Standard deviation: the signal for imminent increasing regional seismic activity is the hydrogeodynamic parameter (water level) where is defined as a jump of daily averaged SDF (standard deviation function). Such approach permits to compare by numbers the daily behavior of the hydrogeodynamic field with those in other days. Among the earthquakes occurred on the territory under consideration in certain time period, the “predicted” one is the earthquake with magnitude M and epicenter distance which is identified by the maximum value of the function: The physical meaning of the function is the surface density of earthquakes energy in the point of measurement.

Investigated period of several earthquakes and hydrogeodynamic parameter in Armenia and Georgia. For comparative analysis using data of water level from the network:

Analysis Comparison of ground-water level in borehole “Noemberyan” (Observatory Network, NSSP of Armenia) and “Akhalkalaki” (Water Observatory, DSH Georgia) for “Van” (Turkey, 23.10.2011, $M=7.2$) [I], “Zaqatala” (Azerbaijan, 07.05.2012, $M=5.4$) [II], “Mingachevir” (Azerbaijan, 07.04.2013, $M=3.8$) [III] earthquakes.



I. Van (Turkey, 23.10.2011, M=7.2 (figure 1))

On the figures below at the first graph in the left corner is the picture of tidal behavior [m], the next shows the energy (J/km^2), the next – magnitude, and the last describes precursors (red columns) and water level signals (blue points). The blue points has been count using normal standard deviation and the red columns so called precursors were obtain by subtraction of the daily standard deviation of today and the previous day. The first graph in the right corner is water mean during 23 October the period of great Turkey (Van) earthquake and the next describes standard deviation of water level.

Figure 1. Map of the epicenters with magnitude $M \geq 3.5$ for time period 01 Sep - 01 Nov 2011

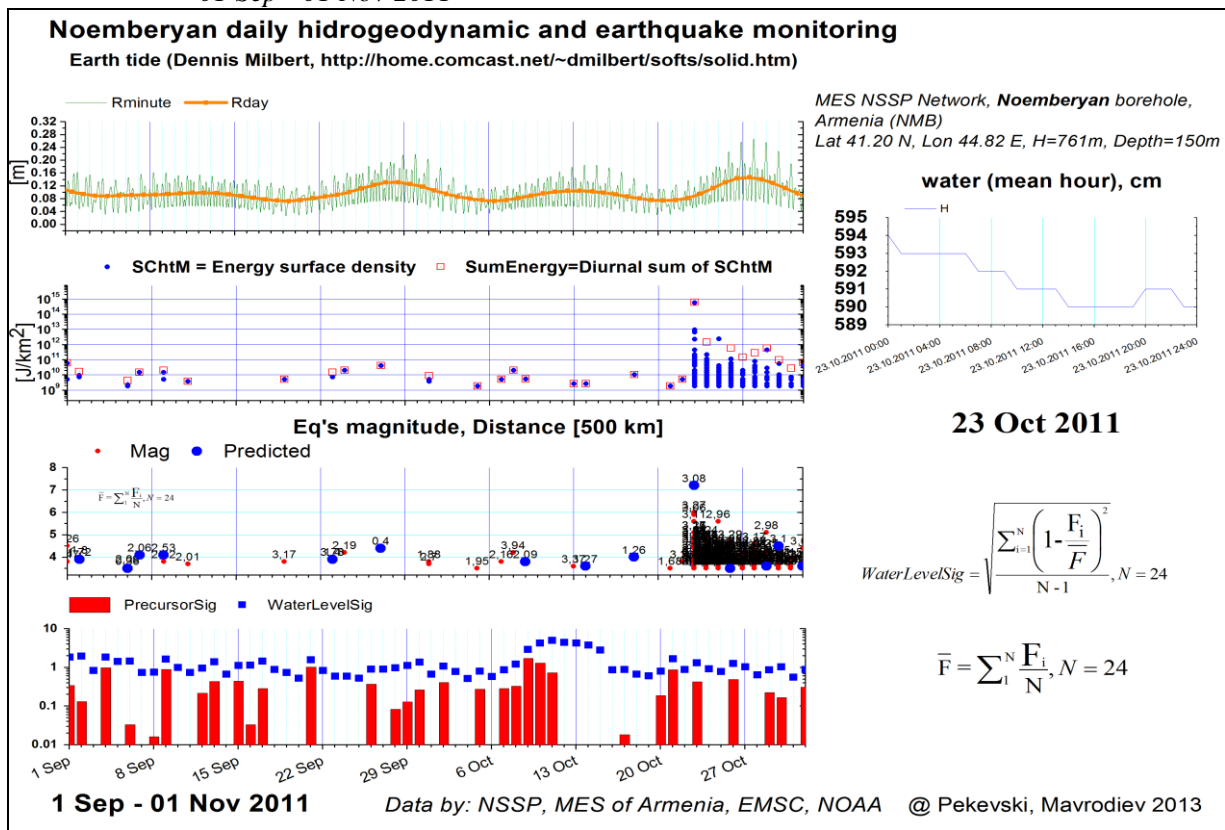


Figure 2. “Noemberyan” borehole daily monitoring including period of earthquake in Van (2011)

On this figure on “Noemberyan” borehole during 23 October Turkey (Van) earthquake $M=7.2$ we can see anomaly, which is expressed by the falling of water level signal during one week before “Van” earthquake (figure 2). The anomaly has place to be during aftershocks too.

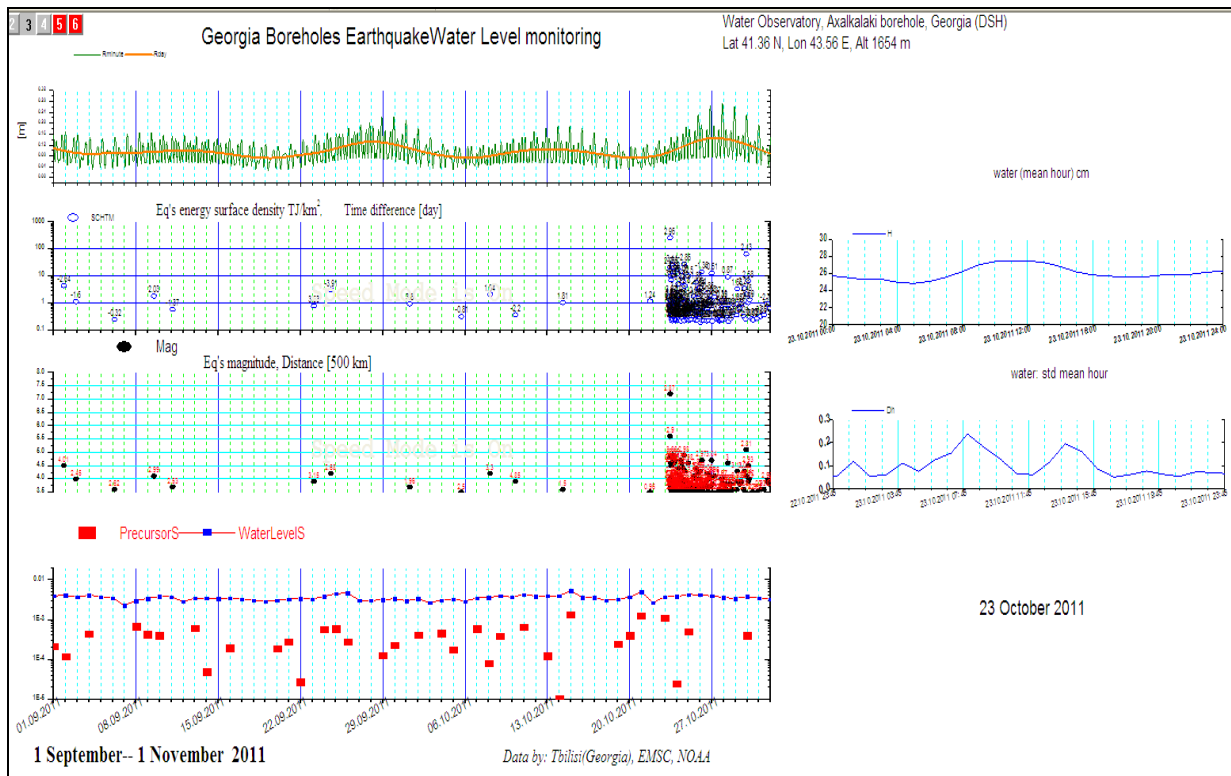


Figure 3. “Akhalkalaki” borehole daily monitoring including period of earthquake in Van (2011)

The same situation is on this figure. Here we have “Akhalkalaki” borehole data for 23 October (figure 3). As we have mentioned above, one week before the earthquake we have the same anomaly at “Akhalkalaki” borehole.

II. Zaqatala (Azerbaijan, 07.05.2012, M=5.4 (figure 4))



Figure 4. Map of the epicenters with magnitude $M \geq 3.5$ for time period 01 Apr - 01 Jun 2012

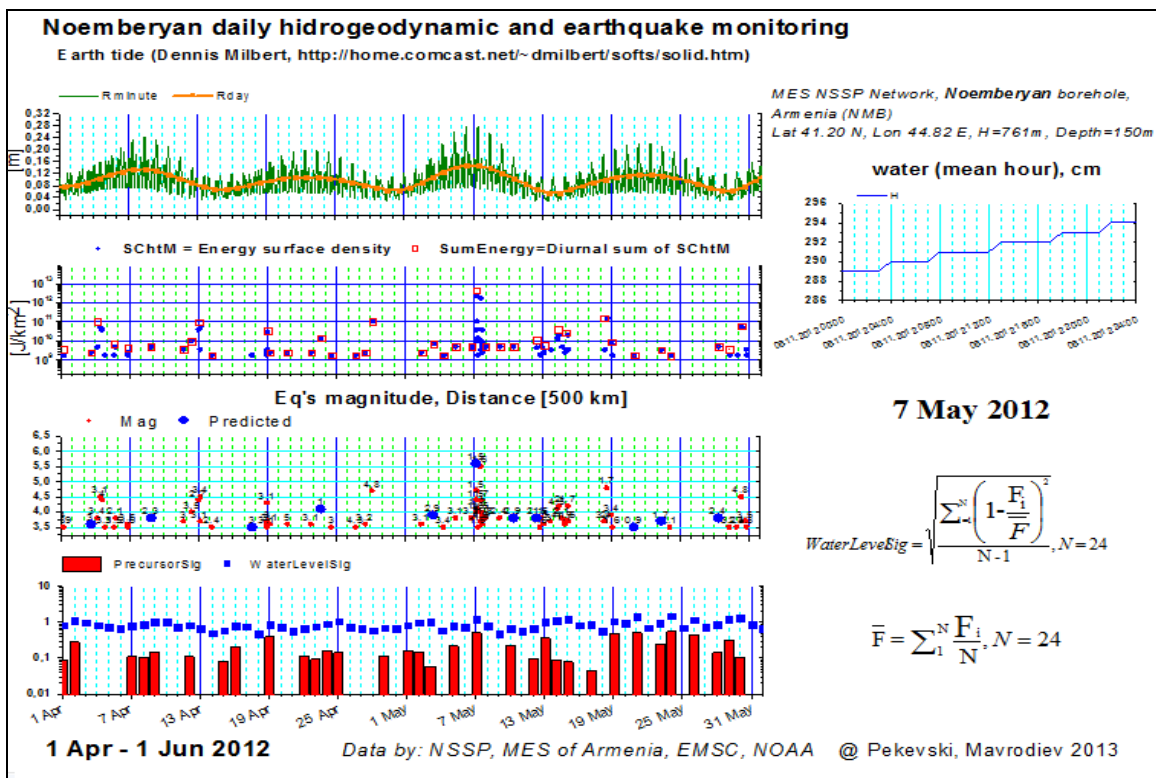


Figure 5. “Noemberyan” borehole daily monitoring including period of earthquake in Zaqatala (2012)

On this figure, which describes “Noemberyan” borehole during “Zaqatala” earthquake (07.05.2013 M=5.4), we also have an anomaly, which appears in falling of water level signal during 3 days before an earthquake (figure 5). Also the anomaly continues during the earthquake.

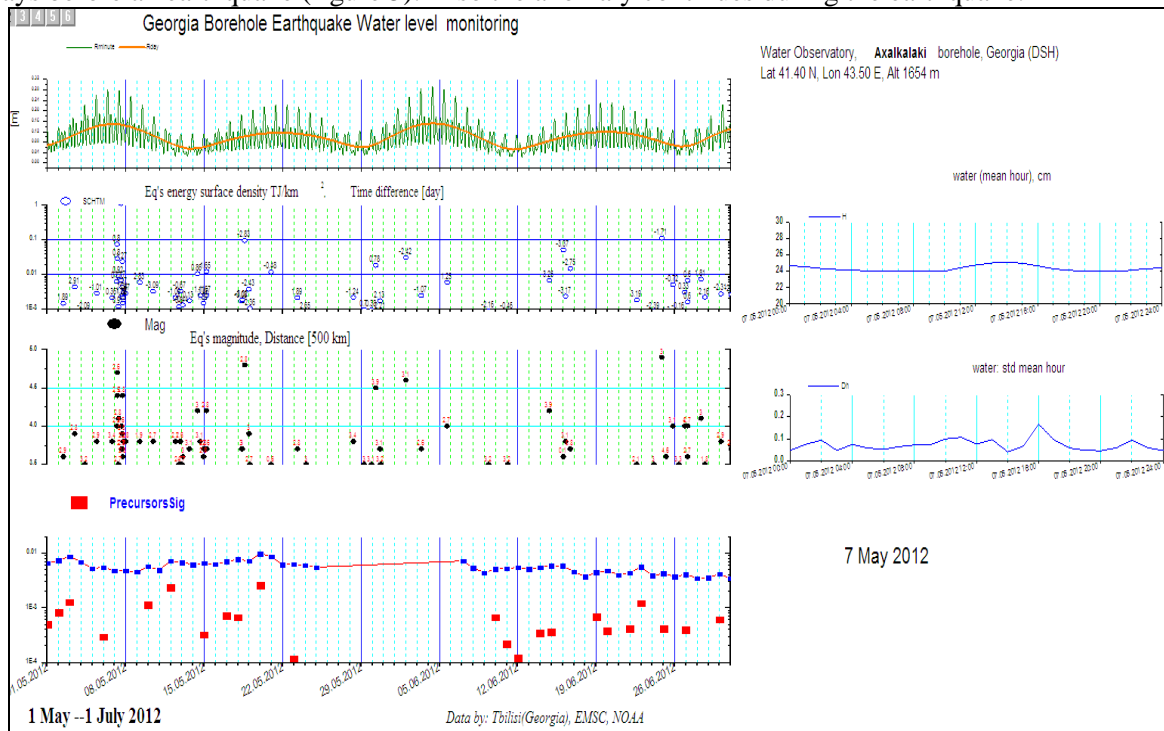


Figure 6. “Akhalkalaki” borehole daily monitoring including period of earthquake in Zaqatala (2012)

The same situation is on “Akhalkalaki” borehole (figure 6). As we see the anomaly starts during 3 days before an earthquake and ends after it.



Figure 7. Map of the epicenters with magnitude $M \geq 3.5$ for time period 01 Mar - 01 May 2013

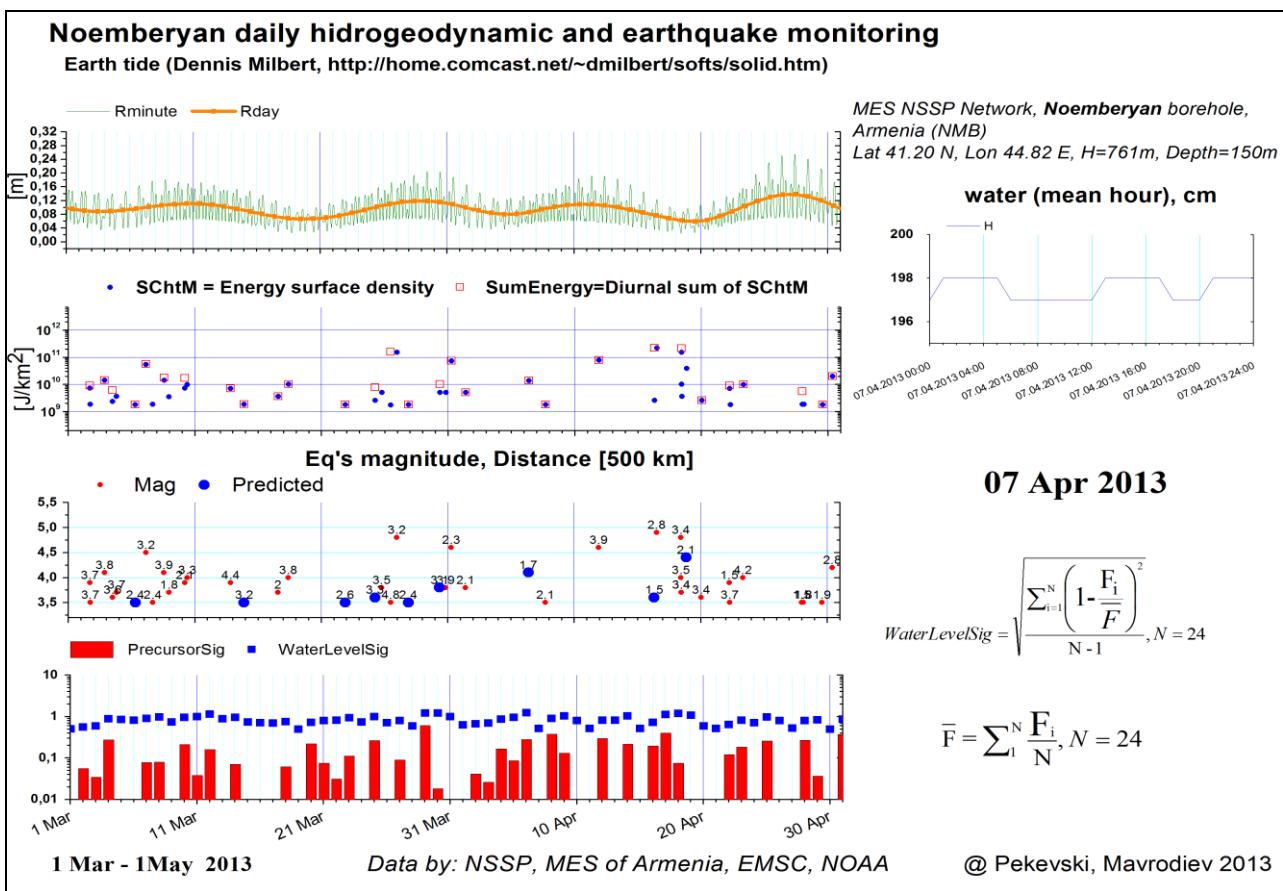


Figure 8. “Noemberyan” borehole daily monitoring including period of earthquake in Mingachevir (2013)

III. Mingachevir (Azerbaijan, 07.04.2013, $M=3.8$ (figure 7))

One more figure of “Noemberyan” borehole for the period of “Mingachevir” earthquake (07.04.2013 $M=3.8$) has anomaly too (figure 8). We see the growing of water level signal during one week before this earthquake and falling after earthquake.

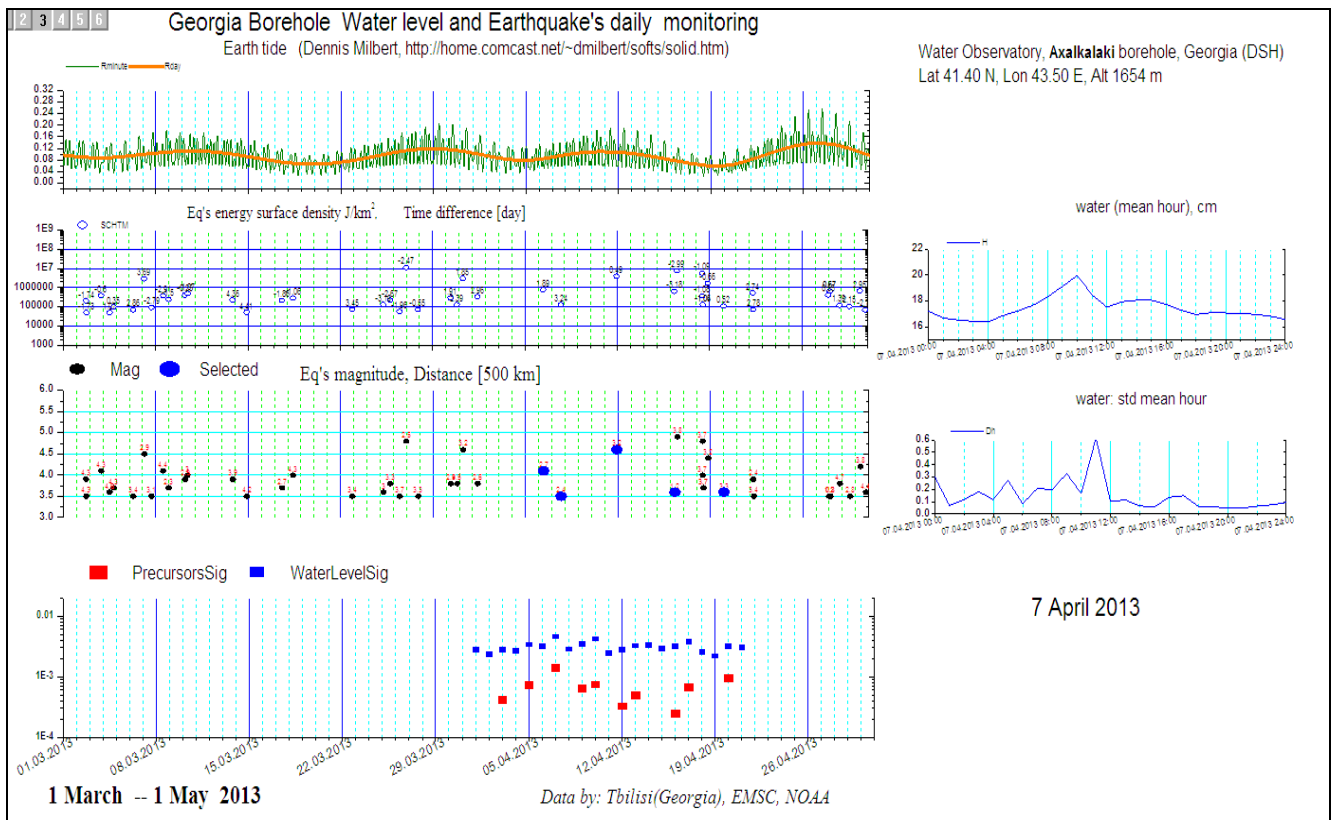


Figure 9. “Akhalkalaki” borehole daily monitoring including period of earthquake in Mingachevir (2013)

The same effect as on “Noemberyan” borehole we have on “Akhalkalaki” well too (figure 9). Growing of water level signal before an earthquake and then falling down after earthquake.

Conclusion

1. Before the earthquake “Van” (Turkey, 23.10.2011, M=7.2), the water level variation in the boreholes “Noemberyan” and “Ahalkalaki” is falling during one week before the earthquake, which means that the expansion process has occurred.

2. The water level variation in boreholes “Noemberyan” and “Ahalkalaki” before the earthquake “Zaqatala” (Azerbaijan, 07.05.2012, M=5.4) also is falling during three days before the earthquake, which means that the expansion process has occurred.

3. The water level variation in boreholes “Noemberyan” and “Ahalkalaki” before the earthquake “Mingachaur” (Azerbaijan, 07.04.2013, M=3.8) is growing during one week before an earthquake and then during it starts to fall down, which means that we have compression process before the earthquake and then expansion process.

The results of the monitoring of water level variation parameter indicated a direct connection between deformation processes imminent earthquakes and tides extreme.

Reference

1. S. Cht. Mavrodiev, L. Pekevski. On reliability of the geomagnetic quake as regional imminent-earthquake precursor, complex research of earthquake’s forecasting possibilities, seismicity and climate change correlations, BlackSeaHazNet Methodological-Coordination Workshop 2-5 May 2011, Ohrid, Republic of Macedonia. BlackSeaHazNet Series, Volume 1, pp 49-63.
2. S. Cht. Mavrodiev, L. Pekevski. On the FP7 BlackSeaHazNet Project and its Possible Application for Harmonic Existence of the Regions. Black Sea Energy Resource Development and Hydrogen

- Energy Problems. Springer, Published in Cooperation with Nato Emerging Security Challenges Division 7-10 October 2012. pp253-271.
3. T. Jimsheladze, G. Melikadze, G. Kikuashvili, S. Cht. Mavrodiiev, L. Pekevski, M. Chkhitunidze. Study of Geomagnetic Variations in Geogia and establishment the Anomaly Nature of Earthquake Precursors, Complex research of earthquake's forecasting possibilities, seismicity and climate change correlations, BlackSeaHazNet Training- SeminarWorkshop 13-16 September, 2011, Tbilisi, Georgia BlackSeaHazet Series Volume 2. pp205-214.
 4. G.S. Vartanyan. Regional Geodynamic Monitoring System for Ensuring Safety in Geological and Exploratory Production of Oil and Gas // Izvestia. Atmospheric and Oceanic Physics. 2010. vol. 46 #8. pp. 952-964.
 5. С.Ю. Баласанян. Сейсмическая Защита и ее организация. Гюмри Эльдorado, 2004г, стр 164 - 169.
 6. A. Sborshchikovi, G. Kobzev, S. Cht. Mavrodiiev, G. Melikadze. Boreholes Water Level and Earthquake's Daily Monitoring Nano Studies 2013,8 pp. 203-212
 7. http://theo.inrne.bas.bg/~mavrodi/everyday_monitoring.html
 8. <http://www.emsc-csem.org/#2>
 9. <http://home.comcast.net/~dmilbert/softs/solid.htm>



Преди Ренесанса - Боянската църква
Before the Renaissance – Boyana church

Бойко Вачев'2004
Boyko Vachev'2004

ANALYSIS OF TEMPORAL VARIATION OF EARTHQUAKE OCCURRENCES IN CAUCASUS FROM 1960 TO 2011

N. Zhukova¹, T. Matcharashvili^{1,2}, T. Chelidze¹

¹M. Nodia Institute of Geophysics, Tbilisi, 0171, Georgia

²Ilia State University, Tbilisi, 0162, Georgia

Abstract:

Frequency of earthquake occurrences in Caucasus is investigated on hourly and daily time scales. The observation period is 51 years, which is sufficiently long to perform a reliable statistics. Several methods (power spectrum, wavelet and Hilbert-Huang transformation) are applied to earthquake time series. Our findings show that earthquakes hourly and daily occurrence is not characterized by the dominant frequencies. However, many different oscillations with periods from hours to years and longer contribute to the frequency content of the earthquake time distribution, although their amplitude is rather low. The variation of the power of cyclic components in the temporal features of earthquakes occurrence is not uniform, but their amplification corresponds to the decrease of released local seismic energy.

Introduction

It is widely accepted that a detailed investigation of the structure of earthquake energy, space and time distribution is very important for earthquake hazard assessment as well as for understanding of fundamental properties of seismic processes.

In particular, the analysis of the temporal features of earthquake occurrences on different time scales represents the focus of intense research. Most of analyses agree that earthquake time dynamics is characterized by switching or intermittent behavior with periods of intense seismic activity interspersed with those of low seismicity [10], [16]. The details of such transition from one state (high seismic activity) to the other (low seismic activity) are still unclear. At the same time it is reasonable to presume that temporal variation of seismic processes should be caused by stress changes in the Earth's crust, which can be dynamically different and of both tectonic and non-tectonic origin [14], [1]. As a consequence, the question of earthquakes' temporal distribution is still an open problem. Many authors emphasized the idea of random nature of seismic processes, which excludes the possibility of regular occurrence of earthquakes [13]. At the same time, evidence of nonrandom features in earthquake generation in energy, space and time domains was shown in several papers [11], [14].

Moreover, several studies claim the presence of cycles in earthquake temporal distribution [9]. For example Metivier [12] reported clear correlation between the phases of the solid Earth tide and the timing of seismic events. These views, though controversial, are in principle consistent with the background tectonics comprising the complex processes of stress accumulation and stress release. In this respect it is important to note that the above mentioned non-tectonic forcing applied to the fault system, though substantially smaller than tectonic forces (few kPa-s vs. MPa-s [7]), often are much more regular in time (e.g. lunar and solar tides, ocean waves, seasonal influences, and thus could reasonably explain the evidence of cyclic components in earthquake occurrences. The ability of such small external influences to affect dynamical behavior of large systems is well known.

Data and Methods of Analysis

We investigated the process of earthquakes time distribution based on the Caucasian earthquake catalogue spanning from 1960 to 2011. Study area represents the segment of the Mediterranean Alpine Belt which is located between the still converging Eurasian and Africa-Arabian lithosphere plates and is a typical wide zone of continent–continent collision. Fig. 1 shows the distribution of earthquakes in the used catalogue, whose main characteristics already have been described in [16].

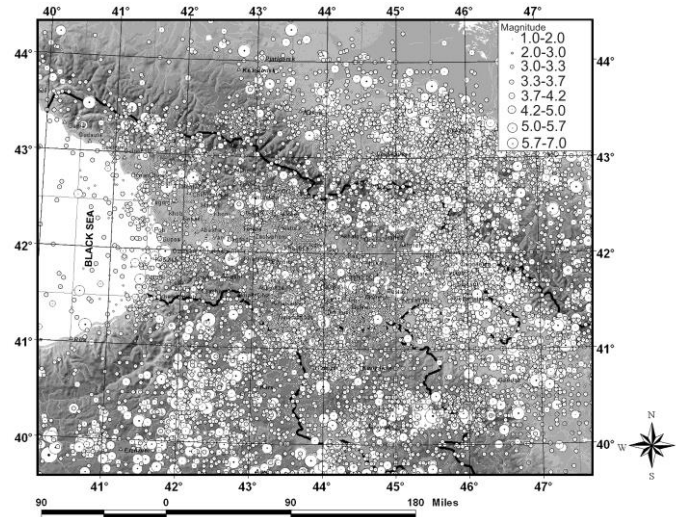


Fig. 1. Epicentral distribution of the earthquakes in Caucasus 1960-2011, declustered catalogue.

The considered catalog for the threshold $M_c=3$ is complete practically for whole analyzed period. In order to remove bias due to the presence of aftershocks, we declustered the catalogue using the Reasenberg’s algorithm and selected only the events with magnitude $M \geq 3.0$. From this catalogue we calculated number of earthquakes occurred in consecutive hours and days of observational period and divided them by the total number of yearly occurred events; we name these data as frequencies of earthquake occurrences (FEO) (Fig. 2). The hourly and daily FEO series were then normalized to zero mean and unit variance.

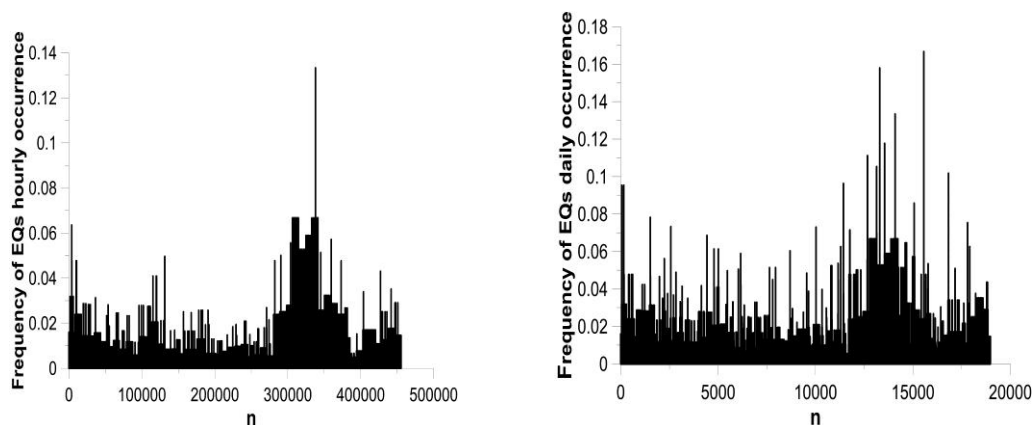


Fig. 2. Hourly (a) and daily (b) FEOs from the declustered Caucasian catalogue (1960-2011, $M \geq 3.0$).

Seismic energy has been calculated from the relation $\log_{10} E_s = 11.8 + 1.5M$ where M is magnitude [8].

To reveal hidden cyclic components in FEO data we used different methods. The well known method of the power spectrum, based on the Fourier transform of the time series, indicates how the power of the series is concentrated at various frequency bands. However, nonlinear and nonstationary features that often characterize seismic processes could produce misleading results and erroneous interpretations if based solely on the power spectrum [4], [6].

Much more efficient tool for our research is the wavelet analysis. The main difference between Fourier-based methods (i.e. power spectrum) and wavelets is that the last one enables a time-frequency representation of the series through decomposition, not based on sinusoidal functions. Wavelets use a so-called “mother function”, from which “daughter” wavelets are obtained by means of a scaling procedure. Mother wavelet functions, localized in both frequency and time domains, slide along the time and contracts or stretches in the high or low frequency regions, respectively, allowing the identification of the dominant modes of variability and their variability through time. These characteristics permit a multi-resolution analysis of a time series.

The wavelet transform of a function $x(t)$ is defined as:

$$W(a,b) = a^{-\frac{1}{2}} \int_{-\infty}^{\infty} x(t)h^*((t-b)/a)dt$$

Where * indicates complex conjugate, a is the scale dilation parameter and b is the translation parameter; a and b physically stand for the inverses of the frequency and the time. $h(t)$ is the mother or analyzing wavelet. In the present work we used the Morlet wavelet as a mother wavelet. The spectral resolution in the wavelet transformation is achieved by selection of the wavelet size (or by dilating or contracting the chosen wavelet) and the temporal resolution follows from the location of the wavelet relative to the signal [6]. We used continuous wavelet transformation (CWT) to calculate the power spectrum variation of the series on time and frequency. The CWT generates a two-dimensional (period/scale and time) wavelet space, on which the time series is represented [6]. However, the CWT is limited by the Heisenberg’s Principle of the time-frequency uncertainty relationship, according to which time and frequency cannot simultaneously be resolved with the same precision.

A further method that we used to perform our investigation of the FEO time series, is the Hilbert-Huang Transform (HHT) [4], which is a new approach to the analysis of non-stationary series, based on the use of an adaptive time-frequency decomposition that does not impose a fixed basis on the data, like in the CWT. Therefore, unlike the CWT, the HHT is not limited by the time-frequency uncertainty relationship. The HHT consists of two parts. In the first part, (the empirical mode decomposition - EMD) the series is decomposed into Implicit Mode Functions (IMFs), putting forward the scale characteristics imbedded in the signal; this is carried out by means of the sifting procedure that is ended according to a certain stop criterion [5] (see, e.g., Fig. 7, where the procedure is illustrated for one of the FEO time series). Each IMF represents a simple oscillatory mode which plays the role similar to a simple harmonic function for spectral analysis. At the same time IMF is much more general because it can have an amplitude and frequency varying with time, contrarily to the constant amplitude and frequency of a simple harmonic. The second part is the Hilbert transformation of the IMFs, yielding the time-frequency representation (Hilbert spectrum) of each IMF.

Indicating as $x(t)$ a real signal and as $X_n(t)$ the IMFs, their Hilbert transform $H[X_n(t)]$ is

$$Y_n(t) = \frac{1}{\pi} P \int_{-\infty}^{\infty} \frac{X_n(\tau)}{t - \tau} d\tau,$$

where P is the operator called Cauchy Principal Value. The analytic signals, $Z_n(t)$ are given by $Z_n(t) = X_n(t) + iY_n(t)$, where i is the imaginary unit. From the analytic signals we can determine the

instantaneous amplitude $A_n(t) = \sqrt{X_n(t)^2 + Y_n(t)^2}$ and phase $\phi_n(t) = \arctan\left(\frac{Y_n(t)}{X_n(t)}\right)$. The instantaneous frequency is given by $f_n(t) = \frac{d\phi_n}{dt}$. The total amplitude (or energy) from each frequency component is given by the marginal spectrum h_f , $h_f = \int_0^T A(f, t) dt$.

Results of analysis

As a preliminary analysis, we calculated the hourly distribution of the average number of earthquakes occurred (Fig. 3 a) and that of the average released energy (Fig. 3 b) in a certain hour of the day, throughout considered time period from 1960 to 2011. Such analysis aiming to check if any significant change in the earthquake occurrence could be associated to a particular hour of the day was important because in earlier reports strong dependence of the probability of earthquake occurrence on the hour of day was claimed for several seismically active regions [15],[3]. From our results in Fig. 3, we see some variations in mean values of the number of earthquakes and the released seismic energy versus the hour of day, but they are not statistically significant. Thus for Caucasian region we can not confirm dependence of the number of earthquakes on the hour of day.

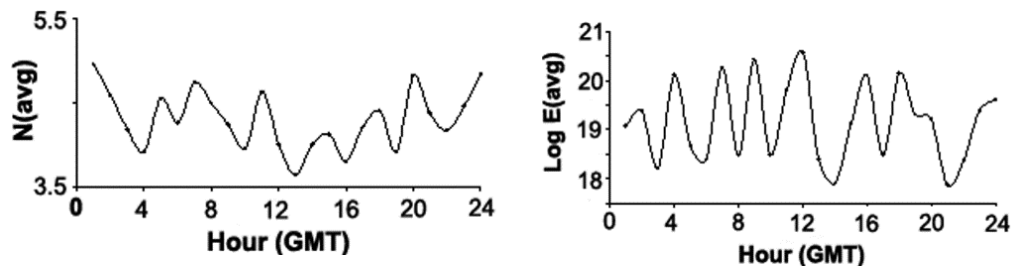


Fig. 3. Mean values of earthquakes (a) and released seismic energy (b) of $M \geq 3.0$ earthquakes occurred hourly in Caucasus from 1960 to 2011.

Next, taking into consideration that averaging procedure could distort and mask subtle features of the time dependent variations in seismic characteristics, we investigated the hourly and daily FEO time series, as described in the previous section, by means of the power spectrum method.

Fig. 4 shows the power spectral density of the daily FEO time series (similar characteristics are found for the hourly FEO time series, not shown here). The power spectrum of the original FEO series (Fig. 4a), does not reveal prevalent cyclic components in the analyzed data obtained from declustered

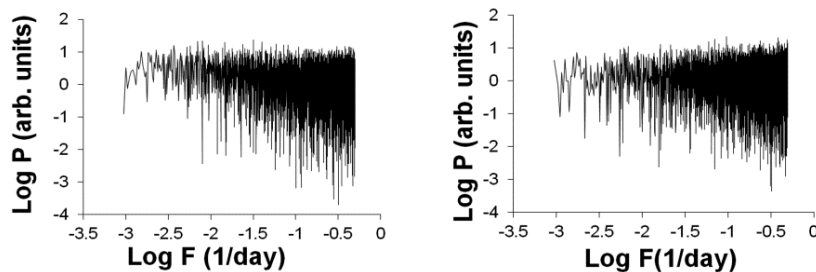


Fig. 4. Power spectrum of original (a) and shuffled (b) daily FEO time series from the declustered Caucasian catalogue 1960-2011, for events with $M \geq 3.0$.

Caucasian earthquake catalogue. It is flat in the higher frequency range, like the power spectrum of the shuffled FEO time series (Fig. 4b) and this is quite reasonable if we consider that a seismic process is very complex phenomenon and debate about its random character is still open. However, although the broadness of the power spectrum of FEO time series, the presence of nonrandom features cannot be excluded, since a seismic process cannot be regarded as a purely random process.

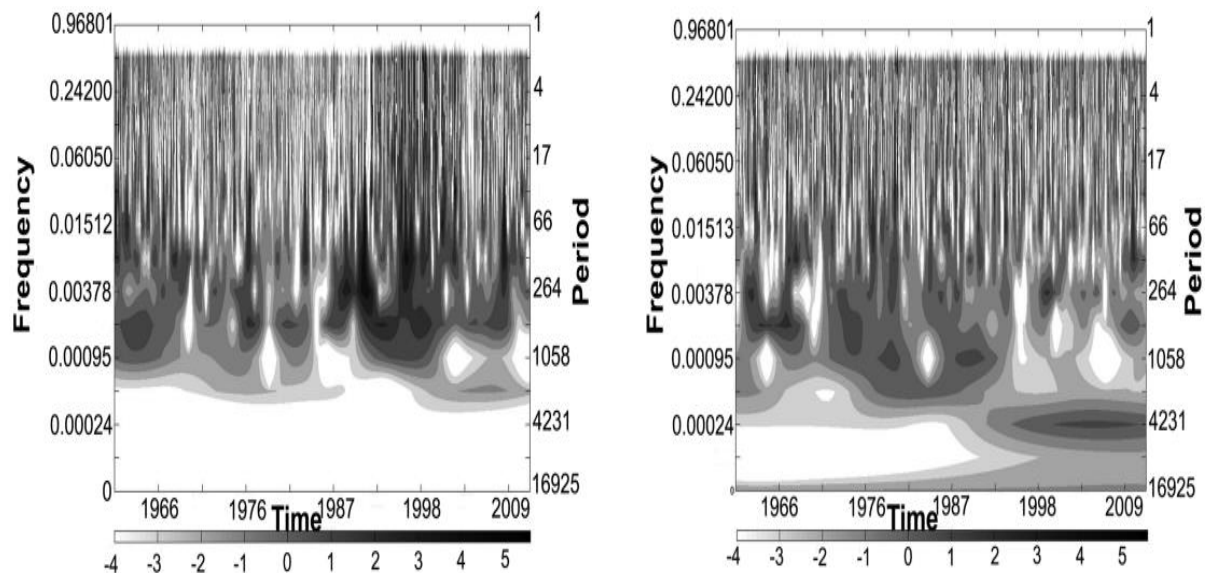


Fig. 5. CWT spectrogram of original (a) and shuffled (b) daily FEO data of filtered and normalized FEO series calculated for the whole available frequency range. Source - declustered Caucasian catalogue, 1960 to 2011.

Fig. 5 shows the CWT spectrogram for the original (Fig. 5a) and shuffled (Fig. 5b) daily FEO time series. It is evident that the shuffled time series shows a higher homogeneity in the temporal distribution of the frequency components with respect to the original data; in particular, the original FEO time series are characterized by a frequency spectrum more intense from approximately 1990 to 2000 than in other periods.

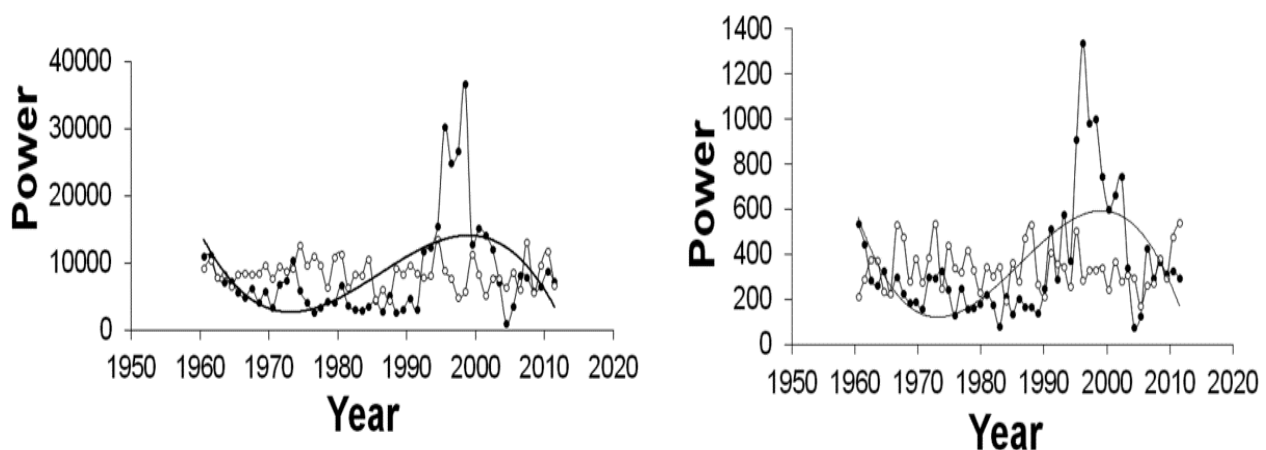


Fig. 6. Power of CWT spectrum vs. time relation of FEO time series obtained from declustered Caucasian catalogue, 1960 - 2011. a) hourly and b) daily time scales. Black and white circles correspond to original and shuffled data. Solid line is the 3th order polynomial fit.

Fig. 6 presents the annual variation of the CWT power. The CWT power for the hourly and daily FEO time series confirms conclusion, derived from analyzing the CWT spectrograms, namely, noticeable changes of the distribution of frequency components between approximately 1990 and 2000; furthermore, the comparison with the CWT power for the shuffled FEO time series corroborates proposition that such changes could not be purely random.

Next, we applied the HHT analysis of the hourly and daily FEO time series. Fig. 7 presents as an example of EMD the 15 IMF-s and the residual of the daily FEO time series.

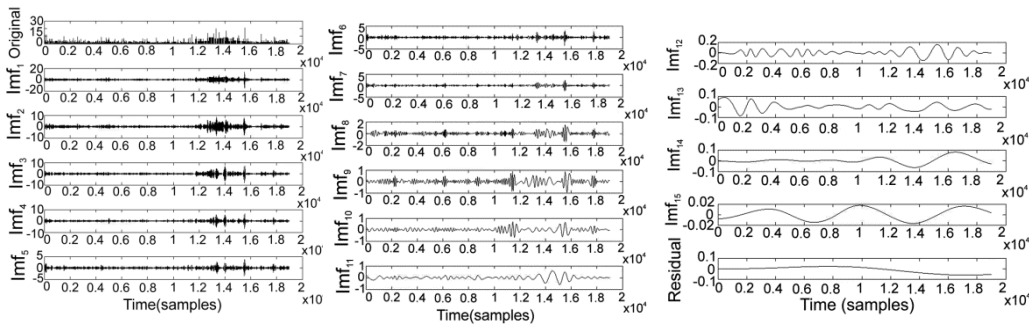


Fig. 7. Original daily FEO data (first row) and their EMD decomposition. Last row corresponds to residual.

We can see that in all the IMFs, except the 13th and the 15th one, the highest amplitudes are observed in the period from about 12000 to 16000 days. The 13th IMF shows high amplitudes at the beginning of observed time interval at low frequency (about 0.00075 1/day). The 15th IMF is characterized by a frequency of approximately 0.00014 1/day with approximately constant amplitude. However, the amplitudes of 13th and 15th IMFs are low and they weakly contribute to the total energy of the original signal. Therefore, we considered only the first 12 IMFs.

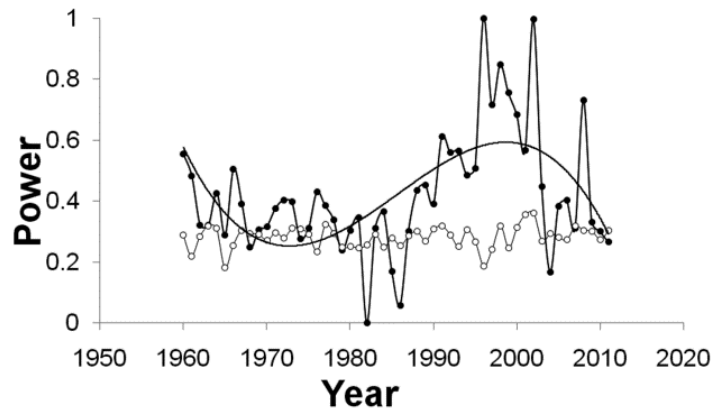


Fig. 8. Log Power vs. time relation of Hilbert Energy Spectrum of daily FEO time series. White circles correspond to Hilbert Energy Spectrum of shuffled data. Solid curve 3th order polynomial fit.

Fig. 8 presents integral power derived from the Hilbert Transform of the 2nd up to the 12th IMF of the Caucasian daily FEO time series for the frequency range between 0.01/day and 0.03/day. Here the relationship of logarithm of the power vs. time actually represents the marginal spectrum, which is in

good agreement with the results of the wavelet analysis of the daily Caucasian FEO data shown in Fig. 7.

The Hilbert power spectrum of the hourly FEO data shows similar to daily data increase of cyclic components for the time period from 1990 to 2000. In order not too overburden text, graphs of these results indicating changes in the frequency content of hourly FEO data from about 1990 to about 2000, are not presented here.

Fig. 9 shows the temporal variation of the number of earthquakes and that of the total seismic energy normalized to the yearly amount of events from 1960 to 2011. Comparing Fig. 9 with Figs. 5, 6 and 8 we can see that the enhancement of strength of same periodic components in the FEO data corresponds approximately to the decrease of the seismic activity, started in late 1980s and continued for about 15-20 years. In the first years of this period the two strongest recorded Caucasian earthquakes, Spitak and Racha, occurred in 1988 and 1991 respectively.

So the territory of Caucasus during this 15-20-year long period can be considered as an area of stress shadow, where the tectonic stress was essentially released.

It seems also important to add here that the declustering procedure performed on the seismic catalogue does not lead to essential changes in CWT power results. The time variation of the CWT power for the FEO time series derived both from the declustered catalogue and from the original one (not shown here) are very similar and this additionally indicate adequacy of used data as well as robustness of the methods applied.

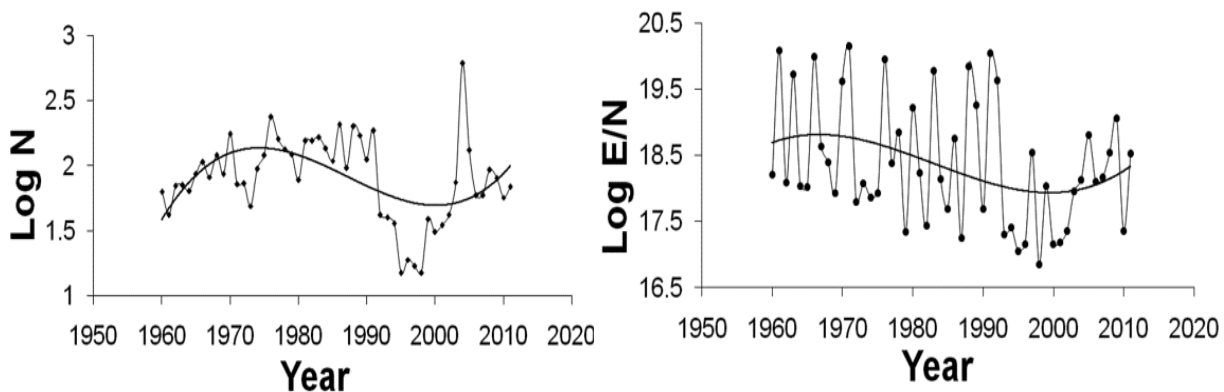


Fig. 9. a) Number of $M>3.0$ earthquakes occurred yearly and b) released yearly seismic energy in Caucasus from 1960 to 2011 normalized to the yearly amount of earthquakes from declustered catalogue. Solid curve is the 3th order polynomial fit.

Discussion

As it follows from results section WT and the HHT analysis shows that though the content of cyclic components in the frequency of earthquakes occurrence distribution in general is uniform, for some time periods the contribution of certain oscillatory modes may significantly increase.

From a dynamical point of view the complicated process of tectonic stress change by its nature is nonrandom though high-dimensional. Therefore, it is difficult to assume that process of tectonic stress change itself may be a source of found enhanced strength of cyclic components in earthquake temporal distribution. On the other hand, factors that often are regarded as causing non-tectonic stress changes are much more regular - mostly quasi-periodic. For example, the tidal forces, one of the non-

tectonic stress factors, consist of 505 to 27000 harmonics containing cycles from hours to years and longer [1]

Among frequency components which amplification is documented in our results we indeed see well known tidal constituents. For example, it is reasonable to link the dominance of the low frequency components clustered around $f = 0.03/\text{day}$ in the 5th and 6th IMF to the long term M_m (moon monthly) constituent with period 27.555 days [1]. The origin of components in the vicinity 0.01/day is not so obvious. We can only guess that this detail can be related to the effect of high-order synchronization connected with M_m period, namely periods of the order of $3 M_m$ [2].

We found that conditions, when the increase of the power of cyclic components may occur (Figs. 6, 8) correspond to the decrease of the local seismic energy release (Fig. 9). This could be explained by the fact that increased seismic activity means more inter-correlated system; contrarily to this, during the decrease of seismic activity, the tectonic system could be less inter-correlated and thus closer to randomness. In this last case, unstable periodic orbits of the considered dynamical system can be easier trapped by different imposed external cycles that indeed strengthen certain cyclic components. Our earlier findings of fragment asperity interaction support conclusion about changed inter-correlations in tectonic system during different stages of seismic cycles

Conclusions

We investigated data on frequency of earthquakes occurrence in Caucasus from 1960 to 2011 at different time scales. Features of the frequency content of analyzed data as well as the time variability of their cyclic components were investigated by means of the WT and the HHT. It was shown that the time series of frequency of earthquake occurrence does not reveal presence of leading cycles. At the same time the temporal distribution of the power of weak cyclic oscillatory modes is not uniform and varies significantly during certain periods. Our analysis indicates that generally, the enhancement of different cyclic components coincides with the time periods of decrease in the amount of released local seismic energy.

References

- [1] Agnew, D. C., 2007. Earth Tides, in *Treatise on Geophysics: Geodesy*. T. A. Herring, ed. Elsevier, New York, 163-195.
- [2] Chelidze, T., Lursmanashvili, O., Matcharashvili, T. Varamashvili, N. Zhukova, N., Mepharidze, 2010. High-order synchronization of stick-slip process: experiments on spring-spring-slider system, *Nonlinear Dynamics*, 59, 1, 259-275.
- [3] Duma, G., Ruzhin, Y., 2003. Diurnal changes of earthquake activity and geomagnetic Sq-variations. *Natural Hazards and Earth System Sciences*, 3, 171-177.
- [4] Huang, N. E., Shen, Z., Long, S.R., Wu, M.C., Shih, H. H., Zheng, Q., Yen, N.-C., Tung, C. C., Liu, H. H., 1998. The Empirical mode decomposition and the Hilbert spectrum for nonlinear and nonstationary time-series analysis. *Proc. R Soc. Lond. A* 454, 903-995.
- [5] Huang, N., Wu, Z., 2008. A review on Hilbert-Huang transform: method and its applications to geophysical studies. *Reviews of Geophysics*, 46, RG2006 / 2008, 1- 23.
- [6] Issac, M., Renuka, G. Venugopal, C., 2004. Wavelet analysis of long period oscillations in geomagnetic field over the magnetic equator. *Journal of Atmospheric and Solar-Terrestrial Physics*, 66, 919-925.
- [7] Iwata, T., 2012. Earthquake triggering caused by the external oscillation of stress/strain changes. *Community Online Resource for Statistical Seismicity Analysis*. doi:10.5078/corssa-65828518.
- [8] Kanamori, H., 1977, The Energy Release in Great Earthquakes, *Journal of Geophysical Research*, 82, 2981-2987
- [9] Kasahara, J., 2002. Tides, earthquakes and volcanoes. *Science*, 297, 348-349.

- [10] Lyakhovsky, V., Ben-zion, Y., Agnon, A., 2001. Earthquake Cycle, Fault Zones, and Seismicity Patterns in a Rheologically Layered Lithosphere. *J. Geophys. Res.*, 106, 4103–4120.
- [11] Matcharashvili, T., Chelidze, T., Javakhishvili, Z., 2000. Nonlinear analysis of magnitude and interevent time interval sequences for earthquakes of Caucasian region. *Nonlinear Processes in Geophysics*, 7, 9-19.
- [12] Metivier, L., Viron, O., Conrad, C. P., Renault, S., Diament, M., Patau, G., 2009. Evidence of earthquake triggering by the solid earth tides. *Earth and Planetary Science Letters*, 278, 370–375.
- [13] Parsons, T., Geist, T. L., 2012. Were global $M \geq 8.3$ earthquake time intervals random between 1900 and 2011. *Bulletin of the Seismological Society of America*, 102 (4), 1583-1592.
- [14] Rundle, J., Turcotte, D., and Klein, W., 2000. *GeoComplexity and the physics of earthquakes*. AGU, Washington.
- [15] Shimshoni, M., 1971. Evidence for Higher Seismic Activity During the Night. *Geophys. J. R. Astr. Soc.*, 24, 97–99.
- [16] Telesca, L., Cuomo, V., Lapenna, V., Macchiato, M., 2001, Intermittent-type temporal fluctuations in seismicity of the Irpinia (southern Italy) region, *Geophys. Res. Lett.*, 28, 3765-3768.
- [17] Vautard, R., Yiou, P., Ghil, M., 1992. Singular-spectrum analysis: A toolkit for short, noisy chaotic signals. *Physica D*, 58, 1-4, 95–126.



Собор святой Троицы, ТбилисиБойко Вачев'2013
Cathedral of the Holy Trinity, Tbilisi Boyko Vachev'2013

UNDERGROUND GEOPHYSICAL OBSERVATIONS IN CAVES

Igor Kachalin^{1,2}, Oleksandr Liashchuk¹, Stanka Šebela³ and Janja Vaupotič⁴

^{1,2}National Antarctic Scientific Centre, Tarasa Shevchenko blvd 16, 01601 Kiev, Ukraine, igor_kachalin@ukr.net; ¹ AtomKomplexPribor, 1 Magnitogorskaya St., Kiev 02660, Ukraine; ³ZRC SAZU, Karst research institute, Titov trg 2, 6230 Postojna, Slovenia; ⁴ Jožef Stefan Institute, Jamova cesta 39, 1000 Ljubljana, Slovenia

Abstract:

In four caves radon (Slovenia and Italy) and gamma ray monitoring was performed to understand the relation between radon and its daughter products. In situ monitoring of natural level of gamma radiation and spectrometry of gamma radionuclides in karst caves was for the first time accomplished in this study. We did not find Cs-137 contamination, but we detected daughter isotopes of Ra-226 and Th-232, such as Rn-222, Rn-220, Bi-214, and Pb-214. Detected radioactive elements have natural origin and are probably connected with natural uranium deposits in north-central Slovenia. The use of the proposed monitoring techniques of radon concentration by monitoring of gamma emitted daughter products can be used for dynamic observation of the possible earthquake radon precursors. The second research included VLF (Very Low Frequency) monitoring in cave. During VLF radio registration we did not receive a good earthquake precursor signal. VLF monitoring in karst cave is a good option for future researches but it has to be continuous for more years with registration in real time mode.

1. Introduction

Within the BlackSeaHazNet Project (FP7 MCA PIRSES-GA-2009-246874) geophysical observations were realized in three karst caves in Slovenia (Postojna Cave System, Županova Jama and Škocjan Caves) and at one cave in Northern Italy (Grotta Gigante). The study was separated into two main topics. The first was the pilot research of allocation of radon and gamma radionuclides in caves and the second was underground VLF (Very Low Frequency) radio signals monitoring for detection of possible earthquake precursor signals.

In all four caves radon and gamma ray monitoring was performed in September – November 2013 to understand the relation between radon and its daughter products. *In situ* monitoring of natural level of gamma radiation and spectrometry of gamma radionuclides in karst caves was for the first time accomplished in this study.

The second research included VLF monitoring in Črna Jama (part of Postojna Cave System). Underground VLF monitoring was periodically settled in 2012 and 2013 for detection of possible preseismic anomalies. Črna Jama, which is not very frequently visited part of Postojna Cave, was chosen as optimal place for first periodical VLF monitoring in Slovene karst cave. Detection of electric, magnetic and seismoacoustic signals in Amare cave (Gran Sasso – L'Aquila, Italy) showed “quite” and “perturbed” state [1]. In 1992 a similar equipment was installed inside Cervo cave, about 50 km SW of the Amare cave. In “quite” state only electric and magnetic signals with highest frequencies appear, which are connected with radio broadcastings and with lightning activity of the Earth. “Perturbed” state is connected with local processes as rainfall, atmospheric-pressure variations and some thermal effects. Micro movements of the limestone blocks that constitute the roof of the caves are invoked for production of seismoacoustic signals [1].

The aim of the underground radon and gamma ray monitoring and VLF monitoring was to determine possible preseismic anomalies and to ascertain suitability of such monitoring in natural karst caves.

2. Methods and results

Gamma ray measurements were performed by radiometric and spectrometric instrument PRS-01 (produced by AtomKomplexPribor, Ukraine), which is designed for determination of qualitative and quantitative composition of gamma-emission radionuclides in field and in laboratory, for investigation of radioactive sources and anomalies, and for gamma-survey of surface. PRS-01 is created taking into account the IAEA recommendations stated in the IAEA TECDOC-1312, (2002) "Detection of Radioactive Material at Borders", which was jointly sponsored by IAEA, WCO, EUROPOL, and INTERPOL, and UNECE document "Recommendations on Monitoring and Response Procedures for Radioactive Scrap Metal".

The gamma measurement technique corresponds as on-walk real time measurements of gamma dose and short/middle time collection of the gamma spectra in defined points of interest. Time of the gamma spectra exposition depended on practical possibilities of measurements and was from few minutes up to few hours for best analyzing of sources of gamma radiation in condition of low-noise natural radiation level. Gamma measurements were accompanied by radon concentration measurements (Fig. 1).

Measurement of radon air concentration in Slovene caves has rich history [2, 3, 4]. But, combined measurements of radon and gamma ray in karst caves were first performed by this study. In the Pisani Rov passage on the Postojna Cave System, maximum radon concentration was 20,000 Bq/m³ and highest gamma doze rate, 526 nSv/h. In the Škocjan Caves maximum radon concentration was 7,500 Bq/m³ and highest gamma doze rate, 550 nSv/h. In the Županova Jama cave maximum radon concentration was 4,930 Bq/m³ and highest gamma doze rate, 290 nSv/h. In the Grotta Gigante (Fig. 2) maximum radon concentration was 2,140 Bq/m³ and highest gamma doze rate, 180 nSv/h.



Figure 1 Combined measurements of radon using radon meter (right) and gamma spectrometer PRS-01(left) in the cave

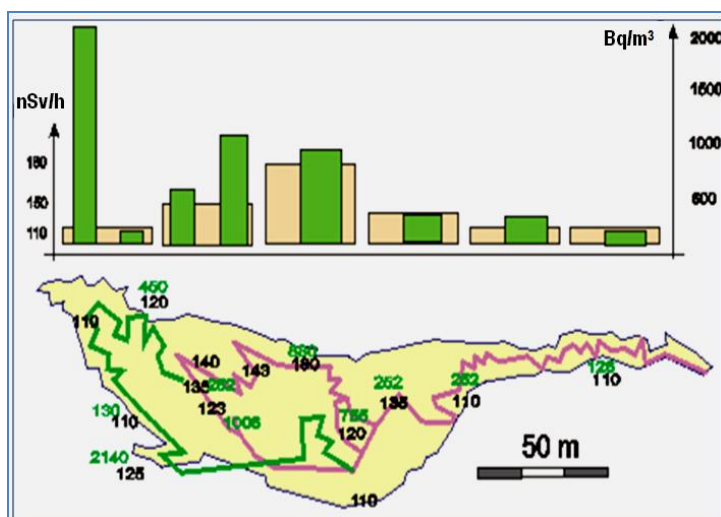


Figure 2 Detected levels of radon concentration (green) and gamma-dose (light brown) in the Grotta Gigante cave

We did not find Cs-137 contamination, but we detected daughter isotopes of Ra-226 and Th-232, such as Rn-222, Rn-220, Bi-214, and Pb-214. Detected radioactive elements have natural origin and are probably connected with natural uranium deposits in north-central Slovenia.

Main source of the gamma radiation is connected with isotopes of Ra-226 and daughter products and a lesser degree (level) from Th-232 series and K-40 isotope. Simple spectrum is shown on Figure 3. We assumed that Cs-137 isotope could be found in Slovenian monitoring sites, but it was not detected at any location of measurements.

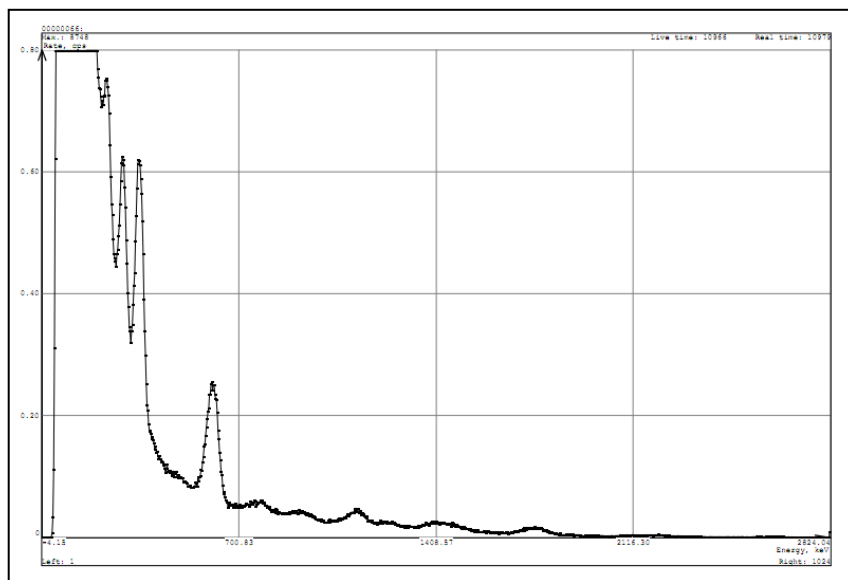


Figure 3 Typical gamma spectrum of natural isotopes Ra-226/Rn-222, daughter isotopes Pb-214 and Bi-214 (Županova Jama, spectrum #66, 3 October 2013)

In the period of 6–7 September, 14–20 September 2012 and 27 September to 11 October 2013, Črna Jama provided the pilot experiment site of the underground registration of the radio

emission of VLF transmitters.

Simple experimental equipment was used for registration of the radio signals in the band of 3 to 45 kHz: computer for digitizing and *in situ* data processing, miniature VLF receiver/amplifier, and 100 m of linear antenna. The complex instrumentation was installed on the bottom of the cave. At the period of installation and tuning of the complex instrumentation few places for long length antenna were tested. The main requirements for the complex installation included: minimal EM noise, power supply 220 V, absence of humans.

The preliminary measurements of the experimental underground registration of VLF signals gave promising results. We propose the use of VLF (with ELF, LF in the future) passive observation in complex with traditional geophysical technologies for monitoring cave conditions and registration of possible preseismic anomalies.

The data processing and complex analyses of the raw data collected by the experimental VLF equipment in Črna Jama (Figs. 4 and 5) are together with meteorological and seismic data and INTERMAGNET data suitable for defining the working regime of the equipment and for detection of possible earthquake precursor signals.

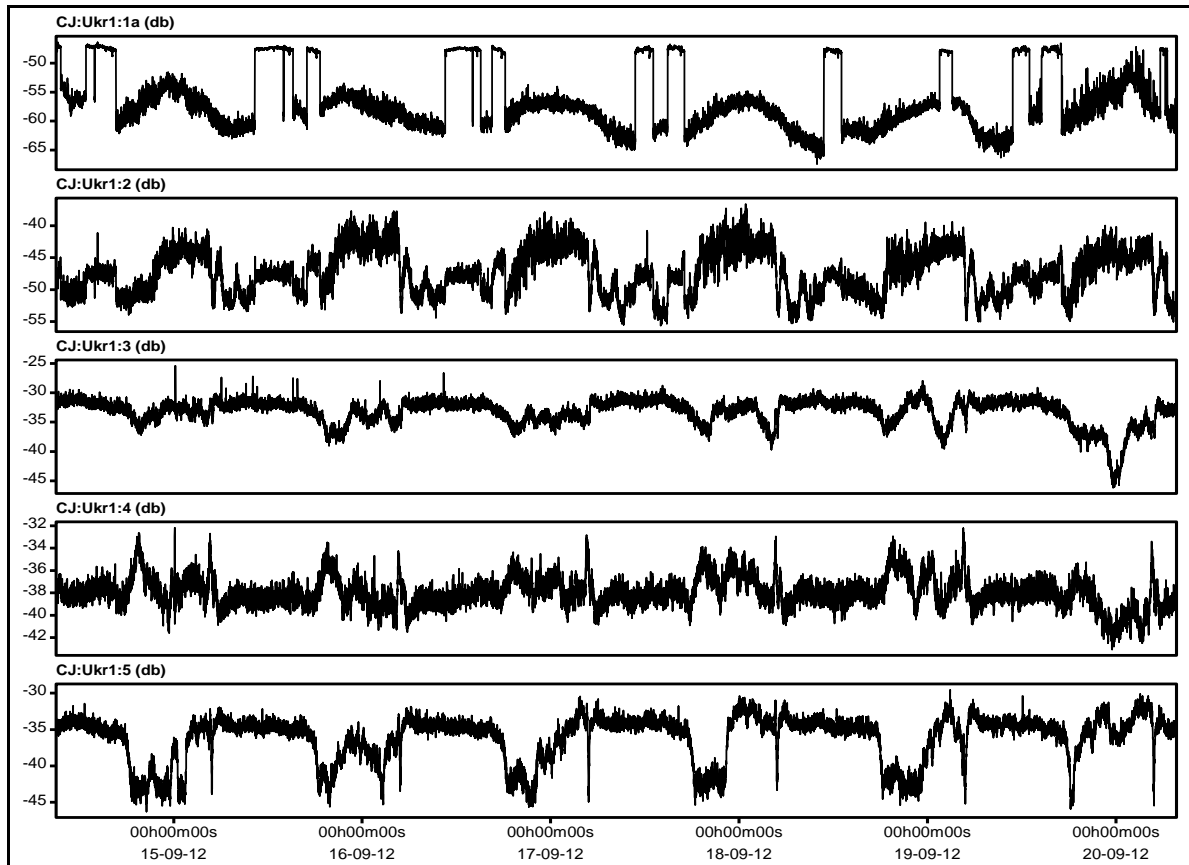


Figure 4 Processed VLF data of one-week observation 14-20 September 2012. Variation of amplitudes of observed VLF frequencies

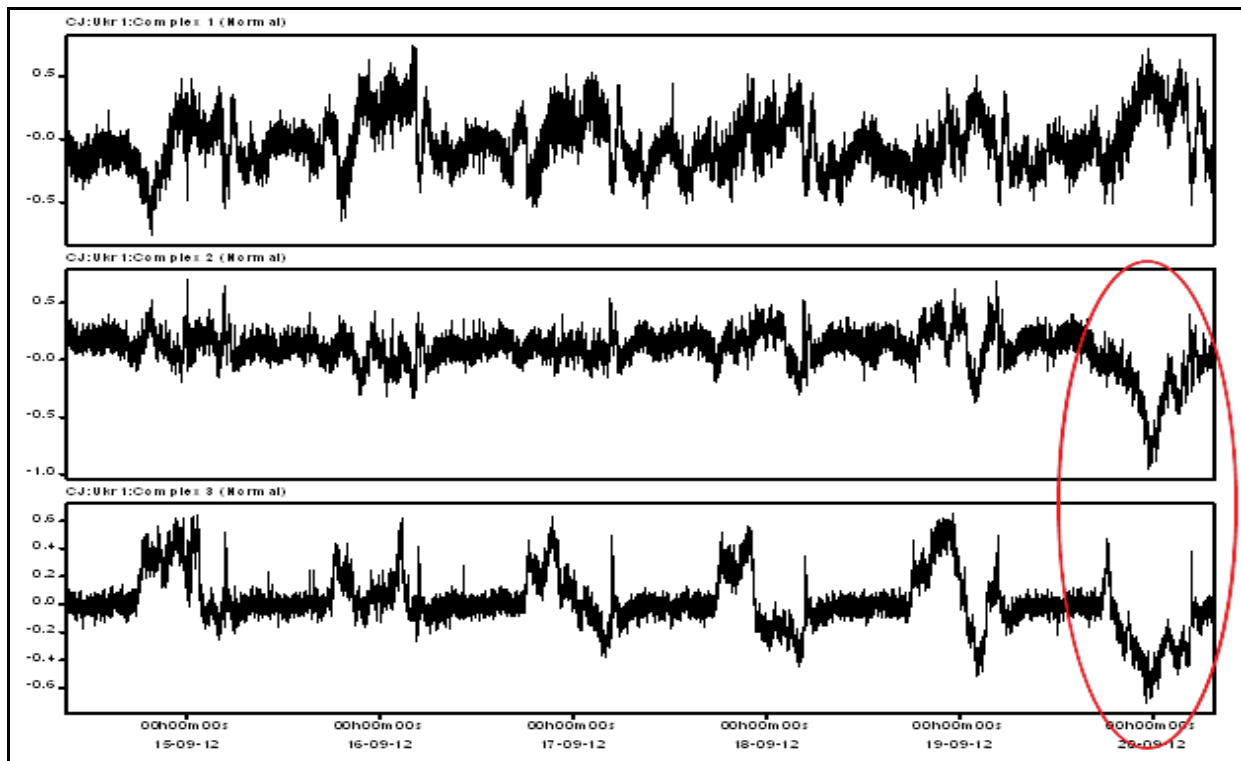


Figure 5 Processed VLF data (14-20 September 2012). By ellipse is shown “modulation” of the VLF signal connected with powerful atmospheric front and changing of the precipitation level

3. Conclusion

The use of the proposed monitoring techniques of radon concentration by monitoring of gamma emitted daughter products with portable gamma spectrometer can be used for dynamic observation of the possible earthquake radon precursors. Using *in situ* gamma measurement method is possible together with fast analysis of the radon concentration level in connection with meteorological, seismological (earthquake precursor) and other situations. Understanding the migration of the “radon cloud” inside of the caves according to cave micro climate is sensitive for development of gamma measurement network. At the time of gamma measurements in the Škocjan Caves and Županova Jama the probable channels of the radon inflow were detected for the first time.

Proposed method of the dynamic monitoring of the radon concentration (speed of the changing of the radon concentration) is useful for continuous radon measurements and discovery of the channels of radon inflow and for safety reasons of personnel and tourists in caves.

The second research included VLF monitoring in Črna Jama (part of Postojna Cave System). In 2012 VLF monitoring covered period of one week and in 2013 we made near one month of continuous underground registration. The experimental underground registration of the VLF radio transmitter is a validated possibility for using this technology of observations. VLF data showed day and night changes and also significant changes between dry and rain period when water from the surface reached the cave chamber through about 30 m of limestone roof. Regular noise probably related to unknown high power customizer, a noise signal like from radar was detected. During VLF monitoring we did not receive a good earthquake precursor signal. VLF monitoring in karst cave is a good option for future researches but it has to be continuous for more years with registration in real time mode.

References:

- [1] F. Bella, P.F. Biagi, M. Caputo, G. Della Monica, A. Ermini, W. Plastino, V Sgrigna and D. Zilpimiani, (1995) Electromagnetic and seismoacoustic signals revealed in karst caves (Central Italy). *Il Nuovo Cimento C.* **18**(1), 19-32
- [2] A. Gregorič, A. Zidanšek, and J. Vaupotič, (2011) Dependence of radon levels in the Postojna Cave on outdoor air temperature. *Nat. hazards earth syst. sci.* **11**(5), 1523-1528
- [3] I. Kobal, M. Ančik and M. Škofljanec, (1988) Variations of ^{222}Rn air concentration in Postojna Cave. *Radiation Protection Dosimetry* **25**(3), 207-211
- [4] J. Vaupotič, (2010) Radon levels in Karst caves in Slovenia. *Acta carsol.* **39**(3), 503-512



Одесская опера 2
Odessa Opera 2

Бойко Вачев'2012
Boyko Vachev'2005

SCHUMAN RESONANCE DEVICE

Georgi Kikuashvili¹, Lazo Pekevski², Schteriumir Mavrodiev³

¹M.Nodia Institute of Geophysics Iv. Javakhishvili Tbilisi State University, Georgia, Ss. Cyril and Methodius University in Skopje, Macedonia, ³Institute for Nuclear Research and Nuclear Energy, Bulgarian Academy of Sciences, Sofia, Bulgaria

The **Schumann resonances** are a set of spectrum peaks in the extremely low frequency (ELF) portion of the Earth's electromagnetic field spectrum. There are global electromagnetic resonances, excited by lightning discharges in the cavity formed by the Earth's surface and the ionosphere.

Schumann resonances occur because the space between the surface of the Earth and the conductive ionosphere acts as a closed waveguide. The limited dimensions of the Earth cause this waveguide to act as a resonant cavity for electromagnetic waves in the ELF band. The cavity is naturally excited by electric currents in lightning. Schumann resonances are the principal background in the electromagnetic spectrum beginning at 3 Hz and extend to 60 Hz.

In the normal mode descriptions of Schumann resonances, the fundamental mode is a standing wave in the Earth–ionosphere cavity with a wavelength equal to the circumference of the Earth. This lowest-frequency (and highest-intensity) mode of the Schumann resonance occurs at a frequency of approximately 7.83 Hz, but this frequency can vary slightly from a variety of factors, such as solar-induced perturbations to the ionosphere. The higher resonance modes are spaced which could be a characteristic attributed to the atmosphere's spherical geometry. The peaks exhibit some spectral width on account of the damping of the respective modes in the atmosphere's dissipative cavity.

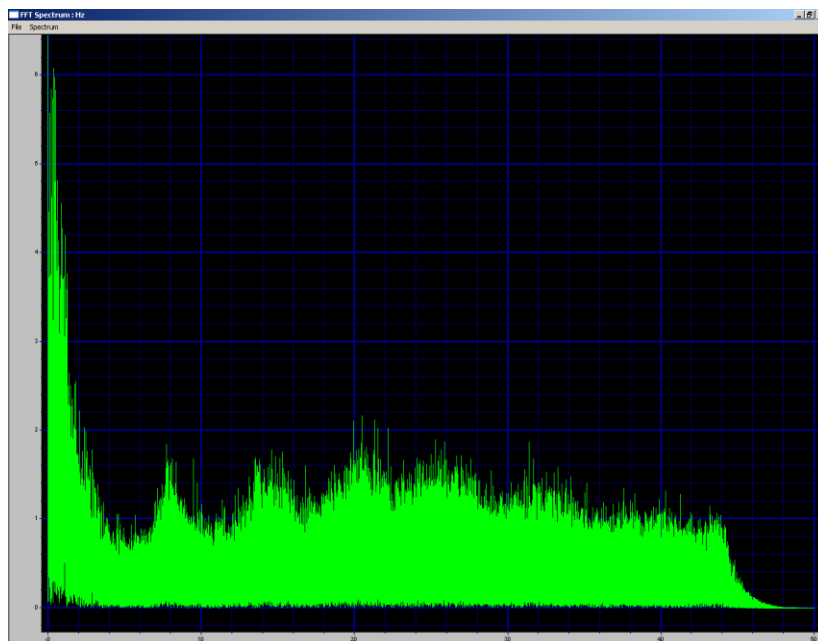
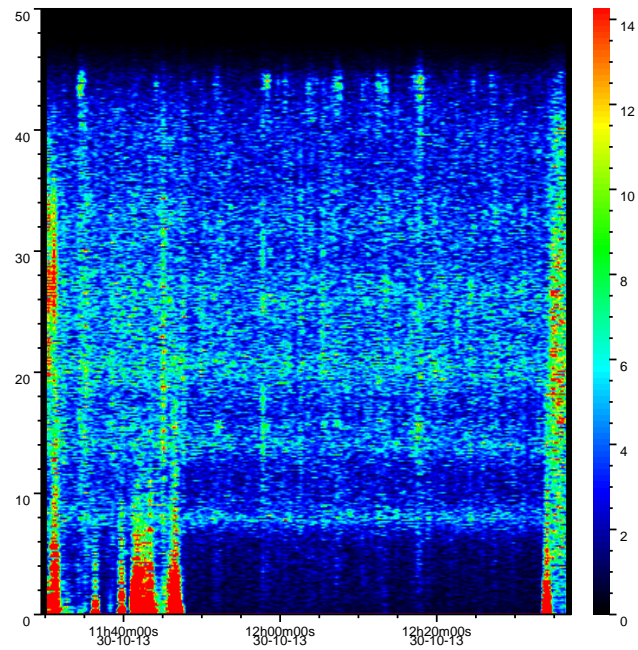
Work done

As an attempt to measure the Schumann's frequencies with an induction antenna build in summer 2012 did not show satisfactory results new antenna was made with much more copper wire windings and better core material (thin iron plates from a big transformer). Both old and new antennas were tested on the mountain Plackovica (near town of Stip, R. Macedonia) because inside and near cities intensive electromagnetic and RF noise makes it impossible to make precise measurements. We used **Kinometrics Q330HRS (26bit)** from Skopje Seismical Observatory for data acquisition at maximum precision and 100Hz sampling rate.

Picture below show moving FFT window of raw recorded data. Intensity at various frequencies are affected by frequency response curve of inductors, so 7.8Hz appears lower intensity than first following harmonics at 15.6, 20.5, 26Hz and 33Hz. As a future plan intensity against frequency will be corrected using measured frequency response of each inductor.

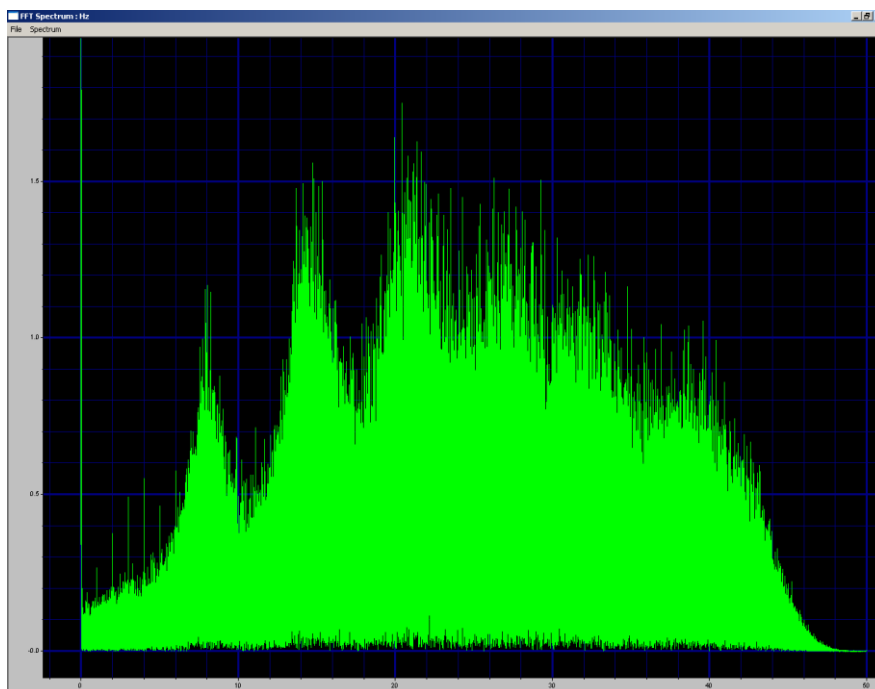
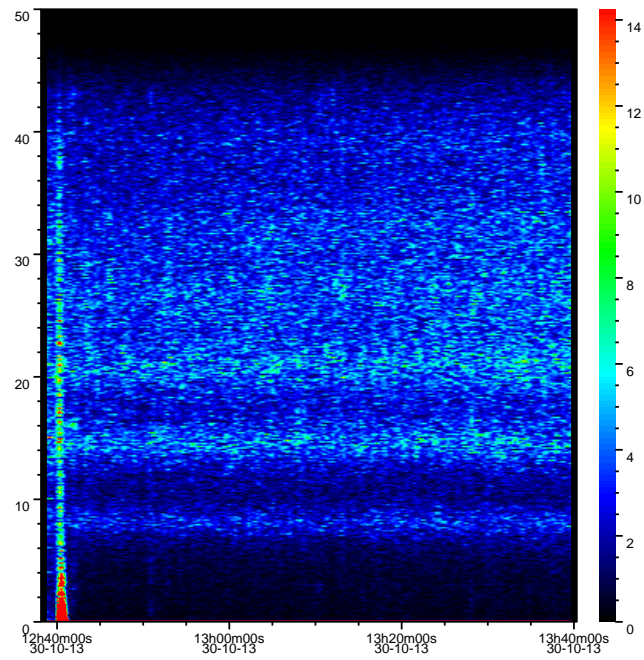
New Antenna

NS orientation

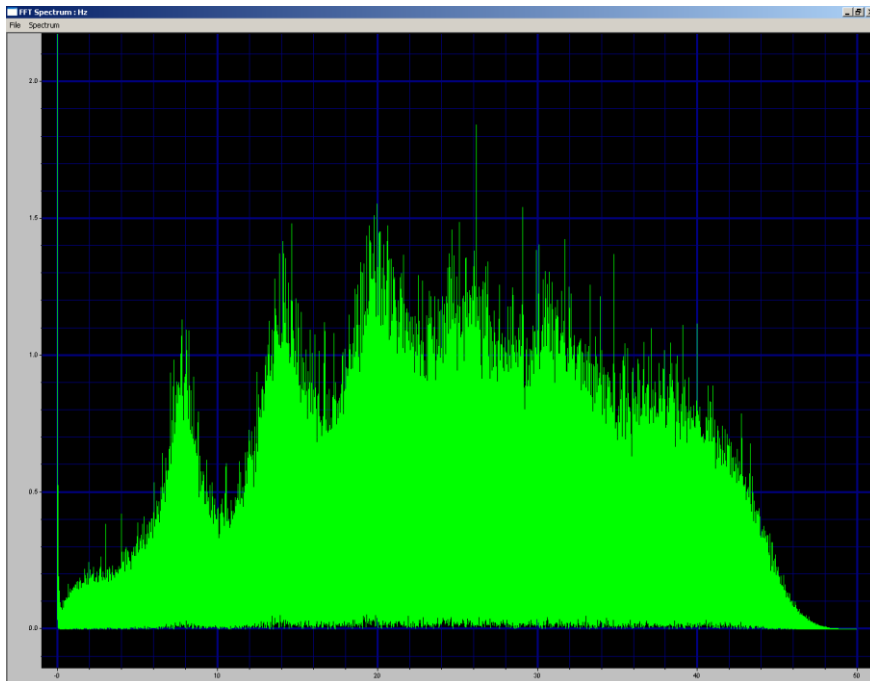
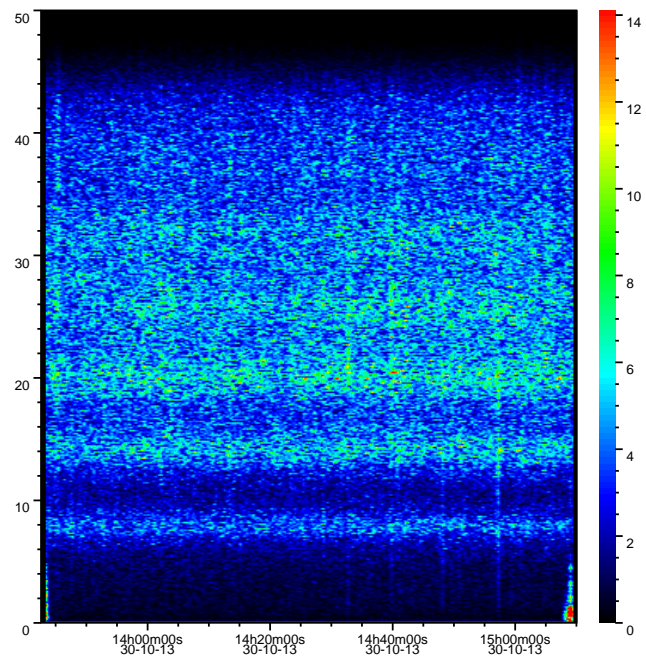


Mean spectrum of recording clearly shows all Schumann resonance peaks.

EW orientation

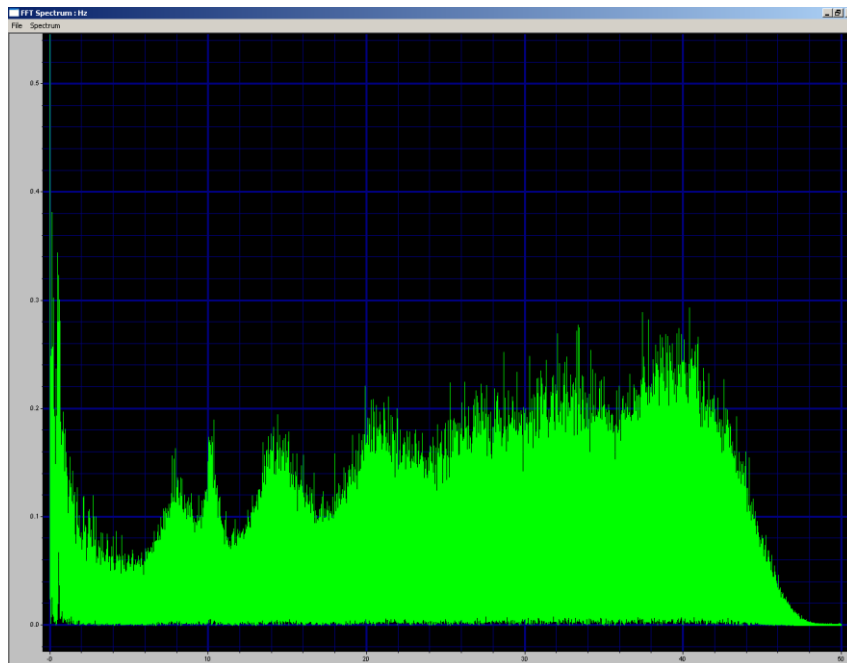
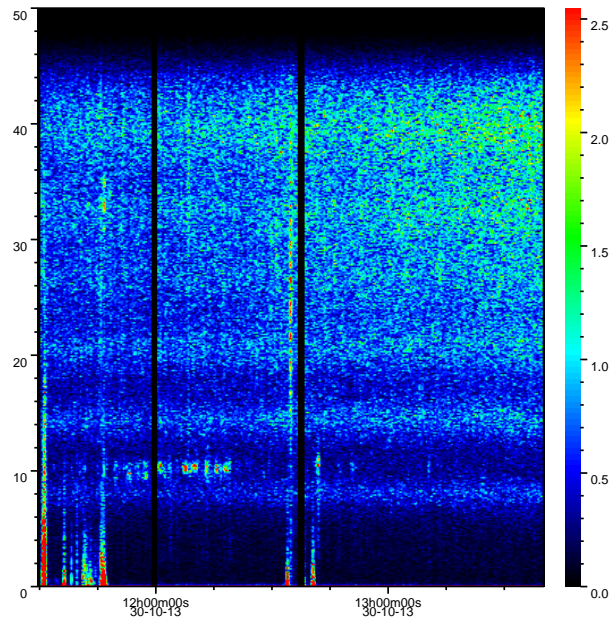


NE-SW orientation

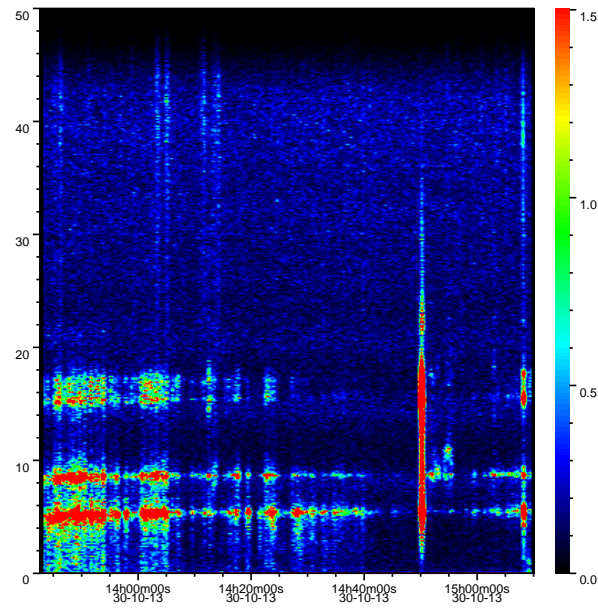


Old Geogia 2012 Antenna

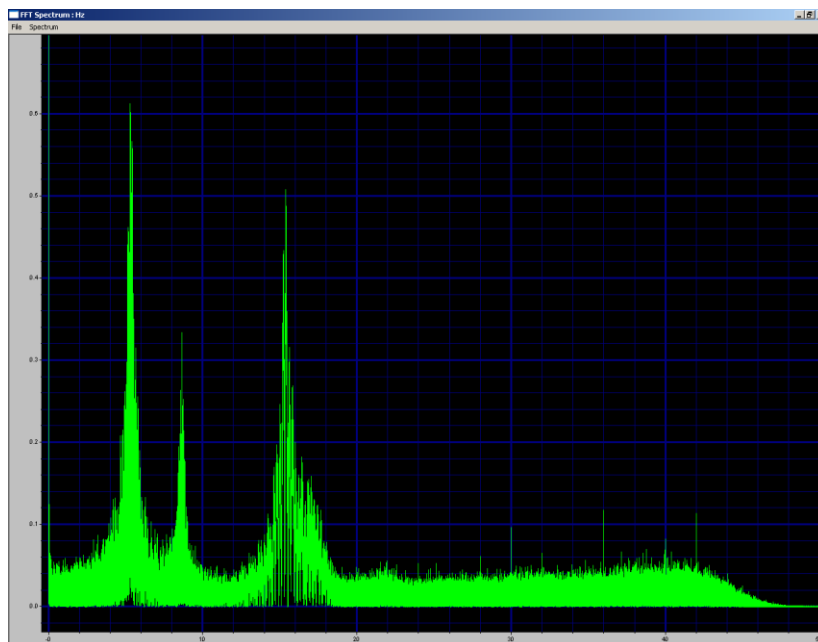
EW orientation



Vertical orientation



In vertical orientation recording is greatly affected by so called telephony noises, caused by physical vibration of antenna, but in quiet regions we still see 7.8, 15.6 and 20.5Hz frequencies.



Sources used:

<http://www.earthbreathing.co.uk/sr.htm>

Hans Michlmayrs blog at <http://www.vlf.it/inductor/inductor.htm>

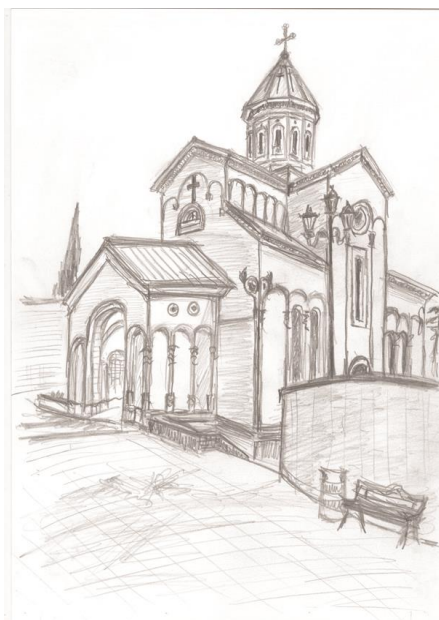
Original work of **Winfried Otto Schumann** (May 20, 1888–September 22, 1974)

Schumann W. O. (1952). "Über die strahlungslosen Eigenschwingungen einer leitenden Kugel, die von einer Luftschicht und einer Ionosphärenhülle umgeben ist". Zeitschrift und Naturforschung **7a**: 149–154. Bibcode:1952ZNatA...7..149S.

Schumann W. O. (1952). "Über die Dämpfung der elektromagnetischen Eigenschwingungen des Systems Erde – Luft – Ionosphäre". Zeitschrift und Naturforschung **7a**: 250–252. Bibcode:1952ZNatA...7..250S.

Schumann W. O. (1952). "Über die Ausbreitung sehr Langer elektrischer Wellen um die Signale des Blitzes". Nuovo Cimento **9** (12): 1116–1138. doi:10.1007/BF02782924.

Schumann W. O. and H. König (1954). "Über die Beobachtung von Atmosphericics bei geringsten Frequenzen". Naturwiss **41** (8): 183–184. Bibcode:1954NW....41..183S. doi:10.1007/BF00638174.



Церковь Кашвети Св. Георгия 3, Тбилиси Бойко Вачев'2013
Kashveti Church „St. George” 3, Tbilisi Boyko Vachev'2013

MEASUREMENT OF GEOMAGNETIC FIELD AT GEOMAGNETIC OBSERVATORY GROCKA (GCK) AND SEISMICALLY ACTIVE AREAS IN SERBIA

Milena Cukavac, Spomenko Mihajlovic

Republic Geodetic Authority, Department for Geomagnetism and Aeronomy, Belgrade, Serbia,
milencukavac@gmail.com, mihas@sezampro.rs

Abstract:

In the complex of geophysical and other methods for investigation various appearances connected with preparation and manifestation of earthquake, seismomagnetic investigations have very important role. Repeated geophysical surveys (for instance seismomagnetic survey) are required for revealing temporal variations of physical rock properties associated with the accumulation of stress. Changes in earth's magnetic field observed prior to earthquakes are to be expected. At geomagnetic observatory Grocka GMO (GCK) digital instruments like three-component and scalar magnetometers are used for monitoring of second registrations of geomagnetic field variations and absolute geomagnetic measurements. Seismomagnetic investigations in the wider area of Kopaonik were initiated immediately after the May 18, 1980 earthquake ($M=6,0$). Also, in the Rudnik area investigations were initiated since 1979 and with some pauses are still managed. At these regions total field intensity surveys have been carried out, using the network of the stations in the wider area affected by the earthquake. Obtained results enabled us to follow spatial and temporal variations of local field changes. The distribution of these changes exhibits characteristic pattern which can be related to the seismicity in certain time period. By the comparison of spatial form of successive measurements, we can obtain different seismicity of that region.

1. Introduction

Investigation of the spatial distribution and temporal changes of physical rock properties have to be held in order to estimate rock strength and failure. The necessary information to depths of tens of kilometers can only be provided by geophysical methods such as seismics, gravity and magnetic surveys, electromagnetic sounding, heat flow measurements, etc. Changes in earth's magnetic field observed prior to earthquakes are to be expected. Changes in radon content of ground water obviously related to the stress field variations have been observed many times in areas of seismic activity.

Earthquakes are caused by the accumulation of stress and strain to the point where rupturing occurs. Strain accumulation is accompanied by precursory phenomena such as ground deformation, changes of physical rock properties, variations of the ground-water level, gas emanation, micro-earthquakes and others. Tectonic forces \rightarrow deformation of rocks \rightarrow increase of strain that rocks are subjected to \rightarrow change of rock magnetization (piezomagnetic effect) \rightarrow local change of geomagnetic field that detects on the Earth surface.

Repeat magnetic surveys are a well known tool for observing and studying the space-time pattern of geomagnetic field changes over a region encompassed by the network of measuring sites

Since the very beginning of earthquake prediction-oriented studies, magnetic methods have been incorporated in complex and multiparameter observations at selected polygons in some of the seismically-active regions of the world (Sasai Y., 1991; Johnston et al., 1979; Oshiman et al., 1983, Zhan, 1989). Data analysis commonly involves removal of variations of ionospheric and

magnetospheric origin as well as the application of procedures in order to define local field changes between two successive surveys (e.g., Sumitomo, 1981) and their subsequent presentation in a form of contour plots. The interpretation of space distribution of the observed magnetic field changes can be supported by model calculations based on particular fault geometry and other relevant parameters characterizing a given focal region (Sasai, 1991). Retrospective analysis of the maps and seismological data in a ten-year period allowed Shapiro (1994) to formulate criteria for forecasting time, location and magnitude of seismic events, being successful in about 70% of the cases.

There has recently been much discussion of large-scale interactions of fault zones and the influence of large-scale processes in the preparation and triggering of earthquakes. The data from standard geomagnetic observatories are basically not appropriate for the detection of a small-magnitude and, in most cases, spatially much localized geomagnetic field changes. Their advantage is continuity in a long-time period which enables the study of regional tectonomagnetic features and long-term precursory changes. Decades of field observations along with theoretical considerations have yielded well-developed methodology in tectonomagnetic effect studies. It is commonly accepted that a network of continually measuring stations in seismically active zones is necessary for recording precursory phenomena.

2. Geomagnetic Observatory Grocka – GMO (GCK)

In the 21st century, at first decade, in observatory practice and development of Geomagnetic Observatory Grocka - GMO (GCK) starts new, modern phase. It is starting epoch of work with automatic instruments, magnetometers and acquisition equipment, which made the digital second registrations of geomagnetic field variations. Observatory Grocka produce geomagnetic data with high resolution and accuracy.

At GMO (GCK) digital instruments: three-component and scalar magnetometers are used for monitoring of second registrations of geomagnetic field variations and process of absolute geomagnetic measurements.

Processing and analyses of second and minute values of geomagnetic field variations and making geomagnetic data class hourly mean, daily, monthly and yearly mean, is done automatically, in program packages, which are done on GMO (GCK).

2.1. Observatory Magnetometer Systems

On Geomagnetic Observatory Grocka (GCK), since 2005 is created and installed referent observatory system: **ADiOS-01 - Automatic Digital Observatory System**. The **ADiOS-01** consists from FLUXGATE MAGNETOMETER, Model FGE version G, normal type, and Overhauser proton magnetometer GSM-90 F. FLUXGATE MAGNETOMETER, Model FGE version G, normal type, is three-component magnetometer (produced by DMI - DANISH METEOROLOGICAL INSTITUTE, DENMARK). Three fluxgate sensors are putted in the orthogonal center-lines system (xyz) and magnetometer to record variations of the geomagnetic field components [dX/dt, dY/dt, dZ/dt] (Table 1.). On Figure 1.a is shown configuration of standard, automatic, digital observatory system; and on Figure 1.b are given the picture of three-component magnetometer FGE, with DIMARK acquisition, on Geomagnetic Observatory Grocka (GCK).

On GMO (GCK) for registrations of variations of total intensity vector of geomagnetic field is in use class Overhauser proton magnetometer GSM-90 F and GSM-19 (made by GEM GEM Systems, Canada; on principle Overhauser effect). Overhauser proton magnetometer on each second recording total intensity values, with resolution of 0.1 nT.

2.2. DIMARK acquisition unit

Digital registrations of geomagnetic field with the FGE–three-component magnetometer and proton magnetometer, recorded according to standard protocol in DIMARK acquisition unit. DIMARK- Geomagnetic data acquisition kit, produced by ELGI-Eötvös Lorand Geophysical Institute, Budapest, Hungary. DIMARK acquisition unit are using for acquisition (recording) data in making process of continuously, digital second and minute registrations of geomagnetic field components. Connect between magnetometer and acquisition unit is realized by optic cable (Figure 1.)

Acquisition of second registrations of geomagnetic field components is doing in MAGADAM1 software, which consist installation program **MAGADAM1.INI** file – that is program for installation of necessary functions for automatic recording of digital geomagnetic data in real time.

In acquisition unit DIMARK record digital registrations of geomagnetic field components, with intervals of recording on 1 second (*sampling interval one second*). Resolution of recording or accuracy of registered variations is to $\Delta A = \pm 0.01$ nT (Table 1.).

2.3. Processing data

Automatic Digital Observatory System, **ADiOS-01**, with FGE threecomponent magnetometer and DIMARK system for acquisition data, makes posible recording of digital registrations of geomagnetic field registrations on one second, in real time. On the basis of these registrations, in next process of processing data, in standard Intermagnet's files (IMF.file), one can get minute values of registered geomagnetic field components. Processing of second registrations and making IMF.files of minute values of geomagnetic field variations, is done by program package MAGADAM 1.

The IMF files of minute values of geomagnetic field variations are main data base for statistical analyses and calculating hourly means, daily means, monthly means and yearly means values of geomagnetic field components.

Class of data, from minute values to yearly means values of geomagnetic field components, are shown in standard tables and adequate diagrams (the magnetograms - diagrams of registered data).

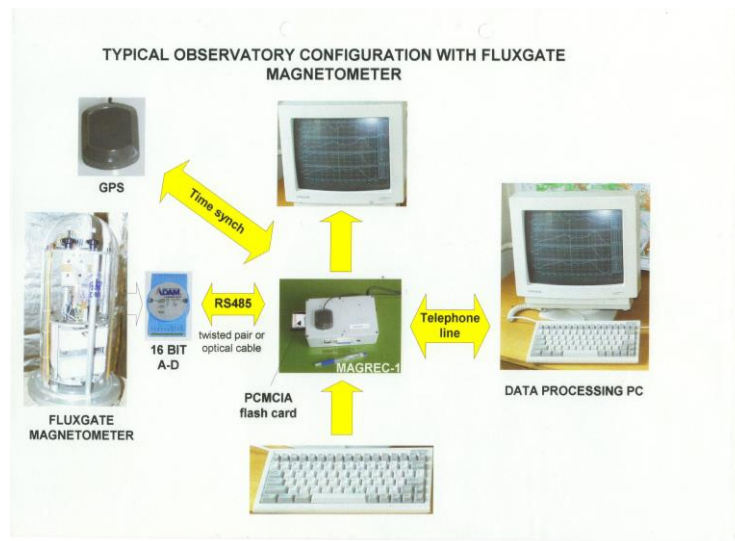
On Geomagnetic Observatory Grocka (GCK) on the basis of digital minutes values of the geomagnetic field components [dX and dY], in program package MAGADAM 2, is doing automatic scalling and calculating observatory indices of geomagnetic activity K_{GCK} .

Observatory geomagnetic measurement results can be applied in a variety of studies. The absolute geomagnetic measurements and daily variation of the geomagnetic field, are used in the performance of geomagnetic surveying, micromagnetic measurements, seismomagnetic survey and magnetovariational measurements.

On the international observatories it is monitored (observed) changes the index of solar-geophysical activities and their impact on the processes and phenomena in the magnetosphere and ionosphere. There are numerous studies that examine solar-geomagnetic disturbances (solar, ionospheric and geomagnetic barrel) and the relationship between these phenomena (events) to climate variations.

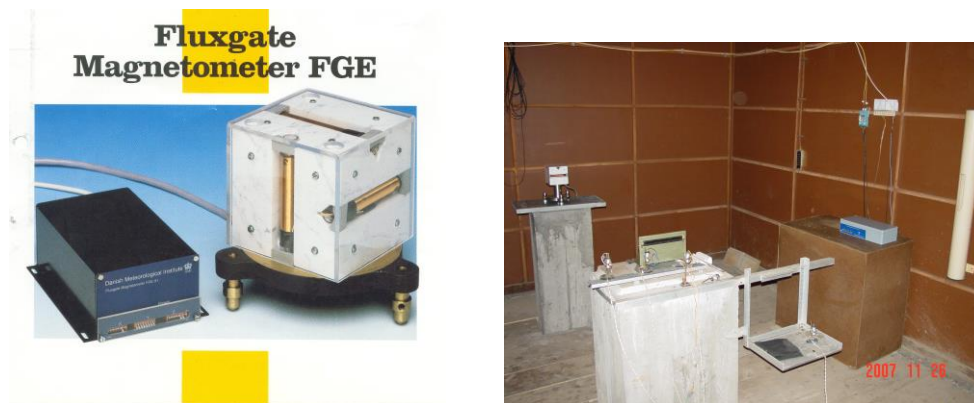
Table 1 Review of observatory instruments for registrations/recording of the geomagnetic field variations

Observatory instruments	GMF Components	Registrations Recording	Resolution and Accuracy	Comment
ADiOS-01 Three-component Fluxgate magnetometer Model FGE DIMARK Acquisition kit	Observatory system X,Y,Z Acquisition unit	Digital, automatic (since 2003.g) Automatic recording	1, 5 sec., 1 min. 1, 5 sec., 1 min. [0.01 nT]	Continuous registrations Recording data
GSM-90F GSM-19	F [nT] F [nT]	Digital (since 2010.g) Digital (since 2004.g)	1, 5 sec., 1 min. [0.01 nT]	Continuous registrations Recording data
Three components Fluxgate Magnetometer MAGSON	dX,dY,dZ [nT]	Digital, automatic (since 2005.g)	1; 5 sec.; 1 min. [0.01 nT]	Continuous registrations Recording data
dIdD - Overhauser Proton Magnetometer GSM-19	D and I [arc min], F [nT]	Digital	1; 5 sec.; 1 min. [0.01 nT]	Continuous registrations Recording data



(a)

Figure 1a Configuration of Automatic Digital Observatory System



(b)

Figure 1b FGE Three-component fluxgate magnetometer and DIMARK acquisition installed on Geomagnetic Observatory Grocka (GCK)

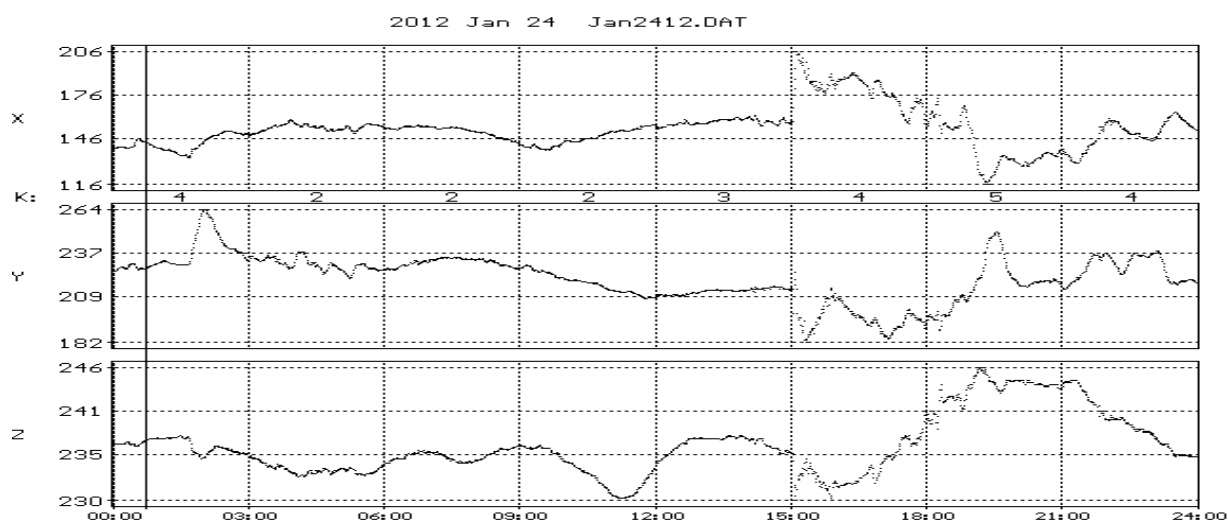


Figure 2 Magnetogram – Diurnal variations of geomagnetic field components (D - magnetic disturbed day) Date: 24 Januar, 2012; Location: Geomagnetic Observatory Grocka

3. Areas of investigations in seismically active regions in Serbia

At the Department for seismomagnetic investigations, seismomagnetic surveys are carried out for more than thirty years. They have been carried out over a number of fixed measuring sites with low gradient geomagnetic field (less than 1 nT/m). Surveys have been carried out with proton precession magnetometers of ± 0.2 nT accuracy applying the following measuring procedure. At each site successive readings were done by proton magnetometer comprising the interval of about 15 minutes, while continuous records of referent station were used to correct values for daily variation.

Seismicity, as the most relevant parameter for the detection of contemporary fault activity in the in Serbia, is relevant source of data (Fig. 3). Most focuses were in the range of 5 to 10 km deep, rarely deeper (15-20 km), and therefore all in the upper crust (depths have been distinguished instrumentally for newer events, at the local stations with short distances).

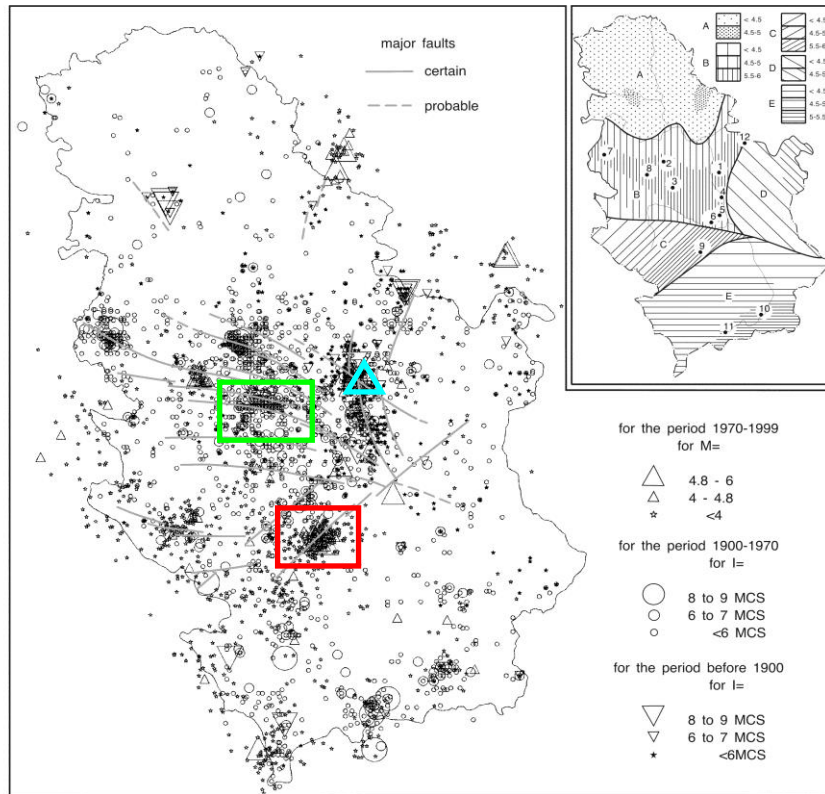


Figure 3 Seismicity of the territory of Serbia and major active faults. Insert: Major seismic zones in Serbia, with marked maximum expected magnitudes:(A)The Pannonian basin (B)Peri-Pannonian margin (C)SW Serbia (D)Eastern Serbia and (E)Southern Serbia, and location of the strongest earthquakes: (1)Svilajnac (2)Lazarevac (3)Rudnik, (4)Svetozarevo (5)Juhor (6)Trstenik (7)Krupanj (8)Mionica (9)Kopaonik (10)Vranje (11)Vitina (12) Golubac. Green square, red square and blue triangle shows area of seismomagnetic measurements.

The seismicity is the best indicator of the fault activity and therefore indicator to the areas that are interesting for the seismomagnetic investigations. Kopaonik thrust region shows high seismicity, Rudnik thrust region is also active (Fig. 3). Earthquakes with maximum magnitude $M=5.5-6$ can be expected in these regions.

In most cases pre- and post-earthquake distributions are almost inverted in space, which is in agreement with the physical nature of processes related to stress accumulation and relaxation. The location of anomalies with respect to the earthquake epicenter, their shape and extension, as well as the direction of axes can be brought into connection with prevailing stress regime in the area concerned and relevant tectonic structure.

4. Seismomagnetic surveys

By discussing the spatial and temporal changes of total intensity on account of the important geological, tectonic and seismological feature of the investigated area, changes in seismicity of area can be given. By the comparison of spatial form of successive measurements one can obtain different stress processes of the region.

Let us now discuss the spatial distribution of local field changes between consecutive surveys. If we look at figure 4a which shows local field changes in the period October 1981 - June 1982 it can be noticed that one negative anomaly with maximum intensity of about 6 nT spreads over the central part of the investigated area, forming with the positive anomaly to the southeast the field of a dipole character, with axis approximately in the direction of the SE boundary of the Kopaonik seismogenic block. This indicates that it might reflect pre and co earthquake processes in the wider area of epicentral region in connection with June 2, 1982 earthquake which epicenter is shown on figure 4a. In the seismically quiet period during June and November 1995, it can be seen that spatial distribution of geomagnetic field is very different from aforementioned period. In seismically-active period, these patterns are governed by the predominant stress regime in the area concerned (Pavlović et al., 1995). Compression axes group generally in NE-SW and dilatation axes in NW-SE direction.

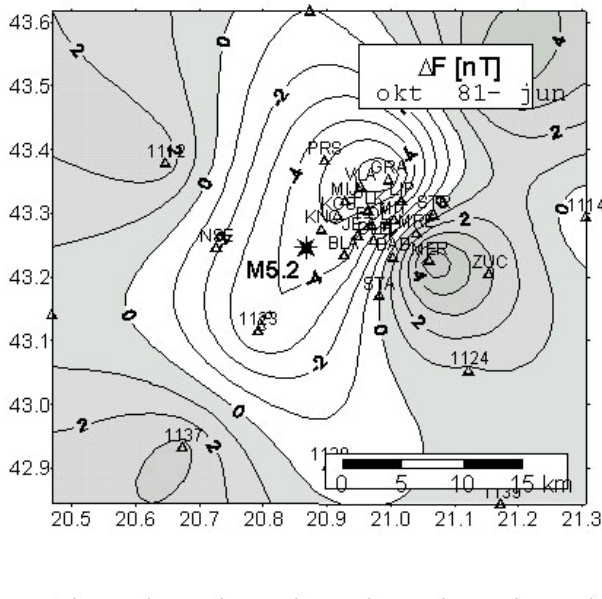


Figure 4a Seismically active period.;

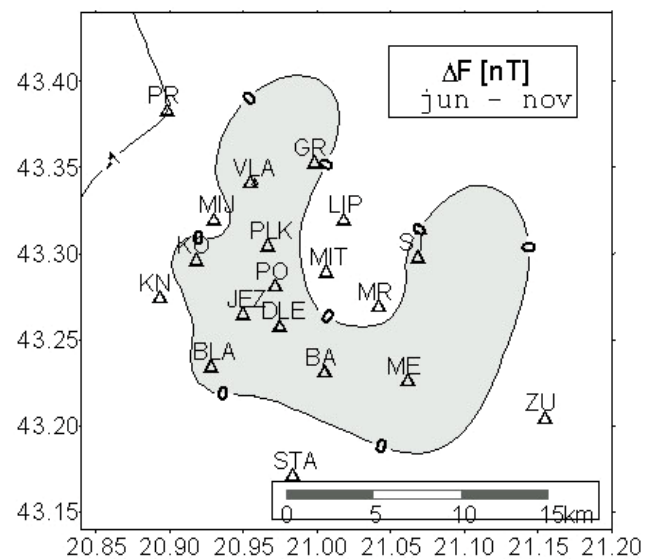


Figure 4b Seismically quite period.

5. Conclusions

In most cases pre- and post-earthquake distributions are almost inverted in space, which is in agreement with the physical nature of processes related to stress accumulation and relaxation. Secondly, the location of anomalies with respect to the earthquake epicenter, their shape and extension, as well as the direction of axes can be brought into connection with prevailing stress regime in the area concerned. It was not our intention to discuss here geological features and tectonic settings of the Kopaonik thrust region, but it should be mentioned that there is also a good correlation with the relevant tectonic structure.

Future of seismomagnetic investigations in Serbia depends on many factors, one is seismicity. Two major seismic activity areas in Serbia are still Kopaonik and Rudnik, we plan to continue our work. Also, it is plan to establish seismomagnetic station for continuous measurements since it will be the best way of conveying response of geomagnetic field to occurred earthquakes.

References:

- [1] Sasai, Y., (1991) "Tectonomagnetic modeling on the basis of the linear piezomagnetic effect", *Bull. Earthq. Res. Inst.* 66, pp. 585-722.
- [2] Johnston, M. J. S., F. J. Williams, J. Mcwhirter and B. E. Williams, (1979) "Tectonomagnetic anomaly during the southern California downwarp", *J. Geophys. Res.* 84, pp. 6026-6030.
- [3] Ohshiman, N., Y. Sasi, Y. Ishikawa, Y. Honkura and H. Tanaka, (1983) "Local changes in the geomagnetic total intensity associated with crustal uplift in the Izu Peninsula, Japan", *Earthq. Predict. Res.*, 2, pp. 209-219.
- [4] Zhan, Z., (1989) "Investigation of tectonomagnetic phenomena in China", *Phys. Earth Planet. Interiors*, 57, pp. 11-22.
- [5] Sumitomo, N.,(1981) "Geomagnetic secular variation anomalies in relation to the recent crustal movement in the southwestern region of Japan", *Bull. Disac. Prev. Res. Inst* 30, 4, pp. 274
- [6] Popeskov, M., (1987) "Geomagnetic field changes in the Kopaonik thrust region, Yugoslavia, in the period 1980-1986", *J. Geomag. Geoelectr.* 39, pp.397-429.
- [7] Radovanović S., Pavlović, R., and B. Glavatović, (1995) "Strong earthquakes of Kopaonik - magnitude $M \geq 4$: Focal plain solution of earthquake (in Serbian with English abstract)", Proceedings of the Symposium on Geology and metallogeny of the Kopaonik Mt., Kopaonik, pp.251-256.
- [8] Rikitake, T., Y. Honkura, H. Tanaka, N. Ohshiman, Y. Sasai, Y. Ishikawa, S. Koyama, M. Kawamura and K. Ohchi, (1980) "Changes in the geomagnetic field associated with earthquakes in the Izu Peninsula, Japan", *J. Geomag. Geoelectr.*, 32, pp. 721-739.



Црква Св. Сави, Београд
Church „St. Sava”, Belgradei

Бойко Вачев'2005
Boyko Vachev'2005

VALIDATION OF SATELLITE MONITORED EARTHQUAKE PRECURSOR ANOMALIES BY GEOCHEMICAL MONITORING

Erhan Alparslan, Cemil Seyis

TUBITAK Marmara Research Centre, Earth and Marine Sciences Institute

Abstract

TUBITAK-MAM Earth and Marine Sciences Institute was a partner in FP7 PRE-EARTHQUAKES project “Processing Russian and European Earth Observations for Earthquake Precursors Studies”, where Universita degli Studi della Basilicata, Italy was the project coordinator and Luft und Raumfahrt (DLR)) from Germany, Fiodorov Institute of Applied Geophysics (FIAD), Russian Space Systems (RSS), Pushkov Institute of Terrestrial Magnetism, Ionosphere and Radio wave propagation of the Russian Academy of Sciences Western Department (WD IZMIRAN) from Russian Federation and Telespazio from Italy were the other partners. During the scope of the project, Earth and Marine Sciences Institute continued the monitoring of soil radon emission at 70 stations across Turkey. Moreover the temperature of spring water and electrical conductivity values were measured on selected sites at hourly intervals. This paper summarizes the validation studies before significant earthquakes in 2012, which were:

- 1) Eastern Anatolia, Karlıova, Bingöl earthquake of magnitude 4.3 on April 4, 2012
- 2) Western Turkey, Izmir Bay earthquake of magnitude 5.0 on May 1, 2012
- 3) Western Turkey, Hisarcik, Kütahya earthquake of magnitude 5.1 on May 3, 2012
- 4) Marmara Sea earthquake of magnitude 5.1 on June 7, 2012 and
- 5) Eastern Anatolia Gökçeli, Kahramanmaraş earthquake of magnitude 5.0 on July 22, 2012

Introduction

Data acquired by the soil radon and/or spring water stations covering the earthquake location were drawn on a graph, illustrating a time series of soil radon gas emissions for a two year period. On a map of Turkey, the locations of the earthquake and geochemical measurement stations are given. The satellite thermal anomaly maps corresponding to these dates were also investigated for any anomalous situation before occurrence of these earthquakes.

Another study in parallel was to check the occurrence of anomalies in our geochemical parameters data corresponding to thermal anomalies detected by our partners and associate partners.

Karlıova / Bingöl Earthquake

Our associate partner, Prof. Dimitar Ouzonov warned us on April 4, 2012 against increased thermal emission on East North Anatolian Fault at 40N, 38E. In fact, in Karlıova, Bingöl region in Eastern Anatolia, an earthquake occurred on April 4, 2012 with a magnitude of 4.3. The soil radon emissions at Yedisu station were checked and an anomalous decline was observed from 180 to 20 alpha counts/15 min reaching its minimum value on the date of the earthquake. Spring water conductivity measured at Yedisu station was on a level of 600 $\mu\text{S}(\text{iemens})/\text{cm}$ for a period of 5 months before the earthquake then it started to increase to a peak of 6000 $\mu\text{S}/\text{cm}$ which is most probably a strong precursor of this earthquake. At Kös station covering this region also, conductivity values showed a decline from 2300 $\mu\text{S}/\text{cm}$ of four months before the earthquake compared to 2100 $\mu\text{S}/\text{cm}$ of 15 days later (Figure 1). This event shows how thermal anomalies detected from satellite images may be integrated with ground observations of geochemical parameters to predict earthquakes.

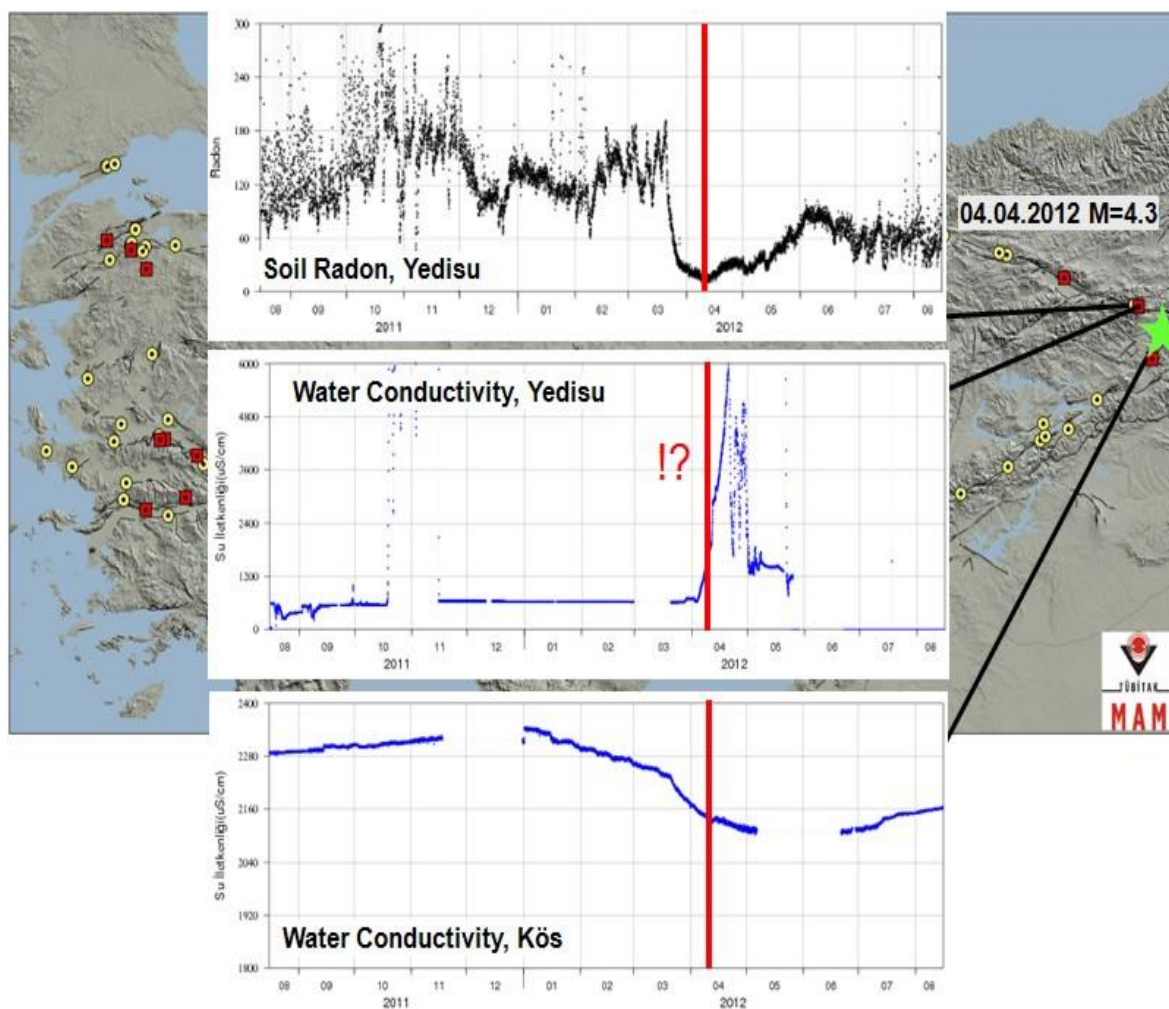


Figure 1. Soil radon and water conductivity anomalies before Karlıova Bingöl earthquake of Magnitude 4.3 on April 4, 2012.

Marmara Sea Earthquakes

Another successful example of the integration of thermal anomaly maps derived from satellite images with geochemical parameter observations is the case of Marmara Sea earthquake of magnitude 5.1 on June 7, 2012. Here soil radon gas emission at Yayaköy station in the vicinity anomalously climbed from 130 alpha counts/15 min on a week ago to 420 alpha counts/15 min on the day of the earthquake. Moreover, water conductivity measured at Balikesir station began to decrease from a peak of 790 μ S/cm to 670 μ S/cm on the day of the earthquake as shown in Figure 2. Thermal anomalies are clearly seen also on maps derived from satellite images as shown in Figure 2.

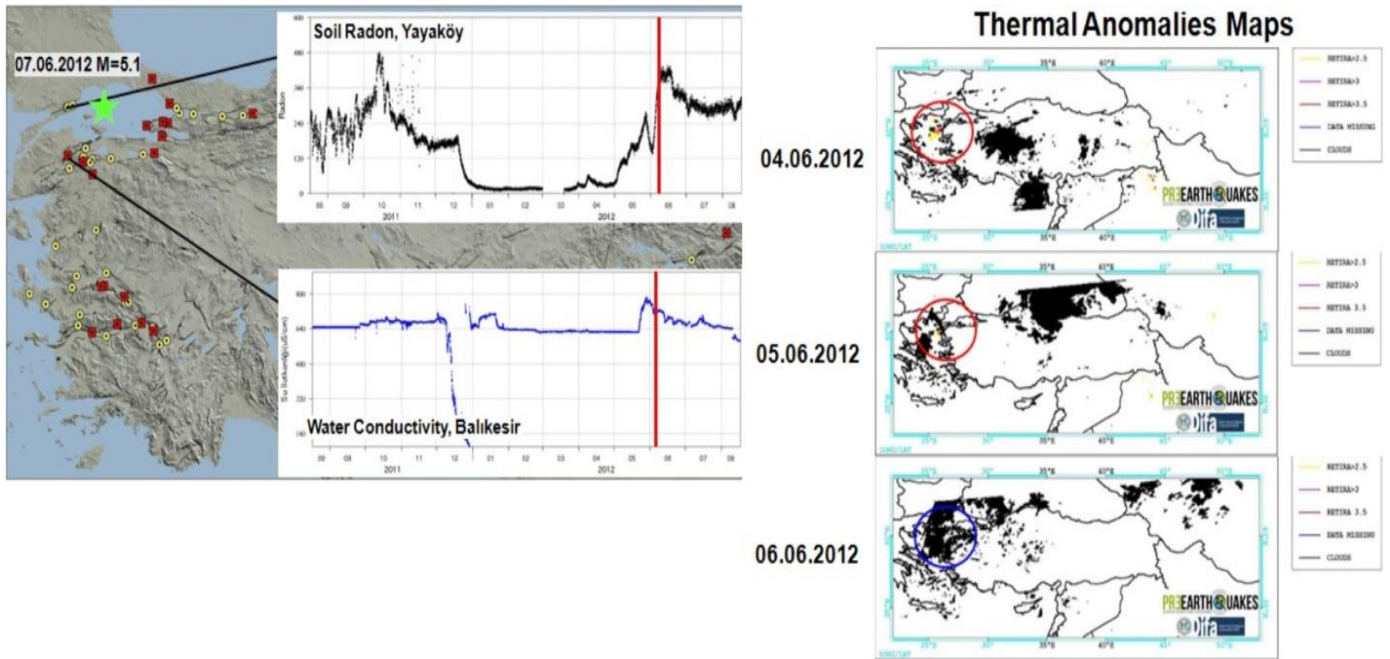


Figure 2. Geochemical parameter measurements vs. thermal anomaly maps derived from satellite images before Marmara earthquake of Magnitude 5.1 on June 7, 2012.

Kahraman Maraş Earthquakes

Although thermal anomaly maps are very useful in prediction of earthquakes as proven by the anomalies detected in eastern Mediterranean on July 20, 2012 just two days before the event and that of September 30, 2012 two weeks before the event, they may not always be supported by ground geochemical parameter measurements, as the measurements in this particular case from the radon and spring water stations in the vicinity did not display any significant anomalous results as can be seen in Figures 3, 4 and 5. More research in this area is needed.

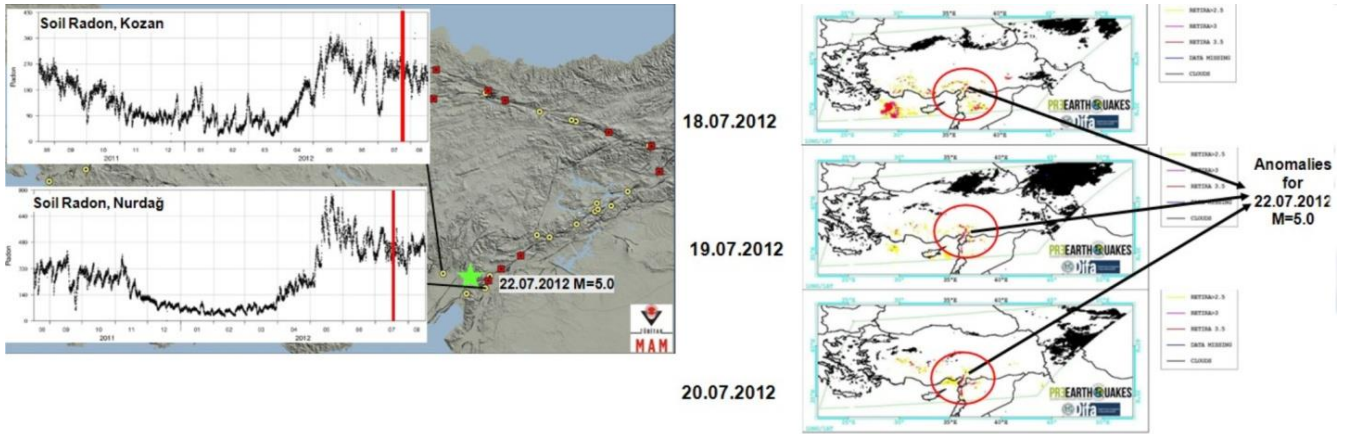


Figure 3: Radon emission measurements vs. thermal anomaly maps derived from satellite images before Kahramanmaraş earthquake of Magnitude 5.0 on July 22 2012.

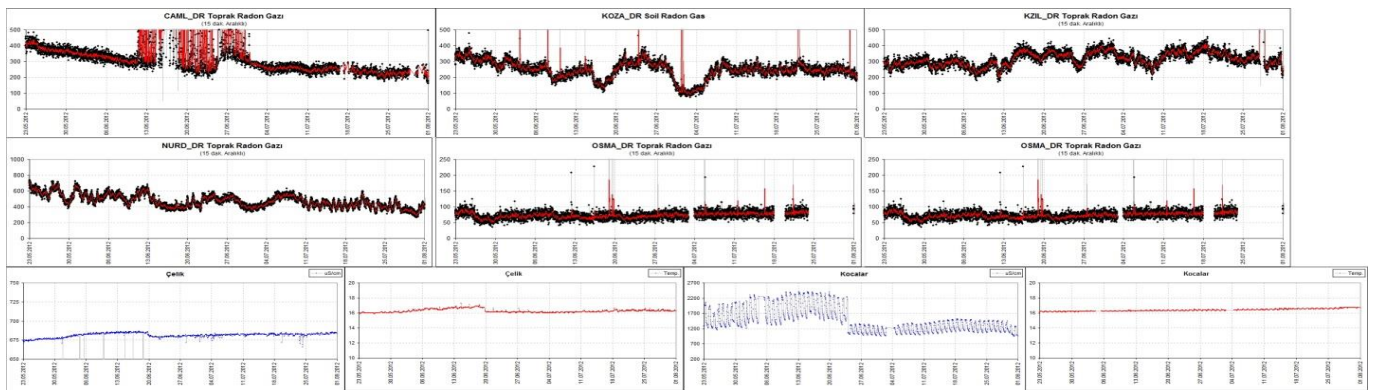


Figure 4: Time series for geochemical parameter measurements from radon and spring water stations in the vicinity before Kahramanmaraş earthquake of Magnitude 5.0 on July 22, 2012.

Aegean Region Earthquakes

Another research carried out was an investigation of an earthquake statistic from micro-seismological stations in the vicinity of regions where thermal anomalies were reported by our associate project partner, Prof. Ouzounov. An anomaly was detected on 19/07/2012 in Aegean Region of Turkey and the largest earthquake that occurred close to the anomaly region was of magnitude 3.6 at depth of 5 km at 26°40'83''E and 37°52'19''N. For the thermal anomaly of 16/10/2011, there occurred an earthquake of magnitude 3.7 at depth of 11.1 km at 28°07'02''E and 40°44'34''N. Finally, for the thermal anomaly of 21/10/2011, there occurred an earthquake of magnitude 3.0 at depth of 6.4 km at 29°07'30''E and 40°42'19''N.

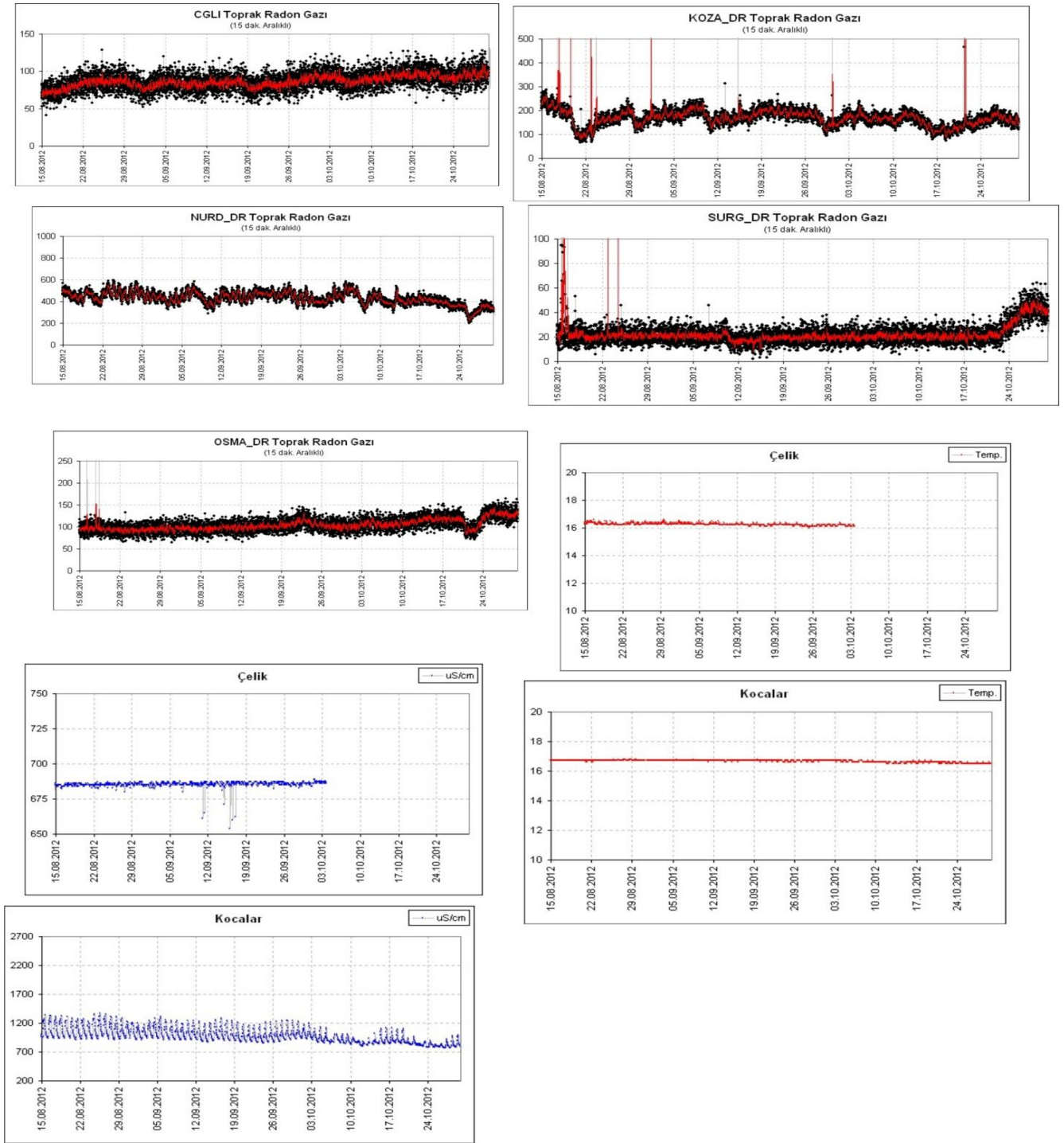


Figure 5. Time series for geochemical parameter measurements from radon and spring water stations before East Mediterranean earthquakes of $M=4.4$ depth 5 km and $M=4.6$ depth 26 km on October 16, 2012.

Results

Thermal anomaly maps derived from satellite images are heavily affected by cloud coverage which negatively affects the integration of this data with ground observation data. However, they also produce valuable earthquake precursor results like in the case of the Kahramanmaraş earthquake in Eastern Turkey on October 16, 2012. In this case thermal anomaly maps derived from satellite images proved to be an essential tool in earthquake precursor studies.

There are earthquake occurrences which are validated both by thermal anomaly maps and geochemical monitoring. However, there are also cases where one or the other gives an alarm on occurrence of a future earthquake. Although there are promising results, more research in this area is needed in order to avoid false alarms.



Часовникът и времето, Кулата в ИзмирБойко Вачев'2008
Clock and time, Izmir tower *Boyko Vachev'2008*

DATA ACQUISITION – DAFIT A NEW TOOLSET FOR TIME EFFECTIVE AND TRACEABLE DATA PREPARATION AND DATA VALIDATION OF TIME SERIES DATA

Ludwig C. Ries

Federal Environment Agency, GAW Global Observatory Zugspitze/Hohenpeissenberg, Zugspitze 5,
D-82475 Zugspitze, Germany, ludwig.ries@uba.de

Keywords: Data Acquisition, quality assurance, data preparation, data validation, automation, standardization

Abstract

Standardized quality assurance according to required data quality objectives is essential for a homogeneous high level of data quality. However data processing and data preparation often times is done individually and in a non-standardized way. As an additional problem interactive data validation can be a very time consuming step with time series data which have been produced with automated measurement equipment.

In front of this background a new methodical approach with a set of time efficient and standardized methods is proposed which also can be used as a tool for future standardization of data quality assurance measurement stations.

In general in order to prepare measurement data a set of methods is required. In the framework of this program the methods are ranked in two groups: first – simpler methods for managing structural changes and corrections in the time series data and second – higher developed methods for assuring a correct time structure, graphical control and flagging non representative data and for the calculation of differently or higher aggregated mean values and statistical values.

By fulfilling the auxiliary condition that data treatment at first has to be finished with application of methods of group one the user is practically free in finding and selecting its way for a solution. Once the user has found an ordered set of methods and parameters which is a sufficient solution for the preparation of the actual data, the solution can be stored as a set of parameters for the individual project. This enables the user for repeating the solution at another time to another set of time series data which are produced with the same data format from the same instrument. This structure is characteristic and useful for continuous environmental monitoring which produces a high amount of time series data with a constant data format.

By saving all intermediate results in a hierarchical way with a fixed naming convention, in a later time the effect of all steps of the application of methods can be traced back in the workflow history. Because the proposed methodology separates methods and its parameters, it can be a good substitution to many situations in data preparation whereas up to now normally for each little change the program source would have to be changed and compiled. This gives an essential facilitation to the whole process of data preparation of time series data in the daily monitoring. The set of methods works with ASCII data files, in case each line has a time stamp with own date and time. The program works on files with arbitrary minute data or higher aggregated time data and provides precision up to the second. Dafit runs on Windows XP-Win 8.

1. General

This paper describes a work flow oriented methodology for efficient data preparation, validation and data flagging of monitoring time series data, following a more general approach. The software was written in order to ease the tedious and time consuming process of time series data preparation and to facilitate its standardization on environmental monitoring stations. It is relatively fast to install and to learn and applicable for all cases, when up to now elementary data preparation was required.

It helps in such situations, when practically the same program for data processing had to be altered only for a little change and then to be recompiled again and again. Methods and parameters and a full history of resulting data from the beginning to the end of processing are separated from each other. All meta-data and processed data are stored in a project. Because the program uses a format interpreter it can process a larger variety of ASCII files, which are produced as an output of different data acquisition programs for different instruments or from larger data acquisition systems which are used at environmental monitoring stations.

1.1 CONCEPT

- Separate methods, parameters and processed data.
- Store parameters and data of a problem in an own project.
- Save each step of processed data, from the beginning to the final result in a hierarchical history (Workflow), which allows backtraceability.
- You receive an ordered set of methods and parameters, stored in the project (Solution).

2. How to work with (Workflow)

The program is directory oriented. At first a directory has to be created for data with a certain time interval, for example, one month. The maximum interval of data which can be processed at once is one year. Then a new project name for this data file is created and stored. In the next step the data structure of the file will be opened with an editor and has to be investigated by the user. At next the user will have to find what preparatory steps with the data file will have to be done in which order to receive a usable file for data validation. Usable file means: Each line contains a datum of one time interval. Each line (time interval) is readable. Missing gaps (sometimes e.g. during a power down, data acquisition does not work.) in the time series data time structure are substituted in the file with a missing data flag. The time stamps are in ascending order.

Finally a plan for the stepwise processing of the data will have to be made.

Besides this the following elementary requirements have to be regarded:

The data file has to be in ascii. Each line of the data file has to contain a date time header with fields of fixed width YYYY or YY, MM, DD, hh, mm (and ss optional). The order of time and date is arbitrary, as the time date fields are interpreted. Each line must contain a minimum of one column of data values and a maximum of 30 columns. At one time only one column can be processed. It is recommended to use list directed data format which means: numbers are separated by a comma or a semicolon, or a blank or tab. The columns after the time data header may consist of numbers and strings in arbitrary order.

2.1. PREPARE AND REPAIR DATA STRUCTURE

After the first preparatory steps which have been explained above, it has to be tested, whether methods from a first group of elementary methods to correct deficiencies in the data structure have to be applied. The application of these methods is optional. Following methods presently are given:

- **Concatenate files** (e.g. daily files to a monthly or annual file or concatenation over an arbitrary interval)
- **Inverse time order** (the data have to be in ascending order)
- **Remove multiple empty lines and multiple separation marks** (for the list directed format each column has to be separated by one separating character).
- **Substitute separation marks** (e.g. TAB by semicolon, or comma or blank)

- **Filter corrupted lines** (sometimes data acquisition produces corrupted lines. This filter detects and removes such lines according to actually defined parameters and produces a log file of removed information.)

After this the application of methods of the following second group of methods has to be planned.

2.2 APPLY HIGHER METHODS FOR TIME STRUCTURE CORRECTION, VALIDATION, FLAGGING AND FINAL AGGREGATION THE FOLLOWING SEQUENCE OF METHODS HAS SHOWN PRACTICAL USABILITY FOR HIGH QUALITY ATMOSPHERIC GAS OR AREOSOL MEASUREMENTS FOR GLOBAL ATMOSPHERE WATCH DATA.

- **Test and repair for a correct and consistent time structure.** This tests check for an equidistant time grid. Each single time step between start time and end time must be contained in the resulting output. In case there is a gap in the data file then it will be substituted with the appropriate time date fields and a missing data code for the missing data value.
- **Aggregate to a time series with higher time resolution in the minute scale** e.g. from 3 sec, 31sec, 146 sec data to 1 minute means. In case already 1 min data exist, then this step has to be omitted.
- **First validation: check interactive plausibility of time series and flag with graphical editor.** Flag spikes, calibrations, outliers etc. (In one minute data files with higher time resolution, typically artifacts like spikes, outliers, short time deviations because of technical issues are found.)
- **Aggregate to a time series with lower time resolution, preferably in the hour scale.** E.g. from 1 min values to 30 min or 1hr mean values.
- **Second validation: interactive check with graphical editor:** Flag non representative episodes, local pollutions etc. (In lower time resolution data, process related information can be read and understood and validated. For example causes for short time sharp shifts in the level of measured values can be detected with a trajectory model like Hysplit or pollution events can be flagged. This step has development potential for inclusion of automated statistical and chemical or physical models for data validation.)

2.3 METHODS OF THE SECOND GROUP FOR AGGREGATION AND VALIDATION ARE:

2.3.1 *Time structure*

This test is contained in the methods 2.3.2 and 2.3.3. It is performed each time when an aggregation of data is calculated.

2.3.2 *Means of even intervals*

This method works with a programmed chain of conditions. It works only for whole minute data. Data intervals with uneven seconds may not be treated. It is slower than method 2.3.3. (Both methods 2.3.2 and 2.3.3 calculate the arithmetic mean, standard deviation, and the percentage of available underlying data. A threshold value for this percentage can be selected. An actual existing percentage over or equal this boundary then allows calculation of a mean value.)

2.3.3 *Means of broken intervals*

This method works with a large array which contains every second of one whole year. According to the start and end time of each mean value for input it's value is stored correctly. In a second step, new

mean values will be calculated according to a selected equidistant time grid with arbitrary grid length in the minute range. With this method a 1min data file can be calculated on the same 1min data file. In that case input equals output, but the time structure has been tested for gaps and gaps have been filled in the output with missing data code.

2.3.4 Graphical editor

The graphical editor has various methods for navigation through large data files. It allows interactive graphical flagging with line editors. This means everything above (or under) an interactively drawn line will be flagged. Additional functions are given for scaling, zoom in and out, selecting a single point and its flags and coordinates, for determination of n, mean and median from selected points in a predefined graphical rectangle. Flagging results and comments can be retrieved and analyzed at any time after the processing of the data. On a modern laptop with an I5 processor one whole year with about 500 thousand data is read in about 25 seconds. It allows simultaneously two hand operation: One hand works with predefined keys and the other operates the computer mouse. Against becoming tired, the function of both hands can be exchanged.

3 Program user interface

3.1 START WINDOW AND GRAPHICAL EDITOR

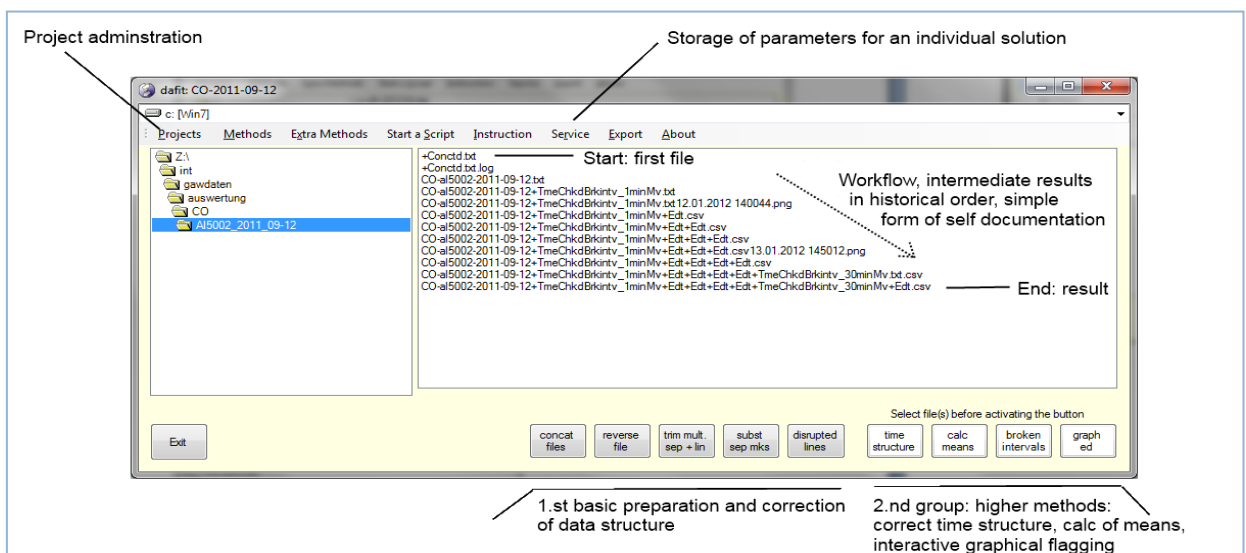


Figure 1

Start window of the program and its essential properties. 1. Create directory and copy data into it. 2. Create project and save. 3. Apply methods for basic preparation and correction 4. Apply higher developed methods for time structure correction, flagging and validation and final aggregation of data

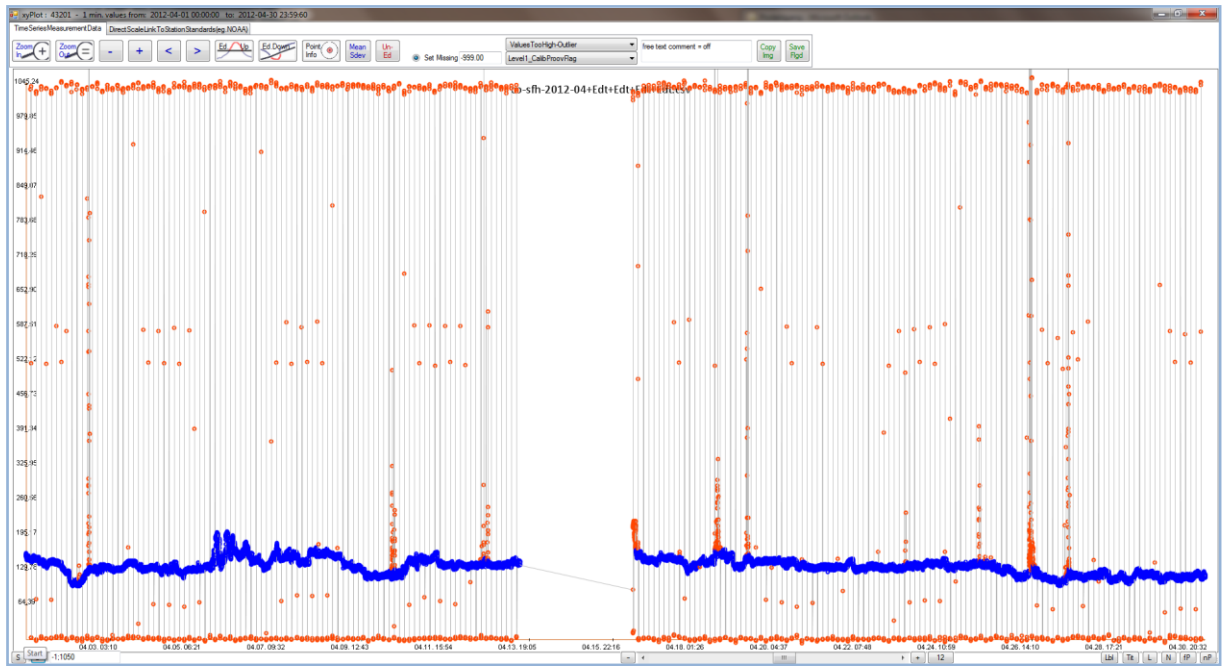


Figure 2

Graphical editor for interactive control, flagging and plausibility check, with several functions for navigating in the data enables for a productive screening, validation and flagging of the processed time series data

Proposed methodology and software can facilitate essentially the process of data preparation of monitoring time series data. Dafit runs on Windows and is free for station personnel and institutions which work for earthquake prediction in public interest or for the UN/WMO Global Atmosphere Watch program (GAW).

References:

L. Ries, Dafit - a new workflow oriented approach for time efficient data preparation, validation and flagging of time series data from environmental monitoring. pp. 651-656. In: Proceedings of the 27th conference on Environmental informatics – Informatics for Environmental Protection, Sustainable Development and Risk Management, Part II, Shaker Verlag, 2013, Aachen, 938.p, ISBN 979.3-8440-1676-5

L. Ries, Standardized and automated data quality assurance at GAW Stations: concept, methods and tools, presentation at GGMT-2013 Conference, Peking.

GAW Technical Report No.206, 16th WMO/IAEA Meeting on Carbon Dioxide, Other Greenhouse Gases and Related Measurement Techniques (GGMT 2011) Wellington, New Zealand, 25-28 October 2011.

L. Ries, How to Keep the Quality Chain - Work Flow-Oriented Data Processing for Global Atmosphere Watch Measurement Stations. pp. 109-112 In: Environmental Informatics and Systems Research . Vol. 2 Workshop and application papers. Eds. Olgierd Hryniewicz, Jan Studzinski, Anna Szediw. Shaker Verlag, 2007, Aachen, 292p

APPLICATION OF MAGNETO-TELLURIC STATION GEOMAG-02 IN GEOELECTRIC RESEARCHES IN BULGARIA

L. Dobrodnyak, I. Logvinov, E. Nakalov, L. Rakhlin, S. Timoshin

In 2013 Bulgarian scientists suggested a task: possibility of application of magnetic-telluric station GEOMAG-02 [1] for identification of subtle texture of behavior of magneto telluric and magneto-variation parameters at geophysics observatories of Bulgaria for identification of connection of these parameters with seismicity.

Magneto-telluric station (MTS) GEOMAG-02 (manufactured by «Research Center Geomagnet», Lviv, Ukraine, email: l.rakhlin@mail.ru) is intended for changing variations of magnetic and electrical fields of Earth in laboratory and field conditions. MTS consists of three-component magnetic field (MF) variation meter based on flux-gate sensor and two-component electric field (EF) variation meter – telluric current based on measuring difference of potentials of non-polarizable electrodes (fig. 1). MTS has built-in CompactFlash type FLASH-card for data acquisition and storage, GPS-receiver for synchronization of data sample, display of station position coordinates and its altitude. Four-line liquid-crystal display for displaying current measurement results and set system parameters. Equipment set includes 5 non-polarizable electrodes of Cu/CuSO₄ type with high long-term parameter stability.



Fig. 1. Variant of MTS set with MF sensor on gimbal mechanic system of automatic stabilization of vertical position.

Equipment is supplied with two MF sensor types: on titanium rotating platform (fig. 2) and on gimbal mechanic system of automatic stabilization of vertical position (fig. 3).

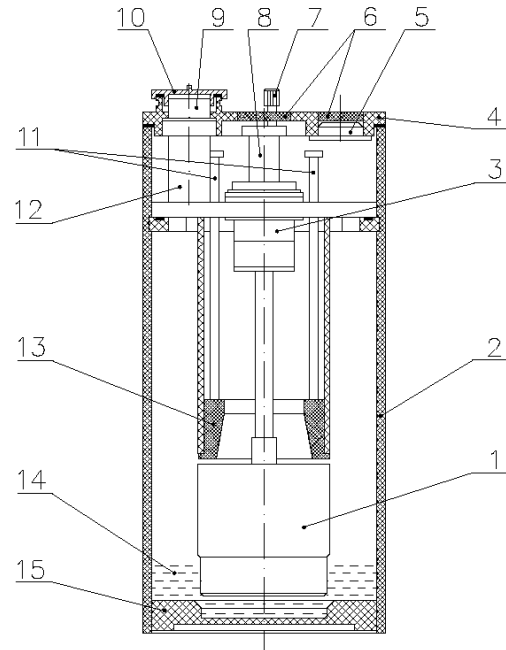


Fig. 2. MF sensor on titanium rotating platform. Fig. 3. MF construction on gimbal mechanic system of automatic stabilization of vertical position.

The first type is expedient to use on stony soils and in laboratory (observatory) conditions, and the second type – use for experimental researches, when it is expedient to dig a sensor to soil for reduction of temperature drift. Both sensor type cases are hermetic.

Every measuring channel has Butterworth fourth order low-pass filters fully identifying frequency characteristics of measuring channels. Filter's cutoff frequency F_0 is selected from the series of (1, 3, 10) Hz depending on set task. Amplitude (AFC) and phase (PFC) frequency characteristics for $F_0=1$ Hz are presented in Fig. 4. Butterworth filters have maximum smooth AFC in pass band frequencies, practically decaying to zero in suppression band frequencies and practically linear phase-frequency characteristics in pass band frequencies. In suppression band frequencies AFC decays with rate of 80 decibel per decade.

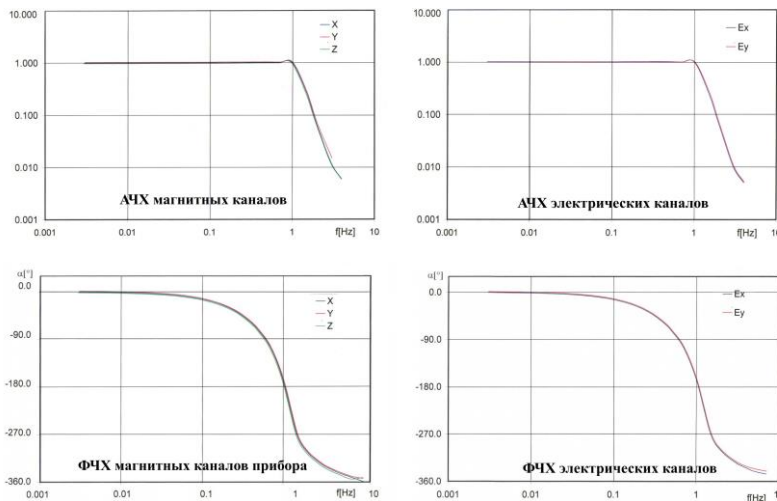


Fig. 4. Amplitude (AFC) and phase (PFC) frequency characteristics of GEOMAG-02.

On output of each measuring channel analogue signals are converted to digital signals by means of 24-bit analogue-digital converters, thereby reading of information from all five measuring channels is performed simultaneously 10 (25) times per seconds depending on set cutoff frequency of

filters Fo. Data averaging during recording to FLASH-card is done for (0.1...60) s. Selection of station operation modes and settings control are extremely simplified and are performed by operator by single menu function controlling button of program. Station settings set by operator are stored to FLASH-memory of processor and are preserved when power supply is off.

Before switching on of data registration, automatic compensation of constant component of full field is performed. After switching on of registration settings header is formed including full field magnetic component value at the time of record start. It allows presenting recorded data taking into account full field values if necessary. Data recording is performed in text format to FLASH-card:

```
; MS:GEOMAG-02 #29-2013
; Date: 2013/06/13; Time: 11:56:00
; Sampling: 0.10 sec
; Latitude: 42 28'33.4"N; Longitude: 023 25'31.8"E; Altitude: 1231.m
; Total Field: X = +19505nT; Y = +00040nT; Z = +41995nT
Date   Time   X [nT] Y [nT] Z [nT] Ex[mV] Ey[mV] Ts[C] Te[C]
;
2013 06 13 11 56 00.00 +0007.91 +0010.03 +0007.92 +009.884 +012.825 +17.1 +18.4
2013 06 13 11 56 00.10 +0007.91 +0010.03 +0007.96 +009.856 +012.899 +17.1 +18.4
2013 06 13 11 56 00.20 +0007.95 +0010.06 +0007.98 +009.831 +012.904 +17.1 +18.4
2013 06 13 11 56 00.30 +0007.96 +0010.02 +0007.94 +009.810 +012.907 +17.1 +18.4
```

Fig. 5 presents typical noise characteristics of magnetic channels.

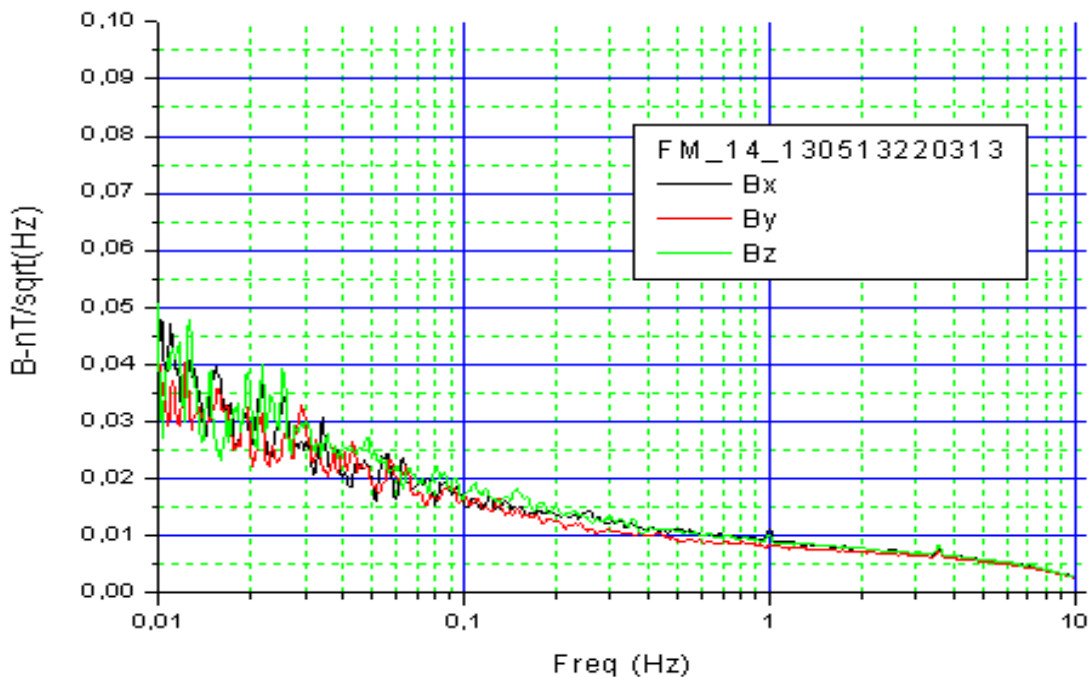


Fig. 5. Typical noise characteristics of magnetic channels of GEOMAG-02.

Main technical characteristics of MTS GEOMAG-02 are:

measuring range of full MF	± 65000 nT;
measuring range of MF variations	± 3200 nT;
resolution of MF variation registration to FLASH-card	0.01 nT;
temperature drift	<0.2 nT/°C;
tolerance of component nonorthogonality of MF sensor	<30 ang. min;
automatic compensation range of contact MF in each component	± 65000 nT;
EF variation measuring range	± 200 mV; ± 2000 mV;
resolution of EF variation registration to FLASH-card	1 μ V;
measuring channel frequency band	DC - 1 (3, 10) Hz;
measuring channel information sampling number	10 (15) 1/sec;
data averaging during recording to FLASH-card	0.1...60 s;
capacity of FLASH-card «CompactFlash» (FAT-16, FAT-32)	64 MB...64 GB;
operating temperature range	- 10... +40°;
connecting cable length between MF sensor and electronic unit	up to 50 m;
power consumption	12 V; 0.1 A.

References

1. Рахлін Л., Гулеюк Л., Накалов Є., Кузнєцов О. Магнітотелурічна станція “GEOMAG-02”//Нові геофізичні технології прогнозування та моніторингу геологічного середовища. Львів: КВ ІГФ НАН України. – 2005. – С.22-23.



Дума - Памятник спасителей, Одесса Бойко Вачев'2012
Duma – The Saviors monument, Odessa Boyko Vachev'2012

STUDY INTERACTION BETWEEN SEISMICITY AND GAS EMISSION ON THE TERRITORY OF GEORGIA

G.Melikadze¹, M. Todadze¹, N. Kapanadze¹, O. Körting², B. Müller³, J. Vaupotič⁴, P. Andreeva⁵, Hr. Kiselinov⁵

¹M. Nodia Institute of Geophysics Iv. Javakhishvili Tbilisi State University; ²Institute of Applied Geosciences, Karlsruhe Institute of Technology, Adenauerring 20b, 76131 Karlsruhe, German; ³Landesforschungszentrum Geothermie, Adenauerring 20b, 76131 Karlsruhe, German; ⁴Jožef Stefan Institute, Slovenia; ⁵Geological Institute, BAS, Sofia, Bulgaria; melikadze@gmail.com

Abstract:

Natural gases emission are a very sensitive indicative for geological, especially for geotectonic state. As it was expected in distributing of gas associations the properties of the geological structure of Georgia has been obviously revealed. In order to study the gas distribution (CO₂, Rn, He, CH₄ etc.) and define its quantitative characteristics the field work was organized in 2013 on the territory of Georgia.

In order to study of regional seismicity influence on gas emission has been organized the real time monitoring of free gas discharge CO₂, and Rn emission, also air temperature and atmosphere pressure on the Borehole # 37 in Borjomi.

1. Field study

In order to study the CO₂ distribution the field work were carried out on the territory Georgia with foreigner colleagues – project coordinator German colleagues as well as Bulgarian and Slovenian ones. For field studies the mobile group was the same way equipped with special devices and moved by car along the pre-defined routes and carried out the sampling of natural and artificial springs. For field measurements they used WTW340i (for pH, conductivity, temperature, free oxygen) as well as SISE INGEM-1 for Radon and Helium measurements. Also, special equipment for gas content measuring had been purchased, namely PGD3-IR (Methan, Oxigen, CO₂ and HS). Selected points were sampled for typical chemical analysis ((Na, Ca, K, Mg, HCO₃, SO₄ და Cl) and the samples were shipped to the laboratory (Tbilisi) for further analyzing.



Fig #1 Water's physical parameters measurement process



Fig #2 Sampling process for hydro- chemical analyze



Fig #3 Geological sampling and gas composition measurement process

The sampled points were mapped by GPS and on the next step the data was processed by ArcMap. By the same software the results of water and gas hydrochemical analysis, as well as geological,

hydrogeological and hydrochemical data of the region have been processed. This gave us the possibility of complex studies.

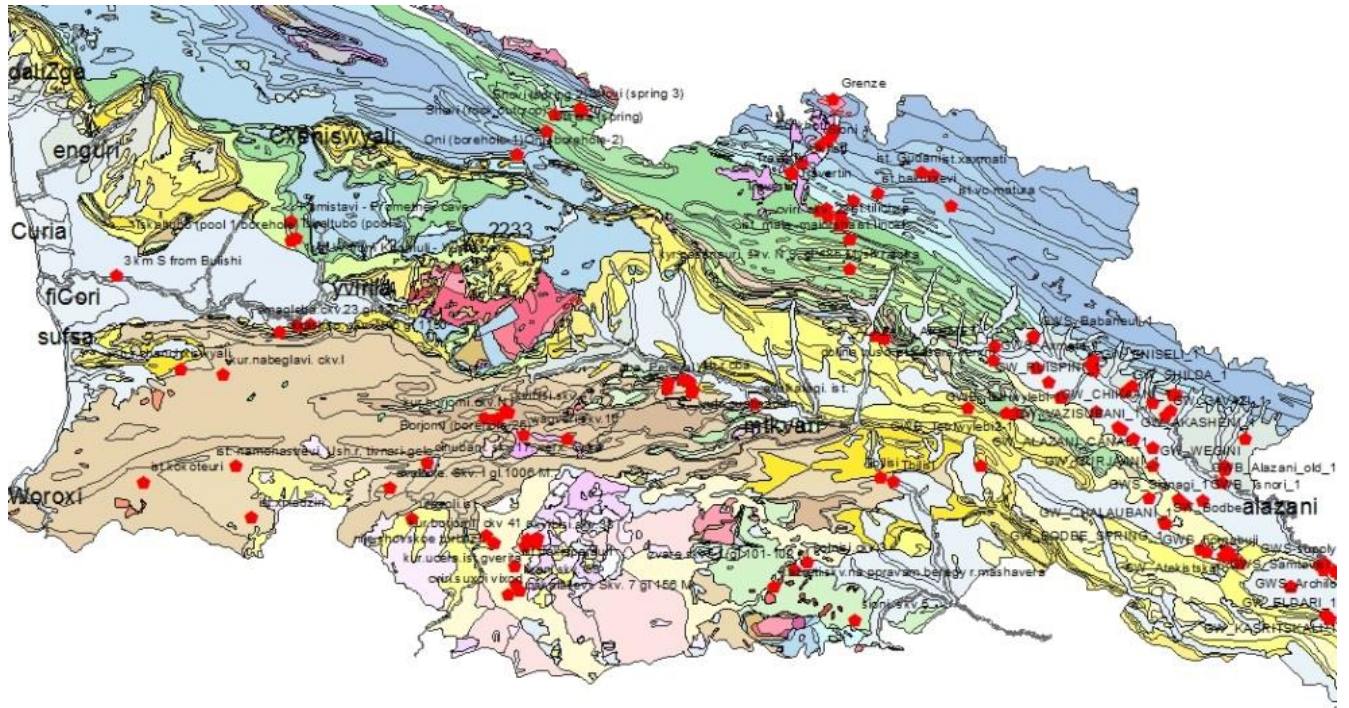


Fig.# 4 Distribution of sampled points in different Geological regions

During field work hydrochemical parameters (Na, Ca, K, Mg, HCO₃, SO₄ and Cl) in underground waters had been observed as well as gas content and general peculiarities of it distribution. For all observed parameters were determined the background values.

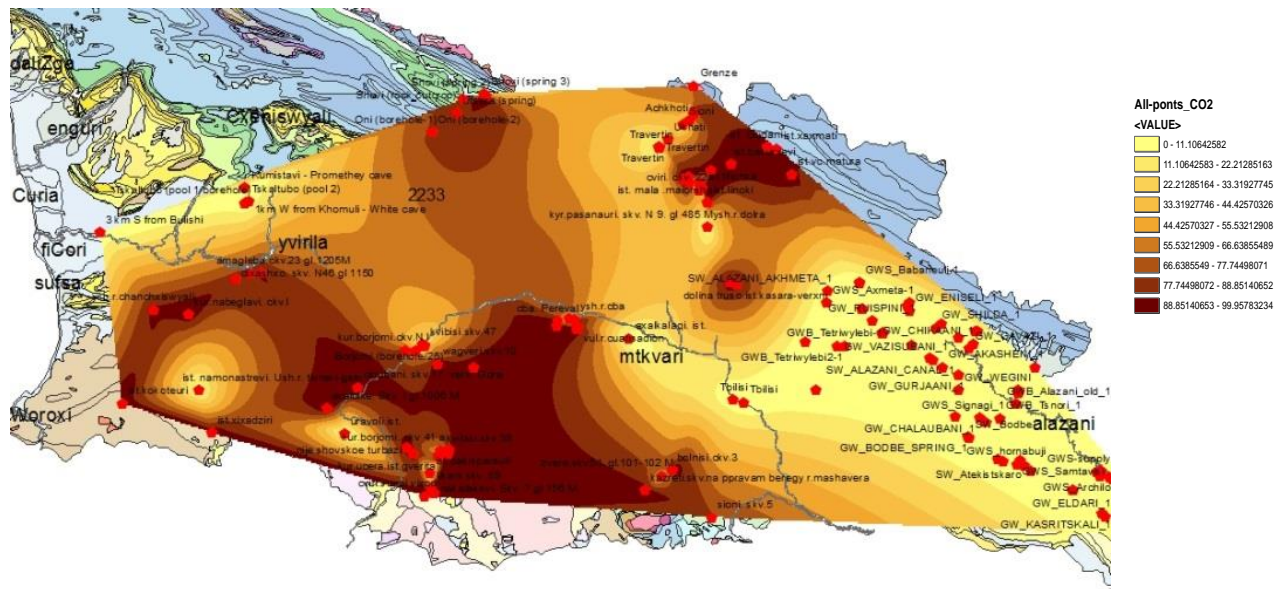


Fig.# 5 Distribution of CO₂ of groundwater in different Geological regions

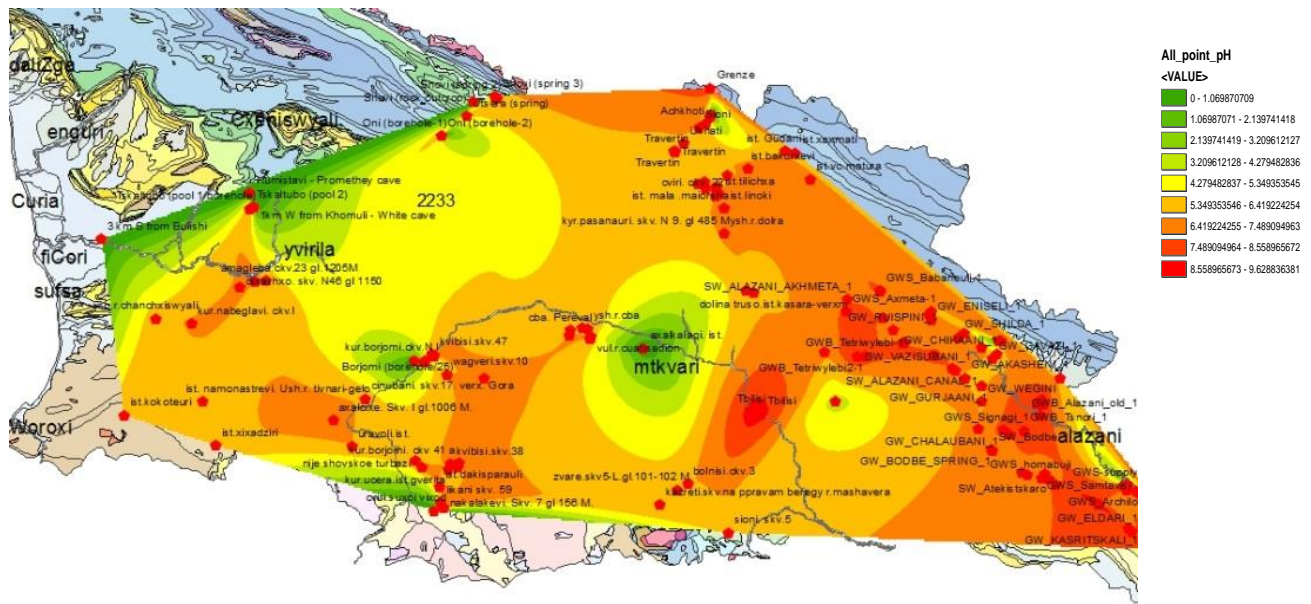


Fig.# 6 Distribution of pH value of groundwater in different Geological regions

2. Discovering of links between rocks, faults and geological structure of Georgia

Natural gases are a very sensitive indicative for geological, especially for geotectonic state. As it was expected in distributing of gas associations the properties of the geological structure of Georgia has been obviously revealed. Researches were done in two zones:

1. the northern zone – containing much carbonic acid gases;
2. The southern zone– with the content of nitrogen and carbonic acid gases.

The northern zone contains two geotectonic elements – the main Caucasian anticline block and the great Caucasian folded ridge without the extreme segments in the east and west [1].

In gas associations of these zones that are connected especially with mineral waters, Carbon dioxide obviously dominates. Investigations do not reveal a clear chemical link between underground waters and carbon dioxide, but the bulk of its exposure is connected with Narzan, the main type of mineral waters on the given territory.

The total content of free CO₂ in the waters of North zone, as it was mentioned above, is 1-2 g/l. So high concentration is related with special groups of underground waters and shows the genetic connections of CO₂ concentration with magmatic-metamorphic processes. So, the It is evident the volcanic origin of CO₂

Carbon dioxide gas exposures in the southern zone are very numerous. Gas factor of Borjomi group as well as Vardzia, Nakalakevi and others often reach 7-10 g/l. Besides, the horizon pressure is quite high (25 atmospheres in a bore hole). Seldom, but dry outlets of carbon dioxide gas are observed anyway. Exposed carbon dioxide amounts to 2 g/l.

All the above mentioned refers to the existence of strong carbon dioxide escalations. Genetic links of carbon dioxide and the young post-magmatic processes cannot be doubtful; besides, the Quaternary lava discovered here refers to the recent volcanic activity.

3. Relation between regional seismicity and gas emission

In order to study of regional seismicity influence on CO₂ emission has been organized the monitoring of free CO₂ emission on the Borehole # 37 in Borjomi. The gas flow meter has been connected to the data logger which is connected data transmitting device. The data (gas discharge, temperature and atmosphere pressure) are logged continuously and can be transferred or checked online at office in Tbilisi. CO₂ emission variation data together with seismic data are analyzed in order to find out their interaction.

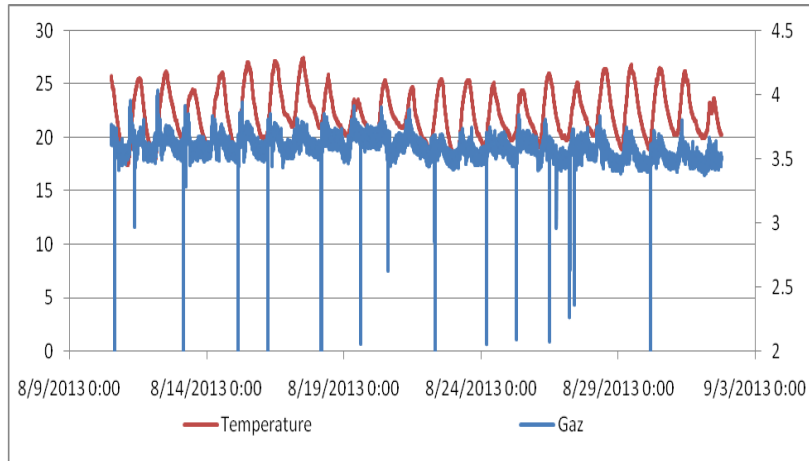


Fig. #7 CO₂ emission and atmosphere temperature variations on the borehole # 37

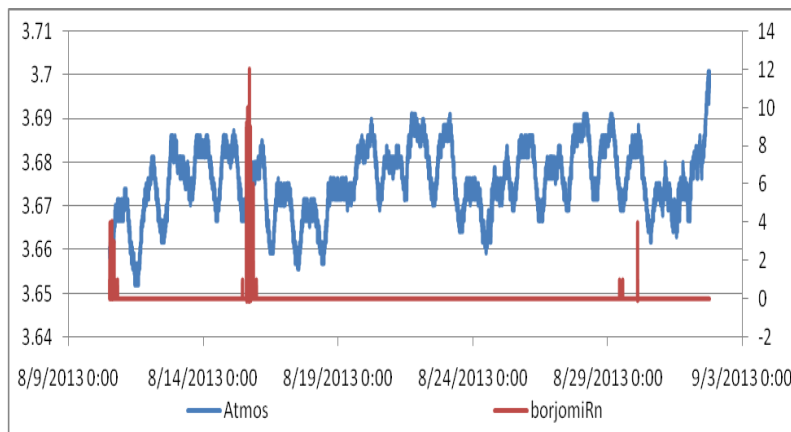


Fig. #8 Radon emission and atmosphere pressure variations on the borehole # 37

As example, we are presenting period of observation August of 2013. During this period was not fixed strong earthquakes and variation was only depending from meteorological factors, such as temperature and atmosphere pressure. Gas discharge is changing between 3.2-3.7 m³/day, but same Rn extraction picks was fixed, which are related with small local earthquakes occurred in this period.

Conclusions

Was study the natural CO₂ distribution on the territory of Georgia and investigated the properties of water samples and of rocks which contain and absorb CO₂ during its emission. Has been organized the monitoring of free CO₂ emission on the Borehole # 37 in Borjomi.

References

[1] Buachidze I. M at all, "Hydrogeology of USSR" Book X, Georgia, "Hedra", Moscow, 1970.

RADON AND THORON LEVELS IN AIR AT SELECTED PLACES IN GEORGIA

N. Kapanadze¹, M. Bezek², J. Vaupotič², G. Melikadze¹

¹ M. Nodia Institute of Geophysics, Ivane Javakhishvili Tbilisi State University, Tbilisi, Georgia

² Jožef Stefan Institute, Ljubljana, Slovenia
melikadze@gmail.com

Abstract

Radon (^{222}Rn) and thoron (^{220}Rn) in air were monitored in a tunnel, and several dwellings, public buildings and spas in Tbilisi, and in the Sataplia and Prometheus caves, using an RTM 1688-2 Radon/Thoron Monitor (SARAD, Germany). While measurement at each point in the cave lasted 20–30 minutes, it did about a day at other places, in order to see the diurnal variations. Highest radon and thoron activity concentrations were found in the Sataplia Cave, being $3094 \pm 340 \text{ Bq m}^{-3}$ and $347 \pm 239 \text{ Bq m}^{-3}$, respectively. Lower values were in the Prometheus Cave ($1472 \pm 236 \text{ Bq m}^{-3}$ and $144 \pm 88 \text{ Bq m}^{-3}$) and at a swimming pool in the Tskaltubo Health Resort ($1110 \pm 115 \text{ Bq m}^{-3}$ and $681 \pm 475 \text{ Bq m}^{-3}$), and were below 200 Bq m^{-3} elsewhere. Thoron/radon activity ratios ranged from 0.03 to 0.17 in the caves and were in the range of 0.09–0.90 at other places, the highest value found in a monk room in the Vardzia-Cave monastery.

Keywords: radon (^{222}Rn), thoron (^{220}Rn), air, dwelling, public building, spa, cave

1. Introduction

For decades, extensive investigations of radon (^{222}Rn , $t_{1/2}=3.82$ days) in various environments worldwide have been performed, while thoron (^{220}Rn , $t_{1/2}=56$ s) was mostly ignored, based on an assumption that at usual ^{232}Th levels in the ground and building material, its activity concentration in indoor air is negligible, because of its short half-life as compared with that of radon. This assumption appeared to be wrong when papers started to report thoron levels, comparable [6] or even higher than those of radon, such as in traditional Japanese houses [3], in Italian buildings made of volcanic material [2], or in cave dwellings in China [9], [11]. It is now well recognised that thoron may contribute significantly to the dose and therefore its inclusion in radon survey is highly recommended [1]; [8]; [10]. Following this recommendation, at several places in Georgia radon and thoron have been simultaneously monitored. In the paper, measurements are described and results presented and commented on.

2. Experimental

For this preliminary study, different places have been selected, from dwellings to public buildings and karts caves. While in a building measurement was carried out in one room, in caves it was done at several points along the tourist path. The survey was performed in summer time (from end of June to middle of July).

A portable RTM 1688-2 Radon/Thoron Monitor (SARAD, Germany) was used. Air is pumped continuously through the chamber at a flow rate of $0.3 \text{ dm}^3 \text{ min}^{-1}$, the positively charged ^{218}Po and ^{216}Po ions, created by ^{222}Rn and ^{220}Rn α -transformations, respectively, are deposited on the detector, and based on α -spectrometry, activity concentrations of ^{222}Rn and ^{220}Rn are obtained. The analysis frequency was ones in 30 minutes. Measurements at various points in the cave lasted 20–30 minutes, while those at other places from one to several days.

3. Results and Discussion

Table 1 shows average values of radon (C_{Rn}) and thoron (C_{Tn}) activity concentrations and C_{Tn}/C_{Rn} ratios, as obtained with continuous measurements in air at selected places. Although measurements were carried out at ten points in the Sataplia Cave and at fourteen points in the Prometheus Cave, only two results are included. Highest radon and thoron levels were observed in the Sataplia Cave, lower in the Prometheus Cave and in the Tskaltubo Health Resort, and were below 200 Bq m^{-3} elsewhere. Thoron/radon activity ratios ranged from 0.03 to 0.17 in the caves and were in the range of 0.09–0.90 at other places, the highest value found in a monk room in the Vardzia-Cave monastery.

Table 1. Average values of radon (C_{Rn}) and thoron (C_{Tn}) activity concentrations and C_{Tn}/C_{Rn} ratios, as obtained with continuous measurements in air at selected places (for the Sataplia Cave and Prometheus Cave, only two results are included)

Place	Date in 2012	C_{Rn} in air Bq m^{-3}	C_{Tn} in air Bq m^{-3}	$C_{Tn}/$ C_{Rn}
Tbilisi, Guest house (1 st floor)	24.6. 11:26 – 25.6. 20:26	12.9 ± 5.4	7.2 ± 5.5	0.56
Tbilisi, Tunnel	26.6. 11:42 – 27.6. 11:42	115 ± 20	28.7 ± 16.5	0.25
Tbilisi, Turkish bath (ground floor)	27.6. 12:55 – 28.6. 16:55	10.0 ± 5.5	6.6 ± 4.6	0.66
Tbilisi, Institute of Geophysics (basement)	29.6. 14:55 – 2.7. 14:55	101 ± 17	13.4 ± 10.1	0.13
Tbilisi, Private house (basement)	2.7. 17:53 – 4.7. 10:53	190 ± 24	17.3 ± 11.8	0.09
Vardzia, Cave monastery (monk room)	7.7. 19:34 – 8.7. 10:34	168 ± 25	151 ± 36	0.90
Vardzia, Cave monastery (cave, at water reservoir)	8.7. 19:33 – 9.7. 8:33	83 ± 24	19.3 ± 12.7	0.23
Tskaltubo, Hotel Imereti (guest room, 1 st floor)	12.7. 00:01 – 12.7. 9:01	34 ± 10	6.3 ± 6.0	0.19
Tskaltubo Health Resort (room with swimming pool)	12.7. 11:39 – 12.7. 12:29	1110 ± 115	681 ± 475	0.08
Satapia Cave (at the end of left branch)	10.7.2012 15:13	1995 ± 279	347 ± 239	0.17
Satapia Cave (at Stony Heart)	10.7.2012 15:43	3094 ± 340	127 ± 88	0.04
Prometheus Cave (Pass)	11.7.2012 16:40	1472 ± 236	55 ± 38	0.04
Prometheus Cave (at Iberia)	11.7.2012 17:20	1297 ± 220	144 ± 88	0.11

Figure 1 presents diurnal variation of radon and thoron activity concentrations in the basement of the Institute of Geophysics (Figure 1a) and in the basement of a private house (Figure 1b). While at the institute both concentrations were highest overnight and lowest at noon, as expected, this pattern was not observed at other places, including also the tunnel. Because the source and behaviour of radon and

thoron are different, a good correlation between radon and thoron levels can hardly be expected, thus resulting in a wide range of C_{Tn}/C_{Rn} . Our range of C_{Tn}/C_{Rn} is narrower than 0.93–2.0 observed in Serbia [12], or 0.05–7 in Hungary [4], [5] or 0.6–6 in Japan [7].

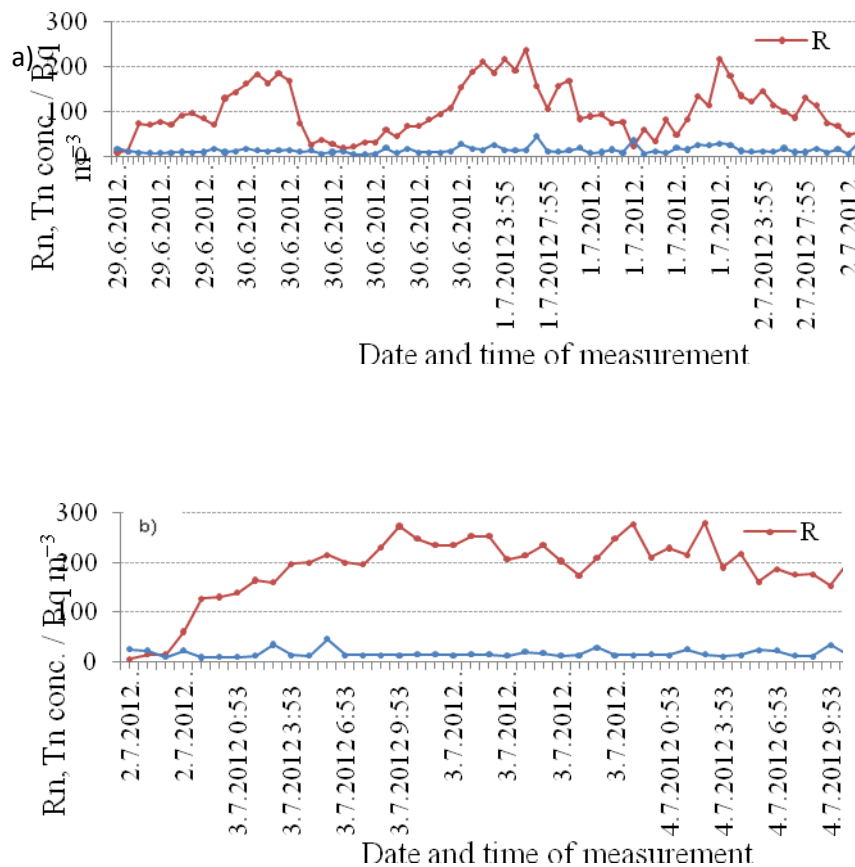


Figure 1. Diurnal variations of radon and thoron activity concentrations in the basement at: a) the Institute of Geophysics and b) in a private house

From average values in Table 1 only, it is not evident that at some places and during some periods of time, thoron level exceeded that of radon. An example is shown in Figure 2 for the monk room in the Vardzia-Cave monastery.

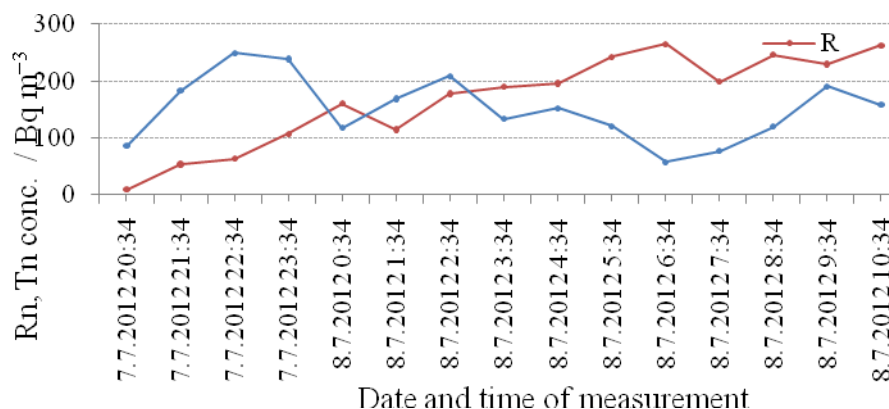


Figure 2. Diurnal variations of radon and thoron activity concentrations in a monk room in Cave monastery

In both caves, radon levels are higher than at other places surveyed, as expected for the caves [9], and are also considerably higher than those of thoron. The tunnel, though underground, is obviously well ventilated and consequently radon levels low (Table 1).

4. Conclusion

According to these preliminary results, Georgia may be considered as a country with moderate thoron levels. Therefore, thoron will not be ignored in our future radon investigations and its contribution to the dose will be considered.

References:

- [1] Akiba S, Tokonami S, Bochicchio F, McLaughlin J, Tommasino L, Harley N. Thoron: its metrology, health effects and implications for radon epidemiology: a summary of roundtable discussions. *Radiat Prot Dosim* 141, 477–481 (2010).
- [2] Bochicchio F, Campos Venuti G, Nuccetelli C, Risica S, Tancredi F. Indoor measurements of ^{220}Rn and ^{222}Rn and their decay products in a Mediterranean climate area. *Environ Int* 22 (Suppl. 1), S633–S639 (1996).
- [3] Doi M, Kobayashi S. Characterization of Japanese wooden house with enhanced radon and thoron concentrations. *Health Phys* 66, 274–282 (1994).
- [4] Kávási N, Németh Cs, Kovács T, Tokonami S, Jobbágy V, Várhegyi A, Gorjánác Z, Vígh T, Somlai J. Radon and thoron parallel measurements in Hungary. *Radiat Prot Dosim* 123, 250–253 (2007).
- [5] Kovács T. Thoron measurements in Hungary. *Radiat Prot Dosim* 141, 328–334 (2010).
- [6] Steinhäussler F, Hofmann W, Lettner H. Thoron exposure of man: a negligible issue? *Radiat Prot Dosim* 56, 127–131 (1994).
- [7] Sugino M, Tokonami S, Zhuo W. Radon and thoron concentrations in offices and dwellings of the Gunma prefecture, Japan. *J Radioanal Nucl Chem* 266, 205–209 (2005).
- [8] Tokonami S, Sun Q, Akiba S, Zhuo W, Furukawa M, Ishikawa T, Hou C, Zhang S, Narazaki Y, Ohji B, Yonehara H, Yamada Y. Radon and thoron exposure for cave residents in Sahnxi and Shaanxi Province. *Radiat Res* 162, 390–396 (2004).
- [9] Tokonami S. Why is ^{220}Rn (thoron) measurement important? *Radiat Prot Dosim* 141, 335–339 (2010).
- Vaupotič J. Radon levels in Karst caves in Slovenia. *Acta Carsol* 39, 503–512 (2010).
- [10] Vaupotič J, Streil T, Žunić Z S, Tokonami S. Diurnal variations of radon and thoron activity concentrations and effective doses in dwellings in Niška Banja, Serbia. *Radiat Prot Dosim* 157, 375–382 (2013).
- [11] Zhang B, Chen B, Gao Y, Wang Y, Cui H, Li Z. Thoron levels in traditional Chinese residential dwellings. *Radiat Environ Biophys* 44, 193–199 (2005).
- [12] Žunić Z S, Čeliković I, Tokonami S, Ishikawa T, Ujčić P, Onischenko A,

USING ENVIRONMENT TRACERS FOR INVESTIGATION OF BLACK SEA POLUSHION

¹G. Melikadze, ¹N. Kapanadze, ¹M. Todadze, ¹Z. Machaidze, ¹A. Chankvetadze, ²Ch Tsabaris, ²E. Androulakaki, ²F. Pappa, ²G. Eleftheriou, ²D. Patiris, ³M. Schubert, ³K. Knoeller, ³R. Stollberg, ³U. Mallast

¹Mikheil Nodia Institute of Geophysics of Ivane Javakhishvili Tbilisi State University
²Hellenic Centre for Marine Research, HCMR (GREECE) - 3
³Helmholtz Centre for Environmental Research – UFZ
melikadze@gmail.com

Abstract

In order to determine the groundwater discharge (SGD) areas into the sea during studies had been implemented and selected the new methodology of using ecological tracers, such as stable isotopes ^{18}O and 2H , radionuclide Rn and Ra and other parameters. On the territory of Kobulety had been defined the groundwater flow direction and the areas of their submarine discharge. Within the identified areas was defined the intensity of eutrofication – the value of nitrate and phosphate content in groundwaters and in the sea. Also, had been studied their distribution on the surface and intensity of outwash into the sea.

1. Introduction

Whereas river and sewage discharge into the sea are bound to distinct locations, thus allowing straightforward quantification of discharge rates and material budgets, the investigation of material transport via submarine groundwater discharge (SGD) is more challenging. Adding to the general difficulties in locating and investigating groundwater sources on the coastal seabed is the spatial and temporal variability that is typical for SGD.

SGD provides a major potential pathway for solute and particulate transport across the aquifer/ocean interface. Nutrients and contaminants carried by the groundwater have a significant potential to cause deterioration of the overall quality of the coastal environment. Related detrimental environmental impacts include contamination and eutrophication of the coastal sea, contamination of seafood, coral reef damage, and harmful algal blooms.

Aqueous tracers provide an appropriate tool for investigating SGD. “Environmental tracers” are defined as natural or anthropogenic substances that are ubiquitously present in the environment originating from defined sources. In contrast to artificially injected tracers they have the general advantage of not contaminating the studied environment by introducing chemicals that may prove persistent into the water body of concern. In addition, due to their ubiquitous occurrence environmental tracers are most suitable for large-scale and/or long-term studies, which are essential for comprehensive SGD investigation.

The scientific aim of the “SGD Black Sea” research project was the application of a multi-tracer approach for SGD research at two exemplary sites on the Black Sea coast. It was the intention to combine several appropriate aqueous tracer methods for SGD localization and quantification and to confirm the achieved findings by a novel approach based on satellite data. The applied satellite-based information allow (i) a water flow accumulation modelling approach based on a terrestrial digital elevation model (DEM) and (ii) an assessment of large scale and long term temperature patterns of the coastal sea. The two suggested study sites have been chosen in order to show strong exposure to anthropogenic pressure on the mountainous eastern coast of the Black Sea (Georgia).

2.1. FIELD WORK ON THE GROUND SURFACE

The coastal zone of study area is located between confluence of river Kintrishi and Kelenderi cape (Sarphi). The coastal zone has a concave form. The coastal zone is built by the sediments transported by rivers. Sediments are distributed by the coastal sea flows –for the south part of study area sea flow changes its directions - from the south to the north.

During the 2012-2013 on the territory of Adjara the field work along the coastline and the surrounding areas had been started. The main research goal was to explore and outline the contaminated areas along the coastline, which represent the potential sources of sea contamination. Along the coastline were sampled every kind of underground water outflow (river, spring, well and borehole). During field work the mobile group was moving by car, which was equipped with special devices (for Ph, conductivity, temperature, free oxygen as well as for Radon and Helium measurements). Besides, the selected points were sampled and the samples were shipped to the laboratory (Tbilisi) for further analyzing.

The sampled points were mapped by GPS and on the next step the data was processed by ArcMap. By the same software was mapped geological, hydrogeological and hydrochemical data. Above mentioned gave us possibility complex studies.

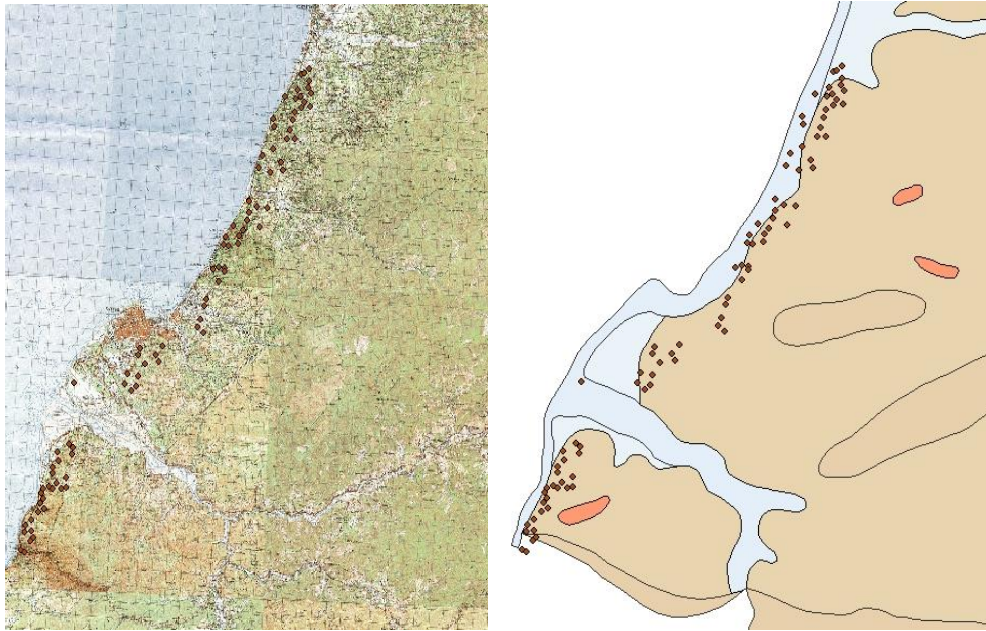


Fig. #1 Dislocation of sampled point on the Topographical and Geological map Had been observed the radon and helium distribution [1], [2] and their background values as well as hydrochemical parameters (Na, Ca, K, Mg, HCO₃, SO₄ and Cl) in underground waters.

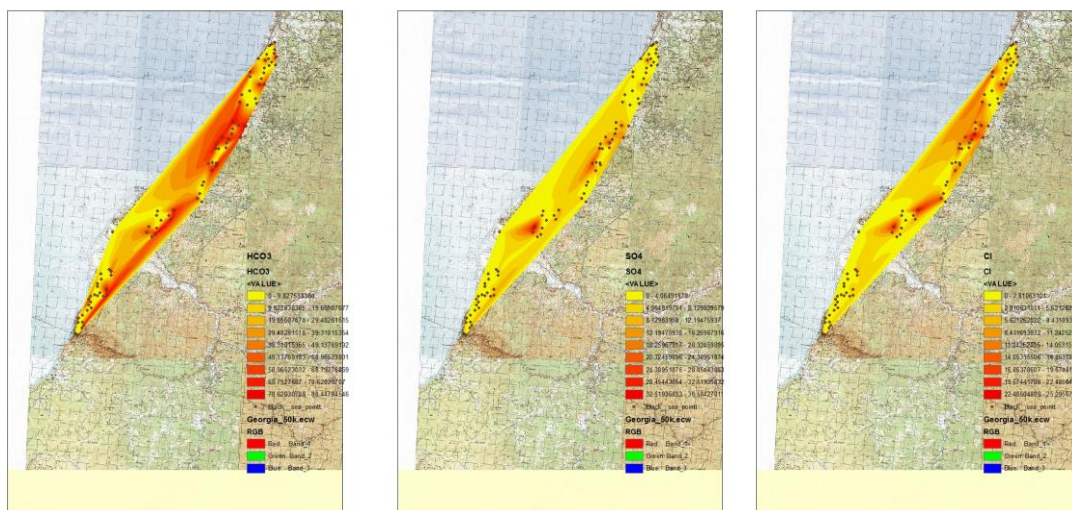


Fig. #2 Distributions of HCO₃, SO₄, Cl in the groundwater along the seaside There are fixed some anomalies located Northern from Batumi and on the territory of Kobuleti

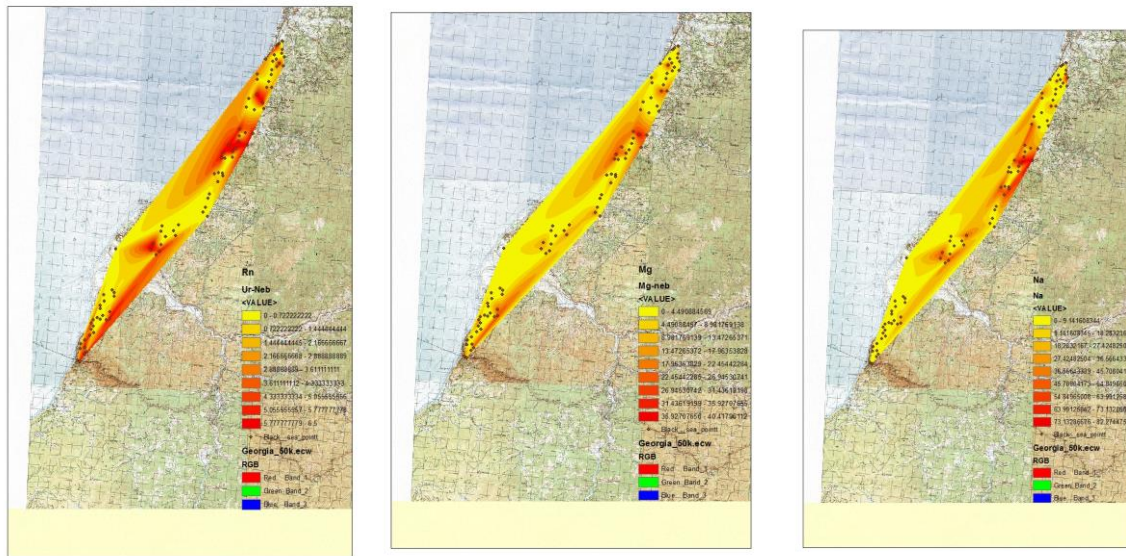


Fig. #3 Distributions of Rn, mineralization and Na in the groundwater along the seaside. During mapping arte fixed anomalies in the distribution of Rn in the groundwater. This zone consisted with anomalies zone of hydrochemical parameters. The observed anomalies may indicate on the polluted areas and represent the object of our interest for further detail studies.

2.2. MARIN SURVEYS

The preparation work for marine expedition had been done together with German colleagues. Namely, the satellite data processing was done by German colleagues. Had been processed and analyzed thermal background data of sea and ground surface.

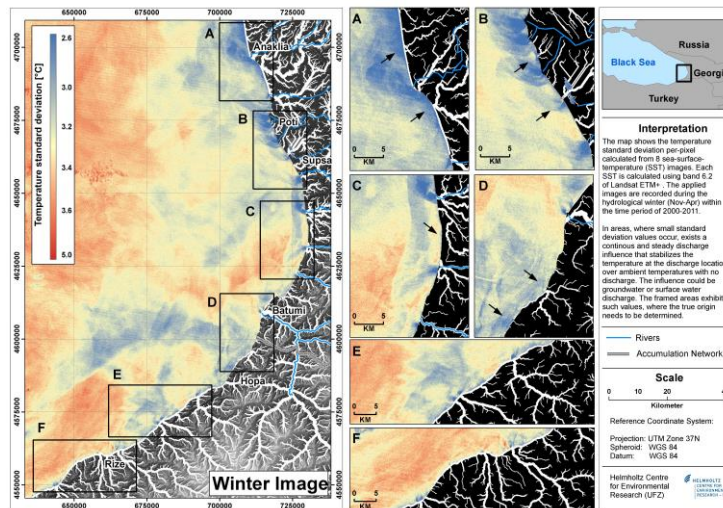


Fig. #4 Satellite data

On the picture shows the cold water discharge areas in the sea at the confluences of rivers as well as at the underground water discharge places. After analyzing two areas had been selected – the one North from Batumi and another one close to Kobuleti, where was expected to reveal the areas of underground waters discharge.

In September 2012 German colleagues arrived in Georgia. During their scientific visit the marine expedition in the Black sea coast was organized. There was done a profile From Batumi till Choloqi by boat and the water physical properties (conductivity, temperature and etc) and Radon concentration were measured continuously.



Fig. #5 Marin investigation



Fig. 6 Illustrates the radon concentrations and the related salinities that were detected along the coastline and on the perpendicular profile. Fig. 7 shows the same information as diagrams.

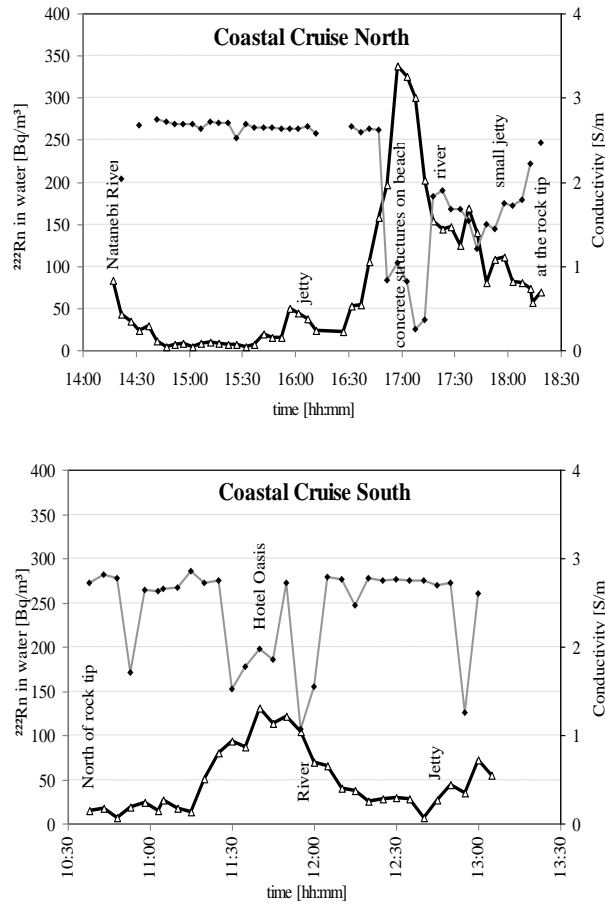


Fig. 7 Radon and salinities data recorded on the north (left) and South (right) profiles during the 1st sampling campaign in September 2012.

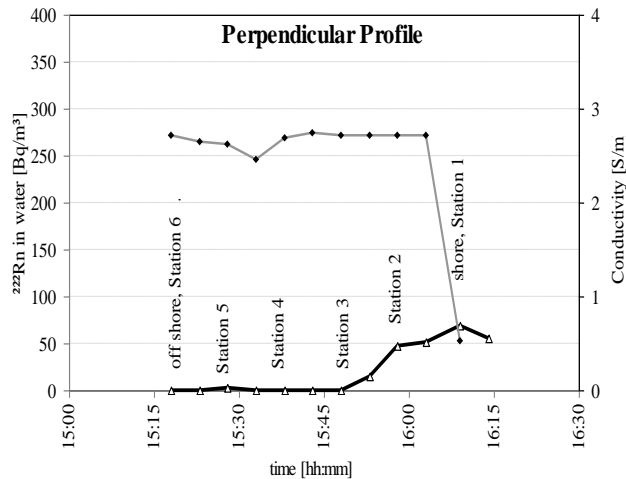


Fig. 8 Radon and salinity recorded during along the perpendicular profile in September 2012. As an additional parameter the pH of the seawater was recorded. As it becomes obvious in Fig. 8A the pH showed a distinct peak at the same location where elevated radon concentrations occur, indicating strong SGD. The data displayed in Fig. 8B, illustrating the findings along the southern part of the coastal survey, do also show a negative correlation between radon and pH, which is however not as distinct as the observation displayed in Fig. 8A.

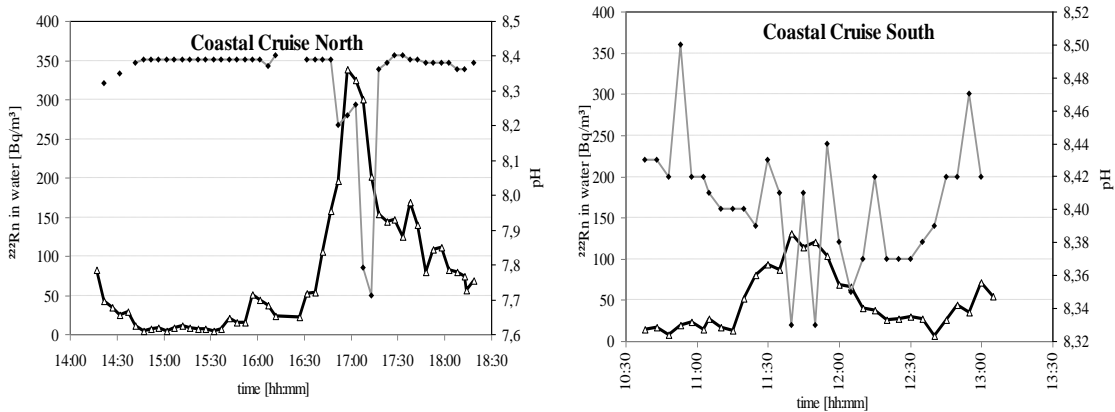


Fig. 9 Radon and pH data recorded during along the north (left) and South (right) part of the coastal survey in September 2012.

Along the perpendicular profiles also had been done sampling of stable isotopes – ^{18}O and ^2H in order to use them as additional tracers. The results showed that mixing of underground water with sea water occurs about 300 meters from the shore and the contribution of underground water is about 5%. By The joint marine and land investigations showed that found anomalous areas can be identified as continuation of each other.

In order to determine the intensity of eutrophication (nitrate and phosphate pollution) had been measured the nitrate and phosphate content in groundwater and sea water in areas of revealed groundwater submarine discharge. Their values are less than the allowable standard for nitrates and range from 0.2 - 3 mg / l and for phosphates 0.18 -1 mg / l.

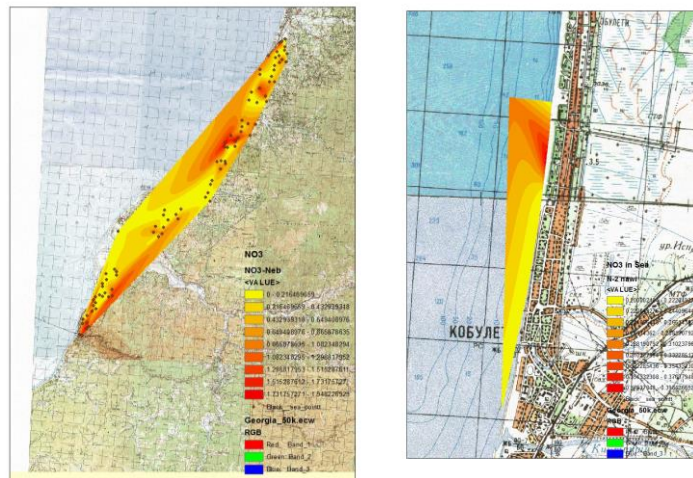


Fig. #10 Distributions of NO_3 in the groundwater (left) and sea water (right) along the seaside

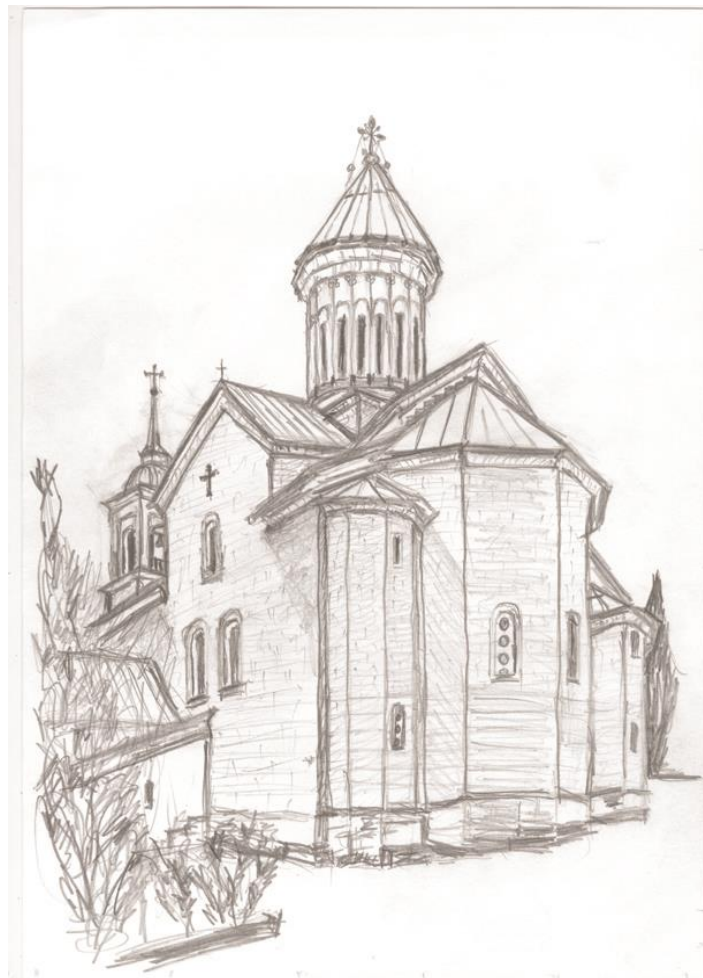
But, the mentioned tendency will decrease in time if the arable lands are not enriched by chemicals in future.

3. CONCLUSIONS

On the territory of Kobulety had been defined the groundwater flow direction and the areas of their submarine discharge; had been defined the surface character of contamination. Within the identified areas was defined the intensity of eutrofication – the value of nitrate and phosphate content in groundwater and in the sea. Also, had been studied their distribution on the surface and intensity of outwash into the sea.

4. REFERENCES

- [1] Janja Vaupotič, Mateja Bezek, Nino Kapanadze, George Melikadze, Teona Makharadze, RADON AND THORON MEASUREMENTS IN WEST GEORGIA, Journal of the Georgian Geophysical Society 2012, in print
- [2] George I. Melikadze, Avtandil G. Amiranashvili, Kahha G. Gvinianidze, David G. Tsereteli, Mariam Sh. Todadze “Correlation Between Radon Distribution and prevalence of lung Cancer in West Georgia”, “Environment and Recourses”, Association of Academics of Science in Asia Workshop, 25-27 September 2009, Izmir, Turkey, pp 176-180



Сионский кафедральный собор, Тбилиси Бойко Вачев'2013
Sioni Cathedral, Tbilisi Boyko Vachev'2013

IDENTIFICATION OF TYPES OF EXOGENIC GEOLOGICAL HAZARDS ALONG BULGARIAN BLACK SEA COAST

Nikolai Dobrev¹, Plamen Ivanov¹, Konstantin Kostov¹, Orlin Dimitrov², Miroslav Krastanov¹,
Valentin Nikolov¹, Boyko Berov¹

¹ Geological Institute, Bulgarian Academy of Sciences, Sofia, Bulgaria

² Institute of Oceanology, Bulgarian Academy of Sciences, Varna, Bulgaria, ndd@geology.bas.bg

Abstract:

This paper regards the exogenic geological hazards affecting the Bulgarian Black sea coastline. They are presented by landslides, rockfalls, abrasion and karst. The most widespread are the landslides which affect almost whole shoreline but most significant of them are located North from Varna. The essential factors of landslide activity are abrasion, rainfalls and earthquakes. However during the last years the technogenic impact increases seriously.

1. Introduction

The contact zone between the sea and the land is place of development of various hazardous geological processes. These processes periodically create damages on the infrastructure, properties and economic activities, and sometimes they cause losses of lives. The variable factors include geology, geomorphology, tectonics and climatic peculiarities create conditions for appearance of various by type and range exogenic geological hazards. This requires need to assess the distribution and variation of geological hazards along the coast. Diversity of processes is imposed mainly by the differentiated tectonic movements and geomorphologic features of the terrain where they originate. A special attention is necessary to be paid to destabilizing factors that are characteristic for the studied area.

2. Geomorphology of the West Black Sea coastal zone

The Bulgarian section of the western shore of the Black Sea, extends from Sivriburun Cape (state border with Romania) in the north to the mouth of Rezovska River at the border with Turkey in the south. In a morphological aspect is distinguished by great diversity. The length of the coastline is 378 kilometers (200 kilometers along the arc of the earth spheroid), of which 200 km are beach. It has a dismemberment coefficient of 1.9. The costal part of the Danubian Plain embraces 37.9% of Bulgarian Black Sea coast, the coast that washes Balkan Mountains take up 12.7%.

The varied relief of Bulgarian Black Sea coast is closely related to the great diversity and complexity of the geological and tectonic structure. Three main geological structures are distinctly outlined, separated each other by faults. They are the following: the Moesian plate, the Balkanides and Srednogorie zone.

Tectonic and lithological features of the coast line are successfully traced from north to south, as well as the part they play in the formation of the resent relief.

The history of development of the relief of the Bulgarian Black Sea coast and its shelf is most closely related with the Neogene and Quaternary evolution of the Black Sea Basin, which is generally accepted, differentiated relatively independently in the second part of Pontian [1].

3. Landslides

Bulgarian Black Sea coast is characterised by complex geological and geomorphological structures. Larger coastal landslides cover higher and steeper slopes of Balchik and Varna areas. Shallow landslides affect the lower steep sea-side banks, built by soft (“washable”) deposits. Black Sea coast is composed of various lithological and engineering geological types of rocks and soils. Sedimentary rocks are divided into complex inhomogeneous engineering complexes.

Until present, landslide phenomena along the Black Sea have been subject to examination and thorough analysis of many scientists. The last detailed and summary information about landslide

processes in Bulgaria and in particular the Black Sea coast have been published in the Map of Geological Hazards in Bulgaria, in scale 1: 500000 [2], Map of Landslides in Bulgaria, in scale 1: 500000 (1999, 2006) and partly in some maps of landslides in administrative districts, in scale 1: 100000 (2000-2002). In the Cadastre of landslides in Bulgaria, 105 landslides were described covering the coastal area of 3 districts: Bourgas, Varna and Dobrich. At present, this Cadastre is updated and therefore is expected to be added data of new landslides. The distribution of landslides and other hazards along the coast is shown in Fig. 1.

Important relationships in the distribution, dynamics and mechanism of different types of landslides have been identified. Influence of a number of destabilizing factors (erosion, abrasion, earthquakes, rainfalls, fluctuations of groundwater levels, technogenic activity, etc.) on landslide activity is estimated. During the assessment of geological hazards in Bulgaria, the landslides are divided into 3 groups as follows: 1) Shallow landslides, 2) Deep-seated landslides and conditionally stable, 3) Deep-seated landslides with periodic (re)activation of some parts of them.

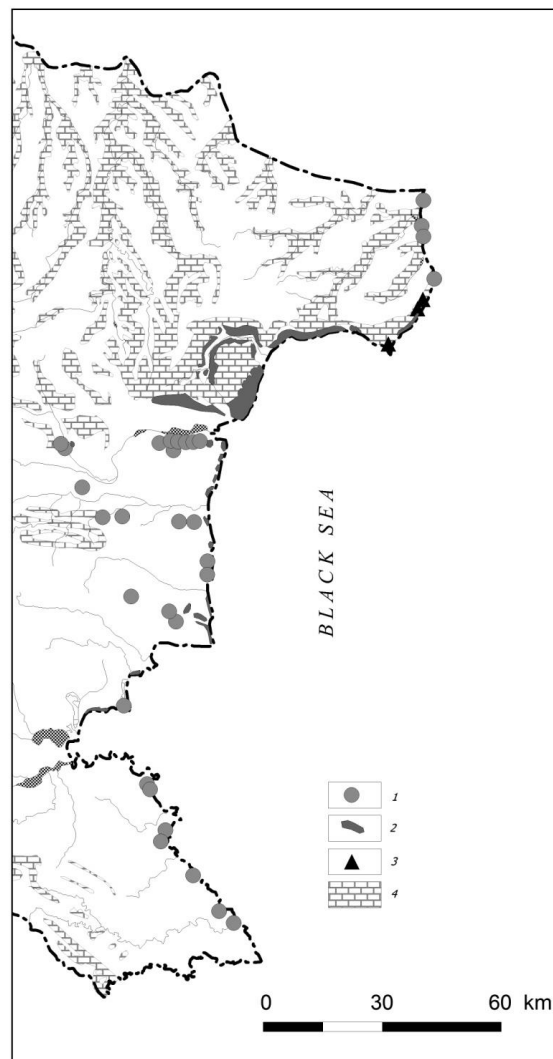


Figure 1 Coastal processes distribution map: 1) landslides with volume $V \leq 1 \text{ mln m}^3$; 2) landslides with volume $V > 1 \text{ mln m}^3$; 3) rockfalls and rocktopplings; 4) karstic areas

Landslides from the first group are the most numerous and widely distributed. They predominate in the southern Bulgarian coast. They have a depth range from 2 to 6-8 m and covering areas of $2-3 \times 10^3 \text{ m}^2$ and more. Their activity is highly influenced by precipitation, erosion and man-made impact.

The landslides of other two groups are deeper (deep-seated). The landslides of the second type have a depth range of 30-40 m (areas over 10^3 m^2). Their morphology is of a typical landslide, with

steps, lower and marshy areas. They are observed in northern Bulgarian Black Sea coast. The danger of them is more potential or dormant according to [3], but under extreme conditions such landslides can be reactivated. Such factors are human impact, earthquakes, storms, intense abrasion and others [4, 5, 6, 7].

The most dangerous landslides are in the third group. They are large (deep-seated), complex type, more than 50 m deep, and their stability is in the limit state of equilibrium. Moreover, it is enough small impact from factors for the triggering the landslide movements, such as abrasion, intense rainfalls, earthquakes and technogenic one to activate the movements along the slope. On the one hand, there is a slow movement in the most deeply situated slip surface, and by other hand, the recent landslides trigger in the upper parts of the existing old deep landslides. Contemporary landslide activation reaching up to the primary (deepest) slip surface (or plastic zone) is rarely occurring. Landslides in the areas of Zlatni Pyasatsi, Albena, and Balchik create such problems.

In most of the landslides in the third group, the slip surface enters with the tens and even hundreds of meters into the sea. Such landslides are these at Zlatni Pyasatsi, Balchik – Kavarna area, and Rusalka – Kamen Bryag area (Fig. 2).

From the Bulgarian-Romanian border to Shabla Cape, the coast is built by Sarmatian shellfish limestone covering with loess clays. In the south to Cape Kaliakra, the thickness of the limestone gradually rises. There are not any landslides around the cape and west of there. They appear again in the strip from Kavarna to Albena (complex type of ancient and recent landslides).

From the Valley of Batova River to Varna, the Sarmatian formations rise even higher (sand covered with limestone, which are situated below the clayey marls). This makes a specific geological structure of the landslides in this area.

Southward of Galata Cape to Kamchia River, the shore is composed mainly of loose soils, with clayey-marly layers, which gradually sink to the south. Here the landslide processes are strongly influenced by abrasion. In Bourgas Depression, the largest landslide affects the coast near Sarafovo Village.

South of Burgas, the Black Sea coast is built mainly of magmatic rocks and the conditions for development of large landslides are strongly limited. Single shallow landslides affect the shoreline up to Bulgarian-Turkish border.



Figure 2 Taukliman Landslide in 1992, lateral spread type (oto N. Dobrev)

4. Rock deformations

Rock deformations along the coast have developed in vertical or very steep rocky slopes on the cliff. Their size is determined by the slope dip and height and joint setting of the massif. The loss of stability on the rocky slopes along the Black Sea can be caused mainly by three factors: abrasion, weathering and earthquakes. Rock deformation can be divided to rockfalls and rocktopples.

The first type of deformation is more common - mainly in places where there is a vertical rock scarp (cliff). The main factor for classical rockfalls is the abrasion. They are found in southern Bulgarian Black Sea coast (around Sozopol Town), and the northernmost part - at Kavarna shoreline,

Kaliakra Cape and to northward. Rockfalls at Cape Kaliakra are characteristic with the largest volumes (Fig. 3).

Rocktopples are less frequently distributed. There are more distributed at plateau's edges where, however, they are in combination with slow landslide movements. They are found mainly in Frangya and Dobrudja plateaux.

Rockfall/rocktopple problem along the Black Sea coast (and not only there) is insufficiently studied yet though its substantial share of geological hazards.



Figure 3 Rockfall at Yailata locality, 20 km north from Kaliakra Cape, in 1976 (photo E. Avramova)

5. Collapse in karstic voids

The karst is developed in Sarmathian limestones in the Northwestern part of the Bulgarian Black Sea coast. According to the scheme of White [8] and from geomorphologic point of view, the karst landforms in the studied area have some features of naked, pavement karst (Fig. 1).

The epikarst landforms are presented mainly by karren. They form classical karren fields, known as “kayryak” according to the local toponimy. The karren fields are widespread along the coast between Shabla and Kaliakra capes, with width between 1.6 and 5 km. Small dolines are developed south of Kavarna [1]. Typical for the area are also the deep blind valleys (Shabla valley, Bolata valley, etc.).

Till now are explored and surveyed 184 caves in the studied area. They are developed in the coastal area between Shabla Cape to the North and Kavarna to the South, in the vicinities of the villages Tyulenovo, Kamen Bryag, Sveti Nicola, Bulgarevo and the town of Kavarna. According to the regionalization of the Bulgarian caves, the described area is a part of the Eastern Dobrudja Cave area (№ 105). The longest cave is Karankut Maara near the village of Sveti Nicola (Table 1).

Table 1: The longest caves in the studied area

Cave	Location	Length (m)
Karankut Maara Cave	Sv. Nicola	236
Tyulenova Cave	Tyulenovo	107
Labirinta Cave	Sv. Nicola	104
Svodestata Nisha Cave	Kavarna	93
Gorchova Maara Cave	Kavarna	87

Typical for the area are the spectacular sea caves in the rock cliffs between the capes of Shabla and Kaliakra. The longest among them is Tyulenova Cave, located 900 m north of the village of Tyulenovo. The 107 m long Tyulenova Cave is one of the last habitats of the monk seal (*Monachus monachus*) – the most endangered sea mammal in Europe.

A lot of the karst caves near the villages Tyulenovo and Kamen Bryag are used as rock monasteries and churches in the Medieval time.

The natural hazards in karst terrains are connected mainly with rock falls and breakdowns. After the Vrancea earthquake of March 4th 1977 are recognized breakdowns of the roofs of two caves in the archaeological reserve “Yailata”, south of the village of Kamen Bryag [9]. The widening of open fractures close to the one of the caves is also established.

During a visit after the Kamen Bryag earthquake of 05.08.2009 ($M_s = 5.0$), small breakdowns are observed at the entrance of the St. St. Constantin and Elena Cave near Kamen Bryag (Fig. 4).

6. Abrasion

Two morphological systems are divided during the engineering geological studies of the coastal zone: abrasional-erosional and abrasional-accumulative.

To abrasional-erosional systems are attached the following processes: mechanical abrasion, termoabrasion, chemical abrasion, erosion by bottom of currents, landslides, rockfalls, and the occurrence of turbid flows. These are a group of processes related to the gravitational movement of rock masses with a result of formation of "negative" forms of relief. Very devastating impact of the pneumatic effect "of instant compression decompression of air in the cracks in (strongly cemented) sediment types in crystalline rocks occur. Cavitation was observed under conditions of high speeds of water masses of the boundary layer of such rock types [10].

Engineering geological conditions of the abrasion-erosion coasts are characterized by data observed in these areas. This can also be done through the section profile with bottom topography and also with data on tidal currents. The latter perform major geologic activity. It is expressed in erosion-dilution and erosion-accumulation - participation in the movement of sediments in the coastal zone.



Figure 4 Breakdown at the entrance of St. St. Constantin and Elena Rock Church after the Kamen Bryag earthquake in 2009 (photo K. Kostov)

The wind is one of the most significant factor of wave abrasion. The overall repeatability of the winds causing meridional transport of water masses is along the coast (NW, N, NE), up more than 63% of the repetition of winds moving (spirit) from the sea to the coast and causing storm. Case of still air over the shelf zone does not exceed 25-30% of all wind situations.

Strong storm with wave height 5 - 7 meters in the deep areas and 3 - 4 m in shallow areas of the Bulgarian shelf are possible once in 100 years. Storm in height from 4.5 to 5.5 m in the deep part and 3.0 to 3.5 m in coastal area are possible once in 50 years. Wave height 3-4 meters in the deep part and 2 to 2.5 m in shallow water portion is recorded once in 10 years. The intensity of emotions varies in seasons. Most is the intensity in autumn and winter and lowest during May and June [11].

Abrasion-accumulative morphosystem is characterized mainly processes: accumulation and movement of sediments, underwater landslides and rockfalling, movement of suspension processes occurring under the influence of exogenous factors, and others.

Lateral part of the marine coastal zone is characterized by exogenic processes: rockfalls, screes, landslides, abrasion, accumulation of sediments and the formation of beaches, erosion processes associated with estuaries, karst, suffosion, loess collapse, eolic processes weathering, human activities [12, 13, 14].

The previous research on the Bulgarian Black Sea coast showed that abrasion processes prevail over accumulation [1, 12]. Shores exposed to impact abrasion than 70% of the length of the coastline. These data require a detailed study of coastal profile for its resistance against the effects of wave and other factors. The dominant influence of wave abrasion (to chemical and biogenic) for the Bulgarian Black Sea coast is established.

Formation of cliffs, niches, caves, bridges abrasion, affecting the stability of coastal slopes etc. take important part in various occurrences of abrasional processes. Landslides and rockfalls at north of Capes Kaliakra and Shabla, between Kavarna and Batova River at the mouth of Provadia River, south of the mouth of the river Karaagach etc. are result of abrasion. Abrasion creates in a shallow terrace with a width greater than 150 m, in places depth of 2-3 m below recent sea level, protecting the coast from the bottom and more intensive wave destruction.

Vegetation (dense seaweed), which develops in these favorable conditions on the bottom and near the coast, with its root system erodes the bedrock [15]. This creates conditions for development of biogenic-type abrasion, such as in Byala, south of Cape Chernia Nos, and others.

During the storm and the breaking of waves on the shore, in the various joints of the cliff burst pressure spray seawater. If this specific wave action is geared towards carbonate sediments, chemical processes of dissolution of carbonates develop. Moreover, in the cracked and karst limestone deposits hollows, crevices, the remains of dissolution are formed. Chemical type of abrasion occurs in this way. Its occurrence is on limestone, marl and some varieties of limy sediments. The event is north of Kaliakra Cape, north and south of Belia Nos Cape in some coastal areas on the southern coast. Biogenic and chemical type abrasion grows together with mechanical abrasion. They have a minor role in the formation of the abrasion cliff in the Black Sea.

Intensive influence of abrasion in Galata-Kamchia area is established, which is dominated by the cape's sections built of susceptible to abrasion weathered sandstone and carbonate sediments. There are landslides with speeds of up to 9 m/yr. Increasing of exogenic processes (including abrasion in other areas and coastal areas, for example, Nesebar, Pomorie, camping Europe etc..) is caused by anthropogenic factors.

Acknowledgements:

The present study has been performed thanking to financial support by the Romania-Bulgaria 2007-2013 Cross border cooperation project MIS ETC 641 – MARINEGEOHAZARD and during the 7FP project BlackSeaHazNet.

References:

- [1] Popov, V., K. Mishev, (1974) Geomorphology of the Bulgarian Black Sea coast and shelf. BAS, Sofia, 268 p (In Bulgarian).
- [2] Iliev-Broutchev, I., ed., et al. (1994) Map of the Geological Hazards in Bulgaria. Scale 1:500000 and Explanatory Text. MTS, Troyan and Publ. House of Bulg. Acad. Sci., Sofia (in Bulg., English Summary).

- [3] UNESCO Working Party on World Landslide Inventory, (1993) A suggested method for describing the activity of a landslide, Bull. IAEG, No.47, Paris, 53-56.
- [4] Evstatiev, D., V. Rizzo (1984) Sull' origine ed evoluzione delle frane nella zonna di Balchik, sul Mar Nero (Bulgaria). Geol. appl. e idrogeol. Bari, Italy, Vol. XIX. 289-305.
- [5] Frangov, G., R. Varbanov, J. Yordanova, M. Stakev (1997) Contemporary activity of the landslides along the Varna and Balchik coast line. Coll.: Coastal fortification along the Bulgarian Black Sea. Bulgarian Academy of Sciences. pp. 20-29. (in Bulgarian).
- [6] Koleva-Rekalova, E., N.Dobrev, P.Ivanov (1996) Earthflows in the Baltchik landslide area, North-eastern Bulgaria. In: Proceedings of the 7th Int. Symp. Landslides, Trondheim, Norway, pp. 473-478.
- [7] Varbanov, R., G. Frangov, D. Evstatiev (1997) New destructive landslides northward from the town of Varna. Journal Minno Delo i Geologia. 5, 6-12 (in Bulgarian).
- [8] White, W., (1988) Geomorphology and Hydrology of Karst Terrains. Oxford University Press, New York, 464 p.
- [9] Avramova, E., S. Stanchev, (1983) The earthquake's influence on the Taukliman landslide complex. In: Vrancea Earthquake in 1977. Its After-Effects in the People's Republic of Bulgaria, BAS, Sofia, 74-84 (In Bulgarian).
- [10] Marinski, G. (1981). An experimental study of the impact of air during shock of liquid column on a flat rigid barrier. S., Techn. misal, 184, 81-86 (in Bulgarian).
- [11] Mihova E. (1990) The role of physico-geographic factors and conditions for formation of recent relief of Bulgarian Black Sea coast. Geological evolution of western part of Black sea basin during Neogene-Quaternary. BAS, Sofia, 431-465 (in Russian).
- [12] Kamenov B, et al. (1970) Study on landslide phenomena along Black sea coast, Report, Geological Institute, BAS, 501 p.
- [13] Shuiskij, J., G. Simeonova. (1976) About the influence of geological structures along sea-side banks on the abrasion processes. Comptes rendus Ac. Bulg. Des sciences, 29, 241-243 (in Russian).
- [14] Simeonova, G. (1989) Formation of coastal zone of water reservoirs at various engineering geological conditions in Bulgaria. PhD Thesis, GI-BAS, Sofia, 234 p. (in Bulgarian).
- [15] Karadjova-Petrova, V.(1975) Quantitative distribution of Cystoseira barbata (Good et Wood) in Bulgarian Black Sea coast. In: Bull . Institute for Fishery Resources, Varna, 14, 18-101 (in Bulgarian).



Возрожденная из пепла, Кафедральная церковь, Одесса Бойко Вачев'2012
The reborn from the ashes, Cathedral Church, Odessa Boyko Vachev'2012

GLOBAL WARMING OR CLIMATE VARIABILITY – THE ROLE OF GEOMAGNETIC FIELD AND LOWER STRATOSPHERIC OZONE

N.A. Kilifarska¹, V.G. Bakhmutov², G. V. Melnyk²

¹National Institute of Geophysics, Geodesy and Geography, Bulgarian Acad. of Sciences, Acad.

G.Bonchev str., bl.3, Sofia 1113, Bulgaria, nkilifarska@geophys.bas.bg

²Institute of Geophysics, National Academy of Sciences of the Ukraine, Palladin av.32, 03680 Kiev, Ukraine, bakhm@igph.kiev.ua

Abstract:

This paper offers a new explanation of the observed rise of surface air temperature until the end of the 20th century and its stabilisation after that. The temporal, as well as the diverse spatial distribution of climate change, we attribute to corresponding variations of helio- and geomagnetic fields. The mechanism of such an influence consists of modulation the intensity, and depth of penetration into the Earth's atmosphere, of highly energetic particles of galactic and solar origin. Releasing their energy at different altitudes, these particles activate ion-molecular reactions of different types, which impact the ozone balance near the stratosphere. The latter controls the temperature and humidity near the tropopause – through an influence on the atmospheric static stability. The highest impact of the upper tropospheric water vapour in the Earth's radiation budget mediates the ozone influence down to the surface, through strengthening or weakening of the greenhouse effect. Thus O₃ abundance near the tropopause reduces humidity and cools the Earth's surface air temperature, while ozone depletion – cools it.

Key words: climate, geomagnetic field, energetic particles, ozone

1. About factors influencing Earth's climate

The question about the dominant factors determining periodical warming and cooling of climate is still one of the hotly debated problems. After several decades of consensus that global warming of the Earth is a result from dramatically increased emissions of CO₂ and other greenhouse gases, the suddenly interrupted raise in the surface air temperature (since the beginning of the millennium) questioned the real driver(s) of climate change with even greater sharpness.

The variations of solar irradiance reaching the Earth's surface have quite small amplitude (~0.1-0.2% during the last 2000 years), which could hardly explain the historically documented abrupt changes in the Earth's climate. Another potential explanation for the great amplitude of climate variability could be the solar UV radiation, the amplitude of which in the middle atmosphere reaches ~10-20%. Up to now, however, there is not a reasonable mechanism capable of explaining the transport of solar energy deposited in the upper and middle atmosphere downward to the surface.

The possibility for dramatic changes in climate, due to variations in orbital parameters of the Earth, seems also unsupported by the recent investigations [1]. The results of Vieira et al. [1] show that the maximum modulation of total solar irradiance for the last 600000 years, due to changes in orbital inclination, is $\sim 3 \times 10^{-3} \text{ W.m}^{-2}$. Compared to the annual variations, determined by the orbital eccentricity ($\sim 1.5 \text{ W.m}^{-2}$), the amplitude of the variability related to the Earth's orbital inclination is much smaller and could hardly be responsible for the documented changes in paleoclimate.

Volcanic activity is another potential factor influencing Earth's climate. However, due to relatively low frequency of recent volcanic eruptions, the duration of their effect on the contemporary surface temperature is limited to $\sim 2\div 3$ years [2].

The regional diversity of climate variability (recent and historical) could hardly be explained in the framework of any homogeneous climate forcing. For example, the simultaneous warming of the west and cooling of the east Antarctica – observed for more than a century and a half [3], or the warmer (than the average temperature of the NH) Greenland – during the Little Ice Age [4] – put questions bagging for a proper answers.

There is another idea – for possible connection between geomagnetic field and Earth's climate (raised in the middle of 20th century) – an interest toward which was regained recently [5-9]. The

main problem of this hypothesis, however, is the absence of mechanism able to explain the way of geomagnetic influence on climate. The single assumption, which is based on the galactic cosmic ray influence on the cloud microphysical processes and cloud formation, seems not supported by the recent measurements [10-14].

In this paper we focus our analysis on the possible relation between geomagnetic field and climate. In doing this, we firstly examine the existence and strength of such a relation over the globe, and secondly offer a causal chain of links, initiated by geomagnetic field, leading to corresponding changes in the surface air temperature.

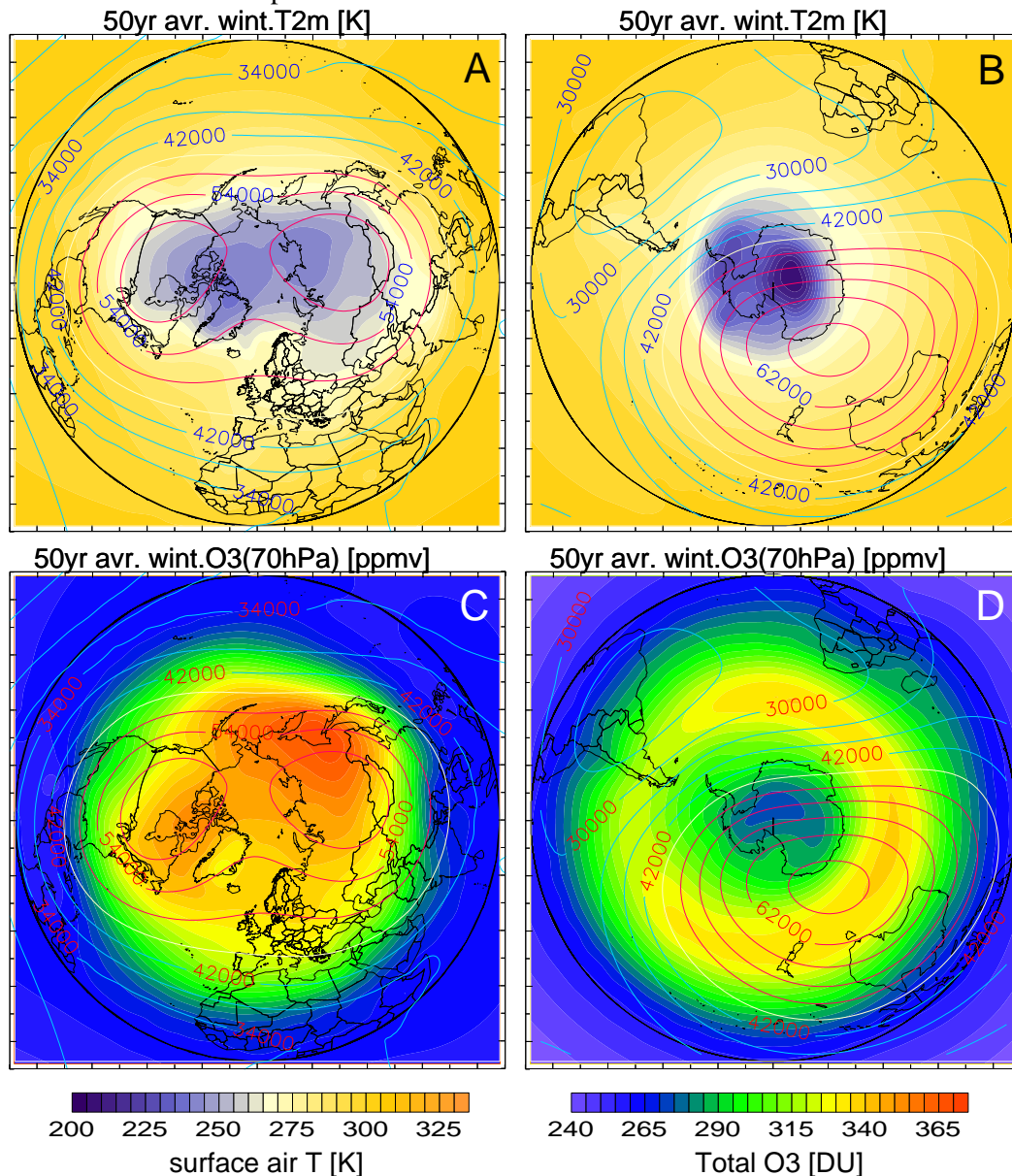


Fig.1 ERA 40&Interim 55-year climatology of surface air T and total ozone density (coloured shading). Overdrawn are contours of geomagnetic field intensity. Note the fairly good correspondence between spatial distributions of the ozone maximum and geomagnetic field intensity (panels C and D).

2. Spatial distribution of geomagnetic field, surface air temperature and total ozone density

The previously reported similarities in spatial distribution of geomagnetic field and surface air temperature [6, 14] is re-examined using the merged data from ERA 40 and ERA Interim re-analyses for the period 1957-2012. Fig. 1 presents comparison of surface air T and total O₃ climatology (color shading) with geomagnetic field intensity (red and blue curves) in both hemispheres. Note the hemispherical asymmetry in the three examined fields – i.e., bifocal structures in the Northern Hemisphere NH (Fig.1, left column) and circular symmetry in the Southern Hemisphere SH (Fig.1,

right column). Unlike the NH, there is a space shift between surface T minimum and the focus of geomagnetic field maximum intensity in the SH. This raises the question: If the geomagnetic field determines the spatial distribution of surface air temperature, why the rule is violated in the SH?

The maximum ozone density, however, corresponds fairly well to the maximal geomagnetic field intensity in both hemispheres – sifted slightly eastward in the NH and elongated around the pole in the SH (Fig.1, panels C and D). In order to estimate whether the spatial similarity between geomagnetic field and ozone is a coincidence, or is a consequence of some physical relation between them, we have analyzed the correlation coefficients of geomagnetic field with GCR and total ozone density. Results are described in the following section.

3. Relations between geomagnetic field intensity, GCR and ozone

The importance of GCR impact in the lower stratospheric O₃ balance is demonstrated in several of our papers [e.g. 15, 16], where the mechanism of this relation is described. On the other hand, the intensity of precipitating energetic particles in the Earth's atmosphere depends not only on the heliomagnetic field strength, but also on the modulation effect of geomagnetic field. Consequently, the connectivity between geomagnetic field and total O₃ density becomes at least quantitatively understandable.

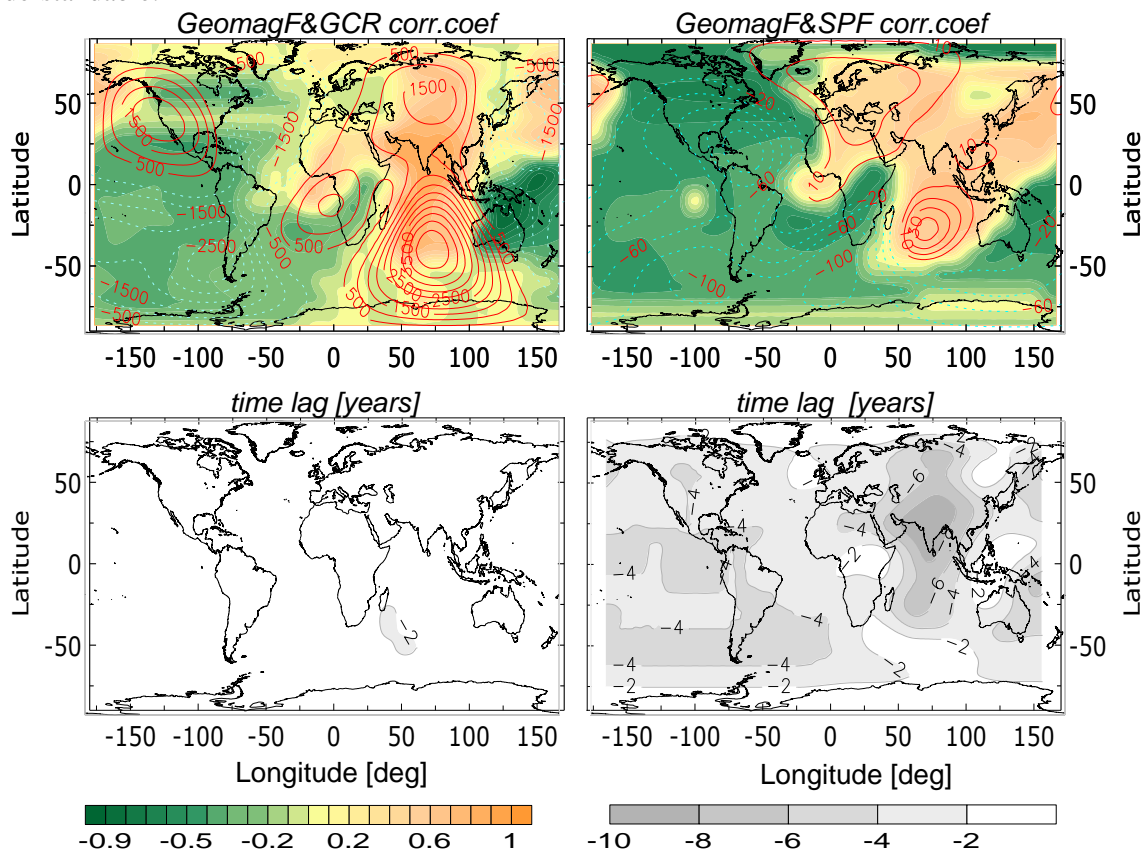


Fig.2 Correlation maps (colored shading) of geomagnetic field intensity with galactic cosmic rays (left) and solar proton flux (right). Overdrawn are contours of longitudinal gradient (left) and secular variations of geomagnetic field (right); red contours denote positive values, blue (dotted) contours – negative one. Time lag in years is shown in the bottom panels.

To gain some numerical estimation of these relations we have calculated the cross-correlation coefficients of geomagnetic field with GCR and solar protons fluxes SPF (with energies $E > 10$ MeV) in each node of our grid (latitude-longitude increment is 10^0). From statistically significant coefficients (at 95% level) we have drawn correlation maps presented in Fig.2 (colored shading). Interestingly, the spatial distribution of geomagnetic field–GCR correlation fairly well resembles the *longitudinal gradient* of geomagnetic field. The correlation of geomagnetic field and solar protons, however, matches the geomagnetic field *secular variations*. These are quite unexpected results, because in the dipole approximation the particles' modulation depends generally on the latitudinal

gradient of magnetic field. Fig.2 illustrates, however, that the deviation of real magnetic field from the dipole approximation – results in more complicated structures of its influence on the energetic particles.

Note that the spatial distribution of the modulation effect of geomagnetic field depends on the energy of precipitating particles. It is well seen not only in different distribution of correlation coefficients with geomagnetic field intensity (compare left and right panels in Fig.2), but also in the time delay of particles' response to magnetic field variability. The response of GCR to the geomagnetic field variations is instantaneous, while that of solar protons is delayed by 2-4 years in average. This could be a result of the fact that during geomagnetic disturbances the Earth's radiation belts are filled with energetic particles, which are released in the atmosphere at later stage – due to magnetospheric instabilities or sub-storm activity.

4.1 Understanding the different geomagnetic influence on solar protons and GCR

In order to understand why the spatial distribution of geomagnetic field modulation depends on the particles' energy, it is worth to remind that any charged particles moving in electromagnetic field is a subject to the action of the Lorentz's force, which could be written in the form:

$$m \frac{d\mathbf{v}}{dt} = q(\mathbf{E} + \mathbf{v} \times \mathbf{B}) ; \quad \mathbf{v} = \frac{d\mathbf{r}}{dt} \quad (1)$$

where: $\mathbf{E}(\mathbf{r},t)$ and $\mathbf{B}(\mathbf{r},t)$ are external electric and magnetic field – functions of the dimensions and time, \mathbf{r} and \mathbf{v} – particle's radius vector and velocity, respectively. In stratosphere and troposphere the electric field is practically zero. Supposing that the z-axis of our coordinate system is along magnetic field line, the solution of the equation of motion (1) – for the guiding centre of a particle moving in magnetic field with parallel gradient (parallel to magnetic field lines) – has the form [17]:

$$v_{\parallel} = v_{\parallel 0} - \frac{v_{\perp}^2}{2 \cdot B_z} \left(\frac{\partial B_z}{\partial z} \right) \cdot t \quad (2)$$

where v_{\parallel} denotes particle's velocity parallel to the magnetic field line, while $v_{\parallel 0}$ – its initial value; v_{\perp} is the perpendicular to magnetic field line component of particle's speed. Equation (2) shows that when a particle enters region of increasing field strength, its parallel to the magnetic field velocity is retarded and at some level could change its direction. Moreover, the non-uniformity of the Earth's magnetic field in the direction perpendicular to \mathbf{B} , together with magnetic field curvature, add additional components affecting the particle's trajectory – known as magnetic drift across the field lines.

The charged particles moving through a matter lose their energy primarily through a scattering on the outer electron shells of molecules filling the medium. This energy loss is usually described by the Bethe formula, which non-relativistic approximation depends inversely on the square of the particles' speed, $1/v^2$ [18], i.e.:

$$-\left[\frac{dE}{dx} \right]_0 = \frac{4\pi \cdot z^2 e^4}{mv^2} \cdot NZ \cdot \ln \left(\frac{2mv^2}{I} \right) \quad (3)$$

where z and Z are respectively charges of incident and target particles; e – electron charge; N – number density; I – mean excitation energy of the target atom (molecule); m – mass of electron and v – speed of incident particle. The Bethe formula indicates that the faster the particle is, the less energy it transfers to the molecules of the medium. Consequently, in regions with higher gradient of geomagnetic field, where according to eq. (9) particles' velocity is slow down, the energy lost by them through scattering on the atmospheric molecules must increase. This means that more secondary electrons and ions are produced.

Comparison of the left and right panels of Fig.2 shows that Earth's field favours the particle precipitation of both types in the central Asia–Indian Ocean longitudinal sector. Its influence on the more energetic GCR, however, is much stronger. This indicates that influence of the parallel magnetic field gradient on the particles' movement is stronger at lower atmospheric levels (where the gradient is higher). Particles releasing their energy at upper levels are less affected, and vary coherently with geomagnetic field variations.

4.2 Modulation of the lower stratospheric ozone by energetic particles of different origin

The distribution of the coherence between GCR and ozone variations over the globe was analyzed by applying the cross-correlation techniques in each grid node. Maps drawn from statistically significant (at 95% level) coefficients are shown in Fig.3. Note the opposite effect of GCR on the total O_3 density in both hemispheres – positive in the NH and negative in the SH.

The effect of solar protons – obtained in the Northern Hemisphere ozone – corresponds to the numerous publications reporting for ozone depletion after intense solar eruptions. Their positive effect in the SH, however, is quite unexpected – suggesting an increase of total ozone density during solar proton events.

At a glance this puzzling behavior is hard to explain. However, having known that geomagnetic field controls the *depth* of particles' penetration in the atmosphere, their different effect on the ozone balance becomes understandable. The variety of ion-molecular reactions – initiated by energetic particles at the level of their absorption – affect the atmospheric chemistry, and particularly the O_3 balance, in a different way. Thus at the Northern Hemisphere high-mid latitudes, GCR are adsorbed near the tropopause, where they activate an autocatalytic cycle for ozone production [15]. In the Southern Hemisphere, however, they penetrate below the tropopause, because of a generally weaker geomagnetic field there. Exceptional is the region around the magnetic pole, where magnetic field intensity is stronger than in the NH. This supposes to be the main reason for a reduced O_3 density near the SH tropopause, because the formation of tetraoxygen O_4^+ ion – far below or far above the tropopause – is obscured by the H_2O vapour abundance at these levels. Due to the higher affinity of the H_2O molecule to the O_2^+ ion, water clusters are created, instead of O_4^+ [20]. As a consequence the O_3 density in the SH is reduced.

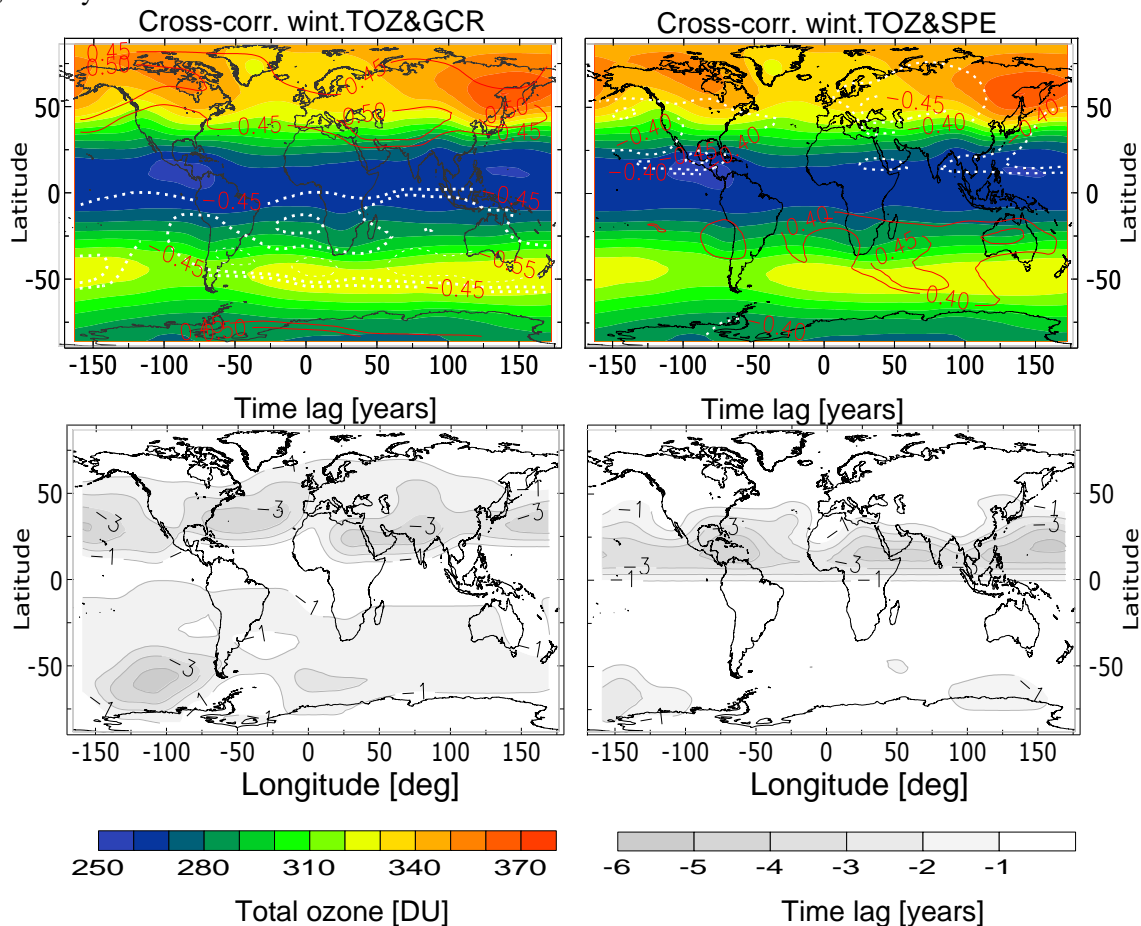


Fig.3 Global distribution of total ozone density with galactic cosmic rays (left) and solar proton fluxes (right). Continuous (red) curves denote positive correlation, dotted (white) curves – negative one. The lower panels show the time delay of ozone response to particles' forcing.

What concerns the solar protons, it is well established that they destruct atmospheric O₃ in the mesosphere and rarely in the upper stratosphere. The weaker geomagnetic field in the SH, however, allows deeper penetration of solar protons, where they destroy the ozone. The reduction of the O₃ optical depth activates, however, another process – its self-restoration at lower levels. This unique feature of the ozone is related to the deeper penetration of the solar UV radiation (when the O₃ at upper levels is destroyed), where it creates ozone (for details see e.g. [19]). Moreover, our previous analysis shows that the deeper the negative O₃ anomaly propagates into the atmosphere, the stronger the ozone self-restoration is at lower stratospheric levels [19].

The efficiency of solar protons in ozone production is, however, weaker due to the sporadic character of solar proton events, as well as to their indirect influence on the lower stratospheric O₃ density. This supposes to be a good explanation for the lower ozone density in the Southern Hemisphere and correspondingly – for the weaker relation between geomagnetic field and climate.

4. How the lower stratospheric O₃ could influence surface air temperature?

4.1 Ozone influence on the lower stratospheric thermodynamical regime

The increased climate sensitivity to variations of the lower stratospheric ozone density is reported by many authors for more than 30 years [21-26]. However, the mechanism of this inter-relation was unclear. In this section we will briefly describe the causal chain of the lower stratospheric ozone influence on climate, proposed by [15, 27], which will help to understand the relations between geomagnetic field and climatic parameters (section 2).

The O₃ is one of the most radiatively active atmospheric gases. Nevertheless, the estimated integral radiative forcing of columnar O₃ on the surface air T is very small [21, 23, 25, 28]. Its local influence on the temperature near the tropopause, however, is well documented [29-31]. Changes in the near tropopause temperature on the other hand affect the amount of humidity at this layer, through modulation of moist adiabatic lapse rate and consequently atmospheric static stability.

The static stability of a given air mass is usually determined by its adiabatic lapse rate. The lower boundary of conditional instability (allowing uplifting of the water vapour) is defined by the moist adiabatic lapse rate, while its upper limit – by the dry adiabatic lapse rate [32, 33]. While the dry adiabatic lapse rate Γ_d is approximately constant, the moist (known also as a *wet* or *saturated*) lapse rate Γ_w depends on the temperature and humidity at a given altitude (see the American Meteorological Society definition of Γ_w , described by eq. 4).

$$\Gamma_w = g \cdot \frac{1 + \frac{H_v \cdot r_v}{R_{sd} \cdot T}}{c_{pd} + \frac{H_v^2 \cdot \varepsilon \cdot r_v}{R_{sd} \cdot T^2}} \quad (4)$$

where: Γ_w is the wet adiabatic lapse rate, [K.m⁻¹]; g – Earth's gravitational acceleration (9.8076, [m.s⁻²]); H_v – heat of vaporization of water (2.501*10⁶ [J.kg⁻¹]); r_v is the ratio of the mass of water vapor to the mass of dry air, known also as a mixing ratio, [kg.kg⁻¹]; R_{sd} – specific gas constant of dry air (287 [J.kg⁻¹.K⁻¹]); ε =0.622; T – temperature of the saturated air, [K]; c_{pd} – the specific heat capacity of dry air at constant pressure, [J.kg⁻¹.K⁻¹].

Equation (4) shows that warming of the air near the tropopause leads to an enhancement of the Γ_w , which reduces the range of conditional instability of air or with other words – increases its stability. Thermodynamically stable conditions prevent uplifting of H₂O vapour across the tropopause. Oppositely, cooling of the tropopause region increases air masses' instability leading to upward propagation of the water vapour.

4.2 Water vapour greenhouse effect

It is broadly accepted that the water vapour in the free atmosphere has the strongest impact into the greenhouse warming of the Earth planet [34, 35]. The actual impact in the greenhouse effect, however, belongs to the humidity near the tropopause [36-38] due to its extremely low temperature and consequently – low emissivity. The colder water vapour has less ability to emit back into the space the absorbed long-wave radiation (emanated by the Earth), trapping it into the troposphere.

Consequently, ozone variability near the tropopause affects simultaneously temperature and humidity variations at the most sensitive for the outgoing long-wave radiation altitudes near the tropopause. This leads to spatial and temporal variations of the Earth's radiation balance (due to the strongest water vapour greenhouse effect) and corresponding changes in the surface air temperature.

5. Evidences supporting the geomagnetic–O₃ influence on climate

In order to estimate the validity of the proposed concept for geomagnetic field–ozone influence on climate, we have analyzed the time series of ozone at 70 hPa and specific humidity at 150 hPa, for the period 1957-2012. The lagged correlations coefficients have been calculated in each point of our grid (steps in lat-long are 10⁰). From statistically significant (at 95%) coefficients we have calculated the correlation map over the globe and results are shown in Fig.4 – for the Northern Hemisphere, and Fig.5 – for the Southern Hemisphere. The correlation contours are overdrawn on the climatological means of surface air temperature anomalies calculated up to the end of 20th century (left columns in the Figs.4) and after that (middle columns).

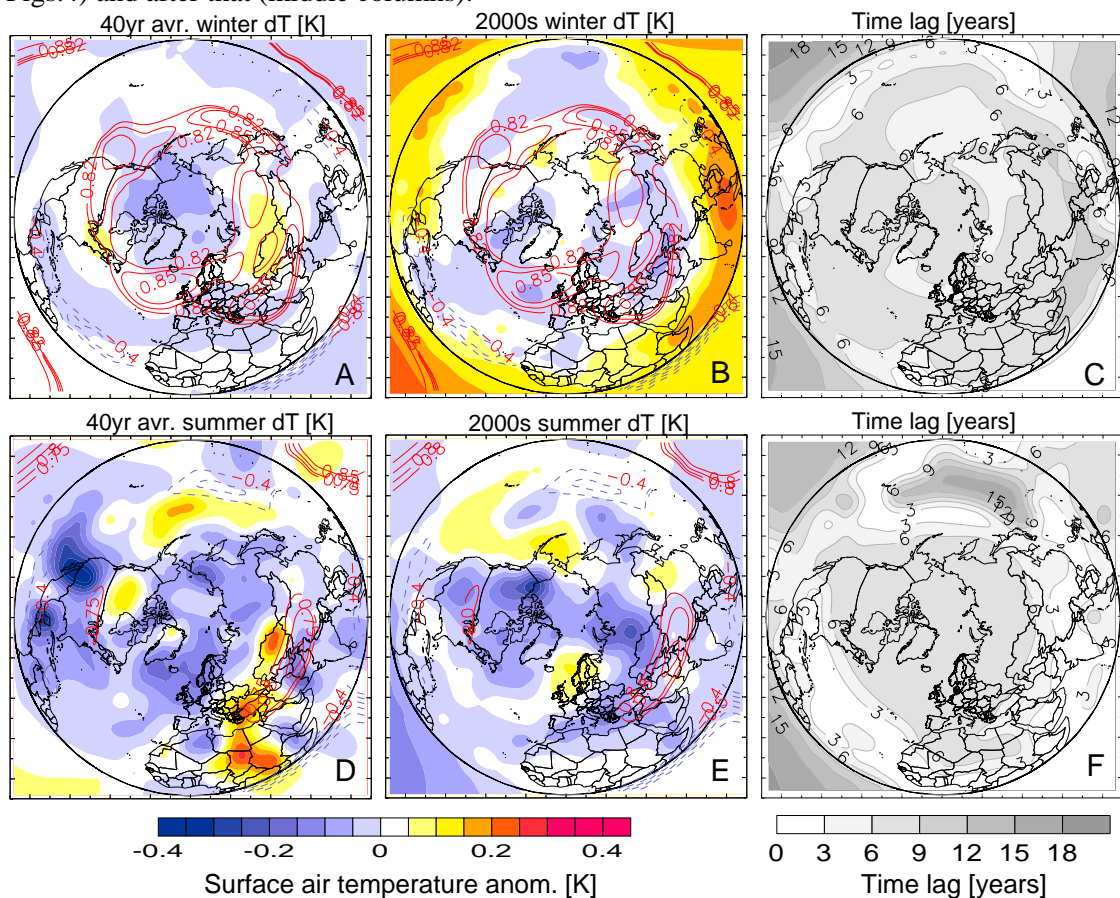


Fig.4a Correlation maps of the Northern Hemisphere O₃ at 70 hPa and specific humidity at 150 hPa (red contours denote positive coefficients) compared with climatological mean of surface air T (colored shading), calculated for the period 1957-2000 (left column) and 2001-2012 (middle column). Upper row presents winter time conditions, lower row – summer conditions. The panels C and F illustrate time delay of humidity response to O₃ forcing. Note that winter temperature inter-annual variations follow fairly well the maximal correlation between lower stratospheric ozone and humidity.

The coherence in temporal variability of the lower stratospheric ozone and water vapour is especially well pronounced in the Northern Hemisphere (Fig.4, panel A). The correlation coefficients are extremely high, so for clarity contours below 0.8 have been omitted. The ozone–humidity correlation resembles quite well the positive surface temperature anomalies (Fig.4, A) during the period of gradual decrease of long-term variations of GCR, and correspondingly decrease of the lower stratospheric O₃ [28].

Since the beginning of the millennium, however, GCR intensity steadily increases, due to weakening of solar activity and correspondingly heliomagnetic field. This is accompanied with more ozone production near the tropopause [16, 17] and with cooling of the surface air – well illustrated in Fig.4, b (for the mechanism of O₃ influence on climate see section 4).

Analysis of the seasonal effect reveals that the ozone influence is most effective in the *winter season* (compare panels A, D and B, E in Fig.4). This effect could be probably related to the annual cycle in the ionization rate of GCR in the lower stratosphere [40]. The latter is manifested by an increased height of the summer maximum ionisation produced by GCR – due to the uplifted denser atmosphere and corresponding upward shift of the Pfozter maximum (the max. of electron-ion pairs produced by GCR). As a result, the ozone density near the tropopause is reduced and its influence on the tropopause temperature and humidity – weakened.

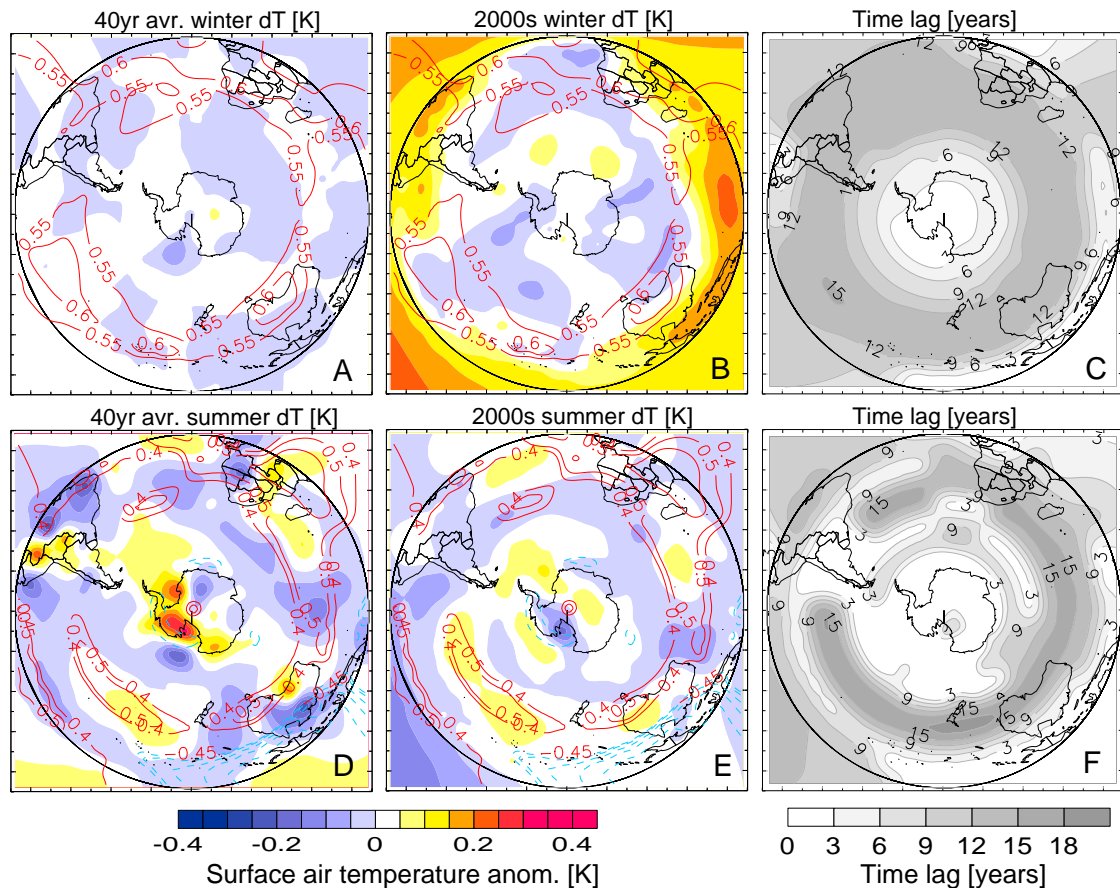


Fig.4b Same as Fig.4a but for the Southern Hemisphere. Note that surface air temperature is sensitive to the near tropopause O₃-humidity connection during the summer season.

The ozone influence on the humidity distribution in the Southern Hemisphere is much weaker – the maximum correlation coefficients are 0.5-0.6, found at mid-latitudes. Interestingly, the surface air temperature responds to the ozone –humidity forcing mainly during the summer season (Fig.5, D and E). The instantaneous negative correlation, obtained in the western Antarctica, illustrates the fact that persistently lower O₃ density in this longitudinal sector is accompanied with persistently higher humidity near the tropopause [17]. The latter reflects in a positive surface air temperature anomalies observed in the region (Fig.5 D and E), due to the increased greenhouse warming of the near tropopause water vapour.

Time lag of the humidity response to O₃ variability in the NH is in the range 5–7 years, independently on the season. In the Southern Hemisphere mid-latitudes, where the O₃-H₂O connectivity is maximal, it is more than 10 years. Over the Antarctica the humidity response to ozone forcing is instantaneous, but the footprint of their effect in the surface air temperature is obtained mainly during the summer season (compare Fig.5, panels A, B and D, E)

6. Data and Method of analysis

Our previous analyses [16, 28] reveal a non-linear character of the relation between lower stratospheric O₃ and GCR. In this study, the main goal was to show spatial distribution of this relation. The replication of the non-linear analysis, however, in each node in our grid (with 10⁰ steps in latitude and longitude, or in total – in 684 points) appears impossible, because of the spatial care required for the monitoring of the optimization procedure convergence (to exclude false deep minima of distance function). For this reason here we apply a lag cross-correlation analysis, the use of which is easily programmable.

The cross-covariance coefficients at lag m have been calculated by moving the axis of the independent variable (i.e. the cause, or the forcing parameter) backward, i.e.

$$c_{xy}(k) = \frac{1}{N-1} \sum_m (Y_t - \bar{Y}) \cdot (X_{t+m} - \bar{X}) \quad \text{for } t = 1 \text{ to } N; \quad m = -1 \text{ to } -k$$

where N is the number of observations in time series. For this reason the time delay is given in our maps as a negative value. The cross-correlation coefficients are calculated through normalization of the cross-covariance on the standard deviations of both time series.

All correlation coefficients presented in this paper are calculated from the mean winter or mean summer values. Cross-correlations of external factors (i.e. long-term variations of galactic cosmic rays as well as the solar proton fluxes) were calculated without any smoothing, while relations between atmospheric parameters themselves – with 3 point running average smoothing. Maps of connectivity between examined parameters have been created from only statistically significant coefficients, determined by applying the two tailed Student's t-test.

7. Conclusions:

The existing hypotheses for geomagnetic field influence on the Earth's climate are based on the assumption for mediating role of galactic cosmic rays (GCR). In order to estimate the physical foundation of such an assumption we have estimated the global distribution of geomagnetic control on the GCR and solar proton flux intensity. Analysis of the correlation coefficients reveals that the intensity of precipitating GCR is well determined by the horizontal gradient of geomagnetic field – the stronger the gradient the more intense is the GCR flux (Fig.2 left). Solar protons are less affected by the magnetic field gradient and simply follow the spatial distribution of geomagnetic secular variations (Fig.2 right).

In addition we have assessed the spatial distribution of the coherent variations between lower stratospheric ozone and energetic particles of both types. We discover that GCR have a positive impact in the ozone balance of the Northern Hemisphere and negative one in the Southern Hemisphere. An intense flux of solar protons, in agreement with the previous findings, reduces the total ozone density in the NH. In the SH, however, total ozone and solar protons correlate positively – what suggests an enhancement of the ozone density with a time lag of 4-6 years. Two different mechanisms explaining the diverse ozone response to the particles' forcing are briefly discussed in section 4.

Analysis of the connectivity between the lower stratospheric ozone and water vapour shows that their variations are tightly synchronised, especially strongly in the Northern Hemisphere. Comparison with the near surface air temperature climatology reveals that the interannual temperature variations during the NH-winter and the SH-summer seasons follow quite well the maximal coherence of the ozone–humidity variations.

In resume we conclude that recent climate variability could be related to the spatial and temporal variations of geomagnetic field. Its influence on climate is mediated by the energetic particles – precipitating regularly or sporadically in the Earth's atmosphere – which in turn affect the ozone balance near the tropopause. Furthermore, the ozone influence on climate consists of: (i) modulation of the temperature and humidity near the tropopause, and (ii) the greatest impact of the water vapour at this level in the Earth's radiation balance. Spatial and temporal variations of geomagnetic field could explain not only the average long-term climate variations during the last half a century, but also the regional diversity of climate variability. The latter could not be reached by any of the global homogeneous climate forcing (i.e. greenhouse gases, variability of solar electromagnetic radiation etc.). Attribution of the recent climate variations to the spatial-temporal variability of heliomagnetic

and geomagnetic fields suggest that the observed global warming (lasting for about a century) as well as the contemporary stabilization of the global surface air temperature could be assessed as just another phase of the continuous climate changes.

Acknowledgements:

This research was supported by the *BlackSeaHazNet FP7* project (PIRSES-GA-2009-246874) and partly by *COST ES1005 TOSCA* (<http://www.tosca-cost.eu>). We are very thankful to the project teams of ERA-40 and ERA-Interim reanalyses, as well as to NOAA National Geophysical Data Center for providing geomagnetic field data.

References:

- [1] Vieira L.E.A., Norton A., Dudok de Wit T., Kretzschmar M., Schmidt G.A., Cheung M.C.M. (2012) How the inclination of Earth's orbit affects incoming solar irradiance. *Geophys. Res. Lett.*, 39, L16104, doi:10.1029/2012GL052950.
- [2] Ward P.L. (2009) Sulfur dioxide initiates global climate change in four ways. *Thin Solid Films* 517 (2009) 3188–3203.
- [3] Schneider D.P., Steig E., van Ommen T.D., Dixon D.A., Mayewski P., Jones J.M., Bitz C.M. (2006) Antarctic temperatures over the past two centuries from ice cores, *Geophys. Res. Lett.*, vol.33, Art. No. L16707.
- [4] Kobashi T., Shindell D.T., Kodera K., Box J.E., Nakaegawa T., Kawamura K., (2013) On the origin of multidecadal to centennial Greenland temperature anomalies over the past 800 yr. *Clim. Past* 9, 583-596, doi:10.5194/cp-9-583-2013.
- [5] Gallet, Y., Genevey, A., Fluteau, F. (2005) Does Earth's magnetic field secular variation control centennial climate change? *Earth Planet. Sci. Lett.* 236: 339–347, doi:10.1016/j.epsl.2005.04.045.
- [6] Courtillot, V., Gallet, Y., Le Mouél, J.L., Fluteau, F., Genevey, A. (2007) Are there connections between the Earth's magnetic field and climate? *Earth Planet. Sci. Lett.* 253: 328–339, doi:10.1016/j.epsl.2006.10.032.
- [7] Bakhmutov, V.G., Martazinova, V.F., Ivanova, E.K., Melnyk, G.V. (2011) Changes of the main magnetic field and the climate in the XX-th century, *Reports of the National Acad. of Sci., Ukraine.* 7: 90-94.
- [8] Usoskin I.G., Kovaltsov G.A., Korte M., Mironova I.A. (2009) Long-term geomagnetic changes and their possible role in regional atmospheric ionization and climate, *Proceedings of the 31st ICRC, ŁODZ*, 1-4.
- [9] Kitaba I., Hyodo M., Katoh S., Dettman D.L., Sato H. (2013) Midlatitude cooling caused by geomagnetic field minimum during polarity reversal, *PNAS*, 110, 1215-1220, doi/10.1073/pnas.1213389110
- [10] Kristjánsson J.E. et al. (2008) Cosmic rays, cloud condensation nuclei and clouds – a reassessment using MODIS data, *Atmos. Chem. Phys.*, 8: 7373-7387.
- [11] Sloan T., Wolfendale A.W., (2008) Testing the proposed causal link between cosmic rays and cloud cover, *Environ. Res. Lett.* 3: 024001, doi:10.1088/1748-9326/3/2/024001.
- [12] Calogovic J., Albert C., Arnold F., Beer J., Desorgher J.J., Flueckiger E.O. (2010) Sudden cosmic ray decreases: No change of global cloud cover, *Geophys. Res. Lett.*, 37: L03802, doi:10.1029/2009GL041327.
- [13] Kulmala M. et al. (2010) Atmospheric data over a solar cycle: no connection between galactic cosmic rays and new particle formation, *Atmos. Chem. Phys.*, 10: 1885–1898.
- [14] Duplissy et al. J. (2010) Results from the CERN pilot CLOUD experiment, *Atmos. Chem. Phys.*, 10, 1635–1647.
- [15] King J.W. (1974) Weather and Earth's magnetic field, *Nature*, 247, 131-134.
- [16] Kilifarska N.A. (2012) Mechanism of lower stratospheric ozone influence on climate. *Intern. Rev. Phys.*, 6(3): 279-290.
- [17] Kilifarska N.A., Bakhmutov V.G., Melnyk G.V. (2013) Geomagnetic influence on Antarctic climate – evidences and mechanism. *Int. Rev. Phys.*, 7 (3), 242-252.

- [18] Moisan, M., Pelletier, J. (2012) Physics of Collisional Plasmas, in: Individual Motion of a Charged Particle in Electric and Magnetic Fields. Springer, 101-202.
- [19] Leung P.T. (1989) Bethe stopping power theory for heavy target atoms, *Phys. Rev. A*, 40(9), 5417-5419.
- [20] Kilifarska N.A., Bakhmutov V.G., Melnyk (2013) Energetic particles influence on the southern Hemisphere ozone variability, *Compt. rend. Acad. bulg. Sci.*, 66, 1613-1622.
- [21] de Petris G. (2003) Atmospherically relevant ion chemistry of ozone and its cation, *Mass Spectrom. Rev.*, 22, 251-271.
- [22] Ramanathan, V., Callis, L.B., Boucher, R.E. (1976) Sensitivity of surface temperature and Atmospheric temperature to perturbations in the Stratospheric ozone and Nitrogen dioxide. *J. Atmos. Sci.* 33: 1092-1112.
- [23] Wang W-Ch., Pinto J.P., Yunk Y.L. (1980) Climatic effect due to the halogenated compound in the Earth Atmosphere. *Atmos. Sci.* 37: 333-338.
- [24] Wang W-Ch., Zhuang Y-Ch., Bojkov R. (1993) Climate implications of observed changes in ozone vertical distributions at middle and high latitudes of the Northern Hemisphere, *Geophys. Res. Lett.*, 20(15): 1567-1570.
- [25] Wirth, V. (1993) Quasi-stationary planetary waves in total ozone and their correlation with lower stratospheric temperature. *J. Geophys. Res.* 98: 8873-8882.
- [26] de Forster, P.M., Shine, K. (1997) Radiative forcing and temperature trends from stratospheric ozone changes. *J. Geophys. Res.* 102(D9): 10841-10855.
- [27] Stuber N., Sausen R., Ponater M. (2001) Stratosphere adjusted radiative forcing calculations in a comprehensive climate model. *Theor. Appl. Climatol.*, 68: 125-135.
- [28] Kilifarska N.A. (2012) Climate sensitivity to the lower stratospheric ozone variations. *J. Atmos. Sol-Terr. Phys.*, 90-91: 9-14.
- [29] Gauss M. et al. (2006) Radiative forcing since preindustrial times due to ozone change in the troposphere and the lower stratosphere, *Atmos. Chem. Phys.*, 6: 575-599.
- [30] de Forster, P.M., Tourpali, K. (2001) Effect of tropopause height changes on the calculation of ozone trends and their radiative forcing. *J. Geophys. Res.* 106(D11): 12241-12251.
- [31] Seidel, D.J., Randel, W.J. (2006) Variability and trends in the global tropopause estimated from radiosonde data. *J. Geophys. Res.* 111: D21101 doi:10.1029/2006JD007363.
- [32] Randel, W.J. et al. (2009) An update of observed stratospheric temperature trends. *J. Geophys. Res.* 114: D02107 doi:10.1029/2008JD010421.
- [33] Young, J.A. (2003) Static stability, in: J.R. Holton, J.A. Curry, J.A. Pyle (Editors), *Encyclopaedia of Atmospheric Sciences*. Academic Press, v.5: 2114-2120.
- [34] North, G.R., Eruhimova, T.L. (2009) *Atmospheric thermodynamics: elementary physics and chemistry*. Cambridge University Press, Cambridge, UK, 267 pp.
- [35] IPCC (2007) (Intergovernmental Panel on Climate Change), *Climate Change 2007: The Physical Science Basis*, edited by Solomon, S., et al., Cambridge Univ. Press, New York. 996 pp.
- [36] Schmidt, G.A., Ruedy, R.A., Miller, R.L., Lacis, A.A. (2010) Attribution of the present-day total greenhouse effect. *J. Geophys. Res.*, 115: D20106, doi:10.1029/2010JD014287.
- [37] Spencer R.W., Braswell W.D. (1997) How Dry is the Tropical Free Troposphere? Implications for Global Warming Theory. *Bull. Amer. Meteor. Soc.* 78(6): 1097-1106 doi:10.1029/2003JD003980
- [38] Smith C. A., Haigh, J.D., Toumi, R. (2001) Radiative forcing due to trends in stratospheric water vapour. *Geophys. Res. Lett.* 28: 179-182.
- [39] Inamdar, A. K., Ramanathan, V., Loeb, N.G. (2004) Satellite observations of the water vapor greenhouse effect and column longwave cooling rates: Relative roles of the continuum and vibration-rotation to pure rotation bands. *J. Geophys. Res.*, 109: D06104 doi:10.1029/2003JD003980
- [40] Forbush, S.E. (1960) Time variations of cosmic rays, Van Allen (editor), AGU special publications, 37: 323-411.

GEOMAGNETIC FIELD–OZONE INFLUENCE ON THE SURFACE AIR TEMPERATURE IN EPICENTRAL REGIONS OF BALKAN'S EARTHQUAKES

N.A. Kilifarska¹, V.G. Bakhmutov², G. V. Melnyk², T. Mozgova²

¹National Institute of Geophysics, Geodesy and Geography, Bulgarian Acad. of Sciences, Acad.

G.Bonchev str., bl.3, Sofia 1113, Bulgaria, nkilifarska@geophys.bas.bg

²Institute of Geophysics, National Academy of Sciences of the Ukraine, Palladin av.32, 03680 Kiev, Ukraine, bakhmutovvg@gmail.com

Abstract:

The problem for a possible warming of the area around the future earthquake's (EQ) epicenter attracts recently the attention of many researchers. However, having in mind that the surface air temperature (T) is controlled in a greater extent by atmospheric processes, we approached to this problem in another way. We start this research with the question – Does surface air T in the day and place of EQ is related to the total ozone density? We have shown previously that these two parameters are strongly connected, describing the mechanism through which the lower stratospheric O₃ could influence the surface air T. Our current analysis reveals that connectivity between both parameters (measured in the day and place of EQs) is quite high in the warmer season.

Due to the fact that the lower stratospheric O₃ density is substantially affected by geomagnetic field, we have examined also the influence of geomagnetic “bursts” on the O₃–T relation. We found that ozone and temperature in the day of EQ are well connected to the sudden increase of magnetic H and Z components (observed for ~1-3 days prior to the EQs). This relation has a seasonal character – being well pronounced in the warmer season (May-September) and missing in the colder season. In addition it is well defined for EQs with epicentral depths more than 15 km. and disappears for shallow seismic events.

1. Problem formulation:

The idea for a possible relation between air surface temperature anomalies and seismic activity dated back to the end of 19 century. Its real exploration began, however, with the satellites era when thermal anomalies across wide regions (based on retrieval of land surface temperature from satellite observations of Earth's infrared emission) became available. Most of the authors report for a positive temperature anomalies observed in a broad region around the future earthquake (EQ) epicenters [1-9]. Other authors [10] have found no relations and argue that the seismic thermal precursors are due to incorrect separation of the surface temperature natural variability.

It is worth to remember that the Earth's surface air temperature (T) is determined generally by the absorbed solar irradiance and to a lesser extent by the geothermal flux – emitted from the lithosphere as a consequence of tectonic activity [11]. The latter is supposed responsible for generation of electromagnetic field in period of earthquakes' preparation [12]. On the other hand, the geomagnetic field measured on the Earth's surface is very frequently influenced from solar and magnetospheric activity – i.e. by magnetic storms and sub-storms. Moreover, some authors suggest that these disturbances in geomagnetic field may serve as a trigger for EQs [13]. Our results from analysis of the EQs in Vrancha region reveal a well pronounced relation to the geomagnetic fluctuations initiated by magnetospheric sub-storms [14-15].

Consequently, despite of the source (internal or external) – the geomagnetic field before the EQs is supposed to be changed [16]. On the other hand our previous investigations [19-22] show that geomagnetic field substantially influences the surface air temperature (T) – through its control over the particles' precipitation, which in turn influence the chemical balance of the lower stratosphere, and particularly the O₃ density.

In the context of geomagnetic changes prior to the EQs, we put the question: Do these changes reflect in the total O₃ density, and correspondingly surface temperature measured in the day and place of the EQ? Moreover, the temperature in a broad area around the EQ's epicenter could be influenced by different lithospheric processes (as is suggested by many authors). All these unresolved questions

have motivated this study, based on the analysis of seismicity in the Balkan region during the period 1957-1990.

2. Data and Methods:

We have analyzed 472 earthquakes (EQs), with magnitudes higher than 2.5, occurred in Balkan Peninsula region with coordinates: (40°-44°N; 18°-26°E) during the period 1957-1990. Time, coordinates and earthquakes' parameters are taken from [20]. In the case of EQs with for- or aftershocks, only the impulse with the highest magnitude has been taken into account.

Data for the air temperature at 2m above the surface (T2m) and total ozone density (TOZ) are from ERA 40 reanalysis, taken at two latitudes (40°N and 42.5°N) and three longitudes (20°E, 22.5°E and 25°E), at 18:00 local time. The temperature and ozone values in all EQs epicenters, occurred in a radius of 1.25° around a given ERA 40 data point, have values determined in that point.

Daily values of geomagnetic filed H and Z components are from *Hurbanovo* observatory (47.52N; 18.12E), Slovakia.

The possible connections between surface air T, atmospheric total ozone density (in the days of EQ strikes) and the maximum daily values of geomagnetic filed (observed for several days before) have been investigated by the use of the standard linear regression method.

3. Relations between surface air temperature and ozone:

Analysis of the lower stratospheric O₃ influence on the surface air temperature over the globe shows that this relation is especially well pronounced at mid-latitudes [21]. The goal of this section is to examine whether this relation changes in days with EQs occurrence, due for example to a lithospheric influence on the surface air T at the final stage of the EQ's preparation. For achieving this goal, we are first examining the manifestation of ozone–T relation over the Balkan Peninsula region using their time series for the entire period 1957-1990. As a representative for the area we have taken the point with coordinates (42.5°N; 22.5°E) – placed in the middle of examined region.

3.1. O₃-T dependence over Balkans for the period 1957-1990

Examination of Fig.1 (presenting scatterplots of columnar O₃ density and surface air T) shows that coherence in their variability is much better pronounced during the summer season (left column). In winter it actually disappears in the mean evening values, but is still tracked in their anomalies (i.e. deviations from decadal means) – compare top and bottom panels of Fig.1, right column.

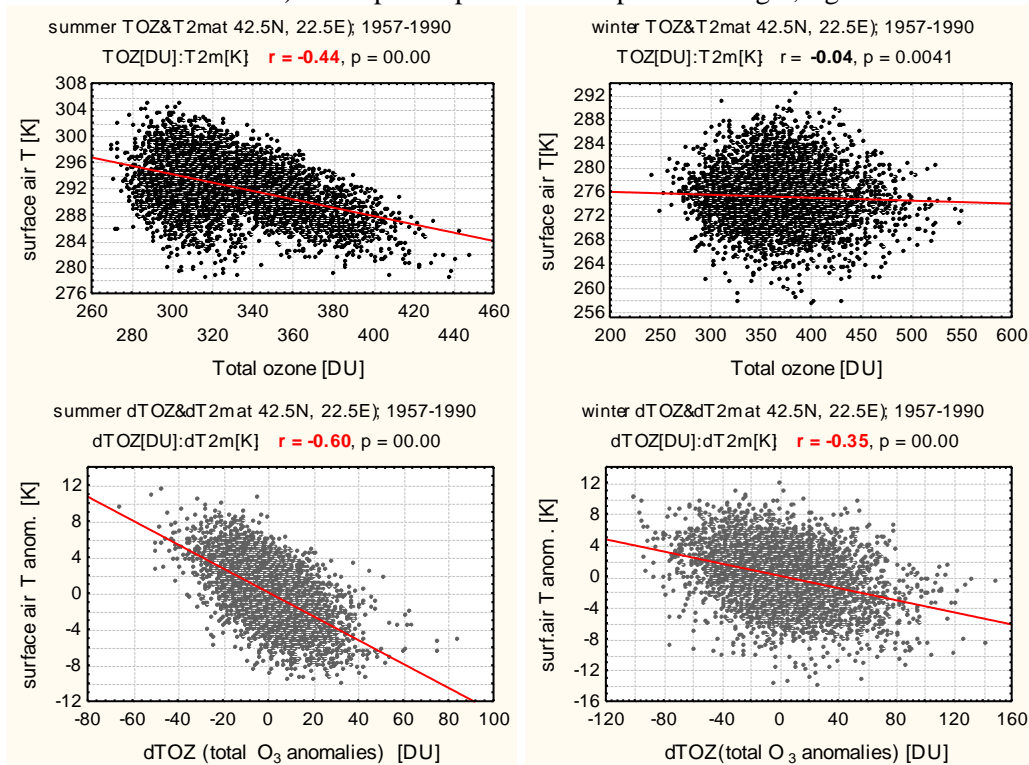


Fig.1 Scatterplots of total ozone and surface air T derived from time series in a point with coordinates

(42.5⁰N; 22.5⁰E), for the period 1957-1990. Left column describes the summer season (May-August), while right column – winter season (December-March). Upper row presents daily mean values, lower row – their anomalies (deviations from the time evolving decadal means)

3.2. O₃-T relation in days with earthquakes – seasonal and depth dependence

Having in mind the seasonal dependence of the O₃-T relation (illustrated in Fig.1), we have divided the days with EQ strikes on two composites corresponding to the warmer season (May-September) and to the colder one (October-April). Applying regression analysis we found that for EQs happened in the colder season, the O₃-T relation is very weak (Fig.2, right column). For EQs occurred in the warmer season, however, this relation becomes even stronger (Fig.2, left column) than that calculated from the whole time series, for the period 1957-1990 (shown in Fig. 1). For this reason we focus our further attention on the EQs occurred in the warmer season.

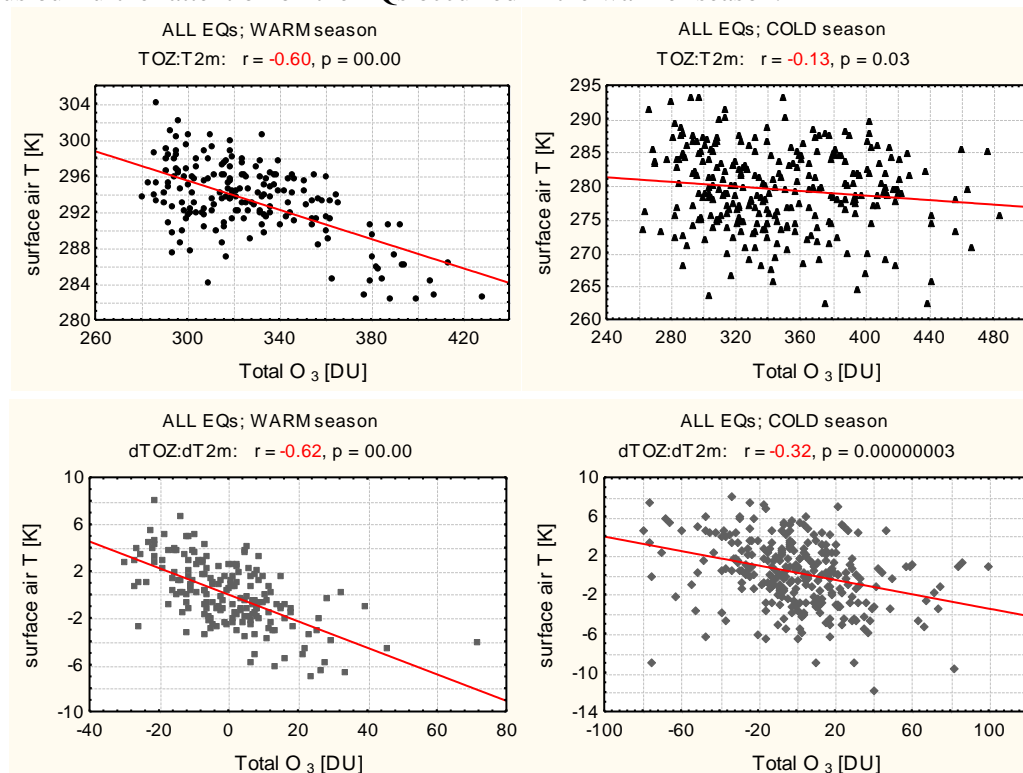


Fig.2 Scatterplots of total ozone and surface air T in the days with EQs, occurred in the *warmer season* (left column) and *colder season* (right column). Note that the relation between ozone and T practically disappears in the colder season.

Analysis of the relation between EQ depth and surface air T reveals in addition the existence of two clusters: (i) the shallow EQs, which do not depend on the surface air T (see Fig.3), and (ii) EQs with epicenters deeper than ~15÷20 km – showing a tendency for temperature dependence; i.e., the higher the T, the deeper the EQ epicenter is (Fig.3).

For this reason the warmer EQs composite has been split on two groups, depending on the depth of the EQs: (i) *shallow* EQs – having depths smaller than 15 km; and (ii) *deep* EQs – with epicenter deeper than 15 km. Results from the application of regression analysis are shown in Fig.4. It is easily seen that relation between ozone and surface air T is strong in both cases, being a bit stronger, however, for the *deep* EQs (compare left and right columns in Fig.4). Moreover, the strong relation between total O₃ density and geomagnetic field intensity [19, 22] gives a hint that the tendency for T dependence on the EQ's depth could be attributed to the geomagnetic field influence on the O₃ density. This hypothesis will be examined in the next section.

4. Geomagnetic field prior to earthquakes and its relations to the ozone and surface air T:

Variability of geomagnetic field on the Earth's surface is strongly influenced by the active processes on the Sun – initiating geomagnetic storms, when hitting the Earth's magnetosphere. In

order to eliminate such an influence, all EQs happened during, or several days after, the geomagnetic storms have been excluded from the analysis. In the warm season they actually were only a few events.

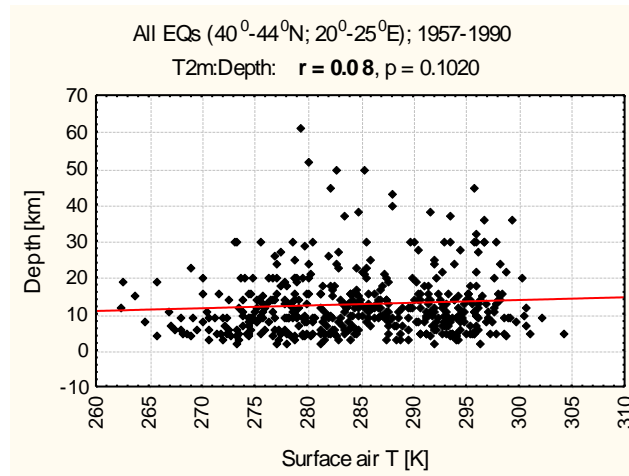


Fig.3 Scatterplots of surface air T and earthquakes' depth derived from all events occurred during the period 1957-1990. Note the clustering regarding the depth of the earthquakes.

Our previous investigations show, however, that midnight sub-storm activity correlates quite well with seismicity in Vranča region [14]. Being aware that separation of external (magnetic substorms) and internal (tectonic processes) forcings of geomagnetic field – are complicated problem, at this stage we will not specify the origin of the magnetic “burst” observed in Hurbanovo observatory for several days prior to the analyzed EQs.

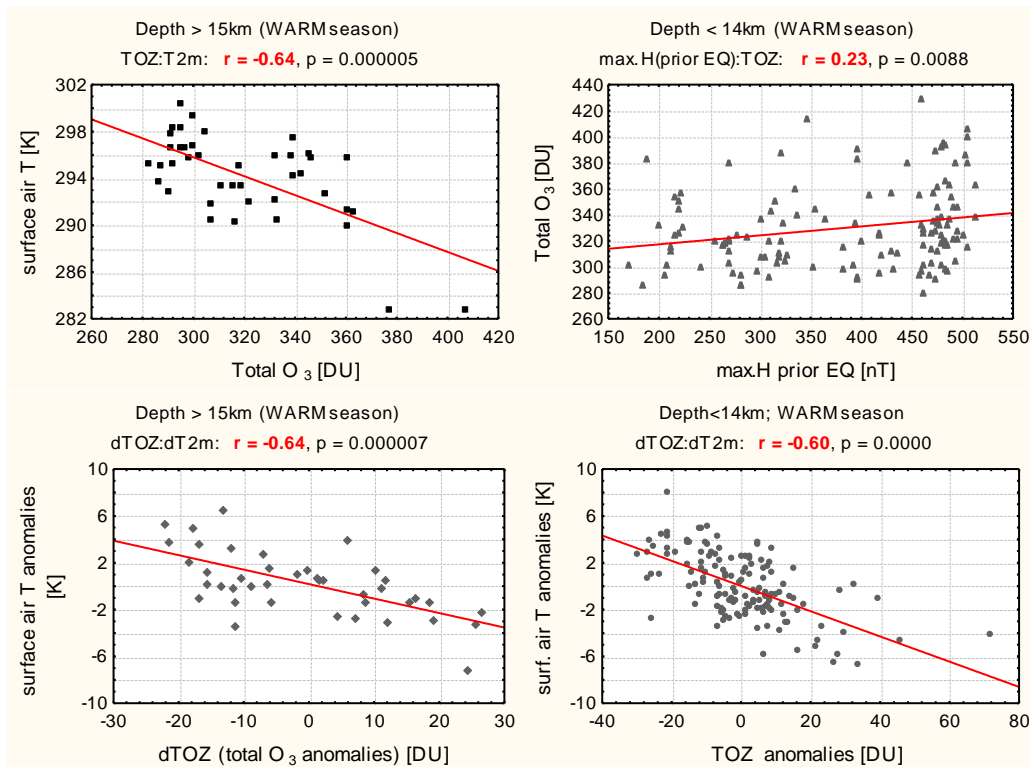


Fig.4 Scatterplots of O_3 -T dependence (top panels) and their anomalies (bottom panels) for the deep EQs (left column) and shallow EQs (right column). EQs occurred in the warmer season (May-September) have been analyzed only.

In order to gain information for the time delay between magnetic “burst” and EQ appearance, we have created the frequency diagram both for *deep* and *shallow* earthquakes. The histogram, shown

in Fig.5, illustrates that the most frequent delay between geomagnetic sudden enhancement and the EQs is about 2 days – for both *deep* and *shallow* EQs. Frequency distribution of the *deep* EQs is close to the lognormal distribution, while that of the *shallow* EQs – to the rayleigh distribution.

Further we have examined the relation between ozone and the maximum daily values of geomagnetic H and Z components (measured prior to the EQs strikes). Results shown in Fig.6 illustrate that fluctuations in geomagnetic field intensity (supposedly associated with EQs' preparation) have a well pronounced influence on the total O₃ density in days with *deep* earthquakes (Fig.6 upper panels). Thus an increase of the magnetic H component by ~300 nT, or strengthening of the magnetic Z component by ~ 400 nT corresponds to an O₃ abundance of about 50 DU. These variations are comparable with the average amplitude deviations from the mean summer value of total O₃ density at mid-latitudes.

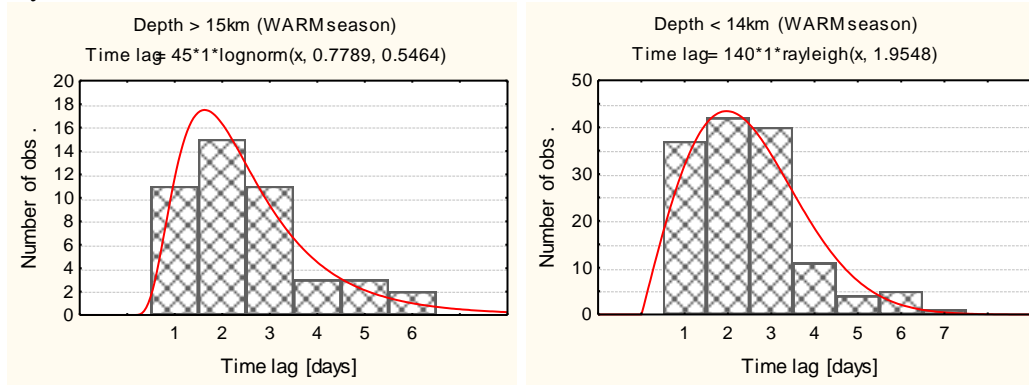


Fig.5 Frequency distribution of time delay between geomagnetic “bursts” and appearance of the EQ’s strikes.

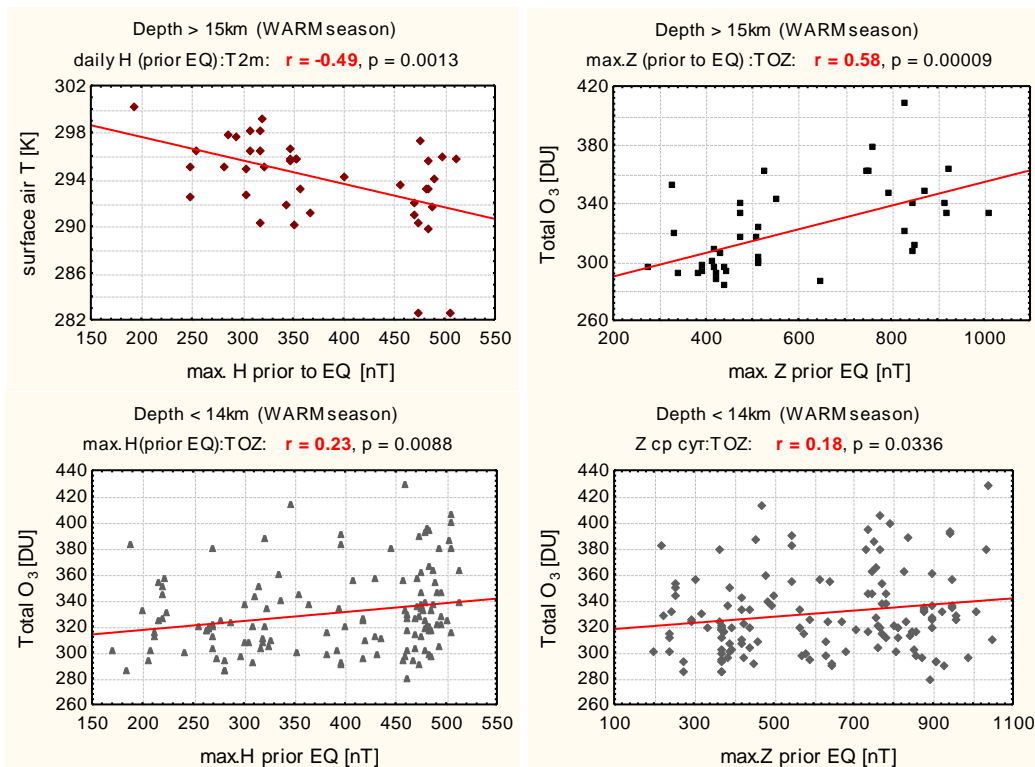


Fig.6 Scatterplots of total O₃ density and maximum values of geomagnetic field H and Z components, measured for several days prior to EQs. Shown is the ozone response to geomagnetic field strengthening prior to *deep EQ* (top row) and *shallow EQ* (bottom row).

The geomagnetic field–O₃ relation, however, is severely weakened in the cases of *shallow* EQs (Fig.6, bottom row). This is an indication that geomagnetic disturbances prior to the *shallow* EQs are less effective in their influence on the total O₃ density.

We have examined also the relation between surface air T and geomagnetic field. Fig.7 shows that it is moderately strong in cases with *deep* EQs and much weaker for *shallow* EQs. Comparison of Figs.6 and 7 suggests that the geomagnetic influence on the surface air T is mediated by the ozone in the case of *deep* EQs. For the *shallow* EQs, however, the regression coefficients between magnetic H and Z components and surface air T are higher than that of the total ozone and geomagnetic field (compare the bottom rows of Figs. 6 and 7). This suggests that surface air T in days with *shallow* EQs is possibly influenced by some factor(s) other than O₃ density – eventually related to the lithospheric processes [11].

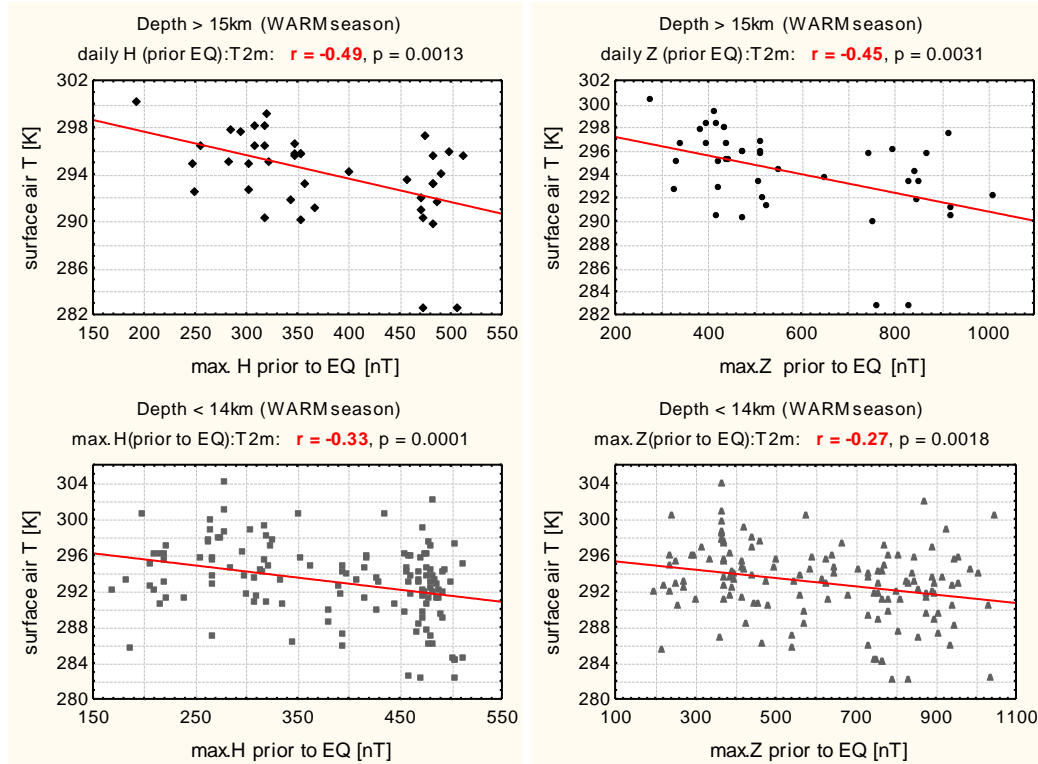


Fig.7 Scatterplots of magnetic H (left column) and Z (right column) components and air temperature near the Earth surface. Upper panels show comparison for the *deep* earthquakes (with depth ≥ 15 km), while lower panels – for *shallow* EQs (with depth <14 km).

5. Spatial distribution of the O₃–T relation over the Balkans’ region in days with EQ:

Besides different coordinates, the examined EQs have occurred in different times. Assuming, however, that they have happened at one and the same moment in time, we could gain an idea for the spatial distribution of the ozone and temperature values in the day of EQs, averaged over the period 1957-1990. This procedure will allow us to detect how the O₃–T relation, in periods of increased seismic activity, is distributed in space. Such a comparison for *deep* EQs, occurred in the warmer season is shown in Fig.8 (top panel). It illustrates that in areas with warmer than average surface air T, the simultaneously measured O₃ value is typically lower than its geometrical mean. With other words – depletion of the total O₃ density is accompanied with warming of the surface air T and vice versa.

For each EQ we also have the values of geomagnetic field measured in Hurbanovo observatory. Mapping the daily mean of the Z component – taken in a day, when peak Z values are detected for ~1-3 days prior to the EQs – we will have the average distribution of geomagnetic “bursts” observed prior to the all examined EQs. Such a map is given in the bottom panel of Fig.8. Its comparison with the average O₃ distribution in the day of the EQ shows that depletion of geomagnetic field is followed by a reduction of total ozone density (blue contours in Fig.8).

The coherence of total O_3 –surface air T variations on a climatic time scales, and correspondingly their relations to geomagnetic field, have been a subject of our previous investigation [14, 15, 18]. Here we have found that such synchronization operates also at shorter time scales (compare top and bottom panels in Fig.8). It appears that even short-term fluctuations in geomagnetic field reflect in corresponding changes in ozone density and air surface temperature. The mechanism of this connectivity includes modulation of the intensity and depth of energetic particles’ penetration in the Earth’s atmosphere, affecting the ozone balance near the tropopause [14, 15].

6. About the seasonality of geomagnetic–ozone influence on the surface air T

An important question raised from the above results is: Why the mechanism for geomagnetic influence on the surface air T (mediated by the lower stratospheric O_3) is effective only during the warmer season?

One possible explanation could be found in seasonality of the daily amplitude of geomagnetic field variations – being higher in the summer season [19]. To estimate the impact of this effect we have regressed ozone and temperature on the amplitude of magnetic Z and H components. Results presented in Fig.9 show that the amplitude of Z variability (i.e. $Z_{max}-Z_{min}$) has a statistically significant effect on the total O_3 density (Fig.9, top panels). More specifically, an enhancement of the amplitude of magnetic Z component leads to O_3 abundance, followed by a cooling of the Earth’s surface. However, the ozone dependence on the amplitude of Z variations is much weaker than its dependence on the “burst” in Z component for 1-3 days prior to the EQ (compare Fig. 9 with Figs.6 and 7).

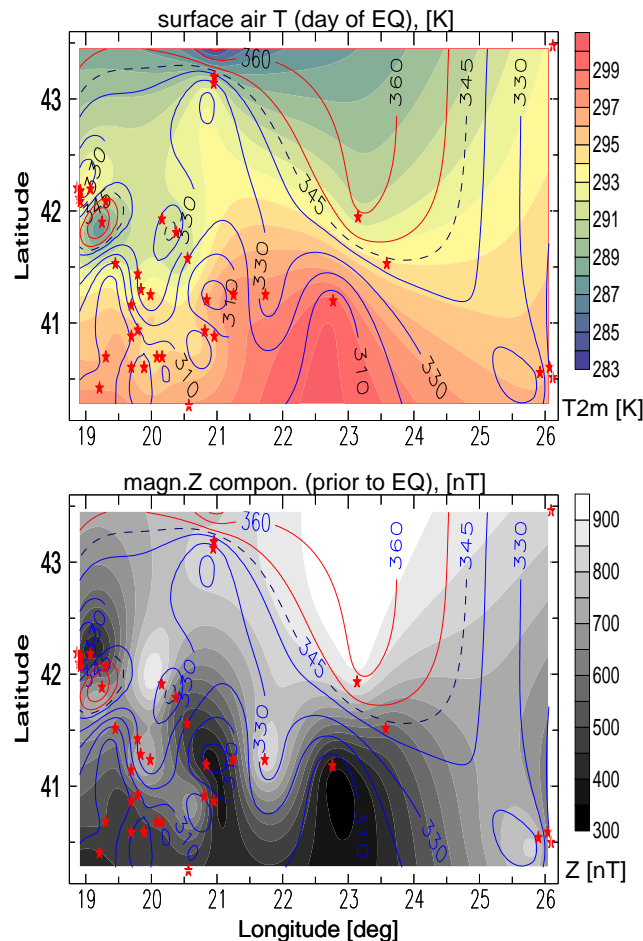


Fig.8 (top) Comparison between surface air T (colored shading) and total ozone density TOZ (contours) measured in days and places of EQs occurred in the warmer season; (bottom) maximal daily values of magnetic Z component (grey shading) measured in Hurbanovo observatory for several days prior to the EQs; overdrawn are contours of total O_3 density in the day of EQs. Blue contours represent TOZ density below the geometrical mean (dashed black contour); red contours – TOZ

values above geometrical mean; red stars denote the epicenters of EQs happened in the warmer season.

The impact of daily amplitude of horizontal H component (i.e. $H_{\max} - H_{\min}$) on the ozone and temperature is surprisingly opposite – i.e. an increase of the H component reduces the O_3 density and leads to the warming of the Earth’s surface (Fig.8, bottom panels). However, this effect is not statistically significant.

One more argument in the explanation of seasonality in geomagnetic field– O_3 –surface air T relation is the summer depletion of the ozone density near the tropopause, due to: (i) uplifting of the ozone layer in the summer season [24], and (ii) reduced impact of GCR on the near tropopause O_3 [21]. This means that ozone fluctuation – induced by the “bursts” in geomagnetic field intensity – are easier detectable on the background of the lower summer O_3 density. Taking into account the higher climate sensitivity to the ozone variability near the tropopause [26–29], the corresponding fluctuations in the surface T are also easily visible (the mechanism of the O_3 influence on surface air temperature is described in [18]).

In the cold season, oppositely the amplitude of daily magnetic variations is reduced and in addition – the whole O_3 profile is shifted downward.

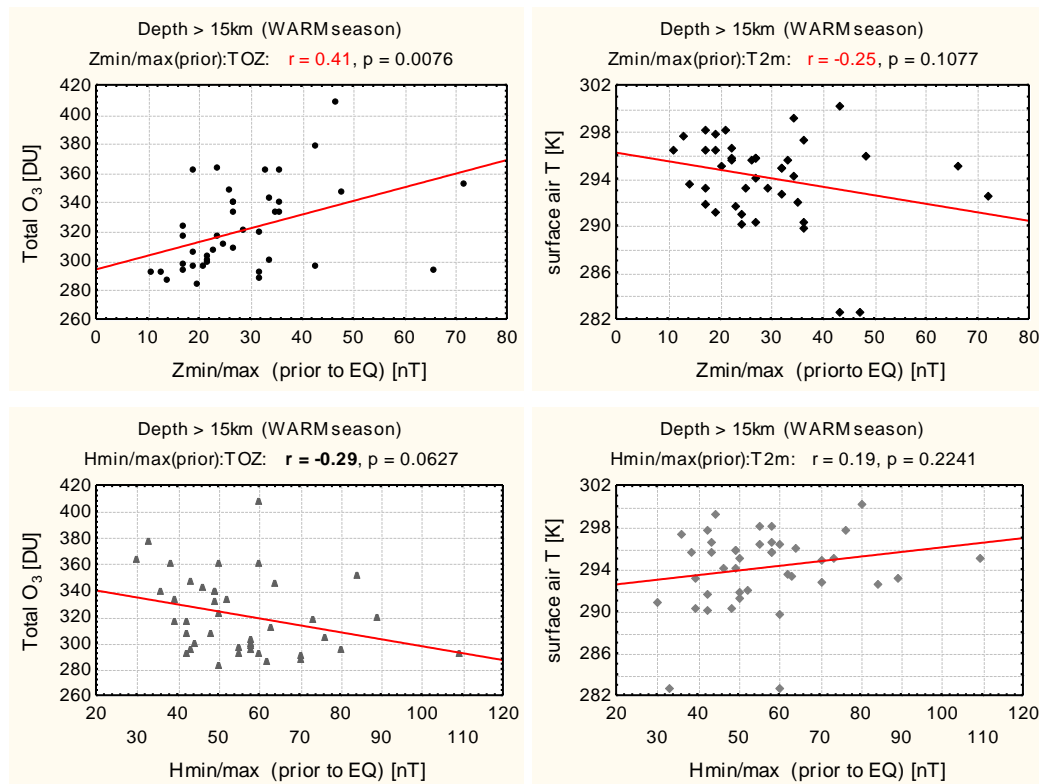


Fig.9 Scatterplots of daily amplitudes of magnetic Z (top panels) and H (bottom panels) components (measured prior to *deep* EQ, in warmer season) with total O_3 density (left column) and surface air T (right column) – measured in the days of seismic events.

7. Discussion and Conclusions:

The broadly explored idea for the surface temperature warming around the future earthquake’s (EQ) epicenter – for several days prior to the strike – raises the question about the reason for such a warming. Most of the authors believe that this is an endogenic warming (i.e. related to the lithospheric processes accompanying the EQ preparation). The surface air temperature (T), however, is controlled in a greater extent by atmospheric processes. Our recent studies [17, 18] have shown in addition that surface air T is strongly influenced by the ozone density near the troposphere. For this reason, besides the temperature, we have analyzed also the total ozone density in the days with earthquake strike. We

have selected all EQs occurred in the region of Balkan Peninsula with coordinates (40° - 44° N; 18° - 26° E), for the period 1957-1990.

The initial goal of this research was to examine whether the O_3 -T relation is changed or broken in days and places of EQs, due for example to the influence of lithospheric processes.

We found that in the *warmer* season the O_3 -T connectivity becomes even stronger in days and places of EQs, (compared to that calculated over the entire examined period) and almost disappears for EQs appearing in the *colder* season.

Having in mind our previous results – for the leading role of geomagnetic field as a factor influencing O_3 density near the tropopause [19, 22], we have analyzed to what extent total ozone density and surface air T are related to geomagnetic field. Results show that for seismic events happening in the warmer season (May-September), with epicentral depth greater than 15 km, the geomagnetic field–ozone–surface air temperature relation is quite strong. However, it almost disappears in cases with shallow EQs in warmer season. It is also negligible during the colder season, independently on the depth of the EQs.

Analysis of the spatial distribution of examined parameters reveals that in regions where the “bursts” in geomagnetic Z component (observed for ~1-3 days prior to the EQ) has values lower than their temporal–geometrical mean for the area – the total O_3 density in the day and place of EQ is reduced. The surface air T at the same time is warmer than its geometrical mean. Oppositely, when the sudden enhancement in magnetic Z component is stronger than average, the O_3 density in the day and place of EQ is enhanced, and the surface air T is colder than the averaged for the area.

Results from this research show that the mechanism of geomagnetic field influence on the surface air temperature, described previously [19, 22], and consisting of: (i.) control over the precipitating energetic particles, (ii.) influence on the lower stratospheric ozone balance; and (iii.) impact on the Earth’s radiation balance (and consequently on the surface air temperature) seems to act on the shorter time scales as well. The effect is seasonally dependent most probably due to the uplifting of the ozone layer in the warmer season and reduced impact of GCR on the near tropopause ozone (for more explanations see [21]). This makes the ozone fluctuations in the warmer season (initiated by changes in geomagnetic field prior to the EQs) easily detectable on the background of the lower near tropopause O_3 density.

Acknowledgements:

This research was supported by the BlackSeaHazNet FP7 project (*PIRSES-GA-2009-246874*) and partly by *COST ES1005 TOSCA* (<http://www.tosca-cost.eu>). We are very thankful to the project teams of ERA-40 and ERA-Interim reanalyses, as well as to NOAA National Geophysical Data Center for geomagnetic field data.

References:

- [1] Wang L., Zhou C. (1984) Anomalous variations of ground temperature before the Tangsan and Haiheng earthquakes (in Chinese). *J. Seismol. Res.*, 7, 649–656.
- [2] Gorny V.I., Salman A.G., Tronin A.A., Shilin B.B. (1988) The Earth’s outgoing IR radiation as an indicator of seismic activity. In: *Proceedings of the Academy of Science, USSR*, vol. 301, 67–69.
- [3] Qiang Z., Xiu-Deng X., Chang-Gong D. (1991) Thermal Infrared anomaly—precursor of impending earthquakes. *Chinese Science Bulletin*, 36 (4), 319–323.
- [4] Tronin A.A. (2000) Thermal satellite data for earthquake research. In: *IGARSS IEEE 2000 International Geosciences Symposium, Taking the Pulse of the Planet: The Role of Remote Sensing in Managing the Environment*, Honolulu, HI, IEEE.
- [5] Tramutoli V., DiBello G., Pergola N., Piscitelli S. (2001) Robust satellite techniques for remote sensing of seismically active areas. *Annali Di Geofisica* 44, 295–312.
- [6] Saraf A.K., Choudhury S. (2003) Earthquakes and thermal anomalies. *Geospatial Today* 2 (2), 18–20.
- [7] Panda S.K., Choudhury S., Saraf A.K., Das J.D. (2007) MODIS land surface temperature data detects thermal anomaly preceding 08 October 2005 Kashmir earthquake. *International Journal of Remote Sensing* 28 (20), 4587–4596.

- [8] Ouzounov D., Freund F.T. (2004) Mid-infrared emission prior to strong earthquakes analyzed by remote sensing data. *Adv. Space Res.* 33, 268–273.
- [9] Pulinet, S.A., Ozounov, D., Karelin, A.V., Boyarchuk, K.A., Pokhmelnikh, L.A., 2006. The physical nature of thermal anomalies observed before strong earthquakes. *Physics and Chemistry of the Earth* 31, 143–153.
- [10] Blacett M., Wooster, M. J., Malamud B.D. (2011) Exploring land surface temperature earthquake precursors: A focus on the Gujarat (India) earthquake of 2001, *Geophys. Res. Lett.*, 38, 115303, doi:10.1029/2011gl048282.
- [11] Saraf A.K., Rawat V., Choudhury S., Dasgupta S., Das J. (2009) Advances in understanding of the mechanism for generation of earthquake thermal precursors detected by satellites. *International Journal of Applied Earth Observation and Geoinformation* 11, 373–379.
- [12] Johstom M.J.S. (2002) Electromagnetic field generated by earthquakes, in: *Intern. Handbook of earthquake and engineering seismology*, vol. 81A, 621-636, Academic Press.
- [13] Sobolev G.A., Zakrzhevskaya N.A., Kharin E.P. (2001) On the Relation between Seismicity and Magnetic Storms, *Izvestiya, Phys. Solid Earth* 37, 917–927.
- [14] Bakhmutov V.G., Sedova F.V., Mozgovaya T.A. (2007) Geomagnetic Disturbances and Earthquakes in the Vrancea Zone. *Izvestiya, Physics of the Solid Earth*, Vol. 43(11) 931–937.
- [15] Bakhmutov V., Melnyk G., Mozgova T., Sedova F., Maksimenko O. (2011) Geomagnetic Field Variations: Monitoring and Application to Environmental Changes, in: *Complex research of earthquake's forecasting possibilities and climate change correlations*, Proceedings of BlackSeaHazNet workshop, 2-5 May, 2011, Ohrid, Repub. Macedonia, 21 - 47.
- [16] Wen S., Chen C.-H., Yen H.-Y., Yeh T.-K., Liu J.-Y., Hattori K., Peng H., Wang C.-H., Shin T.-C. (2012) Magnetic storm free ULF analysis in relation with earthquakes in Taiwan. *Nat. Hazards Earth Syst. Sci.*, 12, 1747–1754.
- [17] Kilifarska N.A. (2012) Climate sensitivity to the lower stratospheric ozone variations. *J. Atmos. Sol-Terr. Phys.*, 90–91, 9–14.
- [18] Kilifarska N.A. (2012) Mechanism of lower stratospheric ozone influence on climate. *Intern. Rev. Phys.*, 6(3), 279-290.
- [19] Kilifarska N.A., Bakhmutov V.G., Melnyk G.V. (2013) Geomagnetic influence on Antarctic climate – evidences and mechanism. *Int. Rev. Phys.*, 7(3), 242-252.
- [20] Shebalin N.V., Leydecker G. (1998) Catalogue for Central and Southeastern Europe (342 BC-1990 AD), *Report No. ETNU CT 93 - 0087, EC, Brussels*.
- [21] Kilifarska N.A., Bakhmutov V.G., Melnyk G.V., (2014) Global warming or climate variability – the role of geomagnetic field and lower stratospheric ozone (this issue).
- [22] Kilifarska N.A., Bakhmutov V.G., Melnyk G.V. (2013) Energetic particles influence on the southern Hemisphere ozone variability, *Compt. rend. Acad. bulg. Sci.*, 66(11), 1613-1622.
- [23] Hwang J., Kim H-P., Park Y-D. (2012) Diurnal and Seasonal Variations in Mid-Latitude Geomagnetic Field during International Quiet Days: BOH Magnetometer. *J. Astron. Space Sci.* 29(4), 329-336.
- [24] Werner R., Stebel K., Hansen H.G., Hoppe U.-P., Gausa M., Kivi R., von der Gathen P., Orsolini Y., Kilifarska N. (2011) Study of the seasonal ozone variations at European high latitudes, *Adv. Space Res.*, 47, 740–747.
- [25] Ramanatan V., Callis L.B., Boucher R.E. (1976) Sensitivity of surface temperature and Atmospheric temperature to perturbations in the Stratospheric ozone and Nitrogen dioxide, *J. Atmos. Sci.*, 3, 1092.
- [26] Wang W-Ch, Pinto J.P., Yunk Y. (1980) Climatic effect due to the halogenated compound in the Earth Atmosphere, *Atmos. Sci.*, 37, 333.
- [27] Wang W-Ch., Zhuang Y-Ch., Bojkov R. (1993) Climate implications of observed changes in ozone vertical distributions at middle and high latitudes of the Northern Hemisphere, *Geophys. Res. Lett.*, 20, 1567.
- [28] de Foster P.M., Shine K. (1997) Radiative forcing and temperature trends from stratospheric ozone changes *J. Geophys. Res.*, 102, 10841.
- [29] Stuber N., Sausen R., Ponater M. (2001) Stratosphere adjusted radiative forcing calculations in a comprehensive climate model, *Theor. Appl. Climatol.*, 68, 125.